



Universiteit  
Leiden  
The Netherlands

## **To bind or not to bind, that is an important question! : Development of covalent probes for adenosine receptors**

Yang, X.

### **Citation**

Yang, X. (2019, December 4). *To bind or not to bind, that is an important question! : Development of covalent probes for adenosine receptors*. Retrieved from <https://hdl.handle.net/1887/81190>

Version: Publisher's Version

License: [Licence agreement concerning inclusion of doctoral thesis in the Institutional Repository of the University of Leiden](#)

Downloaded from: <https://hdl.handle.net/1887/81190>

**Note:** To cite this publication please use the final published version (if applicable).

Cover Page



Universiteit Leiden



The handle <http://hdl.handle.net/1887/81190> holds various files of this Leiden University dissertation.

**Author:** Yang, X.

**Title:** To bind or not to bind, that is an important question! : Development of covalent probes for adenosine receptors

**Issue Date:** 2019-12-04

**To bind or not to bind,  
that is an important question!**

Development of covalent probes for adenosine receptors

*Xue Yang*

The research described in this thesis was performed at the Division of Drug Discovery and Safety of the Leiden Academic Centre for Drug Research (LACDR), Leiden University (Leiden, The Netherlands). Printing of the thesis was financially supported by LACDR, Leiden University.

*Cover design:* Zhuoqun Hou

*Thesis lay-out:* Xue Yang

*Printing:* Ridderprint BV | [www.ridderprint.nl](http://www.ridderprint.nl)

ISBN: 978-94-6375-676-1

© Copyright, Xue Yang, 2019

All rights reserved. No part of this book may be reproduced in any form or by any means without permission of the author.

**To bind or not to bind,  
that is an important question!**

Development of covalent probes for adenosine receptors

**Proefschrift**

ter verkrijging van  
de graad van Doctor aan de Universiteit Leiden,  
op gezag van Rector Magnificus prof.mr. C.J.J.M. Stolker,  
volgens besluit van het College voor Promoties  
te verdedigen op woensdag 4 december 2019  
klokke 10.00 uur

door

***Xue Yang***

geboren te Zhengzhou, Henan, China

in 1988

**Promotores:** Prof. dr. Ad IJzerman  
Dr. Laura Heitman

**Co-promotores:** Dr. Julien Louvel (until June 2016)  
Dr. Daan van der Es (from June 2016)

**Promotiecommissie:** Prof. dr. Hubertus Irth (voorzitter)  
Prof. dr. Joke Bouwstra (secretaris)  
Prof. dr. Mario van der Stelt  
Prof. dr. Eddy Sotelo (Universidad de Santiago de Compostela)  
Dr. Frank Dekker (University of Groningen)

# Contents

<b>Chapter 1</b>	General Introduction.....	<b>7</b>
<b>Chapter 2</b>	Molecular Probes for the Human Adenosine Receptors .....	<b>19</b>
<b>Chapter 3</b>	A Covalent Antagonist for the Human Adenosine A <sub>2A</sub> Receptor .....	<b>57</b>
<b>Chapter 4</b>	Development of Covalent Ligands for G Protein-Coupled Receptors: A Case for the Human Adenosine A <sub>3</sub> Receptor.....	<b>79</b>
<b>Chapter 5</b>	Design, Synthesis and Pharmacological Profiles of LUF7746, A Novel Covalent Partial Agonist for the Adenosine A <sub>1</sub> Receptor.....	<b>113</b>
<b>Chapter 6</b>	An Affinity-based Probe for the human Adenosine A <sub>2A</sub> Receptor.....	<b>141</b>
<b>Chapter 7</b>	Conclusions and Future Perspectives .....	<b>167</b>
	Summary .....	<b>181</b>
	Samenvatting .....	<b>185</b>
	List of publications .....	<b>189</b>
	Curriculum Vitae .....	<b>191</b>
	Acknowledgements.....	<b>193</b>





# **Chapter 1**

## **General Introduction**



**About this thesis**

Most small-molecule drugs are designed to interact with their biological targets under equilibrium binding conditions, whereby the desired drug-protein interaction is a rapid and reversible (non-covalent) process. However, for a drug to exert its effect, it needs to be bound to the target, and hence a common focus of modern drug discovery programs is to maximize the strength of these noncovalent molecular interactions. As an extension to this reasoning, a less conventional strategy termed ‘covalent interactions’ has recently gained reputation in the field of drug discovery [1, 2]. A covalent bond between ligand and receptor can be sufficiently long-lived that it is irreversible within the half-life of the target protein, resulting in a drug-protein complex that is not subject to classical equilibrium kinetics. Accordingly, such drugs were initially less favored owing to concerns over potential nonspecific side effects or off-target toxicity [1, 2]. However, one of the oldest drugs in current clinical practice, aspirin (acetylsalicylic acid), acts as a covalently binding inhibitor [3]. Hence, in this thesis a covalent strategy is applied and shown to be compatible with a target-directed, structure-guided discovery paradigm, with a focus on G protein-coupled receptors as drug targets.

Receptor proteins, located on both the cell surface and within the cell, are the targets through which many drugs produce their beneficial effects in various disease states. The receptor theory was once proposed as the underlying mechanism for drug action by the pioneering scientists Paul Ehrlich and John Newport Langley at the beginning of the 20<sup>th</sup> century. Whereas Langley referred to specific sites affected by nicotine as ‘receptive substances’ [4], Ehrlich simultaneously envisioned chemical ‘side-chains’ on the cell membrane to which toxins could bind [5]. Among the receptors, so-called G protein-coupled receptors (GPCRs) are one of the largest and most important drug target families [6]. This chapter provides a background for the covalent research strategy for GPCRs presented in this thesis, followed by the aim and outline of this thesis.

### 1. G Protein-coupled Receptors (GPCRs)

G protein-coupled receptors (GPCRs) represent a protein superfamily responsible for vision, olfaction, taste and signal transduction by hormones and neurotransmitters [7]. More than 30% of the current clinically used small-molecular drugs target GPCRs [8]. According to Fredriksson and colleagues, this large family in the human genome encompasses five subtypes, including *Rhodopsin* (class A), *Secretin* (class B), *Adhesion* (class B), *Glutamate* (class C), and *Frizzled/Taste2* (class F), shortened to GRAFS [9]. The main structural features of GPCR-family members are the seven hydrophobic, transmembrane,  $\alpha$ -helices, termed as TM1-TM7 (Figure 1). The N terminus, considered a glycosylation site for most GPCRs, together with three extracellular loops (ECL1–ECL3) compose the extracellular section. The intracellular part of the receptor contains a C terminus, three corresponding intracellular loops (ICL1-ICL3) and an amphipathic helix (H8). Due to their similar role in receptor function, such as activation, the seven hydrophobic helices, located in the lipid bilayer, are highly conserved, especially in class A GPCRs.

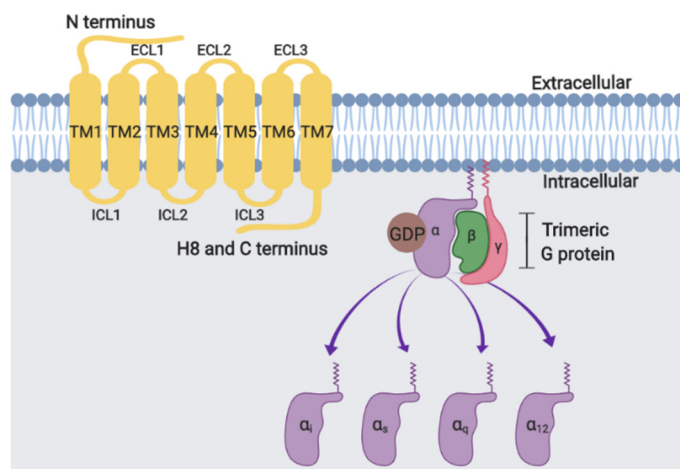


**Figure 1. A schematic representation of an inactive class A G protein-coupled receptor (GPCR).** Class A GPCRs consist of seven hydrophobic  $\alpha$ -helices, termed as TM1-TM7, connected with extracellular loops (ECL1–ECL3) and three corresponding intracellular loops (ICL1-ICL3). The N terminus is directed to the extracellular side, while helix 8 (H8) and C-terminus are located at the intracellular side. Activated G proteins regulate diverse signaling cascades, depending on their subtype ( $\alpha_s$ ,  $\alpha_i$ ,  $\alpha_q$ , and  $\alpha_{12}$  families).

The signaling from the extracellular to intracellular environment is mediated by the heterotrimeric G protein, having three subunits,  $\alpha$ ,  $\beta$  and  $\gamma$  (Figure 1). Activation of the receptor results in a conformational change, causing the G protein-bound guanosine diphosphate (GDP) to be exchanged for guanosine triphosphate (GTP), leading to dissociation of the  $\beta\gamma$ -dimer [10]. The  $\alpha$  subunits of G proteins are divided into four subfamilies:  $G\alpha_s$ ,

$G\alpha_i$ ,  $G\alpha_q$  and  $G\alpha_{12}$ , and a single GPCR can couple to either one or more families of  $G\alpha$  proteins. Each G protein activates several downstream effectors (Figure 1).

### 1.1. Adenosine receptors

Adenosine receptors (ARs) belong to the rhodopsin, or class A subfamily of GPCRs. There are four recognized subtypes for ARs-named  $A_1R$ ,  $A_{2A}R$ ,  $A_{2B}R$  and  $A_3R$ , each of which shows an individual pharmacological profile and tissue distribution [11, 12]. The classification of ARs is traditionally dependent on their differential coupling to adenylyl cyclase (AC), the enzyme responsible for increasing the intracellular concentration of the second messenger cyclic adenosine 5'-monophosphate (cAMP). Activation of the  $A_1R$  and  $A_3R$  will inhibit AC activity, caused predominantly by  $G\alpha_i$  protein interaction, ultimately leading to a decrease of intracellular cAMP. The  $A_{2A}R$  and  $A_{2B}R$  are coupled to the  $G\alpha_s$  protein, resulting in an increase of intracellular cAMP production. So far, only  $A_1R$  and  $A_{2A}R$  have been successfully subjected to structure elucidation, including both inactive [13, 14] and active states [15-17].

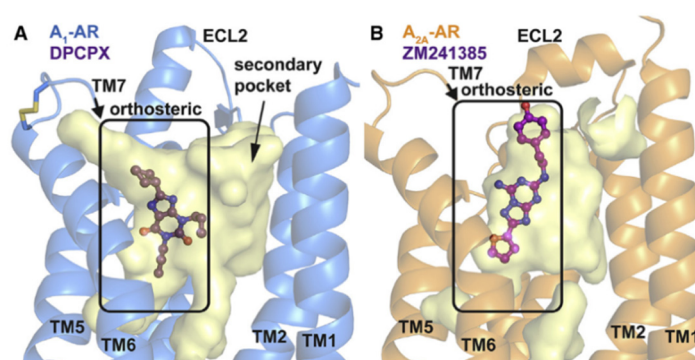


**Figure 2 Crystal structures of the indicated adenosine receptor.** (A) DPCPX, docked into the  $A_1R$  structure, leaves a secondary binding site unoccupied. (B) The  $A_{2A}R$  crystal structure with binding pocket occupied by ZM241385. Reproduced with permission [13].

Figure 2 includes the crystal structures of  $A_1R$  (PDB: 5EUN) docked with antagonist DPCPX and  $A_{2A}R$  co-crystalized with antagonist ZM241385 (PDB: 4EIY) [13, 14]. It was found that the amino acid residues in the orthosteric binding site are highly conserved for both receptor subtypes. However, the  $A_{2A}R$  accommodates an elongated and narrow binding cavity, while in the  $A_1R$ , transmembrane helices TM1, TM2, TM3, TM7 and ECL3 brought a more open and wide binding cavity with a secondary binding pocket. These findings provide important structural insights into a highly valued GPCR target, supporting our research efforts in this thesis.

### **1.2. Adenosine receptor as drug target: focus on A<sub>1</sub>R, A<sub>2A</sub>R and A<sub>3</sub>R.**

Adenosine receptors have distinct distributions through the human body and are important regulators of many different types of physiological and pathological processes. There is accumulating evidence that adenosine receptors are promising therapeutic targets for inflammatory, cardiovascular and neurodegenerative diseases, and cancer [18, 19]. In this thesis, we will only focus on the A<sub>1</sub>R, A<sub>2A</sub>R and A<sub>3</sub>R subtypes as drug targets.

A<sub>1</sub>R is widely expressed throughout the body with particular high abundance at excitatory nerve endings [18]. The activation of receptors inhibits AC activity, activates potassium channels (including K<sub>ATP</sub> channels in neurons and the myocardium), blocks transient calcium channels and increases intracellular calcium ion concentrations and phospholipase C activity (PLC). Adenosine acting via A<sub>1</sub>R plays an important role in various pathological conditions, such as ischemia/hypoxia, epileptic seizures, excitotoxic neuronal injury and cardiac arrhythmias [20]. As a consequence, A<sub>1</sub>R agonists might be considered as therapeutic agents for the treatment of central nervous system (pain) and cardiovascular (arrhythmia) pathologies. Various A<sub>1</sub>R antagonists have been or are currently being explored for clinical applications targeting cognitive and renal dysfunction [19].

High expression levels of A<sub>2A</sub>Rs are found in the brain striatum, spleen, leukocytes and blood platelets [19, 21]. A<sub>2A</sub>Rs mediate vasodilation, modulate angiogenesis and protect tissues from collateral inflammatory damage. In the brain, the A<sub>2A</sub>R influences motor activity, psychiatric behaviors, the sleep-wake cycle and neuronal cell death. The A<sub>2A</sub>R has been validated as a therapeutic/diagnostic target by the clinical use of regadenoson, approved by FDA for myocardial perfusion imaging in patients with suspected coronary artery disease [22]. Furthermore, A<sub>2A</sub>R agonists are being investigated as agents to treat a number of conditions such as asthma, COPD and diabetic foot ulcers, while A<sub>2A</sub>R antagonists have emerged as an attractive approach for Parkinson disease [21] and, more recently, as adjuvants for checkpoint inhibitors in cancer [23].

A<sub>3</sub>Rs have been recognized as a potential therapeutic target and biomarkers due to their overexpression in inflammatory and cancer cells compared to healthy cells [19, 24]. The A<sub>3</sub>R has been shown to couple to the G<sub>i</sub> and G<sub>q</sub> family and its anti-inflammatory activity correlates with the upregulation of nuclear factor- $\kappa$ B (NF- $\kappa$ B) signalling and the phosphoinositide 3-kinase (PI3K)–PKB–AKT signalling pathways. Earlier studies indicated an important role in the central nervous system, immune system, cancer, cardiovascular disease, and eye

disorder. Nevertheless, the medical relevance of the human A<sub>3</sub>R is enigmatic due to paradoxical effects in different therapeutic applications [25]. Currently, agonists are being considered as pharmacological agents for rheumatoid arthritis, psoriasis, glaucoma, and hepatocellular carcinoma.

### 1.3. Targeting adenosine receptors

From a drug discovery perspective, the wide distribution of adenosine receptors in mammalian cell types renders it mandatory to search for high-affinity and highly subtype-selective agonists and antagonists. The development of AR agonists started from structural modification of the endogenous ligand, adenosine, and hence structure-activity relationships for such ribose-containing compounds have been extensively investigated [12, 18, 26]. Besides these several non-ribose agonists have also been shown to reveal high receptor subtype selectivity, such as the A<sub>1</sub>R agonist capadenoson, a clinical drug candidate for atrial fibrillation [27]. Similarly, naturally occurring compounds caffeine and theophylline share a xanthine-based scaffold, contributing to the templates of antagonists for all AR subtypes, while non-xanthine structures have been explored for better water solubility and consequently improved bioavailability [12, 18, 26]. However, the major challenge in developing AR ligands for specific clinical applications is the ubiquitous receptor distribution and associated complex adenosine signaling, which exerts a broad spectrum of physiological and pathophysiological read-outs [19, 28]. The standard pharmacological assays of selectivity and efficacy are not sufficient to reveal a drug candidate's bio-distribution and pharmacokinetics, which may lead to potential side effects responsible for their failure in clinical trials. For example, the A<sub>1</sub>R antagonist rolofylline, a drug candidate for patients with acute heart failure with impaired renal function, failed in clinical trials due to A<sub>1</sub>R-mediated ("on target") safety issues leading to an increased frequency of stroke and seizure activity [29]. Thus, it is desirable to decipher the distinct AR effects dependent on cellular and tissue specificity and disease phase. Moreover, repeated exposure to AR agonists may desensitize receptor activation or reduce receptor signaling over time, and consequently result in the development of ligand tolerance [19, 28]. Moreover, the daily consumption of AR antagonist caffeine, in coffee, tea, etc., undoubtedly complicates clinical trials studying AR-targeted agents [19, 28]. Therefore, despite its medical relevance in various diseases, only a few drugs targeting adenosine receptors have been approved for clinical indications [12, 22, 26].

### 2. Covalent ligands for GPCRs

Covalent ligands, or affinity labels, are defined as compounds that target a specific receptor and feature a reactive moiety that forms a covalent interaction with amino acid residues at or near the binding pocket [30, 31]. Covalent tools should ideally be able to first bind to the receptor non-covalently with high affinity and then form an irreversible interaction with one or more nucleophilic amino acid residues. The archetypical example of a covalent ligand-GPCR complex is the visual pigment rhodopsin, having the 11-cis-retinal chromophore covalently bound via a protonated Schiff's base [32].

#### 2.1. Applications of covalent ligands

Although being one of the largest families of membrane proteins, GPCRs are notoriously difficult to study due to their low expression levels, intrinsic fragility and flexibility, and often low affinity for their endogenous ligand [33]. Covalent ligands may have the potential to address some of these challenges, since they are able to irreversibly bind to GPCRs and contribute to the formation of a stable and conformationally homogeneous ligand-receptor complex [34]. In this way such ligands have emerged already as a promising strategy to facilitate the structure elucidation of GPCRs [31]. For instance, the structures of cannabinoid receptor CB<sub>1</sub> [35] and adenosine A<sub>1</sub> receptor [13] have been resolved in the presence of chemo-reactive ligands contributing to the formation of stable and functional ligand-receptor complexes. The fact that covalent probes are designed to interact irreversibly with residues near the binding site has widened their applications to investigate the topology of the GPCR-ligand binding pocket, receptor signaling and *in vivo* research [31]. For example, the covalent cannabinoid CB<sub>1</sub> receptor agonist, (-)-7-isothiocyanato-11-hydroxy-1,1-dimethylheptylhexahydrocannabinol (AM841), was successfully applied to investigate the ligand binding site in the CB<sub>1</sub> receptor [36, 37], assess its potential use in physiological and pathophysiological *in vivo* studies [38] and demonstrate the differences in binding motifs between the two cannabinoid receptor subtypes, CB<sub>1</sub> and CB<sub>2</sub> [39]. Given the highly dynamic nature of GPCRs and the inherent flexibility of their ligand binding sites, the potential of “freezing” a conformational state of the receptor by a covalently linked agonist or antagonist is very attractive. Moreover, covalent attachment of the ligand/drug to the receptor will lead to an infinitely long residence time or receptor occupancy, and thus might contribute to a sustained on-target pharmacological efficacy and minimized off-target effect [1, 40]. From this perspective, covalent ligands will offer an advantage over conventional reversible ligands



with respect to increased biochemical potency and greater selectivity for the targeted receptors.

## 2.2. Current state and further challenges

More recently, covalent probes equipped with a ligation handle, termed affinity-based probes (AfBPs), have emerged as valuable tools for chemical biology or proteomics studies to gain further insight into receptor localization and target engagement [41-43]. This strategy was inspired by earlier activity-based protein profiling-click chemistry (ABPP-CC), which helped in visualizing and quantifying the activities of drug targets (mainly enzymes) in native biological systems [44, 45]. However, different from mechanism-based enzyme inhibitors, covalent ligands targeting GPCRs have no specific active center to target and are generally armed with a highly electrophilic moiety responsible for the covalent interaction. The abundance of nucleophilic groups in biological systems may cause insufficient target-specific cross-linking [46] and induce low coupling selectivity [47]. In addition, the low expression of GPCRs also hampers successful execution of this otherwise promising technique.

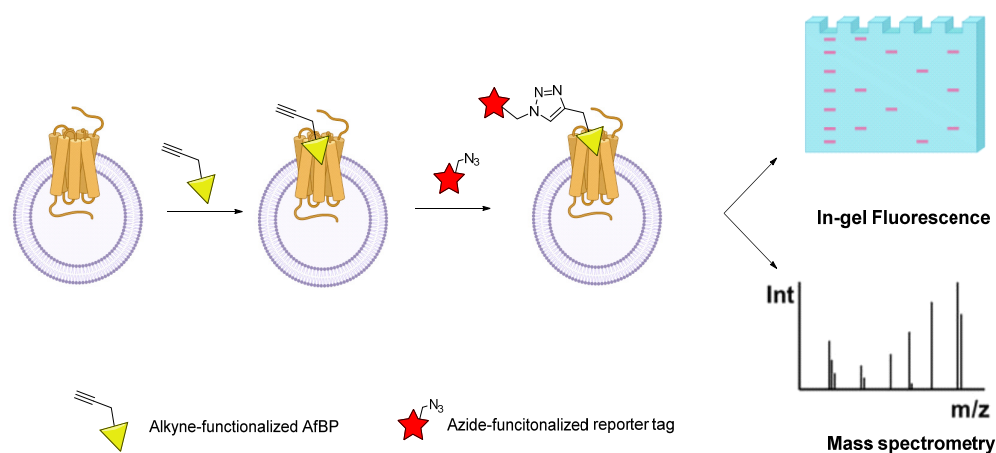


**Figure 3 Schematic representations of two-step affinity-based labeling strategy.** A small bio-orthogonal “ligation handle” is incorporated into a covalent ligand for a GPCR. After binding of the probe to the target receptor the tag is introduced by “click chemistry”. The tagged probe-treated receptors are either visualized/quantified by in-gel fluorescence scanning or mass spectrometry analysis.

As illustrated in Figure 3, AfBPs provide the opportunity to label specific receptors, as they are functionalized probes paired with “clickable” reporter tags (e.g., biotin and/or a fluorophore), via a Huisgen 1,3-dipolar cycloaddition, to form a stable triazole-linked product. In this affinity-based protein profiling (AfBPP) approach the labeled protein targets are separated, visualized or affinity-purified, analyzed via the reporter tag using fluorescent SDS-PAGE, Western Blotting or enriched for multiple LC-MS platforms. It allows monitoring of

## Chapter 1

---

endogenous GPCR expression and engagement and may provide engineered biomarkers for translational drug discovery. Even though the entire GPCR family contains over 800 members, until recently only three subtypes including mGlu5 receptor, cannabinoid CB<sub>2</sub> receptor and adenosine A<sub>2A</sub> receptors have been subject of investigation [41-43], of which the A<sub>2A</sub>R will be the showcase in this thesis.

### 3. Aims and outline of this thesis

In this thesis the development and application of chemical tools and strategies are described to study three subtypes of ARs, A<sub>1</sub>R, A<sub>2A</sub>R and A<sub>3</sub>R. Combined, this research approach may ultimately aid in the discovery and development of novel adenosine receptor-based therapeutics that lack potential side effects as much as possible.

While **Chapter 1** serves as an introduction, **Chapter 2** provides a comprehensive overview of the molecular probes that have been reported to study adenosine receptor distribution, expression levels, occupancy, internalization and pharmacology in both *in vitro* and *in vivo* models. **Chapter 3** describes the development and pharmacological profiling of covalent ligands targeting A<sub>2A</sub>R. The rational design of covalent ligands and a research flow chart to investigate irreversible ligand-receptor interactions have been applied to the A<sub>1</sub>R and A<sub>3</sub>R characterization in **Chapters 4** and **5**. **Chapter 4** describes a design and pharmacological profiling of the first non-ribose covalent partial A<sub>1</sub>R agonist. In **Chapter 5**, a structure-based approach was developed for a compound library based on the existing A<sub>3</sub>R antagonist 1H,3H-pyrido[2,1-*f*]purine-2,4-dione scaffold. The aim of this chapter is to identify a covalent ligand targeting the A<sub>3</sub>R and shed light on the details of its binding site. **Chapter 6** reports on the development of A<sub>2A</sub>R covalent ligands into an affinity-based probe. In the end, two-step affinity labeling with a ZM241385-based probe for A<sub>2A</sub>R target identification was established. **Chapter 7** summarizes the work described in this thesis and presents future prospects and challenges

## References

1. Singh J., Petter R.C., Baillie T.A., and Whitty A. *Nat Rev Drug Discov.* **2011**. 10(4): 307-17.
2. Bauer R.A. *Drug Discov Today.* **2015**. 20(9): 1061-73.
3. Roth G.J., Stanford N., and Majerus P.W. *Proc Natl Acad Sci U S A.* **1975**. 72(8): 3073-6.
4. Langley J.N. *J Physiol.* **1905**. 33(4-5): 374-413.
5. Ehrlich P. *Lancet.* **1913**. 182: 445-451.
6. Alexander S.P.H., Kelly E., Marrion N., Peters J.A., Benson H.E., Faccenda E., Pawson A.J., Sharman J.L., Southan C., Buneman O.P., Catterall W.A., Cidlowski J.A., Davenport A.P., Fabbro

- D., Fan G., McGrath J.C., Spedding M., Davies J.A., and Collaborators C. *Br J Pharmacol.* **2015** 172: 5744-5869.
7. Lefkowitz R.J. *Trends Pharmacol Sci.* **2004.** 25(8): 413-22.
  8. Hopkins A.L. and Groom C.R. *Nat Rev Drug Discov.* **2002.** 1(9): 727-30.
  9. Fredriksson R., Lagerstrom M.C., Lundin L.G., and Schioth H.B. *Mol Pharmacol.* **2003.** 63(6): 1256-72.
  10. Neves S.R., Ram P.T., and Iyengar R. *Science.* **2002.** 296(5573): 1636-1639.
  11. Fredholm B.B., IJzerman A.P., Jacobson K.A., Klotz K.N., and Linden J. *Pharmacol Rev.* **2001.** 53(4): 527-52.
  12. Fredholm B.B., IJzerman A.P., Jacobson K.A., Linden J., and Muller C.E. *Pharmacol Rev.* **2011.** 63(1): 1-34.
  13. Glukhova A., Thal D.M., Nguyen A.T., Vecchio E.A., Jorg M., Scammells P.J., May L.T., Sexton P.M., and Christopoulos A. *Cell.* **2017.** 168(5): 867-877 e13.
  14. Jaakola V.P., Griffith M.T., Hanson M.A., Cherezov V., Chien E.Y., Lane J.R., IJzerman A.P., and Stevens R.C. *Science.* **2008.** 322(5905): 1211-7.
  15. Draper-Joyce C.J., Khoshouei M., Thal D.M., Liang Y.L., Nguyen A.T.N., Furness S.G.B., Venugopal H., Baltos J.A., Plitzko J.M., Danev R., Baumeister W., May L.T., Wootten D., Sexton P.M., Glukhova A., and Christopoulos A. *Nature.* **2018.** 558(7711): 559-563.
  16. Lebon G., Warne T., Edwards P.C., Bennett K., Langmead C.J., Leslie A.G., and Tate C.G. *Nature.* **2011.** 474(7352): 521-5.
  17. Xu F., Wu H., Katritch V., Han G.W., Jacobson K.A., Gao Z.G., Cherezov V., and Stevens R.C. *Science.* **2011.** 332(6027): 322-7.
  18. Jacobson K.A. and Gao Z.G. *Nat Rev Drug Discov.* **2006.** 5(3): 247-264.
  19. Chen J.F., Eltzhischig H.K., and Fredholm B.B. *Nat Rev Drug Discov.* **2013.** 12(4): 265-86.
  20. Varani K., Vincenzi F., Merighi S., Gessi S., and Borea P.A. *Adv Exp Med Biol.* **2017.** 1051: 193-232.
  21. Ruiz M.D., Lim Y.H., and Zheng J.Y. *J Med Chem.* **2014.** 57(9): 3623-3650.
  22. Ghimire G., Hage F.G., Heo J., and Iskandrian A.E. *J Nucl Cardiol.* **2013.** 20(2): 284-288.
  23. Vijayan D., Young A., Teng M.W.L., and Smyth M.J. *Nat Rev Cancer.* **2017.** 17(12): 765-765.
  24. Borea P.A., Varani K., Vincenzi F., Baraldi P.G., Tabrizi M.A., Merighi S., and Gessi S. *Pharmacol Rev.* **2015.** 67(1): 74-102.
  25. Gessi S., Merighi S., Varani K., Leung E., Mac Lennan S., and Borea P.A. *Pharmacol Ther.* **2008.** 117(1): 123-40.
  26. Muller C.E. and Jacobson K.A. *Biochim Biophys Acta Biomembr.* **2011.** 1808(5): 1290-1308.
  27. Jacobson K.A., Tosh D.K., Jain S., and Gao Z.G. *Front Cell Neurosci.* **2019.** 13: 124.
  28. Peleli M., Fredholm B.B., Sobrevia L., and Carlstrom M. *Mol Aspects Med.* **2017.** 55: 4-8.
  29. Teerlink J.R., Iragui V.J., Mohr J.P., Carson P.E., Hauptman P.J., Lovett D.H., Miller A.B., Pina I.L., Thomson S., Varosy P.D., Zile M.R., Cleland J.G., Givertz M.M., Metra M., Ponikowski P., Voors A.A., Davison B.A., Cotter G., Wolko D., Delucca P., Salerno C.M., Mansoor G.A., Dittrich H., O'Connor C.M., and Massie B.M. *Drug Saf.* **2012.** 35(3): 233-44.
  30. Grunbeck A. and Sakmar T.P. *Biochemistry.* **2013.** 52(48): 8625-32.
  31. Weichert D. and Gmeiner P. *ACS Chem Biol.* **2015.** 10(6): 1376-86.
  32. Palczewski K., Kumasaka T., Hori T., Behnke C.A., Motoshima H., Fox B.A., Le Trong I., Teller D.C., Okada T., Stenkamp R.E., Yamamoto M., and Miyano M. *Science.* **2000.** 289(5480): 739-745.

## Chapter 1

---

33. Rosenbaum D.M., Rasmussen S.G., and Kobilka B.K. *Nature*. **2009**. 459(7245): 356-63.
34. Shonberg J., Kling R.C., Gmeiner P., and Lober S. *Bioorg Med Chem*. **2015**. 23(14): 3880-906.
35. Hua T., Vemuri K., Nikas S.P., Laprairie R.B., Wu Y., Qu L., Pu M., Korde A., Jiang S., Ho J.H., Han G.W., Ding K., Li X., Liu H., Hanson M.A., Zhao S., Bohn L.M., Makriyannis A., Stevens R.C., and Liu Z.J. *Nature*. **2017**. 547(7664): 468-471.
36. Picone R.P., Khanolkar A.D., Xu W., Ayotte L.A., Thakur G.A., Hurst D.P., Abood M.E., Reggio P.H., Fournier D.J., and Makriyannis A. *Mol Pharmacol*. **2005**. 68(6): 1623-35.
37. Szymanski D.W., Papanastasiou M., Melchior K., Zvonok N., Mercier R.W., Janero D.R., Thakur G.A., Cha S., Wu B., Karger B., and Makriyannis A. *J Proteome Res*. **2011**. 10(10): 4789-98.
38. Keenan C.M., Storr M.A., Thakur G.A., Wood J.T., Wager-Miller J., Straiker A., Eno M.R., Nikas S.P., Bashashati M., Hu H., Mackie K., Makriyannis A., and Sharkey K.A. *Br J Pharmacol*. **2015**. 172(9): 2406-18.
39. Zhou H., Peng Y., Halikhedkar A., Fan P.S., Janero D.R., Thakur G.A., Mercier R.W., Sun X., Ma X.Y., and Makriyannis A. *ACS Chem Neurosci*. **2017**. 8(6): 1338-1347.
40. Guo D., Hillger J.M., IJzerman A.P., and Heitman L.H. *Med Res Rev*. **2014**. 34(4): 856-92.
41. Gregory K.J., Velagaleti R., Thal D.M., Brady R.M., Christopoulos A., Conn P.J., and Lapinsky D.J. *ACS Chem Biol*. **2016**. 11(7): 1870-1879.
42. Soethoudt M., Stolze S.C., Westphal M.V., van Stralen L., Martella A., van Rooden E.J., Guba W., Varga Z.V., Deng H., van Kasteren S.I., Grether U., IJzerman A.P., Pacher P., Carreira E.M., Overkleeft H.S., Ioan-Facsinay A., Heitman L.H., and van der Stelt M. *J Am Chem Soc*. **2018**. 140(19): 6067-6075.
43. Yang X., Michiels T.J.M., de Jong C., Soethoudt M., Dekker N., Gordon E., van der Stelt M., Heitman L.H., van der Es D., and IJzerman A.P. *J Med Chem*. **2018**. 61(17): 7892-7901.
44. Speers A.E. and Cravatt B.F. *Chem Biol*. **2004**. 11(4): 535-546.
45. Cravatt B.F., Wright A.T., and Kozarich J.W. *Annu Rev Biochem*. **2008**. 77: 383-414.
46. Kung M.P., Mu M., Zhuang Z.P., and Kung H.F. *Life Sci*. **1996**. 58(3): 177-86.
47. Newman A.H. *NIDA Res Monogr*. **1991**. 112: 256-83.

# Chapter 2

## Molecular Probes for the Human Adenosine Receptors

*Xue Yang*

*Laura H. Heitman*

*Daan van der Es*

*Adriaan P. IJzerman*

To be submitted



### 1. Introduction

Adenosine receptors (ARs), which are activated by their endogenous ligand adenosine, belong to the Class A family of G protein-coupled receptors (GPCRs). These receptors have been considered potential therapeutic targets in several disorders, including Parkinson's disease, schizophrenia, analgesia, ischemia and cancer [1]. To date, four subtypes of adenosine receptors have been identified, namely A<sub>1</sub>, A<sub>2A</sub>, A<sub>2B</sub> and A<sub>3</sub>. Activation of A<sub>1</sub> and A<sub>3</sub> receptors leads to inhibition of adenylate cyclase through their interaction with a G<sub>i</sub> protein, whereas A<sub>2A</sub> and A<sub>2B</sub> receptors stimulate the enzyme through a G<sub>s</sub>-linked pathway. Until now, the 3D-structures of the A<sub>1</sub> and A<sub>2A</sub> subtypes have been elucidated [2, 3]; studies on the A<sub>2B</sub> and A<sub>3</sub> subtypes have yet to be successful. Although structure elucidation was relatively successful for adenosine receptors, the membrane-bound GPCRs still prove challenging due to their low expression in native tissue, and their inherent flexibility and instability once extracted from the membrane, which is often needed for further structural studies. Over the past decades a diverse array of molecular probes, bifunctional ligands that can be used to interrogate receptor structure and function, has proven invaluable in GPCR research. From a chemical perspective, a molecular probe can be defined as a small molecule that binds the receptor of interest and enables further studies by virtue of a connected tag or functional group that exhibits specific properties. These conjugated tags or functional groups include radioactive or fluorescent moieties to enable studies on ligand-receptor binding as well as the quantification and visualization of receptors. Moreover, tags containing a reactive warhead capable of irreversibly binding to the receptor have been shown to facilitate structure elucidation, and when made bifunctional, i.e. combined with a click handle, these can be used as affinity-based probes (AfBPs). It emerged as valuable tools for chemical biology or proteomics studies to gain further insight into receptor localization and target engagement [4-6]. This strategy was inspired by earlier activity-based protein profiling-click chemistry (ABPP-CC), which helped in visualizing and quantifying the activities of drug targets (mainly enzymes) in native biological systems [7, 8]. In this review, various chemical probes for human adenosine receptors will be summarized. where we will limit this review to molecular probes comprising radioligands, fluorescent ligands and covalent ligands.

### 2. Radioligands for *in vitro* characterization

Some adenosine receptor agonists and antagonists have been developed in a radiolabeled ('hot') form, so-called radioligands. Often, these are high affinity molecules containing radioactive isotopes such as [<sup>3</sup>H]-, [<sup>125</sup>I]-, and [<sup>35</sup>S]-, which emit radiation that can be detected

and quantified. The majority of radioligands used for *in vitro* assays are labeled with either [<sup>125</sup>I]- or [<sup>3</sup>H]-. [<sup>125</sup>I]-labeled ligands show a higher specific activity (~2,000 Ci/mmol) and shorter half-life ( $t_{1/2}$  = 60 days) compared to tritium-labeled ligands (specific activity ~ 25-120 Ci/mmol and  $t_{1/2}$  = 12.5 years), where the latter are more biologically indistinguishable from the unlabeled parent ligand. These radiolabeled ligands are predominantly used in saturation experiments to measure the radioligand's equilibrium dissociation constant,  $K_D$ , and receptor expression/density ( $B_{max}$ ), in competition displacement experiments to determine the affinity (equilibrium inhibitory constant  $K_i$ ) of non-labelled ('cold') compounds, and in binding kinetics assays to determine a ligand's association ( $k_{on}$ ) and dissociation ( $k_{off}$ ) rate constants [9, 10]. Conventional radioligand binding assays require a filtration step to separate bound from unbound radiolabeled ligands and capture the radioligand-receptor complex. A more recently developed bead-based assay, the scintillation proximity assay (SPA), has emerged as a rapid and sensitive assay to perform high throughput screens in a homogeneous system. Due to the diverse applicability of these techniques in receptor research, a diverse set of radioligands for the different AR subtypes has been developed. All radioligands that are currently commonly used are summarized in Table 1.

### 2.1. Radioligands for the adenosine A<sub>1</sub> receptor

The initial agonist radioligands for A<sub>1</sub>R were all tritiated adenosine-based derivatives. Among them [<sup>3</sup>H]CCPA (Fig. 1; Table 1) showed highest affinity with a  $K_D$  value of 0.61 nM for human A<sub>1</sub>R (hA<sub>1</sub>R) [11]. [<sup>3</sup>H]LUF5834 is a non-nucleoside partial agonist radioligand (Fig. 1; Table 1) with nanomolar affinity ( $K_D = 2.03 \pm 0.52$  nM) for the hA<sub>1</sub>R [12]. Its partial agonistic nature allows this radioligand to bind to both G protein-coupled and -uncoupled receptors. This radioligand proved a versatile tool to estimate the efficacy and the mechanism of action of both agonists and inverse agonists at the hA<sub>1</sub>R.

The reference antagonist radioligand for A<sub>1</sub>R is the xanthine-derived antagonists/inverse agonist [<sup>3</sup>H]DPCPX (Fig. 1; Table 1) [13]. Although this xanthine derivative displays lower affinity at the human ( $K_D = 3.86$  nM) [13] than the rat receptor ( $K_D = 0.18$  nM) [14], it is still a very useful tool for the characterization of A<sub>1</sub>R and consequently discriminate from other subtypes. It has been applied to SPA technology, constituting an alternative platform for real-time measurements of receptor-ligand interactions on hA<sub>1</sub>R [15]. Antagonist radioligands instead of agonists tend to label all receptors present in a cell membrane preparation independent of their coupling to a G protein and are therefore used more frequently in AR research, and GPCR research in general.



### 2.2. Radioligands for the adenosine A<sub>2A</sub> receptor

The reference radioligands for binding assays at A<sub>2A</sub>R include the adenosine-based agonists [<sup>3</sup>H]NECA (Fig. 1 ; Table 1) [13] or [<sup>3</sup>H]CGS21680 (Fig. 1; Table 1) [16]. [<sup>3</sup>H]NECA bound to hA<sub>2A</sub>R with a K<sub>D</sub>-value of 20.1 nM. However, this non-selective radioligand also exhibited remarkably high affinity for hA<sub>3</sub>R with a K<sub>D</sub>-value of 6 nM, threefold higher than at the A<sub>2A</sub> receptor [13]. Later, a more selective radioligand, [<sup>3</sup>H]CGS21680 showed a moderate affinity for human A<sub>2A</sub>R with a K<sub>D</sub> value of 22 ± 0.5 nM and has been used in autoradiographic studies, revealing the distribution of the A<sub>2A</sub>R in the basal ganglia of the human brain and an increased hA<sub>2A</sub>R level in the striatum of schizophrenic patients [17-19]. However, besides its agonistic binding with high and low affinity states to the receptor, application of this agonist radioligand is further limited due to complex binding characteristics related to non-A<sub>2A</sub> binding sites [20] and enhanced affinity by increasing concentrations of Mg<sup>2+</sup> ions [16].

To avoid the issues occurring with agonistic radioligands, two xanthine-based antagonist radioligands [<sup>3</sup>H]XAC (Fig. 1; Table 1) [21] and [<sup>3</sup>H]MSX-2 (Fig. 1; Table 1) [22] were developed to investigate the A<sub>2A</sub>R. Though the unlabeled compound XAC showed poor selectivity for hA<sub>2A</sub>R over hA<sub>1</sub>R (30-fold) and hA<sub>3</sub>R (90-fold) [13], [<sup>3</sup>H]XAC was used to identify the important residues involved in the hA<sub>2A</sub>R binding pocket with a K<sub>D</sub> value of 9.4 ± 2.3 nM [21]. [<sup>3</sup>H]MSX-2 is a styrylxanthine-based antagonist which bound selectively to rA<sub>2A</sub>R (K<sub>D</sub> = 8.04 ± 2.62 nM) [22]. Furthermore, *in vitro* autoradiography using [<sup>3</sup>H]MSX-2 showed the greatest binding in the striatum, which is in line with the expected density of A<sub>2A</sub>R in the mouse, rat and pig brain [23]. A preliminary *ex vivo* study confirmed that [<sup>3</sup>H]MSX-2 penetrated the blood-brain barrier, which is promising for *in vivo* use [23]. Applications of these styrylxanthine derivatives are limited however, due to the tendency to undergo photoinduced isomerization [24]. Meanwhile, two non-xanthine antagonist radioligands were developed as well. [<sup>3</sup>H]ZM241385 (Fig. 1; Table 1) showed a high affinity and low non-specific binding to hA<sub>2A</sub>R [25, 26]. However, this radioligand also binds to A<sub>2B</sub>R with nanomolar affinity (K<sub>D</sub> = 33.6 ± 2.8 nM) [27]. [<sup>3</sup>H]SCH58261 (Fig. 1; Table 1) showed a better selectivity at the hA<sub>2A</sub>R (hA<sub>2B</sub>/hA<sub>2A</sub> = 8352) than [<sup>3</sup>H]ZM241385 and was used in autoradiographic studies to investigate the receptor distribution in the human brain [17, 28]. Similarly, [<sup>3</sup>H]SCH58261 was applied in *ex vivo* binding studies to study A<sub>2A</sub>R receptor occupancy of various ligands in mouse brain [29]. Additionally, this radioligand was applied to high throughput ligand screening in a SPA set-up and showed comparable sensitivity to the conventional filtration assay [30].

### 2.3. Radioligands for the adenosine A<sub>2B</sub> receptor

So far only one selective agonist radioligand has been described for the A<sub>2B</sub>R, which is tritium labeled BAY 60-6583 (Fig. 1; Table 1) [31]. Unfortunately, the specific binding of [<sup>3</sup>H]BAY 60-6583 was too low compared to its high non-specific binding to establish a robust radioligand binding assay. Until now the non-selective agonist radioligand [<sup>3</sup>H]NECA, despite its low affinity, remains the only molecular tool available to study the active A<sub>2B</sub>R conformation [31, 32].

The A<sub>1</sub>R radioligand [<sup>3</sup>H]DPCPX (Fig. 1; Table 1) was also reported to bind hA<sub>2B</sub>R (K<sub>D</sub> = 40 nM) and has been used to determine the affinity of competing ligands [33, 34]. Another commonly used nonselective radioligand is [<sup>125</sup>I]ABOPX (Fig. 1, Table 1) [35]. It bound to A<sub>2B</sub>R with moderate affinity (K<sub>D</sub> = 37 nM) and showed a high specific binding to a hA<sub>2B</sub>R overexpressed cell line. The first A<sub>2B</sub>R-selective antagonist radioligand is [<sup>3</sup>H]MRS1754 (Fig. 1; Table 1), bound to hA<sub>2B</sub>R with a K<sub>D</sub> value of 1.13 ± 0.12 nM [36]. Later, another xanthine analogue radioligand [<sup>3</sup>H]MRE-2029-F20 was reported with comparable affinity and selectivity [37, 38]. Besides, the pyrrolopyrimidine-derivative, OSIP339391 (Fig. 1; Table 1), was labeled with tritium, representing a novel selective and high affinity radioligand for the hA<sub>2B</sub>R [39]. However, all these radioligands showed poor selectivity (less than 100-fold) toward the hA<sub>1</sub>R. More recently, Müller *et al.* investigated the structure-activity relationships of 1-alkyl-8-(piperazine-1-sulfonyl)phenylxanthine derivatives, yielding a new and potent A<sub>2B</sub>-selective antagonist, PSB-603 [40]. Tritium labeled PSB-603 (Fig. 1; Table 1) was subsequently developed and employed as the first high affinity (K<sub>D</sub> = 0.403 nM) A<sub>2B</sub>R-specific radioligand for receptor pharmacological studies. However, the current xanthine-based radioactive tracers are highly lipophilic compounds that exhibit unfavorable non-specific to specific binding ratios; this feature confines their application to receptor studies in isolated membranes.

### 2.4. Radioligands for the adenosine A<sub>3</sub> receptor

Initially, studies on the human A<sub>3</sub>R (hA<sub>3</sub>R) were performed using the non-selective agonist radioligand [<sup>3</sup>H]NECA (Fig.1, Table 1) [13]. For binding studies on the rat A<sub>3</sub>R (rA<sub>3</sub>R), [<sup>125</sup>I]I-APNEA (Fig. 1, Table 1) was the preferred radioligand [41]. Though [<sup>125</sup>I]I-APNEA showed reasonable affinity for the rA<sub>3</sub>R (K<sub>D</sub> = 15.5 ± 2.4 nM), it was shown to be even more potent for the rA<sub>1</sub>R (K<sub>D</sub> = 1.32 ± 0.35 nM) [41, 42]. Another agonist radioligand, [<sup>125</sup>I]I-AB-MECA (Fig. 1; Table 1), showed better affinities for both rA<sub>3</sub>R (K<sub>D</sub> = 1.48 ± 0.33 nM) and hA<sub>3</sub>R (K<sub>D</sub> = 1.86 ± 0.69 nM) [42, 43], but still bound to rA<sub>1</sub>R in nanomolar range (K<sub>D</sub> = 3.42

$\pm 0.43$  nM) [42]. To tackle the selectivity challenge, Klotz *et al.* developed the tritiated agonist radioligand [ $^3\text{H}$ ]HEMADO (Fig. 1, Table 1) [44], which showed high-affinity ( $K_D = 1.10$  nM) and low non-specific binding (1-2% at  $K_D$  value) to hA<sub>3</sub>R. Even though no binding on the rat rA<sub>3</sub>R was observed, the enhanced selectivity versus other AR subtypes (>300 fold) made [ $^3\text{H}$ ]HEMADO a useful tool for A<sub>3</sub>R binding assays. Subsequent efforts in finding a selective ligand for the rA<sub>3</sub>R resulted in [ $^{125}\text{I}$ ]MRS1898 (Fig. 1; Table 1). It selectively binds to rA<sub>3</sub>R with an improved  $K_D$  value of  $0.17 \pm 0.04$  nM [45]. Still, there are some liabilities caused by the high non-specific binding. The truncation of the 5'-position of the ribose moiety generated the latest A<sub>3</sub>R agonist radioligand [ $^{125}\text{I}$ ]MRS5127 (Fig. 1; Table 1) with a  $K_D$  value of  $5.74 \pm 0.97$  nM [46]. Its major advantage is the low degree of non-specific binding ( $27 \pm 2\%$  at a concentration of 5 nM) and its improved selectivity versus the other AR subtypes. These benefits, together with the uniformity of its agonistic nature across species, may render [ $^{125}\text{I}$ ]MRS5127 the preferred chemical tool for characterizing the A<sub>3</sub>R in its active state over other radioligands reported previously. It is fair to say though that commercially available [ $^{125}\text{I}$ ]I-AB-MECA has emerged as a reference radioligand.

Until now, only two antagonist radioligands, [ $^3\text{H}$ ]MRE-3008-F20 (Fig. 1; Table 1) [47, 48] and [ $^3\text{H}$ ]PSB-11 (Fig. 1; Table 1) [49], have been reported. While both derivatives selectively bind the hA<sub>3</sub>R at (sub)nanomolar concentrations, [ $^3\text{H}$ ]PSB-11 shows a much lower degree of non-specific binding ( $2.5 \pm 0.1\%$  at  $K_D$  value) than [ $^3\text{H}$ ]MRE-3008-F20 (ca. 25% at  $K_D$  value). The shortage of these structurally diverse heterocyclic antagonists is their low affinity for the A<sub>3</sub>R in non-human, particularly rodent tissue.

## Chapter 2

**Table 1. Commonly used AR radioligands for *in vitro* studies**

	Radioligands	K <sub>D</sub> <sup>a</sup> (nM)	Functionality	Refs	Commercially Available
A <sub>1</sub>	[ <sup>3</sup> H]CCPA	0.61	Agonist	[13]	Y
	[ <sup>3</sup> H]LUF5834	2.03	Agonist	[12, 50]	N
	[ <sup>3</sup> H]DPCPX	3.86	Antagonist	[13]	Y
A <sub>2A</sub>	[ <sup>3</sup> H]NECA	20.1	Agonist	[13]	Y
	[ <sup>3</sup> H]CGS21680	22	Agonist	[19]	Y
	[ <sup>3</sup> H]XAC	9.4	Antagonist	[21]	N
	[ <sup>3</sup> H]MSX-2	8.04	Antagonist	[22]	Y
	[ <sup>3</sup> H]ZM241385	0.60	Antagonist	[26]	Y
	[ <sup>3</sup> H]SCH58261	2.3	Antagonist	[28]	Y
A <sub>2B</sub>	[ <sup>3</sup> H]NECA	441	Agonist	[31]	Y
	[ <sup>3</sup> H]DPCPX	40	Antagonist	[33]	Y
	[ <sup>125</sup> I]ABOPX	37	Antagonist	[35]	N
	[ <sup>3</sup> H]MRS1754	1.13	Antagonist	[36]	Y
	[ <sup>3</sup> H]MRE-2029-F20	2.8	Antagonist	[37]	Y
	[ <sup>3</sup> H]OSIP339391	0.17	Antagonist	[39]	N
	[ <sup>3</sup> H]PSB-603	0.403	Antagonist	[40]	N
A <sub>3</sub>	[ <sup>3</sup> H]NECA	6.18	Agonist	[13]	Y
	[ <sup>125</sup> I]APNEA	15.5 (r)	Agonist	[42]	N
	[ <sup>125</sup> I]AB-MECA	1.86	Agonist	[43]	Y
	[ <sup>3</sup> H]HEMADO	1.10	Agonist	[44]	Y
	[ <sup>125</sup> I]MRS1898	0.17 (r)	Agonist	[45]	N
	[ <sup>125</sup> I]MRS5127	5.74	Partial agonist	[46]	N
	[ <sup>3</sup> H]MRE-3008-F20	0.80	Antagonist	[47]	N
	[ <sup>3</sup> H]PSB-11	4.9	Antagonist	[49]	N

<sup>a</sup> The data are K<sub>D</sub>-values for radiolabeled compounds (nM) for the indicated human adenosine receptors unless a different species is indicated (r = rat). n.d. = not detectable

## Molecular Probes for the Human Adenosine Receptors

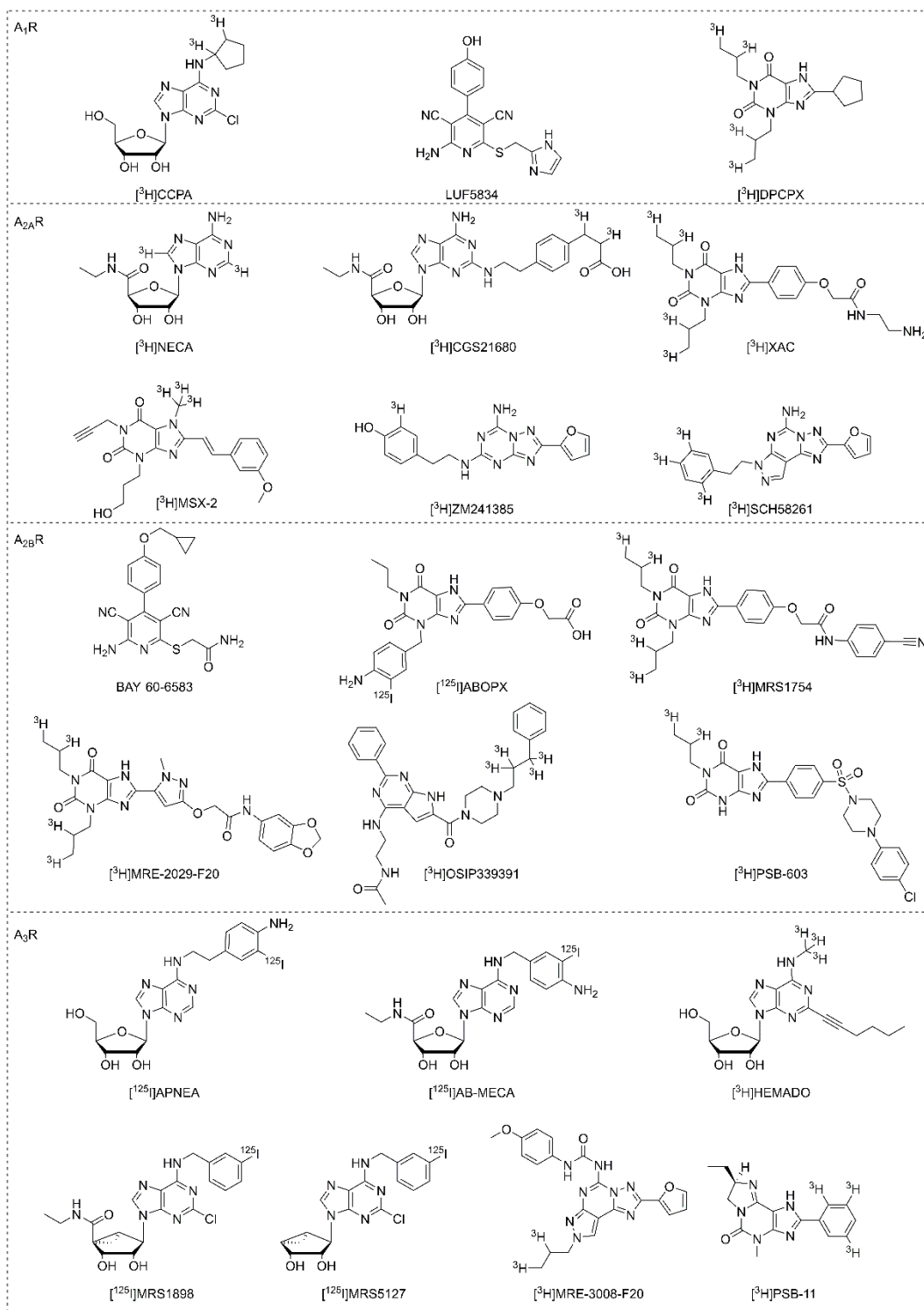


**Fig. 1. Chemical structures of commonly used AR radioligands for *in vitro* studies.** Note: unlabeled version was drawn for radioligands with unknown radioisotope position (i.e. [<sup>3</sup>H]LUF5834 and [<sup>3</sup>H]BAY 60-6583).

### 3. Radioligands for *in vivo* studies –PET/SPECT tracers

While  $\beta$ -emitting ligands serve their purpose in *in vitro* or *ex vivo* experiments, they are not suitable for *in vivo* application. To that end, positron emission tomography (PET) and single-photon emission computed tomography (SPECT) scanning have emerged and are noninvasive quantitative techniques to measure the receptor distribution and function *in vivo*. Over the years an ever-expanding library of [ $^{11}\text{C}$ ]-, [ $^{18}\text{F}$ ]- and [ $^{123}\text{I}$ ]-labelled radiotracers has been developed that enables the determination of receptor binding potentials (BPs) in physiological and pathophysiological studies. Though the decay of these isotopes is much faster than is the case for [ $^3\text{H}$ ]- or [ $^{125}\text{I}$ ]-labeled ligands, the relatively safe  $\gamma$ - and photon-emissions make these tracers suitable for physiological applications. SPECT radioisotopes, such as  $\gamma$ -emitting [ $^{123}\text{I}$ ] ( $t_{1/2} = 13.2$  hours), typically have a much longer half-life than PET tracers labeled with [ $^{11}\text{C}$ ] ( $t_{1/2} = 20.3$  minutes) or [ $^{18}\text{F}$ ] ( $t_{1/2} = 110$  minutes), which allow for longer radiosynthetic protocols and enables SPECT imaging to be conducted for longer time periods. Nonetheless, PET studies of adenosine receptors have been more widely performed due to the higher resolution and sensitivity that can generally be achieved compared to SPECT. In the development of radiotracers for ARs, particularly in the brain and central nervous system, it is desirable to not only optimize for affinity and low non-specific binding capacity, but also for blood–brain barrier permeability. A major challenge is that the short radioligand half-life requires on-site synthesis and rapid purification and validation of the probes. PET and SPECT imaging times, which are also related to radioligand  $t_{1/2}$ , are usually insufficient to allow radioligand–receptor binding to reach an equilibrium; therefore, appropriate kinetic models should be used to correct for this shortcoming. PET imaging of ARs *in vivo*, and the applications thereof in drug discovery have been comprehensively reviewed [51-53]. Here we will focus on the recent applications of clinical PET imaging studies on ARs.

#### 3.1. PET tracers for the adenosine $\text{A}_1$ receptor

Two xanthine derivatives, [ $^{18}\text{F}$ ]CPFPX (Fig. 2, Table 2) and [ $^{11}\text{C}$ ]MPDX (Fig. 2, Table 2), have been extensively employed for the characterization of  $\text{A}_1\text{R}$  in human brain and their results summarized in several reviews [51, 54]. While [ $^{18}\text{F}$ ]CPFPX has a higher affinity for  $\text{A}_1\text{R}$  than [ $^{11}\text{C}$ ]MPDX, the latter has been shown to be much more stable against peripheral metabolism. Using these PET tracers, the cerebral distribution of the  $\text{A}_1\text{R}$  has been successfully visualized and quantified in human brain [55, 56]. From these studies a correlation between  $\text{A}_1\text{R}$  distribution and aging as well as sleep deprivation was established [57, 58]. Additional studies on receptor occupancy using PET tracers, for example

[<sup>18</sup>F]CPFPX in a bolus-plus-constant-infusion PET assay, showed that repeated intake of caffeinated beverages resulted in a 50% occupancy of the cerebral A<sub>1</sub>Rs during the day [59]. This effect might cause adaptive changes and lead to chronic alterations of receptor expression and availability. Furthermore, these PET tracers have been valuable tools for clinical studies on neurodegenerative diseases, revealing the functional mechanisms and pharmacokinetic profiles of new potential drug treatment strategies. In early Parkinson's disease, increased binding of [<sup>11</sup>C]MPDX was found in the temporal lobe, suggesting a compensatory mechanism of A<sub>1</sub>R expression in non-dopaminergic systems in response to the diminished availability of dopamine [60]. With [<sup>18</sup>F]CPFPX a phase-and region-specific change pattern of A<sub>1</sub>R expression in Huntington's disease was detected, providing evidence that adenosinergic targets are involved in the pathophysiology of this disease [61]. More recently, the first partial agonist PET tracer, [<sup>11</sup>C]MMPD (Fig. 2, Table 2), was evaluated in rat brain [62]. It showed suitable blood–brain barrier (BBB) permeability, high specificity and subtype selectivity *in vivo*. This finding may open new routes to visualize receptor occupancy of agonists or partial agonists for the A<sub>1</sub>R in drug development.

### 3.2. PET/SPECT tracers for the adenosine A<sub>2A</sub> receptor

Several radioligands for PET imaging of cerebral A<sub>2A</sub>Rs have been introduced since the 1990s. The initial design of PET tracers for the A<sub>2A</sub>R started from xanthine-based antagonists, leading to the discovery of [<sup>11</sup>C]TMSX (Fig. 2, Table 2), previously abbreviated as [<sup>11</sup>C]KF18446. Though *in vivo* imaging of the human brain in healthy controls and in patients with Parkinson's disease (PD) was relatively successful [63, 64], these xanthine derivatives are prone to photoisomerization, and thus [<sup>11</sup>C]TMSX could only be applied in PET scans under dimmed light. To circumvent this limitation, the first non-xanthine-based PET tracer, [<sup>11</sup>C]SCH442416 (Fig. 2, Table 2), was designed based on a known precursor, SCH58261. An increased binding potential of [<sup>11</sup>C]SCH442416 was observed in the striatum of Parkinson's patients with levodopa-induced dyskinesias (LIDs), providing evidence that A<sub>2A</sub>R is a potential pharmacological target for the management of LIDs [65]. Since the problem of high non-specific binding (and consequential low target-to-non-target ratios) still remains for these ligands [66], Zhou *et al.* incorporated the <sup>11</sup>C-radionuclide into clinical candidate preladenant. PET imaging in rats showed a high uptake of [<sup>11</sup>C]preladenant (Fig. 2, Table 2) in the striatum and low uptake in other regions of the brain, consistent with cerebral A<sub>2A</sub> distribution [67]. Using [<sup>11</sup>C]preladenant in clinical PET-studies, receptor occupancy by istradefylline, an approved A<sub>2A</sub>R antagonist, was measured in patients with Parkinson's disease. It was demonstrated that istradefylline binds to A<sub>2A</sub>R in a dose-dependent manner, consequently

resulting in near-maximal (93.5%) occupancy in the ventral striatum, thus establishing the dosage regimen of such CNS drugs [68]. Subsequently, to extend the half-life of these tracers,  $^{18}\text{F}$ -labeled  $\text{A}_{2\text{A}}$ R antagonist PET tracers have been investigated for human studies. For example, two fluorine-18 labeled SCH442416 analogs, [ $^{18}\text{F}$ ]FESCH (Fig. 2, Table 2) and [ $^{18}\text{F}$ ]FPSCH (Fig. 2, Table 2), were reported as PET tracers used to image the  $\text{A}_{2\text{A}}$ R in rat brain [69]. [ $^{18}\text{F}$ ]FESCH and [ $^{18}\text{F}$ ]FPSCH showed identical striatum-to-cerebellum ratios (4.6 at 37 min and 25 min post injection, respectively), similar to the ratio obtained with [ $^{11}\text{C}$ ]SCH442416. Other examples are preladenant-based ligands, including a SPECT tracer, [ $^{123}\text{I}$ ]MNI-420 (Fig. 2, Table 2) and a PET ligand, [ $^{18}\text{F}$ ]MNI-444 (Fig. 2, Table 2). Both have been successfully applied in  $\text{A}_{2\text{A}}$ R-imaging studies in the human brain [70, 71]. [ $^{123}\text{I}$ ]MNI-420 rapidly entered the human brain and showed the highest specific binding in the striatum, consistent with known  $\text{A}_{2\text{A}}$ R densities. [ $^{18}\text{F}$ ]MNI-444 showed an improved binding potential in the brain compared to [ $^{11}\text{C}$ ]TMSX and [ $^{11}\text{C}$ ]SCH442416, opening up the possibility to more broadly use *in vivo*  $\text{A}_{2\text{A}}$  PET imaging in neuroscience research.

### 3.3. PET tracers for the adenosine $\text{A}_{2\text{B}}$ receptor

So far only two radioligands for use in *in vivo* studies have been developed for  $\text{A}_{2\text{B}}$ R, namely 1- $^{11}\text{C}$ -4 (Fig. 2, Table 2) and - $^{18}\text{F}$ -7a (Fig. 2, Table 2) [72] [73]. The first compound, featuring a triazinobenzimidazole scaffold with moderate potency ( $\text{IC}_{50} = 210.2 \pm 12.3$  nM) toward  $\text{A}_{2\text{B}}$ R, has been applied in PET studies in rats and showed the highest uptake in brown adipose tissue, lungs and testes [72]. With a high chemical stability and good pharmacokinetic profile, this tool compound represented a good lead for the development of  $\text{A}_{2\text{B}}$ R radiotracers. The second  $\text{A}_{2\text{B}}$ R PET tracer was developed on a pyrazine-based antagonist with the potential to penetrate the blood-brain barrier [73]. Despite poor selectivity ( $\text{A}_{2\text{A}}/\text{A}_{2\text{B}}=13$ ,  $\text{A}_1/\text{A}_{2\text{B}}=5$ ) this radiolabeled ligand was further evaluated for its *in vivo* pharmacokinetic profile, revealing the formation of a radio-metabolite capable of penetrating the blood-brain barrier. With these PET studies the stage is set for further  $\text{A}_{2\text{B}}$ R probe design to enhance the selectivity and metabolic stability.

### 3.4. PET tracers for the adenosine $\text{A}_3$ receptor

The first PET tracer for  $\text{A}_3$ R was developed by radiofluorination FE@SUPPY (Fig. 2, Table 2), a selective and potent antagonist for h $\text{A}_3$ R [74, 75]. Though it had already been shown for the parent compound that the affinity for rat  $\text{A}_3$ R was 140 fold lower than for human  $\text{A}_3$ R, [ $^{18}\text{F}$ ]FE@SUPPY was studied for its biodistribution in rats and specific binding in the rat brain was demonstrated using autoradiography [76]. A further preclinical PET study using



[<sup>18</sup>F]FE@SUPPY to image A<sub>3</sub>R revealed a pronounced uptake in xenografted mice injected with cells overexpressing human A<sub>3</sub>R. This “humanized animal model” inspired to evaluate [<sup>18</sup>F]FE@SUPPY in mice xenografted with a human colorectal cancer cell line (HT-29) overexpressing A<sub>3</sub>R as a tumor marker. Unfortunately, this study to visualize the A<sub>3</sub>R *in vivo* was unsuccessful, presumably due to insufficient uptake of [<sup>18</sup>F]FE@SUPPY in the tumors, poor conservation of target expression in xenografts or unfavorable pharmacokinetics of the tracer in mice [77]. In analogy to this, [<sup>18</sup>F]FE@SUPPY:2 (Fig. 2, Table 2) was developed by transforming the fluoroethylester into a fluoroethylthioester [78]. While a higher specific radioactivity was obtained ([<sup>18</sup>F]FE@SUPPY:2 = 340 ± 140 GBq/mol and [<sup>18</sup>F]FE@SUPPY = 70 ± 26 GBq/mol), the uptake pattern for the two PET tracers is distinct. Especially brain to blood ratios are remarkably increased over time for [<sup>18</sup>F]FE@SUPPY whereas those for [<sup>18</sup>F]FE@SUPPY:2 stayed unaltered. Lastly, a pair of structurally similar ligands (i.e. agonist MRS3581 and antagonist MRS5147) were reported as [<sup>76</sup>Br]-labeled potential PET radiotracers [79]. Both ligands showed similar biodistribution in rats: primarily uptake in the organs of metabolism and excretion. However, the uptake of agonist [<sup>76</sup>Br]MRS3581 (Fig. 2, Table 2) was an order of magnitude faster than that of antagonist [<sup>76</sup>Br]MRS5147 (Fig. 2, Table 2), possibly due to the presence of a uronamide group in the agonist to influence its bioavailability and permeation *in vivo*. In contrast, the antagonist [<sup>76</sup>Br]MRS5147 demonstrated an increased uptake in rat testes, an A<sub>3</sub>R-rich tissue, suggesting that the antagonist may also serve as a viable diagnostic molecular probe for pathological conditions with increased A<sub>3</sub>R expression.

## Chapter 2

**Table 2 Recent AR radioligands used for clinical PET or SPECT imaging**

Radioligands	$K_D$ (nM) <sup>a</sup>				Functionality	Ref
	A <sub>1</sub>	A <sub>2A</sub>	A <sub>2B</sub>	A <sub>3</sub>		
A <sub>1</sub>						
[ <sup>18</sup> F]CPFPX	1.26	940	N.D.	N.D.	Antagonist	[51]
[ <sup>11</sup> C]MPDX	4.2 (r)	>100 (r)	N.D.	N.D.	Antagonist	[51]
[ <sup>11</sup> C]MMPD	0.5	71	75	42 % (1 μM)	Partial Agonist	[62]
A <sub>2A</sub>						
[ <sup>11</sup> C]TMSX or [ <sup>11</sup> C]KF18446	1600 (r)	5.9 (r)	N.D.	N.D.	Antagonist	[80]
[ <sup>11</sup> C]SCH442416	1.11	0.05	>10,000	>10,000	Antagonist	[81]
[ <sup>11</sup> C]preladenant	>1000	1.1	>1700	>1000	Antagonist	[82]
[ <sup>18</sup> F]FESCH	42.7% (10 μM)	12.4	N.D.	59.6% (10 μM)	Antagonist	[83]
[ <sup>18</sup> F]FPSCH	1000	53.6	N.D.	1320	Antagonist	[84]
[ <sup>18</sup> F]MNI-444	N.D.	2.8	N.D.	N.D.	Antagonist	[85]
[ <sup>123</sup> I]MNI-420	N.D.	2.0	N.D.	N.D.	Antagonist	[85]
A <sub>2B</sub>						
[ <sup>11</sup> C]”4”	230.3	548.0	210.2	N.A.	Antagonist	[72]
[ <sup>18</sup> F]”7a”	19.0	55.0	4.24	796	Antagonist	[73]
A <sub>3</sub>						
[ <sup>18</sup> F]FE@SUPPY	4030	1720	N.D.	6.02	Antagonist	[77]
[ <sup>76</sup> Br]MRS3581	N.D.	N.D.	N.D.	0.63	Agonist	[79]
[ <sup>76</sup> Br]MRS5147	N.D.	N.D.	N.D.	0.62	Antagonist	[79]

<sup>a</sup> The data are  $K_D$ -values of radiolabeled compounds for human adenosine receptors unless otherwise indicated (r= rat) or % inhibition at the indicated concentration in bracket. N.D. = not determined, N.A. = not active

## Molecular Probes for the Human Adenosine Receptors

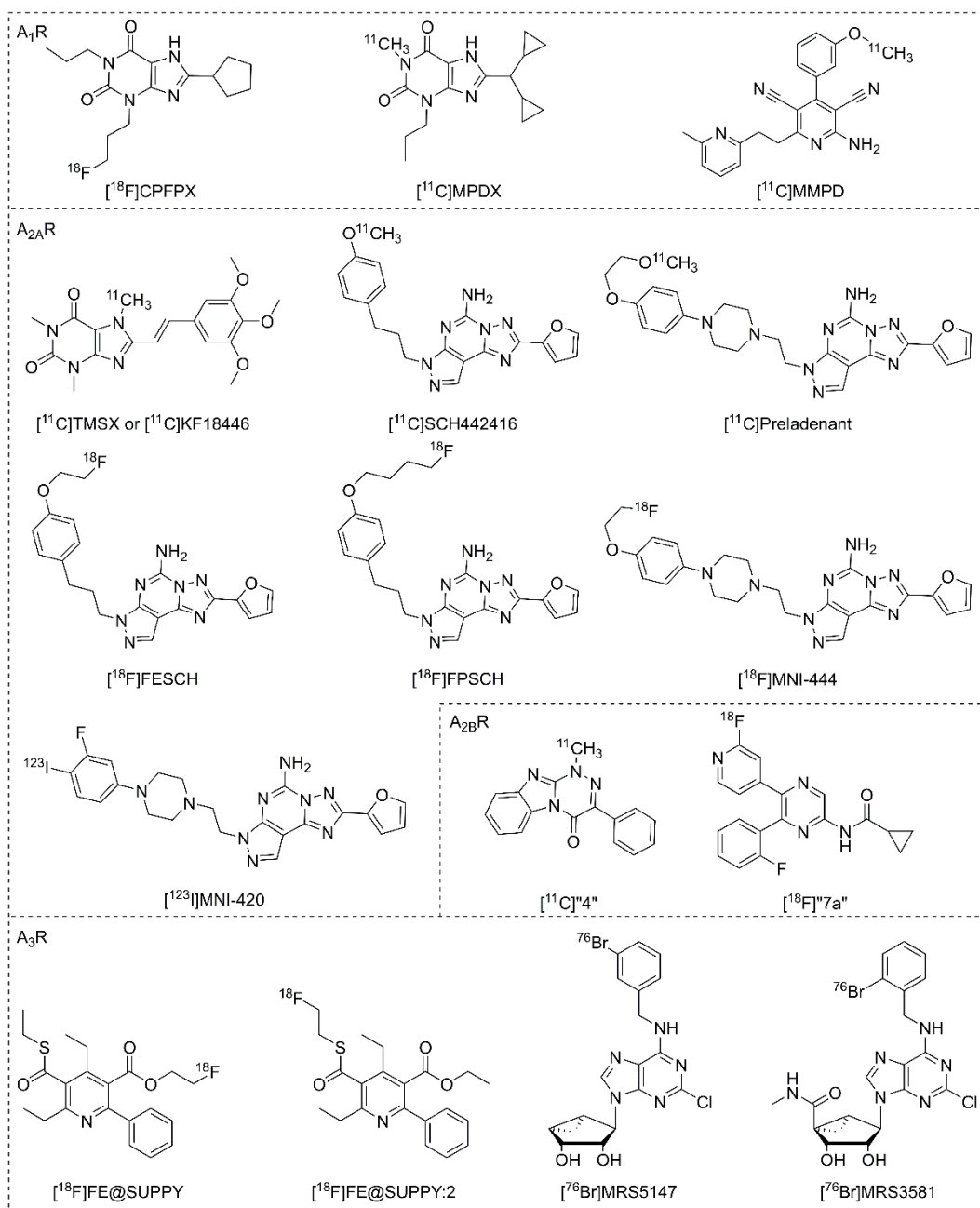


Fig. 2 Chemical structures of AR radioligand tracers for *in vivo* studies

### 4. Fluorescent probes

As an alternative to radiolabeled molecular probes, fluorescent ligands have also been included into the pharmacological toolbox. This approach avoids the safety concerns associated with the disposal of radioisotopes and also provides the opportunity of a “real-time” readout of the ligand-receptor interaction. Fluorescent ligands for GPCRs are usually designed by incorporating a relatively small organic fluorophore, such as a BODIPY-, Alexa Fluor-, rhodamine-, or NBD (nitrobenzoxadiazole) moiety into an existing GPCR agonist or antagonist pharmacophore via a linker. The use of these fluorescent probes can provide more insight in receptor localization, function and regulation, but also on ligand-target binding kinetics, thus contributing to a detailed understanding of receptor physiology and pathophysiology. In addition, the development of newer fluorescent methods and techniques, such as scanning confocal microscopy (SCM), fluorescence polarization (FP), fluorescence correlation spectroscopy (FCS), resonance energy transfer (FRET or BRET) and flow cytometry (FCM), are boosting the potential use of fluorescent probes in drug discovery. The development of fluorescent ligands to characterize adenosine receptors has been the subject of intense investigation, which has been summarized in detail by Kozma *et al.* in 2013 [86]. Here we will therefore summarize and review emerging fluorescent ligands for more recent applications on ARs.

#### 4.1. Fluorescent ligands for the adenosine A<sub>1</sub> receptor

To monitor ligand binding to receptors on the surface of living cells, a Nano-luciferase (NanoLuc) BRET methodology (NanoBRET) has recently been established [87-89]. This approach was also applied to a study of allosteric modulators in intact living cells using fluorescent A<sub>1</sub>R agonists, such as the adenosine-based agonist, ABA-X-BY630 (Fig. 3, Table 5), and two NECA-based ligands, ABEA-X-BY630 (Fig. 3, Table 5) and BY630-X-(D)-A-(D)-A-G-ABEA (Fig. 3, Table 5) [90]. The two positive allosteric modulators tested were shown to increase the specific binding of the fluorescent A<sub>1</sub>R agonists, indicative for a switch of the A<sub>1</sub>R population to a more active receptor conformation.

#### 4.2. Fluorescent ligands for the adenosine A<sub>2A</sub> receptor

MRS5424 (Fig. 3, Table 5) is a fluorescent adduct of agonist APEC with Alexa Fluor 532. Using this probe, allosteric modulation within A<sub>2A</sub>R/D<sub>2</sub>R heterodimers was followed using real-time FRET [91]. A negative allosteric effect on A<sub>2A</sub>R ligand binding and receptor activation was found when the D<sub>2</sub>R agonist quinpirole was added. This heterodimer interaction was further validated in a higher-throughput flow cytometry-based assay with the

fluorescent agonist MRS5206 (APEC-Alexa Fluor 488) (Fig. 3, Table 5) [92]. These experiments provided evidence for a differential D<sub>2</sub>R-mediated negative allosteric modulation of A<sub>2A</sub>R agonist binding, in particular for apomorphine, a drug used in the treatment of PD. Recently, using a fluorescence polarization assay, McNeely *et al.* employed a fluorescent agonist, FITC-APEC (Fig. 3, Table 5), to characterize the binding kinetics of three hA<sub>2A</sub>R ligands [93, 94]. The kinetic parameters of these unlabeled ligands, computed using a numerical solution approach, showed good consistency with those determined in a conventional radioligand binding assay.

Endeavors to enhance selectivity towards hA<sub>2A</sub>R and improve the physicochemical properties of fluorescent ligands led to the discovery of MRS7416 (Fig. 3, Table 5), which is based on the antagonist SCH442416 [95]. As a fluorescent tracer, MRS7416 displayed low nonspecific binding at hA<sub>2A</sub>R in flow cytometry experiments. From molecular docking studies the researchers suggested that the fluorescent AlexaFluor488 moiety present in MRS7416 is binding to the hydrophilic extracellular loops of the receptor. This would make the probe essentially ‘bitopic’, i.e. bridging two separate domains of the hA<sub>2A</sub>R.

### 4.3. Fluorescent ligands for the adenosine A<sub>2B</sub> receptor

The first selective A<sub>2B</sub> fluorescent ligand reported, PSB-12105 (Fig. 3, Table 5), was synthesized by integrating a BODIPY moiety into the pharmacophore of 8-substituted xanthine derivatives [96]. Besides fluorescently labeling CHO cells expressing recombinant human A<sub>2B</sub>R, this ligand was used to establish an A<sub>2B</sub>R binding assay on living cells in a flow cytometry set-up. Barresi *et al.* reported on another series of (non-selective) fluorescent antagonists for labeling A<sub>1</sub>R and A<sub>2B</sub>R [97]. In one of the ligands a fluorescent group, 7-nitrobenzofurazan group (NBD) (Fig. 3, Table 5), was linked to a triazinobenzimidazole scaffold. This fluorescent antagonist showed a clear labeling of bone marrow-derived mesenchymal stem cell membranes, which was largely prevented by pre-incubation with selective agonists for A<sub>1</sub>R and A<sub>2B</sub>R. These findings provide an important basis for the design of novel fluorescent ligands to monitor the expression and localization of A<sub>2B</sub>R in living cells.

### 4.4. Fluorescent ligands for the adenosine A<sub>3</sub> receptor

The non-selective A<sub>1</sub>R/A<sub>3</sub>R antagonist, CA200645, was employed as a tool compound to develop a robust competition binding assay to e.g., screen for new chemical templates and fragments for A<sub>3</sub>R at a live cell high content screening system [87, 88]. Besides, CA200645 was also applied to study the A<sub>3</sub>R localization on intact human neutrophils. It appeared that A<sub>3</sub>R activation induces the formation of filipodia-like extensions and bacterial phagocytosis

## Chapter 2

[98]. Modification of the linker component in CA200645 by the insertion of a dipeptide yielded two  $A_3$ -selective fluorescent ligands, BODIPY 630/650-X-Tyr-Ser-XAC (Fig. 3, Table 5) and BODIPY FL-X-Tyr-Ser-XAC (Fig. 3, Table 5) [99]. Both ligands showed displaceable membrane binding with little non-specific binding in a fluorescent confocal microscopy set-up.

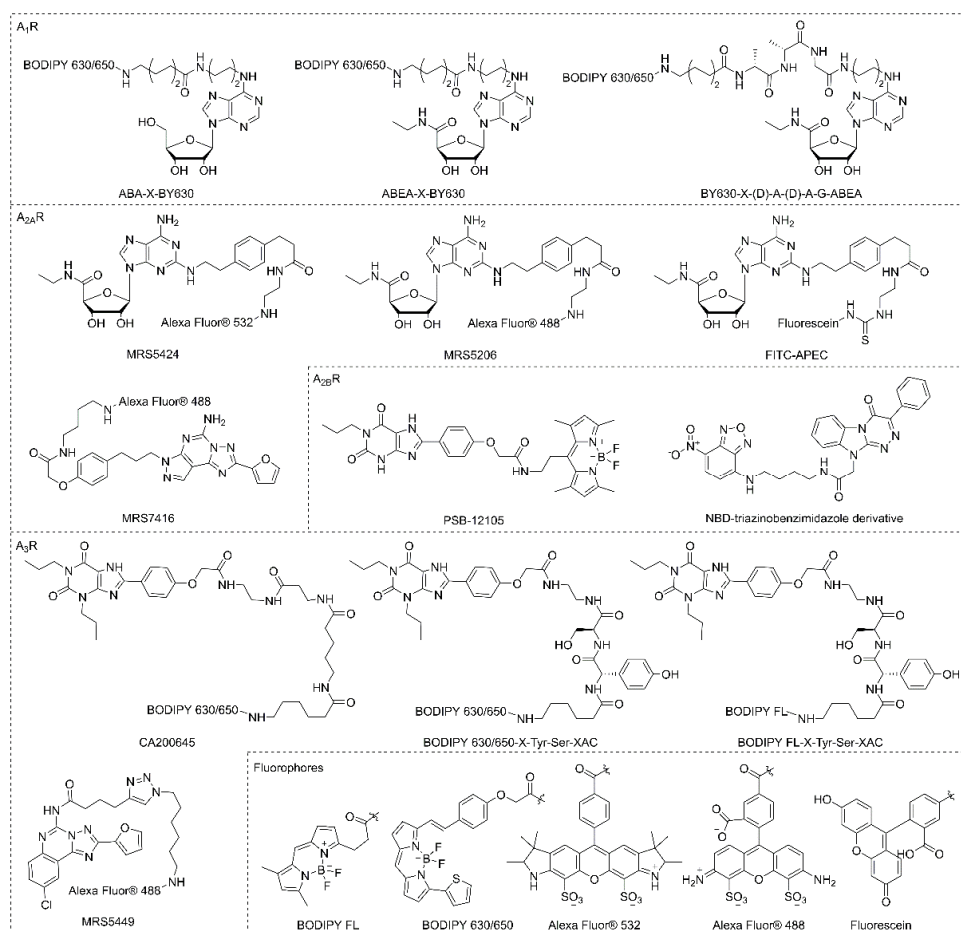


**Fig. 3** Chemical structures of recent fluorescent tools for ARs

A similar strategy to incorporate a (three amino acid) peptide linker was applied to an existing non-selective adenosine-based fluorescent agonist, ABEA-X-BY630, yielding the highly potent fluorescent agonist BY630-X-(D)-Ala-(D)-Ala-Gly-ABEA at  $A_3$ R [100]. This probe was used to visualize the internalization of YFP-tagged as well as untagged receptors, and appeared to promote the formation of intracellular receptor-arrestin3 complexes. In addition, click chemistry serves as a versatile approach to simplify compound synthesis, as it provides the means for facile incorporation of fluorescent tags. CGS15943, a triazolo-quinazoline antagonist scaffold, was extended with an alkyne moiety to be click-conjugated with Alexa Fluor-488, yielding a selective  $A_3$ R fluorescent probe, MRS5449 (Fig. 3, Table 5) [101]. In

flow cytometry this molecular probe was used to quantify hA<sub>3</sub>R and to perform ligand screening in intact cells.

**Table 3 Recent AR fluorescent ligands**

Ligands	pK <sub>D</sub> <sup>a</sup>				Functionality	Ref
	A <sub>1</sub>	A <sub>2A</sub>	A <sub>2B</sub>	A <sub>3</sub>		
<b>A<sub>1</sub></b>						
CA200645	7.47 ± 0.34	N.D.	N.D.	8.21 ± 0.12	Antagonist	[87, 89]
ABA-X-BY630	6.23 ± 0.05	N.D.	N.D.	N.D.	Agonist	[90]
ABEA-X-BY630	5.99 ± 0.15	N.D.	N.D.	N.D.	Agonist	[90]
BY630-X-AAG-ABEA	6.17 ± 0.16	N.D.	N.D.	N.D.	Agonist	[90]
<b>A<sub>2A</sub></b>						
FITC-APEC	N.D.	57 <sup>c</sup>	N.D.	N.D.	Agonist	[93, 94]
MRS7416	1680 <sup>b</sup>	30.3 <sup>b</sup>	N.D.	32 ± 3% <sup>b</sup> (10 μM)	Antagonist	[95]
<b>A<sub>2B</sub></b>						
PSB-12105	≥10 000 <sup>b</sup>	>10 000 <sup>b</sup>	1.83 <sup>b</sup>	>10 000 <sup>b</sup>	Antagonist	[96]
NBD-derivative	1380 <sup>b</sup>	>10 000 <sup>b</sup>	20.7 ± 7.5 % <sup>c</sup>	>10 000 <sup>b</sup>	Antagonist	[97]
<b>A<sub>3</sub></b>						
BODIPY 630/650-X-Tyr-Ser-XAC	7.62 ± 0.13 <sup>d</sup>	N.D.	N.D.	9.12 ± 0.05	Antagonist	[99]
BODIPY FL-X-Tyr-Ser-XAC	6.50 ± 0.04 <sup>d</sup>	N.D.	N.D.	7.96 ± 0.09	Antagonist	[99]
MRS5449	87.0 <sup>b</sup>	73.0 <sup>b</sup>	N.D.	6.4 <sup>b</sup>	Antagonist	[101]

<sup>a</sup> The data are pK<sub>D</sub>-values for compounds for the indicated human adenosine receptors. N.D. = not determined

<sup>a</sup> K<sub>D</sub>-value at the bovine adenosine A<sub>2A</sub> receptor

<sup>b</sup> Data are K<sub>i</sub>-values of compounds (nM) for the indicated human adenosine receptors or % displacement at the indicated concentration in brackets.

<sup>c</sup> cAMP production in CHO cells expressing human A<sub>2B</sub>R at the concentration of 10 nM compound in the presence of 100 nM of NECA. Data are expressed as percentage of cAMP production versus agonist maximal effect (100%).

<sup>d</sup> Data are pK<sub>i</sub>-values for human A<sub>1</sub>R from radioligand binding assay.

### 5. Covalent ligands

Another class of molecular probes is formed by covalent ligands. The term covalent here refers to the ability of these compounds to bind the receptor irreversibly by forming a covalent bond to a specific amino acid residue located at or near the ligand binding site [102]. Some different considerations can be made depending on the type of covalent interaction induced. Generally, high affinity and selectivity for the target receptor will increase receptor occupancy

and decrease non-specific or off-target binding, thus improving specific covalent labeling [103]. Two types of covalent ligands have been developed until now: electrophilic and photoreactive ligands. Choosing the correct functional group (or warhead) that can react with the amino acid residues present in the binding site is essential for successful molecular probe design. Photoreactive ligands possess a light-sensitive group, such as aryl azide, diazirine or benzophenone, which can be irradiated with light of a specific wavelength to yield highly reactive nitrene, carbene or benzophenone-derived diradicals. These reactive species can subsequently form a covalent bond with a neighboring amino acid residue through a variety of insertion reactions [104]. Photoreactive ligands, occasionally combined with mass spectrometry, have been applied in GPCR research to determine the binding site of ligands and to identify the partner-receptor for orphan ligands [105]. When combined with a radioactive label, photoaffinity probes emerge, which can be used to study GPCR localization using autoradiography [106]. Electrophilic ligands on the other hand possess a reactive electrophile as a warhead, such as (iso)thiocyanate, sulfonyl fluoride or a Michael acceptor like acrylamide. These electrophiles react with nucleophilic amino acid residues such as lysine, serine and cysteine near the binding site of the ligand. When combined with *in silico* modeling and site-directed mutagenesis studies, these chemo-reactive ligands often enable characterization of the GPCR-ligand binding site. Additionally, electrophilic covalent ligands have been applied to study receptor reserve, turnover and subtype discrimination [107, 108]. Lastly, binding of a covalent ligand stabilizes the receptor into an active or inactive conformation, which in turn facilitates crystallization of the receptor-ligand complex. This aids in crystallization studies using X-ray or cryoEM, providing valuable insights into the structure and function of GPCRs [109]. A prime example of this is the case of the human adenosine A<sub>1</sub> receptor which was recently co-crystallized with covalent antagonist DU172 [3]. There are numerous reported covalent ligands for adenosine receptors that have in some way contributed to the characterization of these receptors and their ligand binding sites. These ligands will be summarized below and their applications will be discussed.

### 5.1. Covalent ligands for the adenosine A<sub>1</sub> receptor

Arguably the first example of photoaffinity labeling of an adenosine receptor dates back to 1985 when N<sup>6</sup>-2-(4-aminophenyl)ethyladenosine (APNEA), a nonselective adenosine-based agonist with high affinity for both A<sub>1</sub>R and A<sub>3</sub>R, was coupled to the A<sub>1</sub>R [110]. In an attempt to characterize the A<sub>1</sub>R structure, radioiodinated [<sup>125</sup>I]APNEA (Fig. 4, Table 4) was incubated with A<sub>1</sub>R and reacted with crosslinking reagent *N*-hydroxysuccinimidyl 6-(4-Azido-2-nitrophenylamino)hexanoate (SANPAH) *in situ*. Subsequent UV-irradiation resulted in a 38



kDa protein being covalently labeled with the radioligand in rat cerebral cortex and adipocyte membranes. Since this process was completely blocked by co-incubating with a selective A<sub>1</sub>R agonist, this protein was designated as A<sub>1</sub>R. Strictly speaking, this radioactive ligand is obviously not inherently photo-reactive and thus not a photoaffinity probe *per se*. Interestingly, in the same year efforts to develop an inherently photoreactive ligand based on the *R*-PIA scaffold, one of the most selective A<sub>1</sub>R agonists, were successful. A photoactivatable azido group was positioned at the purine core structure, generating the photolabile ligand *R*-AHPIA (Fig. 4, Table 4) [111]. It exhibited similar affinity ( $K_i = 1.5$  nM) and efficacy ( $EC_{50} = 35$  nM) as its parent compound, *R*-PIA, but after photoactivation it showed irreversible inhibition of approximately 40% of the receptor binding sites. Such covalent labeling of A<sub>1</sub>R led to a concentration-dependent reduction of cellular cAMP levels, consistent with activation of rA<sub>1</sub>R and correlating with receptor occupancy [112]. Similar to the case of APNEA, when *R*-AHPIA was radioiodinated to yield [<sup>125</sup>I]AHPIA (Fig. 4, Table 4), SDS-PAGE analysis of rat brain membranes that were incubated with this covalent radioligand and UV-irradiated, showed the appearance of a single protein band of ~35 kDa [111]. Interestingly, even though *R*-AHPIA is about 60-fold selective for the A<sub>1</sub>R, it is also a partial agonist at the A<sub>2A</sub>R, and pretreatment with *R*-AHPIA reduced the stimulatory effect of NECA, indicating persistent binding of the ligand and subsequent reduced activation by a full agonist. [113]. In the search for covalent antagonists, 4-azidophenethyl xanthine derivative [<sup>125</sup>I]BW-A947U (Fig. 4) was synthesized and optimization (analogous to the development of selective A<sub>1</sub>R antagonist DPCPX) gave the next photoactivatable antagonist, [<sup>125</sup>I]azido-BW-A844U (Fig. 4, Table 4) [114-116]. Both ligands are xanthine-based antagonists that have a light-sensitive aryl azide located on the xanthine 3-position. Photoaffinity labeling of partially purified receptor with [<sup>125</sup>I]azido-BW-A844U followed by chemical or enzymatic fragmentation experiments demonstrated that the covalently modified amino acids were located at transmembrane domain III of the A<sub>1</sub>R. This approach provided clear insight into the amino acids surrounding the binding pocket of the A<sub>1</sub>R and thus aided in the development of three-dimensional models of the receptor.

Initial attempts in the development of chemo-reactive agonist ligands for the A<sub>1</sub>R were focused on functionalizing the adenosine scaffold with isothiocyanates or sulfonyl fluorides to serve as warheads [117, 118]. In the first reported case, *p*- and *m*-DITC-ADAC (Fig. 4, Table 4), both adenosine derivatives with nanomolar affinity substituted on the N<sup>6</sup>-position with an isothiocyanate-bearing linker, were synthesized and tested on the A<sub>1</sub>R [119]. At nanomolar

## Chapter 2

concentration both ligands irreversibly occupied approx. half of the A<sub>1</sub>R binding sites. In a functional cAMP accumulation assay both agonists elicited a sustained, antagonist-insensitive, A<sub>1</sub>R-mediated response. Since the incorporation of a warhead via the N<sup>6</sup>-position of the adenosine scaffold was well tolerated and showed no negative effect on the ligands' affinities, a series of adenosine derivatives bearing diverse linker types and warheads were synthesized and examined. Two promising compounds, isothiocyanate **15b** and sulfonyl fluoride **15d** (Fig. 4, Table 4), were validated as irreversible agonists promoting persistent A<sub>1</sub>R-mediated guanine nucleotide exchange activity in a manner resistant to both agonist and antagonist addition [118]. Furthermore, these two ligands demonstrated their capacity to thermo-stabilize purified, detergent-solubilized A<sub>1</sub>R in a ThermoFluor assay to a significantly higher degree than the high affinity agonist NECA could. These thermostabilized receptors with covalently bound ligands allowed purification of the receptor in a monodisperse state, which greatly facilitated structure determination by X-ray crystallography [118].

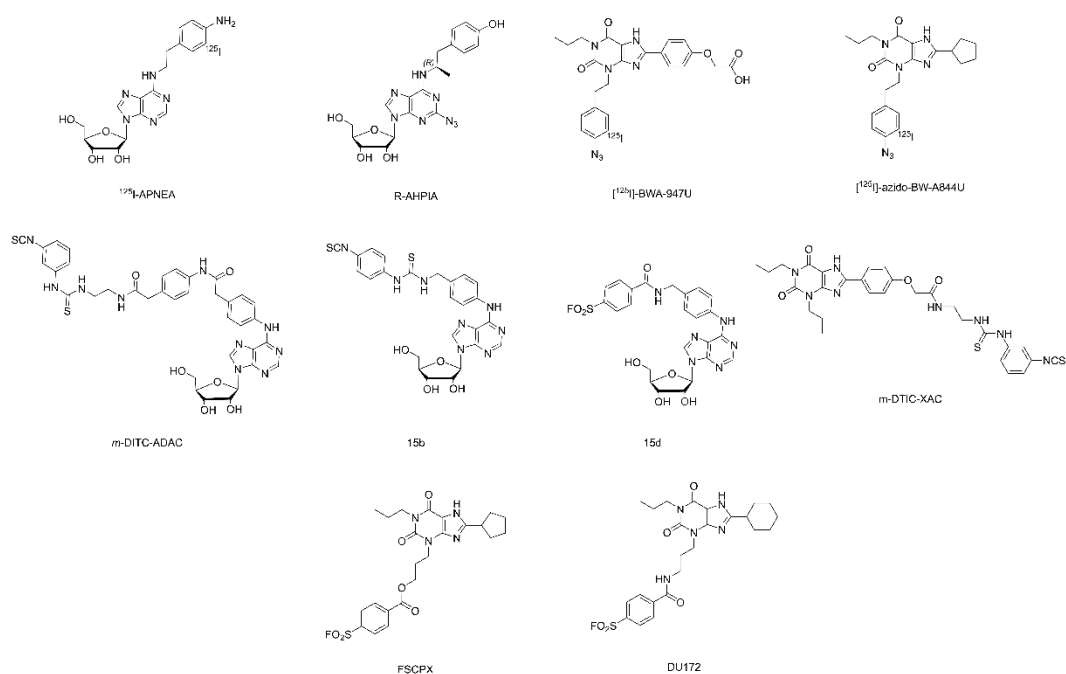


**Fig. 4 Chemical structures of covalent ligands for A<sub>1</sub>R**

With respect to chemo-reactive antagonists two approaches have been explored, both starting from the xanthine scaffold. The first class comprises the 8-substituted 1, 3-dipropylxanthines [117]. One such compound is *m*-DITC-XAC (Fig. 4, Table 4), an isothiocyanate derivative of the relatively non-selective AR antagonist XAC. It was found to be a potent A<sub>1</sub>R antagonist in rat brain ( $K_i = 2.39 \pm 0.35$  nM), and was used to study the receptor reserve in guinea pig atrioventricular nodes [120]. In the second approach the electrophilic fluorosulfonyl group

was placed on the 3-position of the xanthine core, as was done in covalent tool FSCPX (Fig. 4, Table 4) [121]. This compound had a good affinity for the A<sub>1</sub>R (IC<sub>50</sub> = 10 ± 3 nM) and treatment with 10 or 50 nM FSCPX led to reductions in the available A<sub>1</sub>R binding sites of 60% and 74%, respectively. In a follow-up study it demonstrated that FSCPX irreversibly antagonized cardiac A<sub>1</sub>R-mediated responses. Subsequently it was shown that FSCPX was unable to significantly decrease the maximal direct inotropic response to four A<sub>1</sub>R full agonists (NECA, CPA, CHA and adenosine) in guinea pig atria, which demonstrated a considerable A<sub>1</sub>R reserve for direct negative inotropy [122]. In *in vivo* experiments, FSCPX was used successfully as a “receptor knock-down” tool when IV-infusion of FSCPX in conscious rats attenuated CPA-mediated bradycardia [123]. As the ester bond present near the warhead of FSCPX is prone to hydrolysis, a follow-up structural modification was performed with a focus on linker types [124, 125]. This resulted in a closely related analog with improved stability, DU172 (Fig. 4, Table 4). The affinity of DU172 (IC<sub>50</sub> = 24.9 ± 7.6 nM) was in line with that of FSCPX and pretreatment of DDT<sub>1</sub> MF2 cells with DU172 resulted in a concentration-dependent decrease in the A<sub>1</sub>R binding sites, indicating that it behaved as an irreversible ligand indeed. This covalent ligand-receptor interaction has been the basis for the structure elucidation of A<sub>1</sub>R due to improved receptor stability [3].

### 5.2. Covalent ligands for the adenosine A<sub>2A</sub> receptor

For the A<sub>2A</sub>R initial characterization of the receptor was aided by a radio-iodinated analog of APEC, a prototypical ribose-based selective A<sub>2A</sub>R agonist. Similar to the initial A<sub>1</sub>R studies, [<sup>125</sup>I]PAPA-APEC (Fig. 5, Table 4) was cross-linked to the A<sub>2A</sub>R in bovine striatal membranes using SANPAH and was shown to covalently label a 45-kDa protein [126, 127]. Both NECA and R-PIA were able to prevent the covalent labeling of the 45-kDa protein by [<sup>125</sup>I]PAPA-APEC, providing evidence that this protein is the A<sub>2A</sub>R indeed. Subsequently, the photoactivatable azido analog [<sup>125</sup>I]azido-PAPA-APEC (Fig. 5, Table 4) was developed and was used to directly label the same 45-kDa protein in bovine striatal membranes with 3-fold greater efficiency of photo-incorporation [128]. A further characterization of the binding domain was performed by Piersen *et al.*, who performed photoaffinity labeling of the canine A<sub>2A</sub>R overexpressed in COS M6 cells with [<sup>125</sup>I]azido-PAPA-APEC and tracked the cross-linked transmembrane domain V [129]. However, no individual amino acid residues responsible for the covalent interaction were identified. These studies were later repeated with a novel adenosine-based radioligand [<sup>125</sup>I]APE, which showed less hydrophobic interactions than [<sup>125</sup>I]PAPA-APEC and had higher specific radioactivity than [<sup>3</sup>H]CGS21680 [130]. Its azido analog, [<sup>125</sup>I]AzPE (Fig. 5, Table 4), showed saturable, high-affinity binding in rabbit

## Chapter 2

striatal membranes ( $K_D = 1.7 \pm 0.5$  nM), and photolabeling identified a protein of 45 kDa that displayed the appropriate pharmacology of the  $A_{2A}R$ . More recently, photoaffinity labeling is often combined with mass spectrometry analysis to map detailed ligand-receptor binding sites. Muranaka *et al.* incorporated the trifluoromethyl diazirine group into a not-so- $A_{2A}R$ -selective SCH58261 analogue to give photoaffinity ligand NUMBER 9 (Fig. 5, Table 4) [131-133]. When purified h $A_{2A}R$  was photolabeled with this ligand and subjected to protease digestion, cross-link positions were identified with LC-MS/MS. The most likely amino acid candidate for this ligand was Y271<sup>7,36</sup> in transmembrane domain VII. This is the first reported case in which the cross-linked amino acid was elucidated by mass spectrometry, which demonstrates the power of combining mass spectrometry-based proteomics and covalent labeling in the elucidation and characterization of GPCR ligand binding sites.

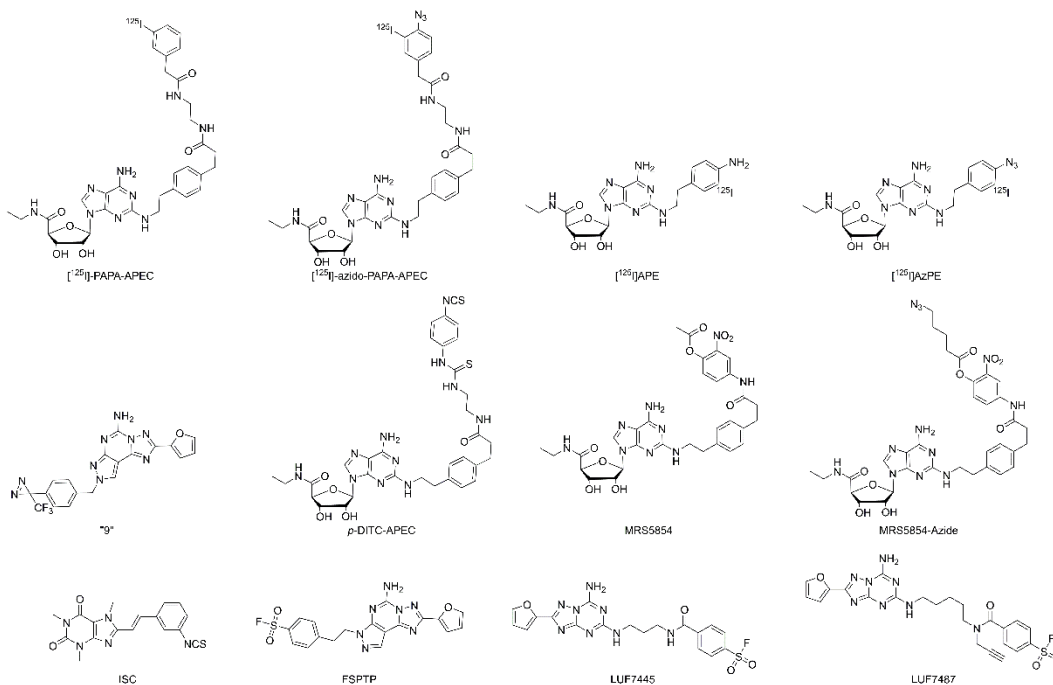


**Fig. 5** Chemical structures of covalent ligands for  $A_{2A}R$

Analogous to the photo-reactive ligands, APEC also served as a parent ligand for the initial design of chemo-reactive ligands for  $A_{2A}R$ . One exemplary compound is *p*-DITC-APEC (Fig. 5, Table 4), which has a reactive 4-isothiocyanatophenyl residue attached to the C-2 substituent of the purine ring [127]. It had good affinity ( $K_i = 7.1 \pm 2.3$  nM at bovine  $A_{2A}R$ ) [127] and, at a concentration of 100 nM, irreversibly blocked 77% of [<sup>3</sup>H]CGS21680 binding in rabbit striatal membranes [134]. In isolated, perfused guinea pig hearts treatment with *p*-DITC-APEC caused a prolonged, persistent, and concentration-dependent coronary vasodilatation, which is evidence of an irreversible activation of  $A_{2A}R$  [135]. More recently,

an APEC-analogue bearing an active 2-nitrophenyl ester was synthesized (MRS5854, Fig. 5, Table 4). This ligand was designed to bind to the receptor irreversibly and subsequently transfer its terminal acyl group to a nucleophilic amino acid residue on extracellular loop 2 (ECL2) of the A<sub>2A</sub>R [136]. This acyl transfer would prevent the ECL2-lysine-mediated recognition of ligands, effectively blocking the receptor. Preincubation of hA<sub>2A</sub>R with MRS5854 followed by extensive washing indeed showed near-complete inhibition of radioligand binding. When ECL2-lysine K153 was mutated to an alanine residue, a partial restoration of B<sub>max</sub> was observed after treatment with MRS5854, confirming that K153 is the anchor point for the covalent interaction. Interestingly, the K<sub>D</sub> for the radioligand used ([<sup>3</sup>H]ZM241385) was not significantly influenced by this mutation, indicating that the targeted lysine residue is not important for ligand binding and that acyl transfer seems to prevent binding by blocking entry to the binding pocket instead of preventing the recognition of ligands. In parallel, the active acyl was replaced by an azido-pentanoate group to generate MRS5854-azide. Though this ligand showed diminished affinity towards the A<sub>2A</sub>R, it nevertheless showed a slight reduction in B<sub>max</sub>, suggesting that at least part of the receptors were covalently labeled with the azido-pentanoate. This azido-group could allow for click-ligation to functionalized alkynes; however, biologic data has not yet been reported.

Three approaches have been taken to develop electrophilic covalent probes for the A<sub>2A</sub>R. The first example is ISC (Fig. 5, Table 4), an isothiocyanate-functionalized xanthine-based antagonist for A<sub>2A</sub>R, which irreversibly binds to 80% of rA<sub>2A</sub>R at 20 μM [137]. A second approach yielded FSPTP (Fig. 5, Table 4), the *para*-fluorosulfonyl derivative of SCH58261, which was used to investigate the level of A<sub>2A</sub>R reserve [138]. More recently, our research group used the molecular structure of the antagonist ZM241385 as a starting point for the design of a third electrophilic covalent ligand. This endeavor yielded LUF7445 (Fig. 5, Table 4), a potent fluorosulfonyl-equipped antagonist with an apparent affinity for the hA<sub>2A</sub>R in the nanomolar range (pK<sub>i</sub> = 8.99 ± 0.008) [139]. Aided by site-directed mutagenesis studies, it was shown that LUF7445 binds to K153<sup>ECL2</sup>, the same residue that was also involved in the acyl transfer of covalent agonist MRS5854. After optimization of the chemical structure, the most potent ligand was retained for further structural modification and was equipped with an alkyne click handle (next to the warhead), resulting in the bifunctional probe LUF7487 (Fig. 5, Table 4) [6]. This affinity-based probe made it possible to visualize the receptor on SDS-PAGE via click-ligation with a sulfonated Cy-3 fluorophore. The hA<sub>2A</sub>R was successfully labeled in cell membranes, making LUF7487 a promising tool compound that sets the stage

for the further development of probes to study GPCRs. The development of affinity-based probes may open the door for the identification and target validation of GPCRs in a more native environment.

### 5.3. Covalent ligands for the adenosine A<sub>3</sub> receptor

While there are no photo-reactive or chemo-reactive ligands available for the A<sub>2B</sub>R (i.e. the so far least studied AR in general), the case for the A<sub>3</sub>R is also still rather minimal. No photo-reactive ligands and only four “classes” of chemo-reactive ligands are available for the A<sub>3</sub>R. MRS1163 (Fig. 6, Table 4), the only irreversibly binding agonist for the A<sub>3</sub>R, was derived from the selective A<sub>3</sub>R agonist IB-MECA [140]. It features a chemo-reactive isothiocyanate moiety, which replaced the iodine substituent on IB-MECA, and showed an apparent K<sub>i</sub> value in the low nanomolar range ( $10.0 \pm 2.3$  nM), which is comparable to IB-MECA. Treatment of rA<sub>3</sub>R with 100 nM of MRS1163 led to a 41% loss in the available receptor binding sites and its irreversible nature was demonstrated by the lack of recovery of A<sub>3</sub>R binding sites after extensive washing.

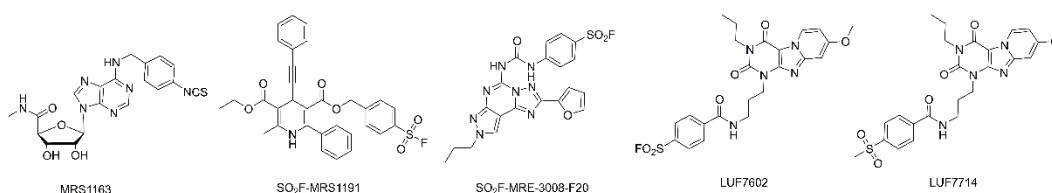


**Fig. 6 Chemical structures of covalent ligands for A<sub>3</sub>R.** Note: LUF7714 is a reversible control ligand for LUF7602.

Using a “functionalized congener approach” the Jacobsen group developed an electrophilic antagonist for the A<sub>3</sub>R based on the 1,4-dihydropyridine template, a selective A<sub>3</sub>R scaffold. A fluorosulfonyl-substituted phenyl group was installed on MRS1191, thereby generating the functionalized congener SO<sub>2</sub>F-MRS1191 (Fig. 6, Table 4) [141]. It was reported to possess greatly improved affinity ( $2.42 \pm 0.32$  nM) over the corresponding sulfonamide compound, which displayed moderate potency of only  $0.292 \pm 0.030$  μM. When 100 nM of compound 19 was incubated with hA<sub>3</sub>R-transfected HEK-293 cell membranes, approximately 56% of the hA<sub>3</sub>R binding sites were irreversibly occupied. A second covalent antagonist was generated based on MRE-3008-F20, a highly potent and selective A<sub>3</sub>R antagonist [142]. By replacing the methoxy group in MRE-3008-F20 with a sulfonyl fluoride moiety an irreversibly binding derivative, SO<sub>2</sub>F-MRE-3008-F20 (Fig. 6, Table 4), was synthesized. At a concentration of 100 nM, SO<sub>2</sub>F-MRE-3008-F20 inhibited binding of the radioligand [<sup>125</sup>I]AB-MECA by 79%. By docking the ligand in a homology model of the A<sub>3</sub>R, it was speculated that two amino

acids, Cys251 or Ser247, are the most probable binding partners for covalent interaction. Recently, our group used a chemical structure-based approach to design covalent antagonists for the hA<sub>3</sub>R [143]. A series of tricyclic xanthine-derived ligands bearing a fluorosulfonyl warhead and varying linkers was synthesized. The most potent ligand, LUF7602 (Fig. 6, Table 4) had high affinity for the hA<sub>3</sub>R ( $pK_i = 8.0 \pm 0.05$ ). Additionally, a nonreactive methylsulfonyl derivative LUF7714 was developed as a reversible control compound. A series of assays, comprising of time-dependent affinity determination, washout experiments, and [<sup>35</sup>S] GTP $\gamma$ S binding assays, then validated LUF7602 as a covalent antagonist. Based on homology-docking, tyrosine Y265<sup>7.36</sup> was identified as potential covalent anchor and when this residue was mutated to phenylalanine the mutant receptor displayed a significant decrease in affinity for LUF7602 ( $pIC_{50} = 7.8 \pm 0.05$  for hA<sub>3</sub>R-WT,  $pIC_{50} = 6.0 \pm 0.3$  for hA<sub>3</sub>R-Y265<sup>7.36</sup>F), while the affinity of LUF7714 ( $pIC_{50} = 5.9 \pm 0.2$  for hA<sub>3</sub>R-WT,  $pIC_{50} = 6.0 \pm 0.1$  for hA<sub>3</sub>R-Y265<sup>7.36</sup>F) was unaltered. It is worth mentioning that this particular tyrosine residue is conserved amongst adenosine receptors, and is also the anchor point of DU172, the aforementioned covalent antagonist for the hA<sub>1</sub>R [124]. Hence, this tyrosine residue potentially represents a universal anchor point for covalent probes designed for adenosine receptors. In general, covalent probes, supported by molecular modeling and site-directed mutagenesis, can serve as powerful tools to characterize the spatial orientation and topography of ligand-receptor binding sites.

## Chapter 2

**Table 4 Covalent ligands for adenosine receptors**

Ligands	K <sub>i</sub> <sup>a</sup>				Functionality	Ref
	A <sub>1</sub>	A <sub>2A</sub>	A <sub>2B</sub>	A <sub>3</sub>		
A <sub>1</sub>						
[ <sup>125</sup> I]APNEA	K <sub>D</sub> = 2 nM (r)	N.D.	N.D.	N.D.	Agonist	[110]
<i>R</i> -AHPIA	1.6 nM (r)	N.D.	N.D.	N.D.	Agonist	[110]
[ <sup>125</sup> I]AHPIA	K <sub>D</sub> = 2 nM (r)	N.D.	N.D.	N.D.	Agonist	[110]
[ <sup>125</sup> I]azido-BW-A844U	K <sub>D</sub> = 0.14 nM (b)	N.D.	N.D.	N.D.	Antagonist	[116]
<i>p</i> -DITC-ADAC	0.469 nM (r)	191 nM (r)	N.D.	N.D.	Agonist	[117]
<i>m</i> -DITC-ADAC	0.867 nM (r)	176 nM (r)	N.D.	N.D.	Agonist	[117]
<i>m</i> -DITC-XAC	2.39 nM (r)	343 nM (r)	N.D.	N.D.	Antagonist	[117]
FSCPX	IC <sub>50</sub> = 11.8 nM	IC <sub>50</sub> = 1200 nM	N.D.	N.D.	Antagonist	[124]
DU172	IC <sub>50</sub> = 21 nM	IC <sub>50</sub> = 2.8 nM	N.D.	N.D.	Antagonist	[124]
A <sub>2A</sub>						
[ <sup>125</sup> I]Azido-PAPA-APEC	N.D.	K <sub>D</sub> = 1.2 nM	N.D.	N.D.	Agonist	[128]
[ <sup>125</sup> I]AzPE	N.D.	K <sub>D</sub> = 1.7 nM	N.D.	N.D.	Agonist	[130]
NUMBER 9	N.D.	39.7 nM	N.D.	N.D.	Agonist	[133]
<i>p</i> -DITC-APEC	276 nM (r)	35 nM (r)	N.D.	N.D.	Agonist	[127]
MRS5854	500 nM	23.0 nM	N.D.	207 nM	Agonist	[136]
MRS5854-azide	30% (10 μM)	4360 nM	N.D.	1810 nM	Agonist	[136]
ISC	20.3 μM	111 nM	N.D.		Antagonist	[137]
LUF7445	372 nM	1.0 nM	0% (1 μM)	49 nM	Antagonist	[139]
LUF7487	19.1 nM	1.5 nM	N.D.	60 nM	Antagonist	[6]
A <sub>3</sub>						
MRS1163	145 nM (r)	272 nM (r)	N.D.	10.0 nM (r)	Agonist	[140]
SO <sub>2</sub> F-MRS1191	41 % (100 μM) (r)	20% (100 μM) (r)	N.D.	2.42 nM	Antagonist	[141]
SO <sub>2</sub> F-MRE-3008-F20	<5 % (100 nM)	50 nM	N.D.	79% (100 nM)	Antagonist	[142]
LUF7602	79 nM	1.3 μM	0% (10 μM)	10 nM	Antagonist	[143]

<sup>a</sup>The data are apparent affinities for the human adenosine receptors or % displacement at the concentration in brackets unless indicated otherwise (r = rat, b = bovine). N.D. = not determined



### 6. Concluding Remarks

Molecular probes, including radioligands, fluorescent and covalent ligands, are important tool compounds that facilitate the biochemical and structural investigation of GPCRs. As shown in this review, these probes provide information about the nature of adenosine receptors, next to a deeper understanding of receptor regulation and the pathological /physiological roles of this GPCR subfamily. In particular, when combined with other techniques such as receptor mutagenesis, X-ray crystallography and homology modelling, these tools provide a powerful platform for molecular receptor pharmacology.

Radioligands are the most developed tools for GPCRs. An established standard radioligand binding assay provides crucial and reliable measurements of GPCRs interacting with their synthetic ligands as well as newly developed probes. The choice of radioligands may influence the quantitative information about the measurement. Binding of an agonist radioligand may reveal different apparent affinity states depending on the receptor states (i.e. G protein-coupled and G protein-uncoupled) or cell-dependent effector coupling. Thus, antagonist radioligands are generally considered more acceptable in receptor classification than agonists. Among the adenosine receptors, there is still an urgent need for the development of better antagonist radioligands for the A<sub>2B</sub>R and A<sub>3</sub>R with high affinity with K<sub>D</sub> values of 1 nM or less, with low non-specific binding and better selectivity. For *in vivo* assays, the development of PET ligands targeting A<sub>2B</sub>R and A<sub>3</sub>R has still been limited to receptor occupancy studies, biodistribution or pharmacokinetic characterization, while PET ligands for A<sub>1</sub>R and A<sub>2A</sub>R have blossomed in clinical studies, particularly for neurological disorders. Studies on A<sub>2B</sub>R and A<sub>3</sub>R are generally considered to be hampered by the low expression level of these receptors in endogenous tissue, insufficient affinity of the tool compound and unclear mechanisms involved in the receptor function. It is anticipated that continued efforts to develop high-affinity and selective PET tracers for adenosine receptors will further our understanding of the role these receptors have in disease conditions.

Concerns about radiation safety and shelf life have fueled the continuing interest in small-molecule fluorescent tools. Recent examples summarized in this review demonstrate that fluorescent probes represent an alternative approach to investigate AR characteristics. However, their use is still sub-optimal due to the often high level of non-specific membrane binding brought by the hydrophobic pharmacophore and fluorophore. Hence, researchers should pay more attention to designing probes with favorable physicochemical properties. Besides, the *in vivo* applications of such tools are still hampered, partly due to their short

## Chapter 2

---

excitation wavelengths and low tissue penetration [144]. Future development of synthetic ligands with a focus on near-infrared (NIR) fluorophores might be advantageous, especially since such wavelengths are not harmful to cells and have a relatively low absorption. Such NIR probes were already employed to study the cannabinoid CB<sub>2</sub> and  $\alpha_1$ -adrenergic receptors [145, 146].

Compared to radioligand and fluorescent probes, covalent ligands do not possess any detectable functionality for direct quantification or visualization of receptors. When combined with site-direct mutagenesis, mass spectrometry and peptide sequencing, they constitute a powerful approach to study adenosine receptor subtype and structure, map ligand binding sites, investigate the physiological and pathological roles of receptors and determine the correlation between receptor occupancy and response. The emergence of the activity-based protein profiling technique inspired researchers to equip probes with click handles to yield bifunctional probes that can be used to visualize receptors for target validation. In this strategy a probe binds the receptor with less perturbation compared to relatively large tags linked to ligand scaffolds beforehand, which bridges the field of chemical biology with the field of molecular pharmacology to better investigate receptor-ligand interactions. In future research, different tags may be introduced; for instance, a biotin-tag would allow for streptavidin-mediated receptor enrichment followed by LC/MS analysis. Of note, the A<sub>2B</sub>R has been known as the more poorly characterized adenosine receptor subtype. This also has limited the development of molecular probes targeting A<sub>2B</sub>R specifically, especially for the covalently binding ligands, where no case has been reported so far. Covalent probes for A<sub>2B</sub>R and A<sub>3</sub>R may also assist in the structure elucidation of these two adenosine receptor subtypes, which are currently still lacking.

For decades, scientists have been continuously developing tool compounds to study adenosine receptors. In this endeavor the use of covalent or reversible probes, whether radiolabeled or fluorescent, has been instrumental, i) to discover new chemical entities, ii) to characterize and interrogate adenosine receptor subtypes both *in vitro* and *in vivo*, and iii) to study their behavior in physiological and disease conditions. This review has summarized evidence for these applications, but, hopefully, it also serves as an invitation to walk another mile to further improve probe characteristics and develop additional tags that interrogate adenosine receptors and other GPCRs in even finer detail.

### References

1. Jacobson K.A., and Gao Z.G. *Nat Rev Drug Discov.* **2006.** 5(3): 247-264.
2. Jaakola V.P., Griffith M.T., Hanson M.A., Cherezov V., Chien E.Y., Lane J.R., IJzerman A.P., and Stevens R.C. *Science.* **2008.** 322(5905): 1211-1217.
3. Glukhova A., Thal D.M., Nguyen A.T., Vecchio E.A., Jorg M., Scammells P.J., May L.T., Sexton P.M., and Christopoulos A. *Cell.* **2017.** 168(5): 867-877
4. Gregory K.J., Velagaleti R., Thal D.M., Brady R.M., Christopoulos A., Conn P.J., and Lapinsky D.J. *ACS Chem Biol.* **2016.** 11(7): 1870-1879.
5. Soethoudt M., Stolze S.C., Westphal M.V., van Stralen L., Martella A., van Rooden E.J., Guba W., Varga Z.V., Deng H., van Kasteren S.I., Grether U., IJzerman A.P., Pacher P., Carreira E.M., Overkleeft H.S., Ioan-Facsinay A., Heitman L.H., and van der Stelt M. *J Am Chem Soc.* **2018.** 140(19): 6067-6075.
6. Yang X., Michiels T.J.M., de Jong C., Soethoudt M., Dekker N., Gordon E., van der Stelt M., Heitman L.H., van der Es D., and IJzerman A.P. *J Med Chem.* **2018.** 61(17): 7892-7901.
7. Speers A.E., and Cravatt B.F. *Chem Biol.* **2004.** 11(4): 535-546.
8. Cravatt B.F., Wright A.T., and Kozarich J.W. *Annu Rev Biochem.* **2008.** 77: 383-414.
9. Flanagan C.A., *Chapter 10 - GPCR-radioligand binding assays*, in *Methods Cell Bio*, A. K. Shukla, Editor. 2016, Academic Press. p. 191-215.
10. Hulme E.C., and Trevethick M.A. *Br J Pharmacol.* **2010.** 161(6): 1219-1237.
11. Klotz K.N., Lohse M.J., Schwabe U., Cristalli G., Vittori S., and Grifantini M. *Naunyn-Schmiedeberg's Archives of Pharmacology.* **1989.** 340(6): 679-683.
12. Lane J.R., Klaasse E., Lin J., van Bruchem J., Beukers M.W., and IJzerman A.P. *Biochem Pharmacol.* **2010.** 80(8): 1180-1189.
13. Klotz K.N., Hessling J., Hegler J., Owman C., Kull B., Fredholm B.B., and Lohse M.J. *Naunyn-Schmiedeberg's Archives of Pharmacology.* **1998.** 357(1): 1-9.
14. Lohse M.J., Klotz K.N., Lindenbornfotinos J., Reddington M., Schwabe U., and Olsson R.A. *Naunyn-Schmiedeberg's Archives of Pharmacology.* **1987.** 336(2): 204-210.
15. Xia L., de Vries H., IJzerman A.P., and Heitman L.H.H. *Purinergic Signal.* **2016.** 12(1): 115-126.
16. Jarvis M.F., Schulz R., Hutchison A.J., Do U.H., Sills M.A., and Williams M. *J Pharmacol Exp Ther.* **1989.** 251(3): 888-893.
17. Svenningsson P., Hall H., Sedvall G., and Fredholm B.B. *Synapse.* **1997.** 27(4): 322-335.
18. Kurumaji A., and Toru M. *Brain Res.* **1998.** 808(2): 320-323.
19. Wan W., Sutherland G.R., and Geiger J.D. *J Neurochem.* **1990.** 55(5): 1763-1771.
20. Lindstrom K., Ongini E., and Fredhohn B.B. *Naunyn-Schmiedeberg's Archives of Pharmacology.* **1996.** 354(4): 539-541.
21. Kim J., Wess J., van Rhee A.M., Schoneberg T., and Jacobson K.A. *J Biol Chem.* **1995.** 270(23): 13987-13997.
22. Muller C.E., Maurinsh J., and Sauer R. *Eur J Pharm Sci.* **2000.** 10(4): 259-265.
23. Sihver W., Schulze A., Wutz W., Stusgen S., Olsson R.A., Bier D., and Holschbach M.H. *Eur J Pharmacol.* **2009.** 616(1-3): 107-114.
24. Hockemeyer J., Burbiel J.C., and Muller C.E. *J Org Chem.* **2004.** 69(10): 3308-3318.
25. Alexander S.P.H., and Millns P.J. *Eur J Pharmacol.* **2001.** 411(3): 205-210.

## Chapter 2

---

26. Guo D., Mulder-Krieger T., IJzerman A.P., and Heitman L.H. *Br J Pharmacol.* **2012.** 166(6): 1846-1859.
27. Xiaodong J., and Jacobson K.A. *Drug Des and Discov.* **1999.** vol. 16,3 (1999): 217-226.
28. Dionisotti S., Ongini E., Zocchi C., Kull B., Arslan G., and Fredholm B.B. *Br J Pharmacol.* **1997.** 121(3): 353-360.
29. El Yacoubi M., Ledent C., Parmentier M., Ongini E., Costentin J., and Vaugeois J.M. *Eur J Neurosci.* **2001.** 14(9): 1567-1570.
30. Bryant R., McGuinness D., Turek-Etienne T., Guyer D., Yu L.M., Howells L., Caravano J., Zhai Y., and Lachowicz J. *Assay Drug Dev Technol.* **2004.** 2(3): 290-299.
31. Hinz S., Alnouri W.M., Pleiss U., and Muller C.E. *Purinergic Signal.* **2018.** 14: 223-233.
32. Casado V., Casillas T., Mallol J., Canela E.I., Lluís C., and Franco R. *J Neurochem.* **1992.** 59(2): 425-431.
33. Robeva A.S., Woodard R.L., Jin X.W., Gao Z.H., Bhattacharya S., Taylor H.E., Rosin D.L., and Linden J. *Drug Develop Res.* **1996.** 39(3-4): 243-252.
34. Bosch M.P., Campos F., Niubo I., Rosell G., Diaz J.L., Brea J., Loza M.I., and Guerrero A. *J Med Chem.* **2004.** 47(16): 4041-4053.
35. Linden J., Thai T., Figler H., Jin X., and Robeva A.S. *Mol Pharmacol.* **1999.** 56(4): 705-713.
36. Ji X.D., Kim Y.C., Ahern D.G., Linden J., and Jacobson K.A. *Biochem Pharmacol.* **2001.** 61(6): 657-663.
37. Baraldi P.G., Tabrizi M.A., Preti D., Bovero A., Fruttarolo F., Romagnoli R., Moorman A.R., Gessi S., Merighi S., Varani K., and Borea P.A. *Bioorg Med Chem Lett.* **2004.** 14(13): 3607-3610.
38. Gessi S., Varani K., Merighi S., Cattabriga E., Pancaldi C., Szabadkai Y., Rizzuto R., Klotz K.N., Leung E., Mac Lennan S., Baraldi P.G., and Borea P.A. *Mol Pharmacol.* **2005.** 67(6): 2137-2147.
39. Stewart M., Steinig A.G., Ma C.L., Song J.P., McKibben B., Castelhana A.L., and MacLennan S.J. *Biochem Pharmacol.* **2004.** 68(2): 305-312.
40. Borrmann T., Hinz S., Lertarelli D.C.G., Li W.J., Florin N.C., Scheiff A.B., and Muller C.E. *J Med Chem.* **2009.** 52(13): 3994-4006.
41. Zhou Q.Y., Li C., Olah M.E., Johnson R.A., Stiles G.L., and Civelli O. *Proc Natl Acad Sci U S A.* **1992.** 89(16): 7432-7436.
42. Olah M.E., Gallorodriguez C., Jacobson K.A., and Stiles G.L. *Mol Pharmacol.* **1994.** 45(5): 978-982.
43. Lane J.R., Beukers M.W., Mulder-Krieger T., and IJzerman A.P. *Biochem Pharmacol.* **2010.** 79(1): 48-56.
44. Klotz K.N., Falgner N., Kachler S., Lambertucci C., Vittori S., Volpini R., and Cristalli G. *Eur J Pharmacol.* **2007.** 556(1-3): 14-18.
45. Gao Z.G., Teng B., Wu H.T., Joshi B.V., Griffiths G.L., and Jacobson K.A. *Purinergic Signalling.* **2009.** 5(1): 31-37.
46. Auchampach J.A., Gizewski E.T., Wan T.C., de Castro S., Brown G.G., and Jacobson K.A. *Biochem Pharmacol.* **2010.** 79(7): 967-973.
47. Varani K., Merighi S., Gessi S., Klotz K.N., Leung E., Baraldi P.G., Cacciari B., Romagnoli R., Spalluto G., and Borea P.A. *Mol Pharmacol.* **2000.** 57(5): 968-975.
48. Baraldi P.G., Cacciari B., Romagnoli R., Varani K., Merighi S., Gessi S., Borea P.A., Leung E., Hickey S.L., and Spalluto G. *Bioorg Med Chem Lett.* **2000.** 10(3): 209-211.

49. Muller C.E., Diekmann M., Thorand M., and Ozola V. *Bioorg Med Chem Lett.* **2002.** 12(3): 501-503.
50. Beukers M.W., Chang L.C., von Frijtag Drabbe Kunzel J.K., Mulder-Krieger T., Spanjersberg R.F., Brussee J., and IJzerman A.P. *J Med Chem.* **2004.** 47(15): 3707-3709.
51. Mishina M., and Ishiwata K. *Int Rev Neurobiol.* **2014.** 119: 51-69.
52. Khanapur S., Waarde A., Ishiwata K., Leenders K.L., Dierckx R.A., and Elsinga P.H. *Curr Med Chem.* **2014.** 21(3): 312-328.
53. van Waarde A., Dierckx R., Zhou X., Khanapur S., Tsukada H., Ishiwata K., Luurtsema G., de Vries E.F.J., and Elsinga P.H. *Med Res Rev.* **2018.** 38(1): 5-56.
54. Paul S., Elsinga P.H., Ishiwata K., Dierckx R.A.J.O., and van Waarde A. *Curr Med Chem.* **2011.** 18(31): 4820-4835.
55. Fukumitsu N., Ishii K., Kimura Y., Oda K., Sasaki T., Mori Y., and Ishiwata K. *J Nucl Med.* **2005.** 46(1): 32-37.
56. Bauer A., Holschbach M.H., Meyer P.T., Boy C., Herzog H., Olsson R.A., Coenen H.H., and Zilles K. *Neuroimage.* **2003.** 19(4): 1760-1769.
57. Meyer P.T., Elmenhorst D., Boy C., Winz O., Matusch A., Zilles K., and Bauer A. *Neurobiol Aging.* **2007.** 28(12): 1914-1924.
58. Elmenhorst D., Elmenhorst E.M., Hennecke E., Kroll T., Matusch A., Aeschbach D., and Bauer A. *P Natl Acad Sci USA.* **2017.** 114(16): 4243-4248.
59. Elmenhorst D., Meyer P.T., Matusch A., Winz O.H., and Bauer A. *J Nucl Med.* **2012.** 53(11): 1723-1729.
60. Mishina M., Ishii K., Kimura Y., Suzuki M., Kitamura S., Ishibashi K., Sakata M., Oda K., Kobayashi S., Kimura K., and Ishiwata K. *Synapse.* **2017.** 71(8).
61. Matusch A., Saft C., Elmenhorst D., Kraus P.H., Gold R., Hartung H.P., and Bauer A. *Eur J Nucl Med Mol Imaging.* **2014.** 41(6): 1210-1220.
62. Guo M., Gao Z.-G., Tyler R., Stodden T., Li Y., Ramsey J., Zhao W.-J., Wang G.-J., Wiers C.E., Fowler J.S., Rice K.C., Jacobson K.A., Kim S.W., and Volkow N.D. *J Med Chem.* **2018.** 61(22): 9966-9975.
63. Mishina M., Ishiwata K., Naganawa M., Kimura Y., Kitamura S., Suzuki M., Hashimoto M., Ishibashi K., Oda K., Sakata M., Hamamoto M., Kobayashi S., Katayama Y., and Ishii K. *PLoS One.* **2011.** 6(2): 17338.
64. Mishina M., Ishiwata K., Kimura Y., Naganawa M., Oda K., Kobayashi S., Katayama Y., and Ishii K. *Synapse.* **2007.** 61(9): 778-784.
65. Ramlackhansingh A.F., Bose S.K., Ahmed I., Turkheimer F.E., Pavese N., and Brooks D.J. *Neurology.* **2011.** 76(21): 1811-1816.
66. Moresco R.M., Todde S., Belloli S., Simonelli P., Panzacchi A., Rigamonti M., Galli-Kienle M., and Fazio F. *Eur J Nucl Med Mol Imaging.* **2005.** 32(4): 405-413.
67. Zhou X., Khanapur S., Huizing A.P., Zijlma R., Schepers M., Dierckx R.A., van Waarde A., de Vries E.F., and Elsinga P.H. *J Med Chem.* **2014.** 57(21): 9204-9210.
68. Ishibashi K., Miura Y., Wagatsuma K., Toyohara J., Ishiwata K., and Ishii K. *Neuropharmacology.* **2018.** 143: 106-112.
69. Khanapur S., Paul S., Shah A., Vatakuti S., Koole M.J.B., Zijlma R., Dierckx R.A.J.O., Luurtsema G., Garg P., van Waarde A., and Elsinga P.H. *J Med Chem.* **2014.** 57(15): 6765-6780.
70. Tavares A.A., Batis J.C., Papin C., Jennings D., Alagille D., Russell D.S., Vala C., Lee H., Baldwin R.M., Zubal I.G., Marek K.L., Seibyl J.P., Barret O., and Tamagnan G.D. *J Nucl Med.* **2013.** 54(10): 1760-1767.

## Chapter 2

---

71. Barret O., Hannestad J., Vala C., Alagille D., Tavares A., Laruelle M., Jennings D., Marek K., Russell D., Seibyl J., and Tamagnan G. *J Nucl Med.* **2015.** 56(4): 586-591.
72. Petroni D., Giacomelli C., Taliani S., Barresi E., Robello M., Daniele S., Bartoli A., Burchielli S., Pardini S., Salvadori P.A., Da Settimo F., Martini C., Trincavelli M.L., and Menichetti L. *Nucl Med Biol.* **2016.** 43(5): 309-317.
73. Lindemann M., Hinz S., Deuther-Conrad W., Namasivayam V., Dukic-Stefanovic S., Teodoro R., Toussaint M., Kranz M., Juhl C., Steinbach J., Brust P., Muller C.E., and Wenzel B. *Bioorg Med Chem.* **2018.** 26(16): 4650-4663.
74. Li A.-H., Moro S., Forsyth N., Melman N., Ji X.-d., and Jacobson K.A. *J Med Chem.* **1999.** 42(4): 706-721.
75. Wadsak W., Mien L.-K., Shanab K., Ettliger D.E., Haeusler D., Sindelar K., Lanzenberger R.R., Spreitzer H., Viernstein H., Keppler B.K., Dudczak R., Kletter K., and Mitterhauser M. *Nuclear Medicine and Biology.* **2008.** 35(1): 61-66.
76. Wadsak W., Mien L.K., Shanab K., Ettliger D.E., Haeusler D., Sindelar K., Lanzenberger R.R., Spreitzer H., Viernstein H., Keppler B.K., Dudczak R., Kletter K., and Mitterhauser M. *Nucl Med Biol.* **2008.** 35(1): 61-66.
77. Balber T., Singer J., Berroteran-Infante N., Dumanic M., Fetty L., Fazekas-Singer J., Vranka C., Nics L., Bergmann M., Pallitsch K., Spreitzer H., Wadsak W., Hacker M., Jensen-Jarolim E., Viernstein H., and Mitterhauser M. *Contrast Media Mol Imaging.* **2018.**
78. Mitterhauser M., Haeusler D., Mien L.-K., Ungersboeck J., Nics L., Lanzenberger R.R., Sindelar K., Viernstein H., Dudczak R., and Kletter K. *Open Nucl Med J.* **2009.** 1: 15-23.
79. Kiesewetter D.O., Lang L., Ma Y., Bhattacharjee A.K., Gao Z.-G., Joshi B.V., Melman A., de Castro S., and Jacobson K.A. *Nuclear Medicine and Biology.* **2009.** 36(1): 3-10.
80. Ishiwata K., Ogi N., Shimada J., Nonaka H., Tanaka A., Suzuki F., and Senda M. *Ann Nucl Med.* **2000.** 14(2): 81-89.
81. Todde S., Moresco R.M., Simonelli F., Baraldi P.G., Cacciari B., Spalluto G., Varani K., Monopoli A., Matarrese M., Carpinelli A., Magni F., Kienle M.G., and Fazio F. *J Med Chem.* **2000.** 43(23): 4359-4362.
82. Neustadt B.R., Hao J., Lindo N., Greenlee W.J., Stamford A.W., Tulshian D., Ongini E., Hunter J., Monopoli A., Bertorelli R., Foster C., Arik L., Lachowicz J., Ng K., and Feng K.-I. *Bioorg Med Chem Lett.* **2007.** 17(5): 1376-1380.
83. Shinkre B.A., Kumar T.S., Gao Z.G., Deflorian F., Jacobson K.A., and Trenkle W.C. *Bioorg Med Chem Lett.* **2010.** 20(19): 5690-5694.
84. Kumar T.S., Mishra S., Deflorian F., Yoo L.S., Phan K., Kecskes M., Szabo A., Shinkre B., Gao Z.G., Trenkle W., and Jacobson K.A. *Bioorg Med Chem Lett.* **2011.** 21(9): 2740-2745.
85. Vala C., Morley T.J., Zhang X., Papin C., Tavares A.A., Lee H.S., Constantinescu C., Barret O., Carroll V.M., Baldwin R.M., Tamagnan G.D., and Alagille D. *ChemMedChem.* **2016.** 11(17): 1936-1943.
86. Kozma E., Jayasekara P.S., Squarzialupi L., Paoletta S., Moro S., Federico S., Spalluto G., and Jacobson K.A. *Bioorg Med Chem.* **2013.** 23(1): 26-36.
87. Stoddart L.A., Vernall A.J., Denman J.L., Briddon S.J., Kellam B., and Hill S.J. *Chem Biol.* **2012.** 19(9): 1105-1115.
88. Arruda M.A., Stoddart L.A., Gherbi K., Briddon S.J., Kellam B., and Hill S.J. *Front Pharmacol.* **2017.** 8: 908.
89. Briddon S.J., Middleton R.J., Cordeaux Y., Flavin F.M., Weinstein J.A., George M.W., Kellam B., and Hill S.J. *Proc Natl Acad Sci U S A.* **2004.** 101(13): 4673-4678.

90. Cooper S.L., Soave M., Jorg M., Scammells P.J., Woolard J., and Hill S.J. *Br J Pharmacol*. **2019**. 176(7): 864-878.
91. Fernandez-Duenas V., Gomez-Soler M., Jacobson K.A., Kumar S.T., Fuxe K., Borroto-Escuela D.O., and Ciruela F. *J Neurochem*. **2012**. 123(3): 373-384.
92. Fernandez-Duenas V., Gomez-Soler M., Morato X., Nunez F., Das A., Kumar T.S., Jauma S., Jacobson K.A., and Ciruela F. *Neurochemistry International*. **2013**. 63(1): 42-46.
93. McCabe R.T., Skolnick P., and Jacobson K.A. *J Fluoresc*. **1992**. 2(4): 217-223.
94. McNeely P.M., Naranjo A.N., Forsten-Williams K., and Robinson A.S. *Slas Discovery*. **2017**. 22(2): 166-175.
95. Duroux R., Ciancetta A., Mannes P., Yu J.H., Boyapati S., Gizewski E., Yous S., Ciruela F., Auchampach J.A., Gao Z.G., and Jacobson K.A. *Medchemcomm*. **2017**. 8(8): 1659-1667.
96. Kose M., Gollos S., Karcz T., Fiene A., Heisig F., Behrenswerth A., Kiec-Kononowicz K., Namasivayam V., and Muller C.E. *J Med Chem*. **2018**. 61(10): 4301-4316.
97. Barresi E., Giacomelli C., Daniele S., Tonazzini I., Robello M., Salerno S., Piano I., Cosimelli B., Greco G., Da Settimo F., Martini C., Trincavelli M.L., and Taliani S. *Bba-Biomembranes*. **2018**. 26(22): 5885-5895.
98. Corriden R., Self T., Akong-Moore K., Nizet V., Kellam B., Briddon S.J., and Hill S.J. *Embo Reports*. **2013**. 14(8): 726-732.
99. Vernall A.J., Stoddart L.A., Briddon S.J., Ng H.W., Laughton C.A., Doughty S.W., Hill S.J., and Kellam B. *Org Biomol Chem*. **2013**. 11(34): 5673-5682.
100. Stoddart L.A., Vernall A.J., Briddon S.J., Kellam B., and Hill S.J. *Neuropharmacology*. **2015**. 98: 68-77.
101. Kozma E., Kumar T.S., Federico S., Phan K., Balasubramanian R., Gao Z.G., Paoletta S., Moro S., Spalluto G., and Jacobson K.A. *Biochem Pharmacol*. **2012**. 83(11): 1552-1561.
102. Jorg M., and Scammells P.J. *ChemMedChem*. **2016**. 11(14): 1488-1498.
103. Adeniyi A.A., Muthusamy R., and Soliman M.E. *Expert Opin Drug Discov*. **2016**. 11(1): 79-90.
104. Robinette D., Neamati N., Tomer K.B., and Borchers C.H. *Expert Rev. Proteomics*. **2006**. 3(4): 399-408.
105. Grunbeck A., and Sakmar T.P. *Biochem*. **2013**. 52(48): 8625-8632.
106. Dorman G., and Prestwich G.D. *Trends Biotechnol*. **2000**. 18(2): 64-77.
107. Morey T.E., Belardinelli L., and Dennis D.M. *Br J Pharmacol*. **1998**. 123(7): 1425-1433.
108. Yasunaga T., Motoyama S., Nose T., Kodama H., Kondo M., and Shimohigashi Y. *J Biol Chem*. **1996**. 271(2): 459-465.
109. Weichert D., and Gmeiner P. *Acs Chem Biol*. **2015**. 10(6): 1376-1386.
110. Stiles G.L., Daly D.T., and Olsson R.A. *J Biol Chem*. **1985**. 260(2): A231-A231.
111. Klotz K.N., Cristalli G., Grifantini M., Vittori S., and Lohse M.J. *J Biol Chem*. **1985**. 260(27): 4659-4664.
112. Lohse M.J., Klotz K.N., and Schwabe U. *Mol Pharmacol*. **1986**. 30(4): 403-409.
113. Lohse M.J., Klotz K.N., and Schwabe U. *Mol Pharmacol*. **1991**. 39(4): 517-523.
114. Earl C.Q., Patel A., Craig R.H., Daluge S.M., and Linden J. *J Med Chem*. **1988**. 31(4): 752-756.
115. Kennedy A.P., Mangum K.C., Linden J., and Wells J.N. *Mol Pharmacol*. **1996**. 50(4): 789-798.
116. Patel A., Craig R.H., Daluge S.M., and Linden J. *Mol Pharmacol*. **1988**. 33: 585-591.
117. Jacobson K.A., Barone S., Kammula U., and Stiles G.L. *J Med Chem*. **1989**. 32(5): 1043-1051.



## Chapter 2

---

118. Jorg M., Glukhova A., Abdul-Ridha A., Vecchio E.A., Nguyen A.T.N., Sexton P.M., White P.J., May L.T., Christopoulos A., and Scammells P.J. *J Med Chem.* **2016.** 59(24): 11182-11194.
119. Zhang J., Belardinelli L., Jacobson K.A., Otero D.H., and Baker S.P. *Mol Pharmacol.* **1997.** 52(3): 491-498.
120. Dennis D., Jacobson K., and Belardinelli L. *Am J Physiol.* **1992.** 262(3 Pt 2): 661-671.
121. Scammells P.J., Baker S.P., Belardinelli L., and Olsson R.A. *J Med Chem.* **1994.** 37(17): 2704-2712.
122. Gesztelyi R., Kiss Z., Wachal Z., Juhasz B., Bombicz M., Csepanyi E., Pak K., Zsuga J., Papp C., Galajda Z., Branzaniuc K., Porszasz R., Szentmiklosi A.J., and Tosaki A. *Arch Pharm Res.* **2013.** 36(3): 293-305.
123. van Muijlwijk-Koezen J.E., Timmerman H., van der Sluis R.P., van de Stolpe A.C., Menge W.M., Beukers M.W., van der Graaf P.H., de Groote M., and IJzerman A.P. *Bioorg Med Chem Lett.* **2001.** 11(6): 815-818.
124. Beauglehole A.R., Baker S.P., and Scammells P.J. *J Med Chem.* **2000.** 43(26): 4973-4980.
125. Beauglehole A.R., Baker S.P., and Scammells P.J. *Bioorg Med Chem Lett.* **2002.** 12(21): 3179-3182.
126. Barrington W.W., Jacobson K.A., Hutchison A.J., Williams M., and Stiles G.L. *Proc Natl Acad Sci U S A.* **1989.** 86(17): 6572-6576.
127. Jacobson K.A., Pannell L.K., Ji X.D., Jarvis M.F., Williams M., Hutchison A.J., Barrington W.W., and Stiles G.L. *J Mol Recognit.* **1989.** 2(4): 170-178.
128. Barrington W.W., Jacobson K.A., and Stiles G.L. *Mol Pharmacol.* **1990.** 38(2): 177-183.
129. Pierson C.E., True C.D., and Wells J.N. *Mol Pharmacol.* **1994.** 45(5): 871-877.
130. Luthin D.R., Lee K.S., Okonkwo D., Zhang P.J., and Linden J. *J Neurochem.* **1995.** 65(5): 2072-2079.
131. Baraldi P.G., Cacciari B., Spalluto G., Pineda de las Infantas y Villatoro M.J., Zocchi C., Dionisotti S., and Ongini E. *J Med Chem.* **1996.** 39(5): 1164-1171.
132. Silverman L.S., Caldwell J.P., Greenlee W.J., Kiselgof E., Matasi J.J., Tulshian D.B., Arik L., Foster C., Bertorelli R., Monopoli A., and Ongini E. *Bioorg Med Chem Lett.* **2007.** 17(6): 1659-1662.
133. Muranaka H., Momose T., Handa C., and Ozawa T. *ACS Med Chem Lett.* **2017.** 8(6): 660-665.
134. Jacobson K.A., Stiles G.L., and Ji X.D. *Mol Pharmacol.* **1992.** 42(1): 123-133.
135. Niiya K., Jacobson K.A., Silvia S.K., and Olsson R.A. *N-S Arch Pharmacol.* **1993.** 347(5): 521-526.
136. Moss S.M., Jayasekara P.S., Paoletta S., Gao Z.G., and Jacobson K.A. *ACS Med Chem Lett.* **2014.** 5(9): 1043-1048.
137. Ji X.D., Gallo-Rodriguez C., and Jacobson K.A. *Drug Develop Res.* **1993.** 29(4): 292-298.
138. Shryock J.C., Snowdy S., Baraldi P.G., Cacciari B., Spalluto G., Monopoli A., Ongini E., Baker S.P., and Belardinelli L. *Circulation.* **1998.** 98(7): 711-718.
139. Yang X., Dong G., Michiels T.J.M., Lenselink E.B., Heitman L., Louvel J., and IJzerman A.P. *Purinergic Signal.* **2017.** 13(2): 191-201.
140. Ji X.D., Gallo-Rodriguez C., and Jacobson K.A. *Biochem Biophys Res Commun.* **1994.** 203(1): 570-576.
141. Li A.H., Chang L., Ji X., Melman N., and Jacobson K.A. *Bioconjug Chem.* **1999.** 10(4): 667-677.



142. Baraldi P.G., Cacciari B., Moro S., Romagnoli R., Ji X., Jacobson K.A., Gessi S., Borea P.A., and Spalluto G. *J Med Chem.* **2001**. 44(17): 2735-2742.
143. Yang X., van Veldhoven J.P.D., Offringa J., Kuiper B.J., Lenselink E.B., Heitman L.H., van der Es D., and IJzerman A.P. *J Med Chem.* **2019**. 62(7): 3539-3552.
144. Iliopoulos-Tsoutsouvas C., Kulkarni R.N., Makriyannis A., and Nikas S.P. *Expert Opin Drug Discov.* **2018**. 13(10): 933-947.
145. Ma Z., Lin Y., Cheng Y., Wu W., Cai R., Chen S., Shi B., Han B., Shi X., Zhou Y., Du L., and Li M. *J Med Chem.* **2016**. 59(5): 2151-2162.
146. Zhang S.J., Shao P., and Bai M.F. *Bioconjug Chem.* **2013**. 24(11): 1907-1911



# Chapter 3

## A Covalent Antagonist for the Human Adenosine A<sub>2A</sub> Receptor

*Xue Yang*

*Guo Dong*

*Thomas J.M. Michiels*

*Eelke B. Lenselink*

*Laura H. Heitman*

*Julien Louvel*

*Adriaan P. IJzerman\**

Purinergic Signal. 2017 Jun;13(2):191-201.

doi: 10.1007/s11302-016-9549-9.



### Abstract

The structure of the human A<sub>2A</sub> adenosine receptor has been elucidated by X-ray crystallography with a high affinity non-xanthine antagonist, ZM241385, bound to it. This template molecule served as a starting point for the incorporation of reactive moieties that cause the ligand to covalently bind to the receptor. In particular, we incorporated a fluorosulfonyl moiety onto ZM241385, which yielded LUF7445 (4-((3-((7-amino-2-(furan-2-yl)-[1,2,4]triazolo[1,5-a][1,3,5]triazin-5-yl)amino)propyl)carbamoyl)benzene sulfonyl fluoride).

In a radioligand binding assay LUF7445 acted as a potent antagonist, with an apparent affinity for the hA<sub>2A</sub> receptor in the nanomolar range. Its apparent affinity increased with longer incubation time, suggesting an increasing level of covalent binding over time. An *in silico* A<sub>2A</sub>-structure-based docking model was used to study the binding mode of LUF7445. This led us to perform site-directed mutagenesis of the A<sub>2A</sub> receptor to probe and validate the target lysine amino acid K153 for covalent binding. Meanwhile, a functional assay combined with wash-out experiments was set up to investigate the efficacy of covalent binding of LUF7445. All these experiments led us to conclude LUF7445 is a valuable molecular tool for further investigating covalent interactions at this receptor. It may also serve as a prototype for a therapeutic approach in which a covalent antagonist may be needed to counteract prolonged and persistent presence of the endogenous ligand adenosine.

**Keywords:** G protein-coupled receptors, A<sub>2A</sub> adenosine receptor, adenosine, covalent antagonist, radioligand binding

### 1. Introduction

G protein-coupled receptors (GPCRs), all membrane-bound proteins, represent one of the largest classes of drug targets, and are the anchor point for approx. one third of all marketed drugs [1]. These proteins are notoriously difficult to handle outside of their natural membrane context, for instance in receptor purification and crystallization. Recently, however, a combination of technological advances has allowed the structure elucidation of an increasing number of these important drug targets [2-4]. In this context covalent modification of the receptor with ligands is emerging as a useful way to investigate ligand-receptor binding domains in membrane proteins, also because such covalent ligands, acting as pharmacological chaperones, tend to stabilize the otherwise fragile receptor proteins.

Covalent binding of both agonists and antagonists to adenosine receptors has known a long history in purinoceptor research. In the 1980s the adenosine A<sub>1</sub> receptor was the preeminent target for such studies [5], eventually leading to the design of a covalently binding fluorosulfonyl derivative of the reference antagonist DPCPX, named FSCPX, which appeared useful also in an *in vivo* setting [6,7]. Likewise the adenosine A<sub>2A</sub> receptor has been subjected to such strategies. One existing example is the *para*-fluorosulfonyl derivative of SCH58261, FSPTP, which was used to investigate the level of adenosine A<sub>2A</sub> receptor reserve for agonist activity [8]. The hA<sub>2A</sub>AR has relevance in various diseases, and thus, agonists for increasing blood flow during cardiac nuclear stress tests [9] and an antagonist for the treatment of Parkinson's disease [10] are on the market, and the receptor may also play a role in cancer-immunotherapy [11]. The hA<sub>2A</sub>AR has also been one of the first GPCRs to be crystallized and a wide variety of crystal structures has been published, including the reported structures co-crystallized with agonist UK-432097 or antagonist ZM241385 [12-14]. Although covalent A<sub>2A</sub>R antagonists have been previously synthesized and investigated in terms of their affinity or potency [8,15-18], little is known about their precise binding mode in the receptor and their effects on the kinetics of interaction.

In this study, we describe our efforts to obtain a covalent antagonist probe for the hA<sub>2A</sub>AR, as a logical extension of our previous research on long residence time antagonists, i.e. compounds that dissociate only slowly from the receptor [19]. We used the antagonist ZM241385 as the starting point in our design efforts, and synthesized a fluorosulfonyl derivative of it, LUF7445. We then validated this compound to bind covalently and inhibit the receptor in a number of *in vitro* experiments, and provide evidence for its point of attachment to the receptor.

### 2. Methods and Materials

*Chemicals and Reagent* The radioligand [<sup>3</sup>H] ZM241385 with a specific activity of 50 Ci × mmol<sup>-1</sup> was purchased from ARC Inc. (St. Louis, MO). Unlabelled ZM241385 was a gift from Dr. S.M. Poucher (Astra Zeneca, Macclesfield, UK). 5'-N-ethylcarboxamidoadenosine (NECA) was purchased from Sigma-Aldrich (Steinheim, Germany). LUF6632 was synthesized in our lab, as published previously [19]. Adenosine deaminase (ADA) was purchased from Boehringer Mannheim (Mannheim, Germany). Bicinchoninic acid (BCA) and BCA protein assay reagent were obtained from Pierce Chemical Company (Rockford, IL, USA). HEK293 cells stably expressing the hA<sub>2A</sub> adenosine receptor (HEK293 hA<sub>2A</sub>AR) were kindly provided by Dr J Wang (Biogen/IDEC, Cambridge, MA, USA). All other chemicals were of analytical grade and obtained from standard commercial sources. *Site-Directed Mutagenesis* Site-directed receptor mutant hA<sub>2A</sub>AR-K153A<sup>ECL2</sup> was constructed by the same procedure reported previously [20]. The wild type pcDNA3.1-A<sub>2A</sub>R plasmid DNA with N-terminal HA and FLAG tags and C-terminal His tag was used as a template for polymerase chain reaction (PCR) mutagenesis. Mutant primers for directional PCR product cloning were designed using the online Quickchange primer design program (Agilent Technologies, Santa Clara, CA), and primers were obtained from Eurogentec (Maastricht, The Netherlands). All DNA sequences were verified by Sanger sequencing at LGTC (Leiden, The Netherlands).

*Cell culture, transfection and membrane preparation* We followed the procedures reported previously [20,21]. Briefly, human embryonic kidney (HEK) 293 cells were grown as monolayers in Dulbecco's modified Eagle's medium supplemented with stable glutamine, 10% newborn calf serum, 50 µg/mL streptomycin, and 50 IU/mL penicillin at 37°C and 7% CO<sub>2</sub> atmosphere. The cells were transfected with mutant plasmid DNA using the calcium phosphate precipitation method, followed by a 48-hour incubation. And HEK293 hA<sub>2A</sub>AR wild type (hA<sub>2A</sub>AR-WT) cells were grown as monolayers on 15 cm ø culture plates to 80%-90% confluency in the same medium as the other HEK293 cells but with the addition of G-418 (500 mg/ml). For both cells were detached from the plates by scraping them into PBS and centrifuged to remove PBS buffer. The pellets were resuspended in ice-cold Tris-HCl buffer (50 mM, pH 7.4) and then homogenized. The cell membrane suspensions were centrifuged at 100,000 × g at 4°C for 20 minutes, after which the procedure was repeated one more time. After this, Tris-HCl buffer was used to resuspend the pellet, and adenosine deaminase was added to break down endogenous adenosine. Membranes were stored in 250 µL aliquots at -80°C until further use. Membrane protein concentrations were measured using the BCA method [22].

## Chapter 3

---

*Radioligand displacement assay* Radioligand displacement experiments were performed as follows. Membrane aliquots containing 10 µg of protein were incubated in a total volume of 100 µL of assay buffer to adjust the assay window to approximately 3000 DPM. Nonspecific binding was determined in the presence of 100 µM NECA and represented less than 10% of the total binding. Then to each tube were added 25 µL cell membrane (10 µg of protein), 25 µL of 2.7 nM radioligand [<sup>3</sup>H] ZM241383, 25 µL of assay buffer [25 mM Tris-HCl, pH 7.4 at 25°C, supplemented with 5 mM MgCl<sub>2</sub> and 0.1% (w/v) 3-[(3-cholamidopropyl) dimethylammonio]-1-propanesulfonate (CHAPS)] and 25 µL of the indicated compounds in increasing concentrations in the same assay buffer. The mixture was incubated at 25°C for 60 min to reach equilibrium. Incubations were terminated by rapid vacuum filtration to separate the bound and free radioligand through 96-well GF/B filter plates using a Perkin Elmer Filtermate-harvester (PerkinElmer, Groningen, Netherlands). Filters were subsequently washed three times with 2 mL of ice-cold buffer (25 mM Tris-HCl, pH 7.4, supplemented with 5 mM MgCl<sub>2</sub>). The filter-bound radioactivity was determined by scintillation spectrometry using a P-E 1450 Microbeta Wallac Trilux scintillation counter (PerkinElmer).

*Radioligand competition association assay* The binding kinetics assay to determine the unlabeled ligands was performed as described previously [21]. Briefly, the association of the radioligand was followed over time in the absence or presence of a concentration corresponding to the IC<sub>50</sub> value of unlabeled ZM241385, LUF6632 and LUF7445. In practice, to the mixture of equal volumes of radioligand, unlabeled compound and assay buffer was added a 25 µL membrane aliquot containing 10 µg of protein at each time point from 0.5 min to 240 min at 25°C. Incubation was terminated as described above (radioligand displacement assay).

*Irreversible binding of LUF7445 to both hA<sub>2A</sub>AR-WT and hA<sub>2A</sub>AR-K153A<sup>ECL2</sup> cell membranes* Both hA<sub>2A</sub>AR-WT and hA<sub>2A</sub>AR-K153A<sup>ECL2</sup> cell membrane aliquots were treated the same way as described in *radioligand displacement assay* to determine their assay window. Then 100 µL assay buffer containing either 1% DMSO (as blank control for total binding and non-specific binding) or 1 µM ligands (ZM241385 or LUF7445, 400 µM stock in assay buffer) was added to 2 mL Eppendorf tubes containing 100 µL cell membrane suspension and 200 µL assay buffer and incubated for 1 h at 25 °C. Subsequently, the mixture was centrifuged at 16,100 × g at 4°C for 5 minutes to remove the buffer with the 'free' ligands. The membrane pellet was resuspended in 1 mL assay buffer and spun for 5 min at 16,100 × g at 4°C. After three washing cycles, the cell pellets were resuspended in 300 µL assay buffer to determine their radioligand binding activity. Afterwards, all the samples were transferred to test tubes on



ice and 100  $\mu$ L (2.7 nM) radioligand [<sup>3</sup>H] ZM241383 was added, followed by a 0.5 h incubation at 25 °C. The incubation was terminated by vacuum filtration through a GF/B filter using a Brandel harvester to separate bound and free radioligand. The filters were washed three times with ice-cold wash buffer (25 mM Tris-HCl, pH 7.4 supplemented with 5 mM MgCl<sub>2</sub>). After harvesting, 3.5 mL of scintillation liquid was added and the filter-bound radioactivity was determined in a Tri-Carb 2900TR liquid scintillation analyser (PerkinElmer). Results are expressed as percentage normalized to the maximum specific binding in the control group (100%).

*Cyclic AMP functional assay* The LANCE ultra-cAMP 384 kit (PerkinElmer, Groningen, Netherlands) was used and all assay components were prepared according to the instructions of the manufacturer. Briefly, cAMP was generated in the stimulation buffer (*N*-2-hydroxyethylpiperazine-*N*-ethane sulfonic acid (HEPES), 5 mM; 0.1% (w/v) BSA; cilostamide, 50  $\mu$ M; rolipram, 50  $\mu$ M; adenosine deaminase (ADA), 0.8 IUmL<sup>-1</sup>). HEK293 hA<sub>2A</sub>AR cells were grown as monolayers to 80%-90% confluency and harvested by centrifugation for 5 min at 200  $\times$  g. Then 5000 cells per well were seeded in a 384 well plate, followed by a 1 h co-incubation with a mixture of 10 nM NECA (prepared in the stimulation buffer) and the antagonists (LUF7445 or ZM241385) at a concentration ranging from 1  $\mu$ M to 1 pM. Then the incubation was terminated by adding cAMP Tracer solution and anti-cAMP solution. Measurements of the generated fluorescence intensity were done on an EnVision Multilabel Reader (PerkinElmer, Groningen, Netherlands).

*Irreversible binding of LUF7445 to HEK293 hA<sub>2A</sub>AR cells assessed in cyclic AMP functional assay* All the assay components were prepared as described in the cAMP functional assay above. HEK293 hA<sub>2A</sub>AR cells were grown as monolayers to 80%-90% confluency and harvested by 200  $\times$  g centrifugation for 5 min. Then cells were pretreated with ligands at the concentration of their IC<sub>80</sub> values (determined in the cAMP functional assay above), or with stimulation buffer (pH 7.4) for 1 hour. Then, the pretreated cells were centrifuged for 5 min at 300  $\times$  g to remove the supernatant at 4 °C, after which the cell pellet was washed three times with 3  $\times$  1 mL stimulation buffer, separated by renewed incubation for 10 min at 25°C. These washed cells were seeded in a 384 well plate (5000 cells/well) as described in the cAMP functional assay above. Briefly, 10 nM NECA (prepared in the stimulation buffer) was co-incubated to stimulate cAMP production, followed by the termination by cAMP Tracer solution and anti-cAMP solution. Measurements of the generated fluorescence intensity were done on an EnVision Multilabel Reader (PerkinElmer, Groningen, Netherlands).

## Chapter 3

---

*Computer Modelling* All calculations were performed using the Schrodinger Suite [23]. The high-resolution crystal structure of the adenosine A<sub>2A</sub> receptor co-crystalized with a ZM241385 was used for the docking studies (PDB:4E1Y) [14]. The crystal structure was prepared using the preparation wizard, protonation states were assigned using PROPKA [24]. After the protein preparation we used the CovDock [25] module to perform covalent docking on residue LYS153EL2. Figures were rendered using PyMol [26].

*Data analysis* All the experimental data were analyzed with GraphPad Prism 6.0 software (GraphPad Software Inc., San Diego, CA). The radioligand displacement curves were fitted to a one-site binding model. Association data for the radioligand were fitted using one-phase exponential association. Values for k<sub>on</sub> were obtained by converting k<sub>obs</sub> values using the following equation: k<sub>on</sub> = (k<sub>obs</sub> - k<sub>off</sub>) / [radioligand], where k<sub>off</sub> values were cited from Guo et al [21]. Association and dissociation rates for unlabelled ligands were calculated by fitting the data in the competition association model using ‘kinetics of competitive binding’ [21, 27].

$$K_A = k_1[L] + k_2$$

$$K_B = k_3[L] + k_4$$

$$S = \text{Sqrt} [(K_A - K_B)^2 + 4 \cdot k_1 \cdot k_3 \cdot L \cdot I]$$

$$K_F = 0.5 (K_A + K_B + S)$$

$$K_S = 0.5 (K_A + K_B - S)$$

$$Q = B_{\max} \cdot k_1 \cdot L \cdot (K_F - K_S)^{-1}$$

$$Y = Q \cdot [k_4 \cdot (K_F - K_S) \cdot K_F^{-1} \cdot K_S^{-1} + (k_4 - K_F) \cdot K_F^{-1} \cdot e^{-K_F \cdot X} - (K_4 - K_S) \cdot K_S^{-1} \cdot e^{-K_S \cdot X}]$$

Where X is the time (min), Y is the specific [<sup>3</sup>H]-ZM241385 binding (DPM), k<sub>1</sub> and k<sub>2</sub> are the k<sub>on</sub> (nM<sup>-1</sup>min<sup>-1</sup>) and k<sub>off</sub> (min<sup>-1</sup>) of [<sup>3</sup>H]-ZM241385 and were obtained from Guo et al [21], L is the concentration of [<sup>3</sup>H]-ZM241385 used (nM), B<sub>max</sub> the total binding (DPM) and I the concentration of unlabeled ligand (nM). Fixing these parameters allows the following parameters to be calculated: k<sub>3</sub>, which is the k<sub>on</sub> value (nM<sup>-1</sup>min<sup>-1</sup>) of the unlabeled ligand and k<sub>4</sub>, which is the k<sub>off</sub> value (min<sup>-1</sup>) of the unlabeled ligand. The residence time (RT) was calculated using RT = 1 / k<sub>off</sub> [27]. Functional concentration-effect curves were fitted to a three-parameter concentration response model. Values are expressed as mean ± S.E.M. of three independent experiments performed in duplicate. Statistical analyses were performed using Student’s unpaired t-test (\*\*\*P < 0.001; \*\*P < 0.01; \*P < 0.05).

### 3. Results

#### 3.1. Design and synthesis of LUF7445

Over the years our research group has explored series of triazolotriazine derivatives based on the reference adenosine A<sub>2A</sub> antagonist ZM241385, 4-(2-(7-amino-2-(furan-2-yl)-[1,2,4]triazolo[1,5-a][1,3,5]triazin-5-ylamino)ethyl)phenol (Figure 1), to investigate their structure-activity and structure-kinetics relationships (SAR and SKR) [21,29]. We identified LUF6632 (Figure 1) as a long residence time (RT) compound compared to other derivatives. This compound prompted us to bring the concept of prolonged receptor occupancy further by aiming for a covalently binding derivative of ZM241385. Hence, LUF 7445 (Figure 1), 4-((3-((7-amino-2-(furan-2-yl)-[1,2,4]triazolo[1,5-a][1,3,5]triazin-5-yl)amino)propyl)carbamoyl)benzene sulfonyl fluoride was synthesized in three steps from sulfone compound 2-(furan-2-yl)-5-(methylsulfonyl)-[1,2,4] triazolo[1,5-a]-[1,3,5]triazin-7-amine as starting reagent. The reaction conditions and other reagents used are described in synthetic Scheme S1 of the SI.

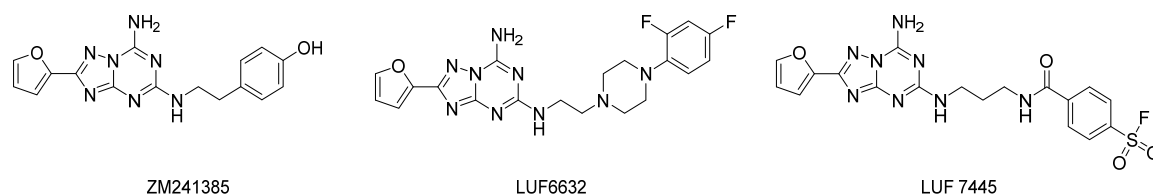


**Figure. 1** Chemical structures of the three hA<sub>2A</sub> receptor antagonists examined in this study.

#### 3.2. Determination of the affinity (K<sub>i</sub>) of LUF7445, LUF6632 and ZM241385 for the A<sub>2A</sub> receptor.

To determine the affinity (K<sub>i</sub>) for the A<sub>2A</sub> receptor LUF7445, LUF6632 and ZM241385 were tested in a [<sup>3</sup>H] ZM241385 displacement experiment (n = 3). All these compounds concentration-dependently inhibited specific [<sup>3</sup>H] ZM241385 binding from human A<sub>2A</sub> receptors overexpressed in HEK293 cell membranes (Figure 2). LUF6632, ZM241385 and LUF7445 showed similar affinities in the subnanomolar range (Table 1). It should be mentioned that the putative covalent nature of the interaction between receptor and LUF7445 precludes the determination of equilibrium binding parameters. Therefore, we expressed LUF7445's affinity for the A<sub>2A</sub> receptor as "apparent K<sub>i</sub>" (K<sub>i</sub><sup>\*</sup>).

## Chapter 3

**Table 1.** (Apparent) affinities of LUF7445, LUF6632 and ZM241385 for the A<sub>2A</sub> adenosine receptor.

Compound	pK <sub>i</sub> <sup>a</sup>	pK <sub>i</sub> <sup>b</sup>
	(0.5h)	(3h)
LUF7445 <sup>c</sup>	8.27±0.042	8.99±0.008***
LUF6632	9.17±0.007	9.26±0.004*
ZM241385	8.89±0.019	8.91±0.006

Data are expressed as means ± SEM of three separate experiments each performed in duplicate. \*P < 0.05, \*\*\*P < 0.001 compared with the pK<sub>i</sub> values in displacement experiments during 0.5h incubation time; Student's t-test.

<sup>a</sup>Affinity determined from displacement of specific [<sup>3</sup>H]ZM241385 binding from the hA<sub>2A</sub>AR at 25°C during 0.5 h incubation; <sup>b</sup>Affinity determined from displacement of specific [<sup>3</sup>H]ZM241385 binding from the hA<sub>2A</sub>AR at 25°C during 3 h incubation; <sup>c</sup>For LUF7445, the covalent antagonist, pK<sub>i</sub> values can only be apparent, as true equilibrium cannot be reached.

### 3.3. Time-dependent characterization of affinity for LUF7445, LUF6632 and ZM241385.

We then tested the time dependency of the affinity of the three compounds. To that end a [<sup>3</sup>H] ZM241385 displacement experiment was performed with an incubation time of both 0.5 hr and 3 hr. As detailed in Table 1, the affinity of LUF6632 slightly and of LUF7445 strongly increased with longer incubation time while ZM241385's affinity did not change. Representative graphs for this effect are in Figure 2, in which the curve representing a concentration-dependent inhibition of specific [<sup>3</sup>H] ZM241385 binding was shifted to the left with time for LUF7445 (Figure 2A), with little (LUF6632, Figure 2B) or no difference (ZM241385, Figure 2C) for the other two compounds.

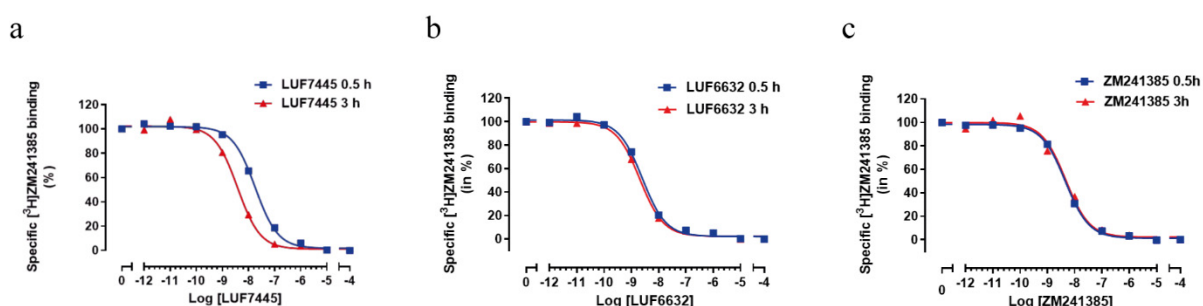


**Figure. 2** Displacement of specific [<sup>3</sup>H] ZM241385 binding from the adenosine hA<sub>2A</sub>AR receptor at 25°C by LUF7445 (a), LUF6632(b) and ZM241385(c) during an incubation of 0.5h (blue curve) and 3h (red curve), respectively. Representative graphs are from one experiment performed in duplicate.

Notably, compared to the long residence compound LUF6632, LUF7445 showed a more pronounced influence with prolonged incubation time, suggesting an increasing level of covalent binding over time. The combined data yielded an approx. 5-fold shift in apparent K<sub>i</sub> value for LUF7445. The affinities of the compound for the other adenosine receptor subtypes are reported in Table S1 of the SI, showing that LUF7445 is very selective towards A<sub>2A</sub> receptors.

### 3.4. Kinetic characterization of LUF6632, LUF7445 and ZM241385 in a competition association binding assay.

The ‘apparent K<sub>i</sub> shift’ of LUF7445 drove us to investigate the irreversible characteristics of LUF7445 binding by performing kinetic assays to determine its dissociation rate from the A<sub>2A</sub> adenosine receptor. In our previous research, the k<sub>on</sub> (k<sub>1</sub> = 0.24 ± 0.05 × 10<sup>8</sup> M<sup>-1</sup>·min<sup>-1</sup>) and k<sub>off</sub> (k<sub>2</sub> = 0.48 ± 0.03 min<sup>-1</sup>) values of [<sup>3</sup>H]-ZM241385 at 25°C have been determined by a traditional association and dissociation assay [21]. Here we derived the kinetic parameters, i.e. the k<sub>on</sub> (k<sub>3</sub>) and k<sub>off</sub> (k<sub>4</sub>) values, for the three unlabeled ligands from a competition association assay (Figure 3). Both LUF6632 (k<sub>on</sub> = 1.53 ± 0.083 nM<sup>-1</sup> min<sup>-1</sup>) and ZM241385 (k<sub>on</sub> = 1.72 ± 0.36 nM<sup>-1</sup> min<sup>-1</sup>) showed a similar association rate, which was significantly faster than for LUF7445 (k<sub>on</sub> = 0.0059 ± 0.00049 nM<sup>-1</sup> min<sup>-1</sup>).

**Table 2.** The (apparent) association and dissociation rate constants of LUF7445, LUF6632 and ZM241385 determined in competition association assays with [<sup>3</sup>H]-ZM241385 binding to HEK293-hA<sub>2A</sub>AR membranes

Compound	k <sub>on</sub> (nM <sup>-1</sup> min <sup>-1</sup> ) <sup>a</sup>	k <sub>off</sub> (min <sup>-1</sup> ) <sup>a</sup>	RT (min)
LUF7445 <sup>b</sup>	(0.0059 ± 0.00049)	(1.37 ± 0.68 × 10 <sup>-11</sup> )	(2.86 ± 0.87 × 10 <sup>11</sup> )
LUF6632	1.53 ± 0.083	0.15 ± 0.021	6.80 ± 0.97
ZM241385	1.72 ± 0.36	1.04 ± 0.13	0.96 ± 0.12

<sup>a</sup>Association [k<sub>on</sub>] and dissociation [k<sub>off</sub>] rate constants were determined by competition association assay at 25°C; all these values were determined by analyzing the data in the mathematical model described by Motulsky and Mahan [27];<sup>b</sup>For LUF7445, no equilibrium is reached between receptors and ligand, hence the Motulsky/Mahan mathematical model [27] for the competition association assay is not valid. The values obtained are therefore considered to provide qualitative insight only, and are in brackets.

As detailed in Table 2, LUF6632 displayed a dissociation rate constant of 0.15 ± 0.021 min<sup>-1</sup> which equals to a receptor RT of 6.80 ± 0.97 min, being 7 fold longer than ZM241385’s RT which was 0.96 ± 0.12 min at 25°C. Figure 3 shows that LUF7445’s behavior was very different, causing an initial ‘overshoot’ of the competition association curve which over time progressed to negligible radioligand binding at 240 min. Analyzing this curve with the (equilibrium) Motulsky and Mahan model [27] led to a negligible dissociation rate (k<sub>off</sub> = 1.37 ± 0.68 × 10<sup>-11</sup> min<sup>-1</sup>) and an almost infinite RT for LUF7445 (values between brackets in

Table 2). These data provided further evidence for a putative irreversible binding mode between LUF7445 and the hA<sub>2A</sub> adenosine receptor. This data is qualitatively summarized in a simplified scheme in the SI (Scheme 2).

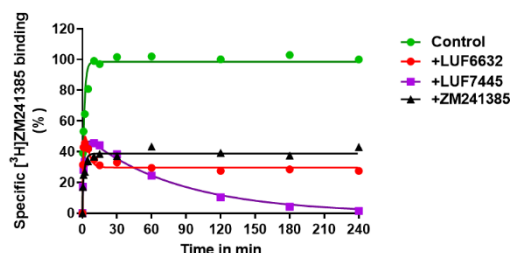


**Figure. 3** Competition association binding assay with [<sup>3</sup>H] ZM241385 in the absence or presence of indicated compounds at 25°C. Representative graphs are from one experiment performed in duplicate (see Table 2 for kinetic parameters).

### 3.5. Binding mode of LUF7445 in the hA<sub>2A</sub>AR binding pocket

Although the radioligand binding results above characterized LUF7445 as an irreversibly binding ZM241385 derivative, it remained to be tested what the target residue of the reactive warhead is. We therefore constructed a binding model based on the reported adenosine A<sub>2A</sub> X-ray crystal structure (PDB code: 4EIY) and chemical structure of LUF7445.

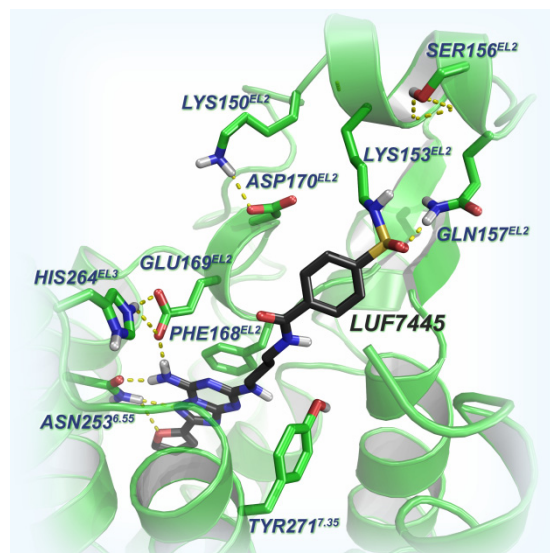


**Figure. 4** Binding model of LUF7445 in the hA<sub>2A</sub> adenosine receptor-binding pocket based on the hA<sub>2A</sub> adenosine receptor crystal structure (PDB code: 4EIY). The black carbon sticks represent the structure of LUF7445. The important residues and H-bonds for ligand recognition are indicated by yellow dashed lines.

From the docking result, the ZM241385 core structure, shown as black carbon sticks in Figure 4, is in the same position as ZM241385 in the A<sub>2A</sub> crystal structure, participating in H-bond formation with residues such as His264, Glu169, Phe168 and Asn253. Due to the flexibility

of the three-carbon linker a lysine residue in close proximity of the ligand, K153<sup>ECL2</sup>, could interact with the 4-fluorosulfonylbenzoic warhead in LUF7445 to form a covalent sulfonyl amide.

### 3.6. Lysine K153<sup>ECL2</sup> residue is the possible anchor point for covalent bond formation.

To investigate the structural nature of the interaction between the ligands and receptor, we therefore mutated the potential target lysine residue to alanine (A<sub>2A</sub>AR-K153A<sup>ECL2</sup> receptor) to compare with the wild type receptor and perform a “wash-out” experiment. Following preincubation with either LUF7445 or ZM241385, cell membranes overexpressing mutant A<sub>2A</sub>AR-K153A<sup>ECL2</sup> or wild type A<sub>2A</sub>AR were washed three times to remove the non-covalently bound ligands. After this repeated washing cell membranes were incubated with the radioligand [<sup>3</sup>H]ZM241385 to assess the remaining radioligand binding.

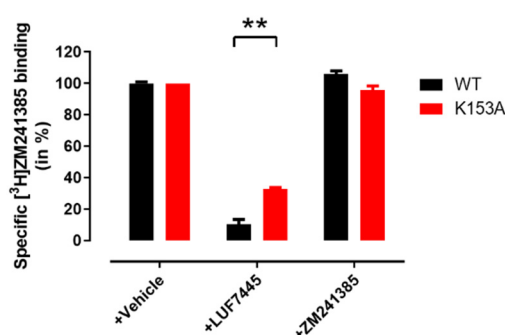


**Figure 5.** Involvement of Lys153 in the binding of LUF7445. HEK293 cell membranes overexpressing wild type or K153A mutant hA<sub>2A</sub> AR were pretreated with buffer (vehicle) or 1 μM of LUF7445 or ZM241385 for 1h followed by 3 wash cycles. The membranes were then subjected to a standard [<sup>3</sup>H] ZM241385 radioligand binding assay to measure remaining specific [<sup>3</sup>H] ZM241385 binding. Results were obtained from three independent experiments performed in duplicate. Data are normalized to 100% of the vehicle group response. Error bars indicate SEM values. \*\*Significant difference between groups (P<0.01); Student’s t-test

In the absence of antagonist (labeled ‘+ vehicle’ in Figure 5) both the mutant A<sub>2A</sub>AR-K153A<sup>ECL2</sup> and the wild type A<sub>2A</sub>AR receptor containing membranes had a similar recovery of radioligand binding, which we normalized to 100% recovery. LUF7445 caused a significant decrease of radioligand binding on the A<sub>2A</sub>AR WT cell membranes with only 10.4 ± 3.0% recovery of specific binding despite the extensive washing, while more radioligand binding was ‘saved’ at the cell membranes overexpressing A<sub>2A</sub>AR-K153A<sup>ECL2</sup> (32.8 ± 0.9% remaining). As a control, both cell membrane preparations preincubated with ZM241385 showed that ZM241385 was rapidly washed off the membranes, as a full recovery of radioligand binding was observed.



### 3.7. Functional characterization of LUF7445 and ZM241385 in cAMP assay

Functional characterization of these compounds in a cAMP assay on the HEK cells expressing the hA<sub>2A</sub>AR showed their antagonist behavior. The cAMP production was stimulated by the addition of the reference agonist NECA (10 nM). Both LUF7445 and ZM241385 caused a concentration-dependent inhibition of NECA's effect (100% in the absence of antagonist, see Figure 6a). The potency of LUF7445 ( $pIC_{50} = 8.10 \pm 0.044$ ) was somewhat lower than of ZM241385 ( $pIC_{50} = 8.71 \pm 0.13$ ). Again, it should be mentioned that LUF7445 precludes a true equilibrium affinity determination.

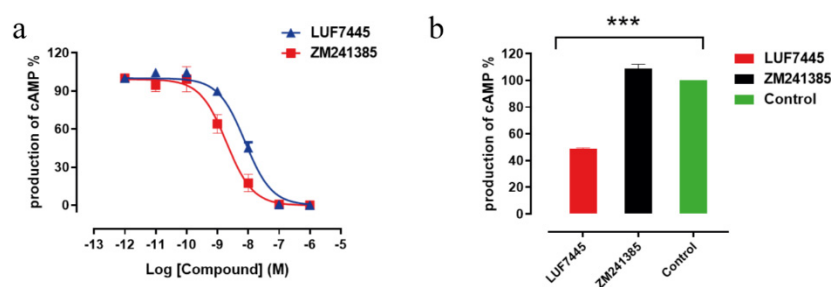


**Figure.6** Functional characterization of LUF7445 and ZM241385 on hA<sub>2A</sub> AR expressed in HEK293 cells (a) Concentration-inhibition curves for LUF7445 and ZM241385 in a cAMP assay in the presence of 10 nM NECA (100%). Results were obtained from three independent experiments performed in triplicate. (b) Recovery of cAMP production. Cells were pretreated with a concentration corresponding to the IC<sub>80</sub> value (retrieved from **Fig.6a**) of the indicated compound, or with buffer (control) for 1 hour. Then, 3 wash cycles were applied, followed by adding 10 nM NECA to stimulate cAMP production. Data are expressed as means  $\pm$  SEM of three separate experiments each performed in duplicate. \*\*\*Significant difference between groups ( $P < 0.001$ ); Student's t-test

From Figure 6a we determined the IC<sub>80</sub> values of the two compounds, which concentrations were then used to pretreat the HEK-A<sub>2A</sub>AR cells, followed by three wash steps. Thereafter, we stimulated the cAMP production in these cells with 10 nM NECA, resulting in a sustained inhibition of cAMP production in the presence of LUF7445 ( $48 \pm 1\%$ ), while ZM241385 showed no difference in restoration of cAMP production compared to the control cells in the absence of any indicated compound (Figure 6b). Apparently, the cAMP production induced by NECA in the presence of LUF7445 was inhibited under conditions where a reference antagonist did not, further validating LUF7445 as a covalent antagonist forming an irreversible bond with the hA<sub>2A</sub>AR.

## 4. Discussion

Covalent ligands for GPCRs are emerging as a useful tool for receptor structure-elucidation and the chartering of the ligand-receptor binding pocket. As an example, the 3D architecture



of the beta<sub>2</sub>-adrenergic receptor in an active conformation has been recently determined in the presence of a covalently binding derivative of noradrenaline [4,30]. In the current study we designed and synthesized a covalent antagonist (LUF7445) to investigate ligand-receptor interaction in the binding pocket of the hA<sub>2A</sub>AR, and compared its behavior to the reference antagonist ZM241,385 and the long residence time ZM-derivative LUF6632 [19]. All three compounds showed a high affinity for the hA<sub>2A</sub>AR.

The rational ligand design came from the reported crystal structures of the hA<sub>2A</sub>AR bound to ZM241385, providing a clear blueprint of ligand-binding interactions [13,14,31]. A deep, planar, and narrow cavity holds the aromatic core and furan ring of ZM241385, while the phenylethylamine substituent is directed to the extracellular region (EL2 and EL3). The architecture of the ligand binding pocket offered us a good starting point for the structural modification of ZM241385. Therefore, instead of the 4-hydroxyphenylethylamine side chain in ZM241,385, the electrophilic fluorosulfonyl group, chosen to permit a possible nitrogen-to-sulfur bond between the ligand and a nearby free amino group in the receptor, was introduced and incorporated in a linker to yield LUF7445.

A first hint of the covalent nature of LUF7445 was found in incubation time-dependent radioligand displacement assays. A longer incubation time rendered LUF7445 more potent in displacing the radioligand from the receptor, while this was not or hardly the case for ZM241384 and LUF6632, respectively. LUF6632 had previously been identified as an antagonist with a long residence time (>300 min) at the receptor, when assessed at 4 °C [19]. The current set of experiments was performed at 25 °C, making LUF6632 dissociate faster (RT = 6.8 min, Table 2) from the receptor with no substantial pK<sub>i</sub> shift in affinity at the two incubation times. Similar experiments on other GPCRs, such as CB<sub>1</sub> cannabinoid receptor [32,33] and histamine H<sub>2</sub> receptor [34], demonstrated that the covalent interaction between the ligand and the receptor resulted in a time-dependent affinity change.

However, it is far from conclusive to identify a presumed covalent ligand from an affinity shift alone, as pseudo-irreversible interactions can also occur caused by slow dissociation rates. From a kinetic perspective, a covalent ligand refers to a ligand that stays at the receptor for an infinite time period. If the incubation time is long enough, all receptors will be occupied by the covalent compound, rendering competitive radioligand binding impossible. In accordance with this, a continuing decrease of specific radioligand binding was observed in the kinetic experiments over a 4 h incubation at 25 °C (Figure 3). The inadequacy of the

## Chapter 3

---

Motulsky-Mahan equations [27] to fit this data is further evidence for the non-equilibrium features of the binding of LUF7445 to the receptor. Furthermore, extensive washing did not free the receptors from LUF7445, as demonstrated by the lack of [<sup>3</sup>H]ZM241385 binding (Figure 5, WT receptor), compared to a full recovery of membranes pretreated with ZM241385. This confirms the washing steps did remove the reversible ligand from the receptors, and in return validates the irreversible binding of LUF7445 to the hA<sub>2A</sub>AR. Similar findings were obtained on the adenosine A<sub>1</sub> receptor and histamine H<sub>4</sub> receptor where preincubation of a covalently binding ligand concentration-dependently decreased radioligand binding after extensive washing of the cell membrane preparation [7, 35].

Based on the ZM241385 binding mode of the hA<sub>2A</sub>AR, we hypothesized that LUF7445 covalently interacts with a lysine residue, K153<sup>ECL2</sup>, resulting in a sulfonamide bond formation (Figure 4). Hence, the K153A<sup>ECL2</sup> mutant construct, potentially preventing the covalent bond from being formed, was made to perform a similar wash-out experiment as described above. Since ZM241385 showed a similar affinity for both the K153A<sup>ECL2</sup> mutant (pK<sub>i</sub> = 7.83 ± 0.04) and WT receptors (pK<sub>i</sub> = 7.91 ± 0.05) [20], we assumed that the difference in radioligand binding recovery was not due to a point mutation within a receptor binding site, which has the potential of altering ligand binding properties. Moreover, in the absence of either LUF7445 or ZM241385, the apparently same binding capacity (data not shown) proved that the washing steps had little influence on the integrity of both WT hA<sub>2A</sub>AR and mutant A<sub>2A</sub>AR-K153A<sup>ECL2</sup>. The mutation led to a three-fold increase of binding recovery indicating a substantially decreased level of covalent binding to the cell membranes, resulting from a decreased possibility to form a covalent bond between the warhead and a target residue. The mutation did not lead to a full recovery of radioligand binding, however, suggesting that other unidentified residues may play a similar role. Likewise, Nijmeijer et al identified a cysteine amino acid to be the linking residue for the covalent probe at the histamine H<sub>4</sub> receptor mentioned above [35], and it may be that the very reactive fluorosulfonyl warhead in LUF7445 also targets other residues such as cysteines [36].

A covalent antagonist will decrease the maximal agonist-induced effect by a permanent occupancy of the available receptors, which was indeed demonstrated in the functional assay. The concentration-effect curves obtained in the cAMP functional assay showed an antagonistic behavior of LUF7445 (Figure 6A). A much lower stimulation by AR receptor agonist NECA was observed as the number of available receptors was most likely reduced by the irreversible binding of LUF7445 (Figure 6B). A similar experiment at the adenosine A<sub>1</sub>

receptor showed that the irreversible binding by FSCPX decreased the maximal effect in the agonist dose-response curves [37]. All these results contributed to our hypothesis that LUF7445 is an insurmountable antagonist for the hA<sub>2A</sub>AR indeed, and that the fluorosulfonyl group present in LUF7445 reacts with K153<sup>ECL2</sup> via a covalent modification.

Besides in clinical trials for Parkinson's disease, A<sub>2A</sub> antagonists have risen to prominence as a future add-on to cancer combination therapy. Under chronic hypoxic conditions within the tumor microenvironment, increased accumulation of extracellular adenosine around the tumor tissue activates A<sub>2A</sub>ARs in the vicinity, which promotes peripheral tolerance by inducing T-cell anergy and the generation of adaptive regulatory T cells [38]. In contrast, blockade of A<sub>2A</sub>ARs plays a vital role in retardation of tumor growth, relieving immune cells from their repressed conditions, reducing the metastasis of tumors [39], and thus boosting antitumor immunity. As a consequence, potent A<sub>2A</sub> receptor antagonists are now being considered as potential therapeutics in diminishing the rate of cancer development [40,41]. The starting point of our design strategy, ZM241385, has been reported to significantly inhibit melanoma growth and reinforce the antineoplastic immune response, when combined with anti-CTLA4mAb [42]. However, *in vivo* tumor rejection during treatment with ZM241385 failed to take place most likely because of ZM241385's short half-life [11]. In addition, we speculate that the relatively short receptor residence time of ZM241385 at physiological temperature is another aspect that allows the massive amounts of adenosine produced in the tumor environment to continue to activate the A<sub>2A</sub>AR. Thus, a covalently binding antagonist such as LUF7445 may be a better proposition under these conditions.

### 5. Conclusion

The structure-based design of LUF7445, an antagonist for the human A<sub>2A</sub>AR, is reported in this study. In a number of *in vitro* assays, we obtained accumulating evidence for the covalent nature of the ligand's interaction with the receptor. More specifically, LUF7445 appeared to bind covalently to a lysine residue in the extracellular domain of the receptor (K153<sup>ECL2</sup>). Its antagonistic nature was confirmed in a functional assay, as it blocked hA<sub>2A</sub>AR-mediated cAMP accumulation by agonist NECA. The results contribute to a better understanding of long-lasting effects caused by ligands covalently reacting/interacting with GPCRs. In itself LUF7445 may be a probe to explore the added value of covalent antagonists for the adenosine A<sub>2A</sub> receptor in certain disease states such as cancer immunology, in which high adenosine levels are causative. In the end, rational design of covalent probes may have further value in

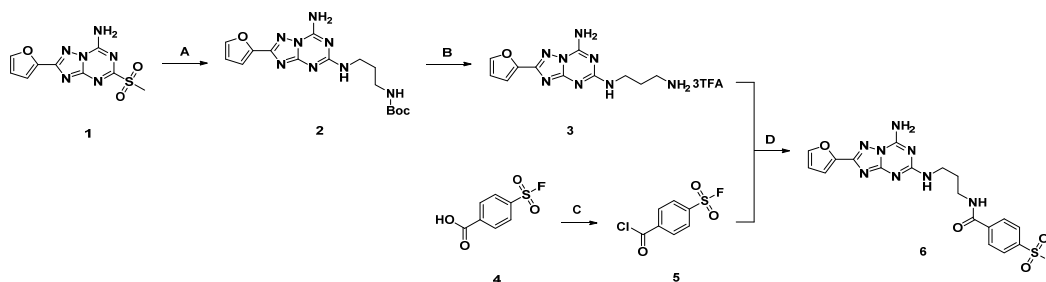
new technologies such as activity-based protein profiling with the perspective of imaging or structural probing of GPCRs.

### 6. Supporting information

#### 6.1. Chemistry

All solvents and reagents were purchased from commercial sources and were of analytical grade.  $^1\text{H}$  NMR spectra were recorded on a Bruker AV 400 liquid spectrometer ( $^1\text{H}$  NMR, 400 MHz) at ambient temperature. Chemical shifts are reported in parts per million (ppm), are designated by  $\delta$ . Coupling-constants are reported in Hz and are designated as  $J$ . Analytical purity of the final compounds was determined by high pressure liquid chromatography (HPLC) with a Phenomenex Gemini 3 $\mu$  C18 110A column (50  $\times$  4.6 mm, 3  $\mu\text{m}$ ), measuring UV absorbance at 254 nm. Sample preparation and HPLC method was as follows: 0.5 mg of compound was dissolved in 1 mL of a 1:1:1 mixture of  $\text{CH}_3\text{CN}/\text{H}_2\text{O}/\text{tBuOH}$  and eluted from the column within 15 min, with a three component system of  $\text{H}_2\text{O}/\text{CH}_3\text{CN}/1\%$  TFA in  $\text{H}_2\text{O}$ , decreasing polarity of the solvent mixture in time from 80/10/10 to 0/90/10. All compounds showed a single peak at the designated retention time and are at least 95% pure. Liquid chromatography–mass spectrometry (LC–MS) analyses were performed using Thermo Finnigan Surveyor – LCQ Advantage Max LC-MS system and a Gemini C18 Phenomenex column (50  $\times$  4.6 mm, 3  $\mu\text{m}$ ). The sample preparation was the same as for HPLC analysis. The elution method was set up as follows: 1–4 min isocratic system of  $\text{H}_2\text{O}/\text{CH}_3\text{CN}/1\%$  TFA in  $\text{H}_2\text{O}$ , 80:10:10, from the 4th min, a gradient was applied from 80:10:10 to 0:90:10 within 9 min, followed by 1 min of equilibration at 0:90:10 and 1 min at 80:10:10. Thin-layer chromatography (TLC) was routinely performed to monitor the progress of reactions, using aluminum coated Merck silica gel F254 plates. Purification by column chromatography was achieved by use of Grace Davison DAVISIL silica column material (LC60A 30–200 micron). Solutions were concentrated using a Heidolph laborota W8 2000 efficient rotary evaporation apparatus and by a high vacuum on a Binder APT line Vacuum Drying Oven. The procedure for the synthesis of similar compounds is given as a general procedure.

Scheme 1. Synthesis route of LUF7445.



Reagents and conditions: A) *tert*-Butyl (3-aminopropyl) carbamate, MeCN, reflux, 60 h; B) TFA, DCM, room temperature, 0.5 h; C) SOCl<sub>2</sub>, reflux, 2 h; D) triethylamine, dry dioxane, 70 °C, 18 h.

***tert*-Butyl (3-((7-amino-2-(furan-2-yl)-[1,2,4]triazolo[1,5-*a*][1,3,5]triazin-5-yl)amino)propyl)carbamate (2)** 2-(Furan-2-yl)-5-(methylsulfonyl)-[1,2,4]triazolo[1,5-*a*][1,3,5]triazin-7-amine (**1**) (280 mg, 1 mmol, 1 eq), which was synthesized as previously reported [20], was suspended in acetonitrile (to give a 0.1 M solution). *tert*-Butyl (3-aminopropyl)carbamate (0.19 mL, 1.10 mmol, 1.1 eq) was added. The mixture was heated to 70 °C for 60 h. The final crude mixture was purified using flash column chromatography (DCM:EtOAc → EtOAc). Flash column (DCM:EtOAc, 50% → 100% EtOAc) gave a yellowish solid (310 mg, 0.83 mmol, 41% yield). <sup>1</sup>H NMR (400 MHz, DMSO-*d*<sub>6</sub>) δ 8.50–7.94 (m, 2H), 7.91–7.83 (m, 1H), 7.48–7.40 (m, rotamer 1, 0.30H), 7.36 (t, *J* = 5.6 Hz, rotamer 2, 0.70H), 7.04 (d, *J* = 3.3 Hz, 1H), 6.90–6.76 (m, 1H), 6.67 (dd, *J* = 3.0, 1.7 Hz, rotamer 3, 0.85H), 6.49–6.39 (m, rotamer 4, 0.15), 3.24 (q, *J* = 6.7 Hz, 2H), 2.97 (q, *J* = 6.4 Hz, 2H), 1.72–1.56 (m, 2H), 1.37 (s, 9H) ppm.

**N<sup>5</sup>-(3-aminopropyl)-2-(furan-2-yl)-[1,2,4]triazolo[1,5-*a*][1,3,5]triazine-5,7-diamine (3)** Boc protecting groups were removed by dissolving (**2**) (374 mg, 1 mmol, 1 eq) in DCM, adding TFA (3.9 mL, 50 mmol, 50 eq) and removal of solvents after the reaction was finished. The remaining material was co-evaporated thrice with H<sub>2</sub>O and once with acetone, affording the triple TFA salt in quantitative yield. <sup>1</sup>H NMR (400 MHz, DMSO-*d*<sub>6</sub>) δ 8.61–8.04 (m, 2H), 7.88 (s, 1H), 7.70 (brs, 3H), 7.63–7.53 (m, 1H), 7.12–7.01 (m, 1H), 6.68 (dd, *J* = 3.3, 1.7 Hz, rotamer, 0.95H), 6.64–6.59 (m, rotamer, 0.05H), 3.40–3.28 (m, 2H), 2.85 (q, *J* = 6.7 Hz, 2H), 1.89–1.68 (m, 2H) ppm.

**4-Fluorosulfonyl benzoylchloride (5)** Commercially available 4-fluorosulfonylbenzoic acid (500 mg, 2.45 mmol, 1 eq) was dissolved in thionyl chloride (8.89 mL, 122.4 mmol, 50 eq) and heated at 70 °C under N<sub>2</sub> atmosphere. After 2 h, all material was dissolved and the thionyl chloride was removed by evaporation. The crude product was co-evaporated twice with

## Chapter 3

toluene to give a brown liquid that solidified when it cooled down to room temperature. The resulting product was used directly in the next step.  $^1\text{H NMR}$  (400 MHz, Acetone- $d_6$ )  $\delta$  8.52 (d,  $J = 8.5$  Hz, 2H), 8.39 (d,  $J = 8.7$  Hz, 2H).

**4-((3-((7-amino-2-(furan-2-yl)-[1,2,4]triazolo[1,5-*a*][1,3,5]triazin-5-yl)amino)propyl)carbamoyl) benzene sulfonyl fluoride (6) LUF7445(3)** (TFA salt, 322 mg, 0.83 mmol, 1 eq) was added to dry dioxane (5 mL). **(5)** (184 mg, 0.92 mmol, 1.1 eq) was added along with triethylamine (0.3 mL, 2.49 mmol, 3 eq). The mixture was heated to 70 °C for 18 h. The reaction was finished, solvents were removed and a flash column (EtOAc→ 99% EtOAc + 1% AcOH) was used. Subsequent washing with acetone of the obtained solids gave the title compound as a white solid (77mg, 0.18 mmol, 22% yield).  $^1\text{H NMR}$  (400 MHz, DMSO- $d_6$ )  $\delta$  8.90 (t,  $J = 6.0$  Hz, 1H), 8.52–8.02 (m, 6H), 7.87 (s, 1H), 7.58–7.44 (m, 1H), 7.04 (d,  $J = 3.3$  Hz, 1H), 6.68 (dd,  $J = 3.3, 1.8$  Hz, 1H), 3.36-3.33 (m, 4H), 1.80 (pent,  $J = 6.3$  Hz, 2H) ppm. **HPLC**: 96.7%, RT 7.40 min. **LC-MS**: [ESI+H] $^+$ : 461.13

### 6.2. Biology.

Table S1. Affinities of LUF7445 at the other adenosine receptor subtypes. Data are expressed as means  $\pm$  SEM or percentage displacement at 1  $\mu\text{M}$  of three separate experiments each performed in duplicate.

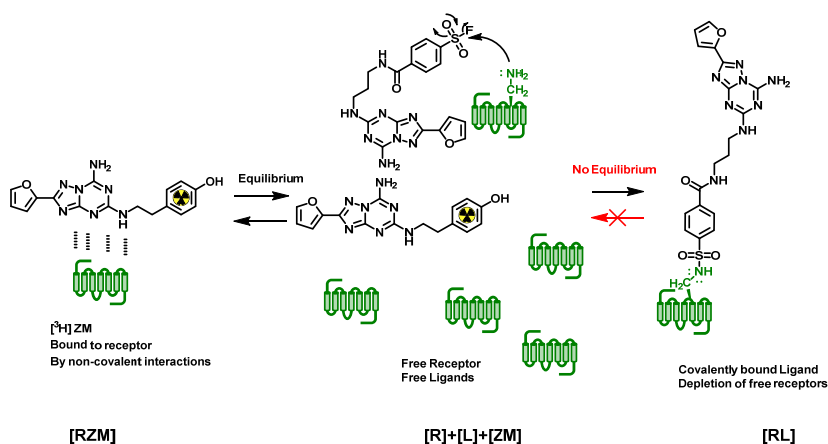
Compound	$pK_i$ or displacement at 1 $\mu\text{M}$ (%)			
	hA $_1$ <sup>a</sup>	hA $_{2A}$ <sup>b</sup>	hA $_{2B}$ <sup>c</sup>	hA $_3$ <sup>d</sup>
LUF7445	6.43 $\pm$ 0.095	8.99 $\pm$ 0.008	0.0% (2.0, -4.7, -2.6)	7.31 $\pm$ 0.083

<sup>a</sup>Affinity determined from displacement of specific [ $^3\text{H}$ ]DPCPX binding on CHO cell membranes stably expressing human adenosine A $_1$  receptors at 25°C during 3h incubation;

<sup>b</sup>Affinity determined from displacement of specific [ $^3\text{H}$ ]ZM241385 binding from the hA $_{2A}$ AR at 25°C during 3h incubation;

<sup>c</sup>% displacement at 1  $\mu\text{M}$  concentrations of specific [ $^3\text{H}$ ]PSB603 binding on CHO cell membranes stably expressing human adenosine A $_{2B}$  receptors at 25°C during 3h incubation;

<sup>d</sup>Affinity determined from displacement of specific [ $^3\text{H}$ ]PSB-11 binding on CHO cell membranes stably expressing human adenosine A $_3$  receptors at 25°C during 3h incubation



Scheme 2. Simplified representation of interaction between LUF7445 and hA<sub>2A</sub>AR during a competition association assay. The radiolabeled ZM-receptor complex ([RZM]) is being measured. If a compound L, such as LUF7445, binds covalently, the equilibrium shifts to the right ([RL]). The longer the incubation, the more receptors will be occupied by LUF7445.

### References

1. Overington J.P, Al-Lazikani B, Hopkins A.L *Nat Rev Drug Discov.* **2006** 5 (12):993-996.
2. Katritch V, Cherezov V, Stevens R.C *Annu Rev Pharmacol Toxicol.* **2013** (53):531-556.
3. Rosenbaum DM, Rasmussen SGF, Kobilka BK. *Nature.* **2009** 459 (7245):356-363.
4. Lagerstrom MC, Schiöth HB. *Nat Rev Drug Discov.* **2008** 7 (4):339-357.
5. Jacobson KA, Barone S, Kammula U, Stiles GL. *J Med Chem.* **1989** 32 (5):1043-1051.
6. Srinivas M, Shryock JC, Scammells PJ, Ruble J, Baker SP, Belardinelli L. *Mol Pharmacol.* **1996** 50 (1):196-205
7. van Muijlwijk-Koezen JE, Timmerman H, van der Sluis RP, van de Stolpe AC, Menge WMPB, Beukers MW, van der Graaf PH, de Groote M, IJzerman AP. *Bioorg Med Chem Lett.* **2001** 11 (6):815-818.
8. Shryock JC, Snowdy S, Baraldi PG, Cacciari B, Spalluto G, Monopoli A, Ongini E, Baker SP, Belardinelli L. *Circulation.* **1998** 98 (7):711-718.
9. Ruiz MD, Lim YH, Zheng JY. *J Med Chem.* **2014** 57 (9):3623-3650.
10. Schwarzschild MA, Agnati L, Fuxe K, Chen JF, Morelli M. *Trends Neurosci.* **2006** 29 (11):647-654.
11. Ohta A, Gorelik E, Prasad SJ, Ronchese F, Lukashev D, Wong MKK, Huang XJ, Caldwell S, Liu KB, Smith P, Chen JF, Jackson EK, Apasov S, Abrams S, Sitkovsky M. *P Natl Acad Sci USA.* **2006** 103 (35):13132-13137.
12. Xu F, Wu HX, Katritch V, Han GW, Jacobson KA, Gao ZG, Cherezov V, Stevens RC. *Science* **2011** 332 (6027):322-327.
13. Jaakola VP, Griffith MT, Hanson MA, Cherezov V, Chien EYT, Lane JR, IJzerman AP, Stevens RC. *Science* **2008** 322 (5905):1211-1217.
14. Liu W, Chun E, Thompson AA, Chubukov P, Xu F, Katritch V, Han GW, Roth CB, Heitman LH, IJzerman AP, Cherezov V, Stevens RC. *Science.* **2012** 337 (6091):232-236.
15. Barrington WW, Jacobson KA, Hutchison AJ, Williams M, Stiles GL. *P Natl Acad Sci USA.* **1989** 86 (17):6572-6576.
16. Moss SM, Jayasekara PS, Paoletta S, Gao ZG, Jacobson KA. *ACS Med Chem Lett.* **2014** 5 (9):1043-1048.

## Chapter 3

---

17. Niiya K, Jacobson KA, Silvia SK, Olsson RA. *Naunyn Schmiedebergs Arch Pharmacol.* **1993** 347 (5):521-526.
18. Ji XD, Gallo-Rodriguez C, Jacobson KA. *Drug Dev Res.* **1993** 29 (4):292-298.
19. Guo D, Xia LZ, van Veldhoven JPD, Hazeu M, Mocking T, Brussee J, IJzerman AP, Heitman LH. *ChemMedChem.* **2014** 9 (4):752-761.
20. Guo D, Pan AC, Dror RO, Mocking T, Liu R, Heitman LH, Shaw DE, IJzerman AP. *Mol Pharmacol.* **2016** 89 (5):485-491.
21. Guo D, Mulder-Krieger T, IJzerman AP, Heitman LH. *Brit J Pharmacol.* **2012** 166 (6):1846-1859.
22. Smith PK, Krohn RI, Hermanson GT, Mallia AK, Gartner FH, Provenzano MD, Fujimoto EK, Goeke NM, Olson BJ, Klenk DC. *Anal Biochem.* **1985** 150 (1):76-85.
23. Xiao WB, Nishimoto H, Hong H, Kitaura J, Nunomura S, Maeda-Yamamoto M, Kawakami Y, Lowell CA, Ra CS, Kawakami T. *J Immunol.* **2005** 175 (10):6885
24. Bas DC, Rogers DM, Jensen JH. *Proteins* **2008** 73 (3):765-783.
25. Zhu K, Borrelli KW, Greenwood JR, Day T, Abel R, Farid RS, Harder E. *J Chem Inf Model.* **2014** 54 (7):1932-1940.
26. Motulsky AG. *Biomed Pharmacother.* **1984** 38(4):185-186.
27. Motulsky HJ, Mahan LC. *Mol Pharmacol.* **1984** 25 (1):1-9.
28. Copeland RA. *Methods Biochem Anal.* **2005** 46:1-265.
29. de Zwart M, Vollinga RC, Beukers MW, Slegers DF, Kunzel JKVD, de Groot M, IJzerman AP. *Drug Dev Res.* **1999** 48 (3):95-103.
30. Weichert D, Kruse AC, Manglik A, Hiller C, Zhang C, Hubner H, Kobilka BK, Gmeiner P. *P Natl Acad Sci USA* **2014** 111 (29):10744-10748.
31. Segala E, Guo D, Cheng RK, Bortolato A, Deflorian F, Dore AS, Errey JC, Heitman LH, IJzerman AP, Marshall FH, Cooke RM. *J Med Chem.* **2016** 59 (13):6470-6479.
32. Li C, Xu W, Vadivel SK, Fan PS, Makriyannis A. *J Med Chem.* **2005** 48 (20):6423-6429.
33. Ogawa G, Tius MA, Zhou H, Nikas SP, Halikhedkar A, Mallipeddi S, Makriyannis A. *J Med Chem.* **2015** 58 (7):3104-3116.
34. Kijima H, Isobe Y, Muramatsu M, Yokomori S, Suzuki M, Higuchi S. *Biochem Pharmacol.* **1998** 55 (2):151-157.
35. Nijmeijer S, Engelhardt H, Schultes S, van de Stolpe AC, Lusink V, de Graaf C, Wijtmans M, Haaksma EEJ, de Esch IJP, Stachurski K, Vischer HF, Leurs R. *Brit J Pharmacol.* **2013** 170 (1):89-100.
36. Narayanan A, Jones LH. *Chem Sci.* **2015** 6 (5):2650-2659.
37. Lorenzen A, Beukers MW, van der Graaf PH, Lang H, van Muijlwijk-Koezen J, de Groot M, Menge W, Schwabe U, IJzerman AP. *Biochem Pharmacol.* **2002** 64 (8):1251-1265.
38. Zarek PE, Huang CT, Lutz ER, Kowalski J, Horton MR, Lindens J, Drake CG, Powel JD. *Blood.* **2008** 111 (1):251-259.
39. Beavis PA, Divisekera U, Paget C, Chow MT, John LB, Devaud C, Dwyer K, Stagg J, Smyth MJ, Darcy PK. *P Natl Acad Sci USA.* **2013** 110 (36):14711-14716.
40. Leone RD, Lo YC, Powell JD. *Comput Struct Biotech.* **2015** 13:265-272.
41. Mahoney KM, Rennert PD, Freeman GJ. *Nat Rev Drug Discov.* **2015** 14 (8):561-584.
42. Iannone R, Miele L, Maiolino P, Pinto A, Morello S. *Am J Cancer Res.* **2014** 4 (2):172-1



# Chapter 4

## Development of Covalent Ligands for G Protein-Coupled Receptors: A Case for the Human Adenosine A<sub>3</sub> Receptor

*Xue Yang,*

*Jacobus P.D. van Veldhoven,*

*Jelle Offringa,*

*Boaz J. Kuiper,*

*Eelke B. Lenselink,*

*Laura H. Heitman,*

*Daan van der Es*

*Adriaan P. IJzerman\**

J Med Chem. 2019 Apr 11;62(7):3539-3552.

doi:10.1021/acs.jmedchem.8b02026



### Abstract

The development of covalent ligands for G protein-coupled receptors (GPCRs) is not a trivial process. Here, we report a streamlined workflow thereto from synthesis to validation, exemplified by the discovery of a covalent antagonist for the human adenosine A<sub>3</sub> receptor (hA<sub>3</sub>AR). Based on the 1*H*,3*H*-pyrido[2,1-*f*]purine-2,4-dione scaffold, a series of ligands bearing a fluorosulfonyl warhead and varying linker was synthesized. This series was subjected to an affinity screen, revealing compound **17b** as the most potent antagonist. In addition, a nonreactive methylsulfonyl derivative **19** was developed as a reversible control compound. A series of assays, comprising time-dependent affinity determination, washout experiments and [<sup>35</sup>S]GTPγS binding assays, then validated **17b** as covalent antagonist. A combined in silico hA<sub>3</sub>AR-homology model- and site-directed mutagenesis study was performed to demonstrate that amino acid residue Y265<sup>7,36</sup> was the unique anchor point of the covalent interaction. This workflow might be applied to other GPCRs to guide the discovery of covalent ligands.

## 1. Introduction

The adenosine A<sub>3</sub> receptor (A<sub>3</sub>AR) is one of four G protein-coupled receptor subtypes stimulated by adenosine [1]. Different from the other subtypes (A<sub>1</sub>, A<sub>2A</sub> and A<sub>2B</sub>) A<sub>3</sub>AR was identified by molecular biology studies prior to its pharmacological characterization [2]. The initial studies indicated its important role in both physiological and pathophysiological conditions, such as cell proliferation, cell differentiation, neuroprotection, cardioprotection and apoptosis [3]. Nevertheless, the medical relevance of the human adenosine A<sub>3</sub> receptor (hA<sub>3</sub>AR) is enigmatic due to its dichotomy in different therapeutic applications [3]. In this regard, there is a continuing interest in the development of the selective ligands of the hA<sub>3</sub>AR to investigate its pharmacological effects. For instance, selective A<sub>3</sub>AR antagonists have been applied for the treatment of glaucoma [4] and respiratory tract inflammation such as asthma [5]. In particular, a tricyclic xanthine derivative, 1-benzyl-8-methoxy-3-propyl-1*H*,3*H*-pyrido[2,1-*f*]purine-2,4-dione (compound **1**, Figure 1a), has been reported to exert high affinity for the hA<sub>3</sub>AR [6-8].

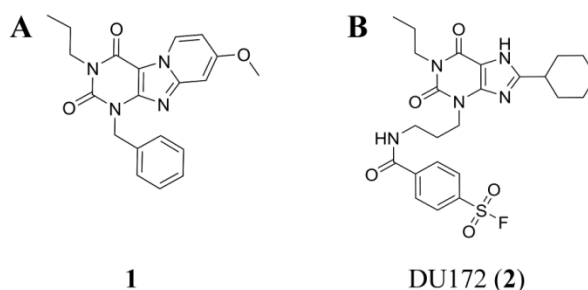


**Figure 1.** (A) Reference antagonist (**1**) for hA<sub>3</sub>AR. (B) DU172 (**2**), a covalent antagonist for hA<sub>1</sub>AR.

Initial efforts to study the structural biology of GPCRs suffered from numerous limitations, such as low expression, dynamic conformational states, and inherent instability. Covalent ligands, i.e., compounds that irreversibly bind to the receptor and possess a reactive moiety to target specific amino acid residues, helped to solve some of these obstacles [9]. This is also the case for adenosine receptors. For example, the structure of the human adenosine A<sub>1</sub> receptor, having the highest similarity to hA<sub>3</sub>AR among all adenosine receptors subtypes (61% of sequence homology) [10], has been elucidated by X-ray crystallography with a covalent antagonist DU172 (**2**) (Figure 1b) [11]. However, the application of covalent ligands in hA<sub>3</sub>AR studies has been limited to the characterization of the receptor type [12-14], far from providing a comprehensive study of receptor structure elucidation, pharmacological characteristics and ligand-receptor binding description.

To this end, we devoted our efforts to the discovery of a well-defined covalent antagonist based on xanthine analogue **1** mentioned above. Inspired by the resemblance in chemical structure between the potent hA<sub>3</sub>AR antagonist **1** and irreversible adenosine A<sub>1</sub> receptor antagonist **2**, we incorporated the reactive moiety, a fluorosulfonyl benzoyl group, connected to a spacer, at the N<sup>1</sup> position of the scaffold. Using a structured approach to bring the reactive fluorosulfonyl group in close proximity to a nucleophilic amino acid residue, we diversified the type of linker, linker length and position of the fluorosulfonyl substituent on the phenyl group, resulting in a series of analogues with a wide range of affinities. Our efforts led to the discovery of a best-in-class antagonist, **17b**, which bound to hA<sub>3</sub>AR with an apparent affinity in the nanomolar range. To keep the chemical structure similarity, we replaced the warhead with a methylsulfonyl moiety to obtain a non-reactive derivative **19** as a reversible control compound. **17b** was then validated to covalently bind and inactivate the hA<sub>3</sub>AR in an insurmountable manner. Molecular modelling suggested the fluorosulfonyl functionality of **17b** in close proximity to Y265<sup>7,36</sup>, which was identified as the unique anchor point of the covalent interaction in a subsequent mutagenesis study. The confirmed binding mode between this novel covalent antagonist and hA<sub>3</sub>AR opens the door for exploring other ligand binding motifs and will benefit receptor stabilization and further structure elucidation of the hA<sub>3</sub>AR.

## 2. Results and Discussion

### 2.1. Design of Covalent hA<sub>3</sub>AR Antagonists

In previous studies, our research group disclosed several series of hA<sub>3</sub>AR antagonists based on the pyrido[2,1-*f*]purine-2,4-dione scaffold [6-8]. Using compound **1**, a nanomolar probe from the previous series, as the starting point, we further designed and synthesized compounds based on a previously suggested binding mode of the pyrido[2,1-*f*]purine-2,4-dione scaffold [7]. When examining the suggested binding mode of this scaffold, we noted that this scaffold inserted into the binding pocket with a receptor interaction between TM3, TM6 and EL2. Two key H-bonds include the carbonyl-oxygen at the C<sup>4</sup>-position with residue N250<sup>6,55</sup> and the methoxy substituent at the C<sup>8</sup>-position bonding to Q167<sup>EL2</sup>. Taking this into account, we reasoned the only available space to incorporate the reactive warhead is limited to C<sup>1</sup>-position substituents.

To explore the chemical space required to optimally position the warhead in close proximity to a nucleophilic amino acid residue, we examined various linker systems, connecting the warhead and the pyrido[2,1-*f*]purine-2,4-dione scaffold. First, variation in the length of the spacer, between two and four carbon atoms, may offer more steric freedom allowing the

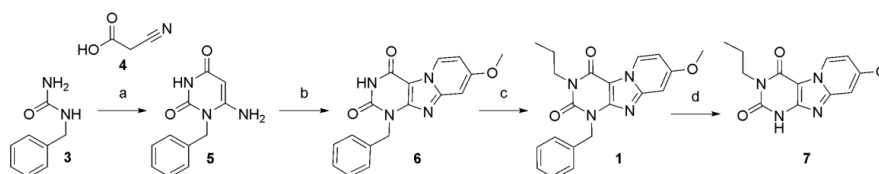
## Chapter 4

fluorosulfonyl group to orient toward an adjacent nucleophilic residue in the receptor binding site [15, 16]. Additionally, the type of chemical bond connecting the warhead to the spacer was varied between the slightly differently oriented ester or amide bond. Finally, since the exact position of an appropriate nucleophilic residue is unknown, the sulfonyl fluoride moiety was positioned at either the 3- or 4-position of the phenyl ring. To this end, four series of compounds **13a-c**, **14a-c**, **17a-c** and **18a-c**, bearing three different spacer lengths, ester or amide linkage and 3- or 4-fluorosulfonylphenyl warhead were targeted for synthesis.

### 2.2. Synthesis.

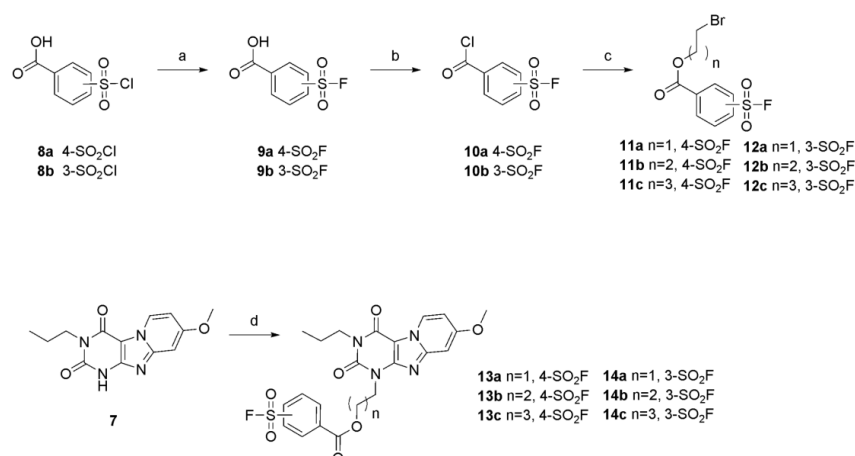
**Scaffold.** The scaffold, 8-methoxy-3-propyl-1*H*,3*H*-pyrido-[2, 1-*f*]purine-2, 4-dione (**1**), was synthesized according to the previously published procedure [6-8]. Starting from the commercially available benzylurea (**3**), the fused tricyclic intermediate (**6**) was generated by excess NBS bromination and 4-methoxypyridine cyclization (Scheme 1). Then alkylation at the N<sup>3</sup>-nitrogen by 1-bromopropane in dry DMF, using dry potassium carbonate as a weak base, afforded the reference compound (**1**) in 73% yield. Removing the benzyl protecting group by palladium hydroxide afforded the fused xanthine core (**7**).

**Scheme 1.** Synthetic route towards scaffold **7**



Reagents and conditions: (a) i) Ac<sub>2</sub>O, 80 °C, 2 h; ii) Et<sub>2</sub>O, rt, 1 h; iii) 3M NaOH, 85 °C, 1 h; iv) HCl (37%), 25%; (b) i) NBS, MeCN, 80 °C; ii) 4-methoxypyridine, 80 °C, 64%; (c) 1-bromopropane, DBU, MeCN, 70 °C, 73%; (d) Pd(OH)<sub>2</sub>/C, HCOONH<sub>4</sub>, EtOH, reflux, 40%.

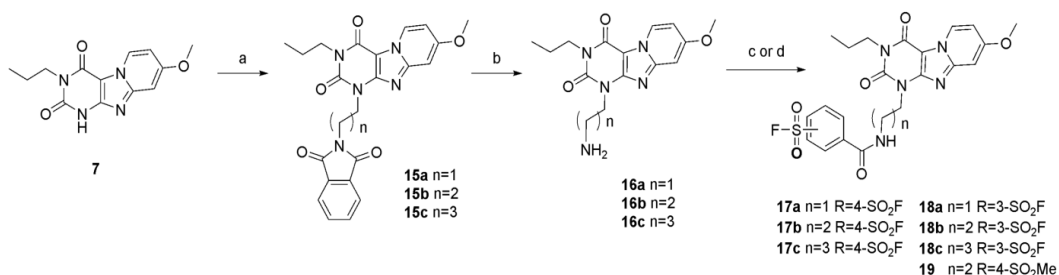
**Ester Linker** The fluorosulfonyl warhead is notorious for its reactivity resulting in undesired side reactions or hydrolysis under several harsh reactions [17]. So we adopted a convergent synthetic strategy in which the fluorosulfonyl phenyl linker unit was prepared separately and attached directly to scaffold **7** at the N<sup>3</sup> position. This approach offers the flexibility to accommodate a variety of different linker lengths. The warhead was synthesized from commercially available chlorosulfonylbenzoic acids (**8a** and **8b**) (Scheme 2), followed by a 2 M solution of potassium bifluoride treatment to afford fluorosulfonylbenzoic acids (**9a** and **9b**) in good yields. [18] The next step converted the carboxylic acids to acid chlorides (**10a** and **10b**) by excess thionyl chloride treatment. These acyl chlorides are prone to hydrolysis and

**Scheme 2.** Synthetic route towards the bromoalkyl fluorosulfonylbenzoates **13a-c** and **14a-c**


Reagents and conditions: (a) 2M KHF<sub>2</sub> solution, dioxane, rt, 1h, 87%-90%; (b) SOCl<sub>2</sub> reflux; (c) corresponding bromoalkylalcohol, anhydrous dioxane, 100 °C, 18h, 55%-83%, (d) **11a-c** or **12a-c**, K<sub>2</sub>CO<sub>3</sub>, anhydrous DMF, 50 °C, 5%-57%.

were thus used in the next step reaction without further purification. To incorporate the acyl chlorides with the corresponding bromoalkylalcohols, compounds **10a** and **10b** were heated to 100 °C with the addition of bromoalkylalcohols to afford the desired bromoalkyl fluorosulfonylbenzoates (**11a-c** and **12a-c**) in decent yields. The final step was to couple the core to the corresponding bromoalkyl fluorosulfonylbenzoates. In order to preserve the functional fluorosulfonyl group, the reactions were carried out under mild conditions at low temperature. Additionally, excess DMF was removed by multiple washing steps, instead of vacuum removal at high temperature. Six final products (**13a-c** and **14a-c**) were obtained in acceptable yields.

**Amide Linker** A similar synthetic approach was initially pursued to prepare analogues with an amide linker. However, the basicity and instability of bromoalkylamine caused complex side reactions with itself and with the warhead, ending up with an unacceptably low yield of amide-linked building blocks. An alternative synthetic route was devised, where 1-phthalimidopropyl bromide was attached directly to the N<sup>3</sup> position of scaffold **6**, to afford the substituted intermediates **15a-c** (Scheme 3). Liberation of the amine took place by treatment with hydrazine monohydrate in methanol to obtain compound **16a-c** in moderate yield. Then **16b** and **16c** were acylated with acyl chlorides **10a** and **10b**, respectively, to obtain **17c** and **18b**. However, impurities brought by the acylation reaction were not easily removed by column chromatography or preparative TLC.

Scheme 3. Synthetic route towards the amide-linker antagonists **17a-c**, **18a-c** and **19**

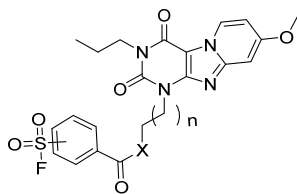
Reagents and conditions: (a) N-(bromoalkyl)phthalimide, K<sub>2</sub>CO<sub>3</sub>, DMF, 100 °C, 5-96%; (b) N<sub>2</sub>H<sub>4</sub>·H<sub>2</sub>O, MeOH reflux, 86-90%; (c) EDC, corresponding acid (**9a-b**), CHCl<sub>3</sub> or CH<sub>2</sub>Cl<sub>2</sub>, rt; (d) SOCl<sub>2</sub>, K<sub>2</sub>CO<sub>3</sub>, dry DMF, 40 °C, 3-78%

To overcome this, we used peptide coupling conditions with the corresponding benzoic acids (**9a** and **9b**) to convert the free amine to the target compounds (**17a-b**, **18a** and **18c**) in good yields (Scheme 4). A similar synthetic strategy was adapted to obtain reversible ligand **19** as a control compound.

### 2.3. Pharmacological Evaluation.

**Determination of the apparent affinity ( $K_i$ ) of synthesized ligands.** To determine the binding affinity for the hA<sub>3</sub>AR receptor, all compounds were tested in a radioligand displacement binding assay in the presence of 10 nM [<sup>3</sup>H]PSB-11 at 25 °C according to previously reported procedures [7, 19]. All compounds were able to concentration-dependently inhibit specific [<sup>3</sup>H]PSB-11 binding to the hA<sub>3</sub>AR. As detailed in Table 1, all putative covalent compounds, except the two carbon linker compounds (**13a**, **14a**, **17a** and **18a**), displayed high affinities for the hA<sub>3</sub>AR ( $K_i < 100$  nM). It should be mentioned that the putative covalent nature of the interaction between hA<sub>3</sub>AR and ligands precludes the determination of equilibrium binding parameters. Therefore, we expressed the ligands' affinity for the hA<sub>3</sub>AR as "apparent  $K_i$ ". Of note, **17b**, bearing three carbon atoms with amide linkage and positioning the sulfonyl fluoride at the 4-position of phenyl ring, interacted with hA<sub>3</sub>AR with comparable affinity (10 nM) as the parent compound **1**. High affinity is desirable for covalent ligand design, as it allows sufficient receptor occupancy with the electrophilic warhead in proximity to a nucleophilic residue in the binding site over time concomitant with putatively negligible or less interaction with off-targets. Thus, we chose compound **17b** for further studies. However, featuring an electrophilic fluorosulfonyl functionality, **17b** was no longer a close analogue of compound **1**, while a non-reactive control compound, chemically similar to the designed



**Table 1.** Apparent Affinities of Pyrido[2,1-*f*]purine-2,4-dione Derivatives **13-19**.


Compound	n	X	R <sup>1</sup>	pK <sub>i</sub> ± SEM <sup>a</sup> or disp. at 10 μM (%)
<b>13a</b>	1	O	4-SO <sub>2</sub> F	6.7 ± 0.1
<b>13b</b>	2	O	4-SO <sub>2</sub> F	7.7 ± 0.1
<b>13c</b>	3	O	4-SO <sub>2</sub> F	7.5 ± 0.1
<b>14a</b>	1	O	3-SO <sub>2</sub> F	6.4 ± 0.1
<b>14b</b>	2	O	3-SO <sub>2</sub> F	7.0 ± 0.05
<b>14c</b>	3	O	3-SO <sub>2</sub> F	7.1 ± 0.05
<b>17a</b>	1	NH	4-SO <sub>2</sub> F	27%
<b>17b</b> (LUF7602)	2	NH	4-SO <sub>2</sub> F	8.0 ± 0.05
<b>17c</b>	3	NH	4-SO <sub>2</sub> F	7.5 ± 0.05
<b>18a</b>	1	NH	3-SO <sub>2</sub> F	18%
<b>18b</b>	2	NH	3-SO <sub>2</sub> F	7.5 ± 0.01
<b>18c</b>	3	NH	3-SO <sub>2</sub> F	6.8 ± 0.1
<b>19</b> (LUF7714)	2	NH	4-SO <sub>2</sub> Me	6.3 ± 0.03

<sup>a</sup> Data are expressed as means ± SEM of three separate experiments each performed in duplicate. Apparent affinity determined from displacement of specific [<sup>3</sup>H]PSB-11 binding from the hA<sub>3</sub>AR stably expressed on CHO cell membranes at 25 °C during 2 h incubation.

covalent ligand, is needed for the further pharmacological characterization. A non-substituted phenyl to replace the warhead might impose different steric and electronic characteristics of the ligand. To avoid this, we performed a conservative structural modification to replace the reactive warhead with an electron-withdrawing methylsulfonyl group, yielding derivative **19** as a nonreactive control compound.

## Chapter 4

**Table 2.** (Apparent) Affinities of **17b** and **19** for all adenosine receptor subtypes, hA<sub>3</sub>AR-WT and hA<sub>3</sub>AR-Y265F<sup>7,36</sup>

cpd	hA <sub>1</sub> AR <sup>a</sup>	hA <sub>2A</sub> AR <sup>b</sup>	hA <sub>2B</sub> AR <sup>c</sup>	hA <sub>3</sub> AR		hA <sub>3</sub> AR-WT <sup>f</sup>	hA <sub>3</sub> AR-Y265F <sup>7,36g</sup>
	pK <sub>i</sub> ± SEM		Displ. (%) at 1 μM	pK <sub>i</sub> <sup>d</sup> (pre-0 h)	pK <sub>i</sub> <sup>e</sup> (pre-4 h)	pIC <sub>50</sub> ± SEM <sup>e</sup>	
<b>17b</b> <sup>h</sup>	6.1 ± 0.03	5.9 ± 0.09	0% (7, -7)	6.9 ± 0.06	8.0 ± 0.01**	7.6 ± 0.05	6.0 ± 0.3*
<b>19</b>	4.8 ± 0.20	5.2 ± 0.20	0% (-10, -13)	6.2 ± 0.03	6.1 ± 0.06 <sup>NS</sup>	5.9 ± 0.02	6.1 ± 0.1 <sup>NS</sup>

Values represent mean ± SEM of three separate experiments each performed in duplicate or percent age displacement at 1 μM of two separate experiments each performed in duplicate.

<sup>a</sup>Affinity determined from displacement of specific [<sup>3</sup>H]DPCPX binding on CHO cell membranes stably expressing human adenosine A<sub>1</sub> receptors at 25 °C during 2 h incubation;

<sup>b</sup>Affinity determined from displacement of specific [<sup>3</sup>H]ZM241385 binding on HEK293 cell membranes stably expressing human adenosine A<sub>2A</sub> receptors at 25 °C during 2 h incubation;

<sup>c</sup>% displacement at 1 μM concentration of specific [<sup>3</sup>H]PSB-603 binding on CHO cell membranes stably expressing human adenosine A<sub>2B</sub> receptors at 25 °C during 2 h incubation.

<sup>d</sup>Displacement of specific [<sup>3</sup>H]PSB-11 binding on CHO cell membranes stably expressing hA<sub>3</sub>AR at 25 °C during 0.5 h incubation.

<sup>e</sup>Displacement of specific [<sup>3</sup>H]PSB-11 binding from CHO cell membranes stably expressing hA<sub>3</sub>AR preincubated with antagonist for 4 h at 25 °C, followed by a 0.5 h co-incubation with [<sup>3</sup>H]PSB-11. P < 0.01\*\* compared with the pK<sub>i</sub> values in displacement experiments during 0.5 h incubation time; NS: no significant difference compared with the pK<sub>i</sub> values in displacement experiments during 0.5 h incubation time; Student's test.

<sup>f</sup>Displacement of specific [<sup>3</sup>H]PSB-11 binding from CHO-K1 cell membranes transiently transfected with hA<sub>3</sub>AR-WT at 25 °C during 2 h incubation

<sup>g</sup>Displacement of specific [<sup>3</sup>H]PSB-11 binding from CHO-K1 cell membranes transiently transfected with hA<sub>3</sub>AR-Y265F<sup>7,36</sup> at 25 °C during 2 h incubation. P < 0.01\* compared with the pIC<sub>50</sub> values in displacement experiments on hA<sub>3</sub>AR-WT. NS: no significant difference compared with the pIC<sub>50</sub> values in displacement experiments on hA<sub>3</sub>AR-WT membranes; Student's test.

<sup>h</sup>For **17b**, pK<sub>i</sub> values are apparent affinity values as no dynamic equilibrium can be obtained.

To better understand the time-dependent binding characteristics of these compounds, we carried out radioligand displacement assays under two different protocols. In detail, the CHO cell membranes overexpressing hA<sub>3</sub>AR were either pre-incubated with the indicated compound for 4 h, followed by a 0.5 h co-incubation or only co-incubated for 0.5 h with the radioligand [<sup>3</sup>H]PSB-11. As detailed in Table 2, both compounds had comparable binding affinity in the low micromolar range (pK<sub>i</sub> = 6.9 ± 0.06 for **17b** and pK<sub>i</sub> = 6.2 ± 0.03 for **19**) at 0.5 h incubation time. However, compound **17b** showed a significantly increased affinity (pK<sub>i</sub> = 8.0 ± 0.01) when it was pre-incubated with hA<sub>3</sub>AR, while the affinity of compound **19** did not change (pK<sub>i</sub> = 6.1 ± 0.06).

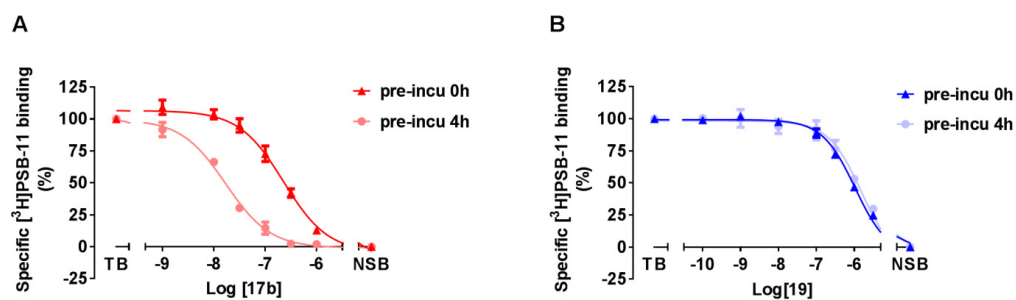


**Figure 2.** (A) Displacement of [<sup>3</sup>H]PSB-11 binding from hA<sub>3</sub>AR at 25°C by **17b** with and without a pre-incubation of 4 h. (B) Displacement of [<sup>3</sup>H]PSB-11 binding from hA<sub>3</sub>AR at 25°C by **19** with and without a pre-incubation of 4 h. Data represent the mean ± SEM of three individual experiments performed in duplicate.

The effect of pre-incubation on the affinity of **17b** and **19** is illustrated in Figure 2, i.e. the [<sup>3</sup>H]PSB-11 displacement curve was shifted to the left with an increased incubation time for compound **17b** (Figure 2A), while no difference was observed for compound **19** (Figure 2B). Presumably this time-dependent binding affinity of compound **17b** (i.e. resulting from an increased receptor occupancy over time) is a result of an increasing level of covalent binding. Similar results on other GPCRs, such as β<sub>2</sub> adrenergic receptor [20] and A<sub>2A</sub> adenosine receptor [21], showed that covalent bond formation generates an increased affinity over time. Meanwhile, control compound **19** showed no substantial pK<sub>i</sub> shift in affinity at the two incubation times, indicating that a dynamic equilibrium was achieved at both incubation times. We can thus speculate that the possible covalent interaction between compound **17b** and the receptor may be attributed to the presence of a reactive warhead. Finally, we tested **17b** and **19** for their affinity on the other adenosine receptor subtypes, and learned that the two compounds were at least modestly selective for the hA<sub>3</sub>AR (Table 2). Finally, we tested **17b** and **19** for their affinity on the other adenosine receptor subtypes, and learned that the two compounds were at least modestly selective for the hA<sub>3</sub>AR (Table 2).

**Kinetic characterization of the covalent ligand.** Subsequently, the significant shift in “apparent K<sub>i</sub>” drove us to explore the binding kinetic profile of **17b** at the hA<sub>3</sub>AR, and specifically its dissociation rate and residence time (RT). Previously, the k<sub>on</sub> (k<sub>1</sub> = 0.281 ± 0.04 × 10<sup>8</sup> M<sup>-1</sup>·min<sup>-1</sup>) and k<sub>off</sub> (k<sub>2</sub> = 0.3992 ± 0.02 min<sup>-1</sup>) values of [<sup>3</sup>H]PSB-11 at 25 °C had been determined in our laboratory by traditional association and dissociation assays. Here we performed a competition association assay to characterize the binding kinetics of **17b** and **19** following previously reported procedures from our research group [7]. Using the on- and off-rate constants from [<sup>3</sup>H]PSB, the k<sub>on</sub> (k<sub>3</sub>) and k<sub>off</sub> (k<sub>4</sub>) values for **17b** were determined using the equations from the (equilibrium) Motulsky and Mahan model [22]. **17b** had a much

## Chapter 4

slower association rate ( $k_{\text{on}} = 3.48 \pm 0.22 \times 10^5 \text{ M}^{-1} \text{ min}^{-1}$ ) than the radioligand and a negligible dissociation rate ( $k_{\text{off}} = 1.38 \pm 0.22 \times 10^{-12} \text{ min}^{-1}$ ), yielding an almost infinite residence time ( $\text{RT} = 7.63 \pm 1.19 \times 10^{11} \text{ min}$ ), indicative of irreversible receptor binding by **17b**. The inadequacy of the Motulsky-Mahan equations to fit this data is further evidence for the non-equilibrium features of the binding of **17b** to the receptor. Compound **19** showed fast association and dissociation rate constants (Figure 3). Unfortunately, the data did not converge in the fitting procedure, possibly due to the low binding affinity of compound **19** ( $K_i = 525 \text{ nM}$ ).

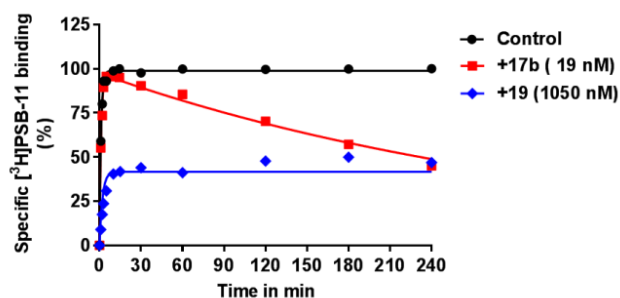


**Figure 3.** Competition association assay of [ $^3\text{H}$ ]PSB-11 in the absence (control) or presence of **17b** and **19** at the indicated concentration. Association and dissociation rate constants for the unlabeled ligands were calculated by fitting the data to the equations described in the experimental section (“data analysis”). Representative graphs are from one experiment performed in duplicate.

As detailed in Figure 3, the control curve represented the association curve of radioligand [ $^3\text{H}$ ]PSB-11 alone, approaching equilibrium over time. Compound **19** equally associated to and dissociated from the receptor and reached equilibrium within 30 min, evidenced by the same curve shape as the control curve. Of note, **17b**’s behavior caused an initial ‘overshoot’ of the competition association curve, followed by a linear decline over time indicating that no equilibrium was reached. The shape of **17b**’s kinetic curve is a quintessential example for the irreversible interaction, similar to the reported covalent ligands’ behavior for the adenosine  $A_{2A}$  receptor [21] and mGlu2 receptor [23].

**Wash-resistant interaction between 17b and  $hA_3AR$ .** Inspired by the negligible dissociation of compound **17b** from the  $hA_3AR$ , we performed a “washout” experiment to ascertain the irreversible binding between the ligand and receptor. A protocol previously reported by our laboratory [21] was adapted. We first exposed  $hA_3AR$  cell membranes to **17b** or **19** both at

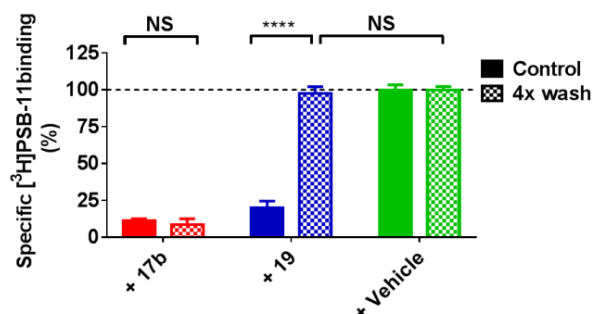


**Figure 4.** hA<sub>3</sub>AR membranes pre-incubated with buffer (vehicle) or a  $10 \times K_i$  concentration of indicated ligand, followed by no washing (Control) or four-cycle washing treatment (4x wash) before being exposed to [<sup>3</sup>H]PSB-11. Data represent the mean  $\pm$  SEM of three individual experiments performed in duplicate, normalized to the vehicle (set at 100%). Statistics were determined using unpaired Student's *t* test. NS: no significant difference, \*\*\*\**P* < 0.0001, significant difference between indicated groups.

10-fold  $K_i$  for 2 h, and without washing the samples were supplemented with [<sup>3</sup>H]PSB-11 to assess the competitive binding capacity of the receptor ('Control group' in Figure 4). For washed samples, hA<sub>3</sub>AR cell membranes were subjected to four-cycle washing steps to remove unbound ligand following the pre-incubation ('4x wash group' in Figure 4), after which the membranes were exposed to [<sup>3</sup>H]PSB-11 to determine the remaining binding capacity. In the absence of ligand (labeled '+ vehicle' in Figure 4), we normalized membranes' binding ability to 100%. Following preincubation with **17b**, membranes containing the hA<sub>3</sub>AR lost most of the ability to bind to the radioligand ( $11.3 \pm 1.2\%$  binding remaining). Furthermore, after the pre-incubation, membranes were washed by cycles of centrifugation in an attempt to regenerate binding capacity. However, washing steps failed to restore hA<sub>3</sub>AR binding of [<sup>3</sup>H]PSB-11 ( $8.7 \pm 3.8\%$ ). This was in contrast to preincubation of the hA<sub>3</sub>AR-expressing membranes with ligand **19**, in which binding function was completely restored from  $19.8 \pm 4.7\%$  to  $97.6 \pm 4.5\%$  following four washing steps. This result indicates **19** is a reversible ligand which can be rapidly washed off the membranes, while **17b** forms a wash-resistant bond between the ligand and the receptor. Similar experiments on other GPCRs, such as adenosine A<sub>1</sub> [24, 25] and A<sub>2A</sub> [21] receptors and the metabotropic glutamate receptor 2 (mGluR2) [23], demonstrated that the covalent interaction between the ligand and the receptor resulted in a wash-resistant bond formation.

**Insurmountable antagonism caused by covalent interaction.** To further evaluate the effect of irreversible inhibition by covalent ligand **17b** on receptor function, we performed a membrane functional assay using [<sup>35</sup>S]GTP $\gamma$ S, which is a typical readout for activation of receptor-coupled G<sub>i/o</sub> proteins [26].

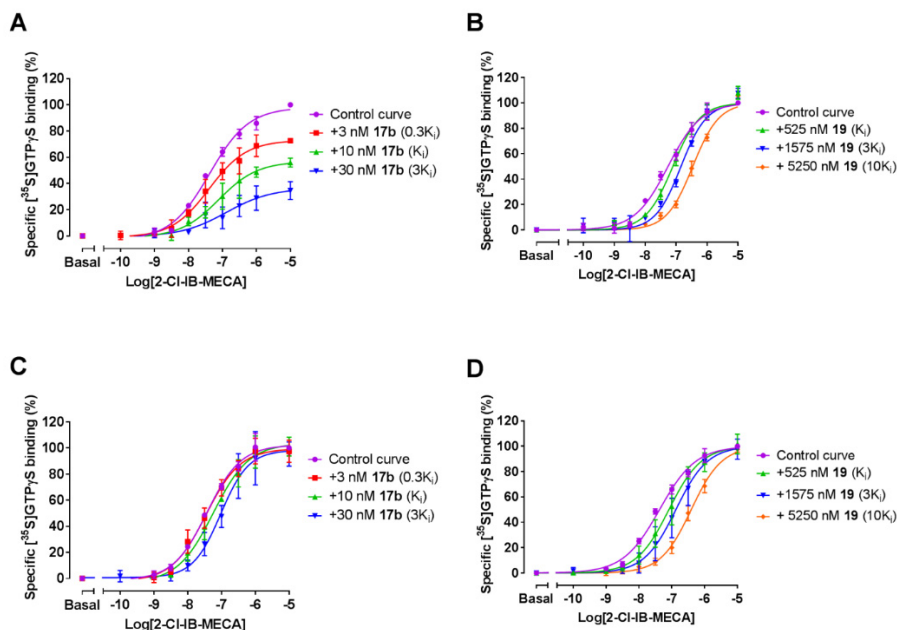


**Figure 5.** Effects of **17b** and **19** on hA<sub>3</sub>AR activation as measured by [<sup>35</sup>S]GTPγS binding. (A, B) Compound **17b** (A) or **19** (B) were pre-incubated with hA<sub>3</sub>AR stably expressed on CHO cell membranes (25 °C) for 60 min prior to the addition of 2-Cl-IB-MECA at a concentration ranging from 0.1 nM to 10 μM for 30 min. (C, D) Compound **17b** (C) or **19** (D) were co-incubated with 2-Cl-IB-MECA, at a concentration ranging from 0.1 nM to 10 μM, for 30 min. The agonist curves were generated in the presence of increasing concentrations of antagonists, namely 0.3-, 1-, 3-, 10-fold their respective K<sub>i</sub> values. Data are from three independent experiments performed in duplicate, normalized according to the maximal response (100%) produced by 10 μM 2-Cl-IB-MECA alone. The shift in agonist EC<sub>50</sub> values was determined to perform Schild analyses.

Pretreatment of hA<sub>3</sub>AR with increasing concentrations of ligand **17b**, prior to the stimulation with hA<sub>3</sub>AR agonist 1-[2-chloro-6-[[3-iodophenyl)methyl]amino]-9H-purin-9-yl]-1-deoxy-N-methyl-β-D-ribofuranuronamide (2-Cl-IB-MECA), produced rightward shifts of agonist concentration-response curves with a concomitant decline in maximal stimulation (Figure 5a). Therefore, the covalent ligand **17b** generated insurmountable antagonism in the pre-incubation experiment. In contrast, pretreatment of hA<sub>3</sub>AR with **19**, followed by 2-Cl-IB-MECA agonist exposure resulted in surmountable antagonism (Figure 5b), i.e. shifting dose-response curves to the right with no alteration of its maximum effect. The extent of the shifts was used to construct a Schild plot as previously described [7], which would have a slope of unity if the interaction is competitive and the pA<sub>2</sub>-value corresponds to the pK<sub>i</sub> of the antagonist. The slope for **19** was found to be 1.1 ± 0.1 and the compound's pA<sub>2</sub> value was 5.9 ± 0.1, comparable with its pK<sub>i</sub> value (6.3 ± 0.03), suggesting that **19** competed with 2-Cl-IB-MECA for the same receptor binding site.

**Table 3.** Functional Analysis of hA<sub>3</sub>AR Antagonism from [<sup>35</sup>S]GTPγS Binding Assays

compound	Pre-incubation		Co-incubation		mode of antagonism
	pA <sub>2</sub>	Schild slope	pA <sub>2</sub>	Schild slope	
<b>17b</b>	N.A.	N.A.	7.4 ± 0.1	1.1 ± 0.1	Competitive Insurmountable
<b>19</b>	5.9 ± 0.1	1.1 ± 0.1	6.2 ± 0.1	1.0 ± 0.1	Competitive Surmountable

Values represent mean ± SEM of three separate experiments each performed in duplicate.

To unravel the molecular mechanism responsible for the insurmountable antagonism of **17b**, we also co-incubated either **17b** or **19** with hA<sub>3</sub>AR in the presence of 2-Cl-IB-MECA. Both ligands produced a rightward shift of the agonist's concentration–response curve (Figure 5c and 5d) with no suppression of maximal response, indicative of surmountable antagonism. The Schild plot showed that both antagonists inhibited receptor activation in a competitive manner, with their Schild-slopes close to unity (1.1 ± 0.1 for **17b**, 1.0 ± 0.1 for **19**, Table 3). In addition, **19**'s pA<sub>2</sub> value was in agreement with that from the pre-incubation experiments (6.2 ± 0.1, Table 3), and the pA<sub>2</sub> value of **17b** was also comparable with its pK<sub>i</sub> value (7.4 ± 0.1 vs 8.0 ± 0.05). Taken together, both ligands fully competed with 2-Cl-IB-MECA bound to hA<sub>3</sub>AR. Notably, it is likely that the insurmountable behavior relates to covalent binding of **17b** due to an irreversible blockade that reduces the total receptor population available.

**Binding model for 17b in the hA<sub>3</sub>AR receptor-binding pocket.** To examine the interaction between receptor residues possibly involved in covalent binding, we docked **17b** into a ligand optimized homology model on the basis of the A<sub>2A</sub> receptor crystal structure (PDB: 4EIY [27]), as described previously [7]. As detailed in Figure 6, the core structure of compound **17b** interacted with the TM3, TM6 and EL2 regions. Additionally, the carbonyl-oxygen at the C<sup>4</sup>-position participated in H-bond formation with residue N250<sup>6.55</sup> and the methoxyl moiety at the C<sup>8</sup>-position functioned as H-bond acceptor with Q167<sup>EL2</sup>. Interestingly, the latter is a unique residue in hA<sub>3</sub>AR, as it is not conserved in other subtypes of adenosine receptors. Due to the flexibility of the three-carbon linker, the tyrosine residue Y265<sup>7.36</sup> is in close proximity of the ligand, and could therefore interact with the 4-fluorosulfonylbenzoic warhead to form a covalent sulfonyl amide. Similarly, the same residue Y271<sup>7.36</sup> located within the human adenosine A<sub>1</sub> receptor has also been reported to covalently interact with the fluorosulfonyl warhead of compound **2** [11]. Comparison of the binding modes of compound **2** and ligand **17b** in an A<sub>1</sub>/A<sub>3</sub> receptor overlay showed that key interactions between ligands and binding sites are preserved, such as a hydrogen bond with N<sup>6.55</sup> (Figure S1).



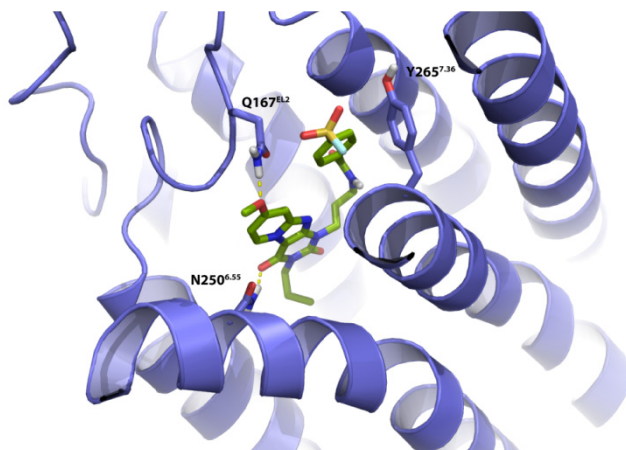


**Figure 6.** Proposed binding mode of compound **17b** (green carbon sticks) in a homology model (violet ribbons) of hA<sub>3</sub>AR. The hA<sub>3</sub>AR homology model was based on the high-resolution antagonist-bound crystal structure of the adenosine A<sub>2A</sub> receptor (PDB: 4EIY [27]). Atoms color code: red = oxygen, blue = nitrogen, white = hydrogen, yellow = sulfur, cyan = fluorine. Hydrogen bonds between ligand and receptor are indicated by yellow dashed lines. Residue Y265<sup>7.36</sup> is in the proximity of the fluorosulfonyl warhead.

**Y265<sup>7.36</sup> as an anchor point for the covalent bond.** Based on the docking study, we postulated that Y265<sup>7.36</sup> is the anchor point for covalent bond formation. To investigate our hypothesis this tyrosine was mutated to phenylalanine (hA<sub>3</sub>AR-Y265F<sup>7.36</sup>), to remove the nucleophilic reactivity of the phenolic hydroxyl group. First we performed standard [<sup>3</sup>H]PSB-11 displacement assays to investigate the binding affinity of **17b** and **19** using CHO-K1 cell membranes transiently transfected with either wild type (hA<sub>3</sub>AR-WT) or mutant receptors (hA<sub>3</sub>AR-Y265F<sup>7.36</sup>). As shown in Table 2 and Figure 7, the affinity of control compound **19** on hA<sub>3</sub>AR-Y265F<sup>7.36</sup> (pIC<sub>50</sub> = 6.09 ± 0.11) was similar to the affinity to hA<sub>3</sub>AR-WT (pIC<sub>50</sub> = 5.95 ± 0.03), indicating that the mutation has no impact on the binding affinity of the reversible ligand. In marked contrast, **17b**'s affinity was decreased nearly 43-fold relative to WT, from an IC<sub>50</sub> value of 27 nM to 1072 nM, indicative of the loss of irreversible interaction. Moreover, there were no marked affinity differences on hA<sub>3</sub>AR-Y265F<sup>7.36</sup> between **17b** and **19**. This suggests that the chemically dissimilar ligands **17b** (reactive) and **19** (nonreactive) exhibit a similar binding interaction with hA<sub>3</sub>AR-Y265F<sup>7.36</sup>. We thus speculate the amino acid in position 7.36 plays a prominent role in the covalent bond formation between the fluorosulfonyl warhead and receptor. To support this idea, we repeated the “washout” assay on hA<sub>3</sub>AR-Y265F<sup>7.36</sup>. Membranes treated with **17b** at 10-fold IC<sub>50</sub> inhibited the specific [<sup>3</sup>H]PSB-11 binding to 7.2 ± 0.6%. After extensive washing, hA<sub>3</sub>AR-Y265F<sup>7.36</sup> showed a complete recovery of [<sup>3</sup>H]PSB-11 binding to 91 ± 2% (Figure 7c). This full recovery for mutant hA<sub>3</sub>AR-Y265F<sup>7.36</sup> is in sharp contrast to the findings in the wild type washout assay (Figure 4), indicating Y265F<sup>7.36</sup> completely prevented the wash-resistant bond formation. In



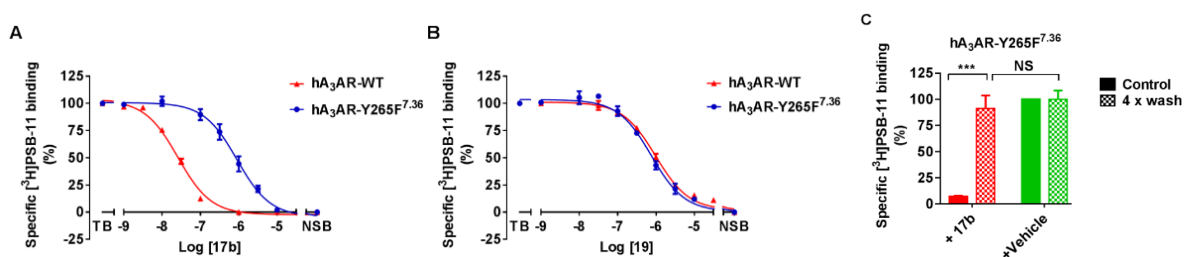


**Figure 7.** (A, B) Displacement of specific [<sup>3</sup>H]PSB-11 binding from transiently transfected hA<sub>3</sub>AR-WT and hA<sub>3</sub>AR-Y265F<sup>7.36</sup> at 25°C by compound **17b** (A) and **19** (B) during an incubation of 2 h. (C) hA<sub>3</sub>AR-Y265F<sup>7.36</sup> cell membranes were pretreated with buffer (vehicle) or 10 × IC<sub>50</sub> of compound **17b** for 2 h followed by no washing (Control) or four-cycle washing treatment (4x wash) before exposed to [<sup>3</sup>H]PSB-11. Data represent the mean ± SEM of three individual experiments performed in duplicate, normalized to the vehicle (set at 100%). NS: no significant difference between groups; \*\*\*Significant difference between groups (P<0.001); Student's *t*-test

other words Y265<sup>7.36</sup> is the unique amino acid residue involved in the covalent attachment of **17b**'s fluorosulfonyl group within the hA<sub>3</sub>AR binding pocket. A similar approach was also adopted to pinpoint the anchor point between covalent probes and other subtypes of GPCRs, such as the adenosine A<sub>2A</sub> receptor [21] mGlu2 receptor [23] and cannabinoid CB<sub>1</sub> receptor [28]. **17b** can be a useful structural biology tool as it would be expected to stabilize the 7TM domain in its inactive state, thereby potentially facilitating crystallization of receptor material. This could be highly valuable for the structure elucidation of hA<sub>3</sub>AR which up to now remains unreported. Furthermore, understanding the precise molecular interactions between ligand and receptor may stimulate the more rational design of novel ligands. Such ligands may have improved receptor subtype selectivity, fewer undesirable side effects, and enhanced potency and efficacy, leading to potentially attractive therapeutic agents that produce their effects by modulating the functionality of the adenosine system. Given that GPCR-targeted covalent drugs went through clinical success across various indications,[29] our covalent compound **17b** may serve as a probe to explore the problematic translation of hA<sub>3</sub>AR ligands into clinical utility in certain disease states such as eye disorder glaucoma, in which an increased A<sub>3</sub> adenosine receptor mRNA and protein level have been detected.

### 3. Conclusions

By introducing a reactive sulfonyl fluoride warhead onto the 1-benzyl-3-propyl-1*H*,3*H*-pyrido [2,1-*f*]purine-2,4-dione scaffold, we designed and synthesized a series of novel covalent hA<sub>3</sub>AR antagonists. Compound **17b** acted as the most potent antagonist, with a time dependent apparent affinity in the low nanomolar range. Meanwhile, we removed the warhead and inserted a methylsulfonyl moiety into the scaffold, to obtain ligand **19** as a reversible control compound. Ligand **17b** was then validated as covalent antagonist through its wash-

resistant nature and insurmountable antagonism in [<sup>35</sup>S]GTP $\gamma$ S binding assays. *In silico* homology-docking suggested that Y265<sup>7,36</sup> is responsible for the covalent interaction. Site-directed mutagenesis showed that removal of the nucleophilic tyrosine phenolic hydroxyl group resulted in the complete loss of covalent binding, validating that Y265<sup>7,36</sup> is the only anchor point of reactive covalent ligand **17b**. The results contribute to a better understanding of pharmacological behaviors caused by covalent interaction with GPCRs. In the end, we developed a structured approach to quickly obtain a well-defined covalent ligand. Besides, we envisioned that a methylsulfonyl replacement would be suitable for providing a non-reactive sulfonyl-bearing control compound. The rational design of covalent probes may have further value in receptor structure elucidation or in new technologies such as affinity-based protein profiling [15, 30] with the perspective of imaging or structurally probing GPCRs.

### 4. Experimental Section

**4.1. Chemistry** All solvents and reagents were purchased from commercial sources and were of analytical grade. Demineralized water is simply referred to as H<sub>2</sub>O, and was used in all cases unless stated otherwise (i.e. brine). <sup>1</sup>H were recorded on a Bruker AV 400 liquid spectrometer (<sup>1</sup>H NMR, 400 MHz) at ambient temperature and <sup>13</sup>C NMR spectra was performed on a Bruker AV 600 liquid spectrometer (<sup>13</sup>C NMR, 125 MHz) at indicated temperature. Chemical shifts are reported in parts per million (ppm), using residual solvent as the internal reference in all cases. The values are given in  $\delta$  scale. Coupling-constants are reported in Hz and are designated as *J*. Analytical purity of the final compounds was determined by high performance liquid chromatography (HPLC) with a Phenomenex Gemini 3 $\mu$ m C18 110Å column (50  $\times$  4.6 mm, 3  $\mu$ m), measuring UV absorbance at 254 nm. Sample preparation and HPLC method was as follows: 0.3-1.0 mg of compound was dissolved in 1 mL of a 1:1:1 mixture of MeCN/H<sub>2</sub>O/tBuOH and eluted from the column within 15 minutes at a flow rate of 1.3 mL/min with a three component system of H<sub>2</sub>O/MeCN/1% TFA in H<sub>2</sub>O. The elution method was set up as follows: 1–4 min isocratic system of H<sub>2</sub>O/MeCN/1% TFA in H<sub>2</sub>O, 80:10:10, from the 4th min, a gradient was applied from 80:10:10 to 0:90:10 within 9 min, followed by 1 min of equilibration at 0:90:10 and 1 min at 80:10:10. All final compounds showed a single peak at the designated retention time and are at least 95% pure. Liquid chromatography–mass spectrometry (LC-MS) analyses were performed using Thermo Finnigan Surveyor - LCQ Advantage Max LC-MS system and a Gemini C18 Phenomenex column (50  $\times$  4.6 mm, 3  $\mu$ m). High resolution mass spectrometry (HRMS) analyses were performed using a Thermo Scientific™ LTQ Orbitrap XL™ Hybrid Ion Trap-Orbitrap Mass

Spectrometer. The sample preparation was the same as for HPLC and HRMS analysis. The compounds were eluted from the column within 15 minutes after injection, with a three component system of H<sub>2</sub>O/MeCN/0.2% TFA in H<sub>2</sub>O, decreasing polarity of the solvent mixture in time from 80:10:10 to 0:90:10. Thin-layer chromatography (TLC) was routinely consulted to monitor the progress of reactions, using aluminum coated Merck silica gel F254 plates. Purification by column chromatography was achieved by use of Grace Davison Davisil silica column material (LC60A 30-200 micron). Solutions were concentrated using a Heidolph Laborota W8 2000 efficient rotary evaporation apparatus. All reactions in the synthetic routes were performed under nitrogen atmosphere unless stated otherwise. The procedure for a series of similar compounds is given as a general procedure for all within that series, annotated by the numbers of the compounds.

**1-benzyl-8-methoxy-3-propyl-1*H*,3*H*-pyrido[2,1-*f*]purine-2,4-dione (1)** [7, 8]. To a stirred suspension of **6** (6.0 g, 19 mmol, 1.0 equiv) in MeCN (120 mL) were added 1-bromopropane (5.6 mL, 57 mmol, 3.0 equiv) and DBU (50 mL, 57 mmol, 3.0 equiv). This mixture was stirred at 70 °C overnight. Conversion of starting material was confirmed by TLC (2% MeOH in CH<sub>2</sub>Cl<sub>2</sub>) and the solvent was removed under vacuum. The residue was suspended in CH<sub>2</sub>Cl<sub>2</sub> (200 mL) and the organic phase was washed with 1M HCl (200 mL), H<sub>2</sub>O (200 mL), brine (200 mL) and dried over MgSO<sub>4</sub>, filtered and concentrated *in vacuo*. The crude was purified by column chromatography (0.5% MeOH in CH<sub>2</sub>Cl<sub>2</sub>) to obtain **1** as a white solid (5.0 g, 14 mmol, 73%). <sup>1</sup>H NMR (400 MHz, CDCl<sub>3</sub>): δ 8.82 (d, *J* = 7.6 Hz, 1H), 7.58 – 7.51 (m, 2H), 7.34 – 7.22 (m, 3H), 6.98 (d, *J* = 2.0 Hz, 1H), 6.74 (dd, *J* = 7.4, 2.2 Hz, 1H), 5.36 (s, 2H), 4.04 – 3.97 (m, 2H), 3.92 (s, 3H), 1.76 – 1.65 (m, 2H), 0.97 (t, *J* = 7.4 Hz, 3H)

**6-amino-1-benzyl-1,3-dihydropyrimidine-2,4-dione (5)**[7, 8]. The synthesis of the compounds adapted from the procedure reported before [7, 8]. Benzylurea (**3**) (25 g, 167 mmol, 1.0 equiv) and **4** (16 g, 191 mmol, 1.1 equiv) were dissolved in acetic anhydride (100 mL). This mixture was stirred at 80 °C for 2 h. After the mixture was cooled to room temperature, diethyl ether (150 mL) was added followed by 1 hour of stirring at room temperature. The precipitate was filtered off and suspended in a mixture of EtOH (75 mL) and H<sub>2</sub>O (150 mL). This mixture was heated to 85 °C and 3 M NaOH (aq.) (50 mL) was added dropwise. After 1 h, the mixture was concentrated and neutralized dropwise with HCl (37 %). The precipitate was filtered off and washed with acetone, obtaining **5** as a white solid (9.0 g, 42 mmol, 25%). <sup>1</sup>H NMR (400 MHz, DMSO-*d*<sub>6</sub>): δ 10.42 (brs, 1H), 7.48 – 7.08 (m, 5H), 6.85 (brs, 2H), 5.03 (s, 2H), 4.60 (s, 1H)

## Chapter 4

---

**1-benzyl-8-methoxy-1*H*,3*H*-pyrido[2,1-*f*]purine-2,4-dione (6)** [7, 8]. To the intermediate (**5**) (9.0 g, 42 mmol, 1.0 equiv) and NBS (15 g, 83 mmol, 2.0 equiv) was added MeCN (100 mL). This mixture was stirred at 80 °C. After 1.5 h conversion of starting material was confirmed by TLC (10% MeOH in CH<sub>2</sub>Cl<sub>2</sub>), 4-methoxypyridine (13 g, 125 mmol, 3.0 equiv) was added and the reaction mixture was stirred at 80 °C for 4.5 h. After cooling to room temperature, the precipitate was filtered off and washed with diethyl ether and MeOH, yielding product **6** as a white solid (8.5 g, 26 mmol, 64%). <sup>1</sup>H NMR (400 MHz, DMSO-*d*<sub>6</sub>): δ 11.31 (br s, 1H), 8.70 (d, *J* = 7.2 Hz, 1H), 7.38 – 7.16 (m, 6H), 6.90 (dd, *J* = 7.4, 2.2 Hz, 1H), 5.18 (s, 2H), 3.89 (s, 3H)

**8-methoxy-3-propyl-1*H*,3*H*-pyrido[2,1-*f*]purine-2,4-dione (7)** [7, 8]. To a mixture of the intermediate **1** (1.1 g, 3.0 mmol, 1.0 equiv), Pd(OH)<sub>2</sub>/C (2.0 g, 14 mmol, 1.0 equiv) and ammonium formate (0.20 g, 3.0 mmol, 1.0 equiv) was added EtOH (250 mL). During the reaction, five portions of ammonium formate (0.20 g, 3.0 mmol, 1.0 equiv) was added, after which completion of the reaction was observed on TLC (5% MeOH in CH<sub>2</sub>Cl<sub>2</sub>). The reaction was filtered over Celite and the residue was extracted with hot DMF. Purification of the crude product by column chromatography using 2-10% MeOH in CH<sub>2</sub>Cl<sub>2</sub> to obtained **5** as a white solid (0.30 g, 1.2 mmol, 40%). <sup>1</sup>H NMR (400 MHz, DMSO-*d*<sub>6</sub>): δ 12.05 (s, 1H), 8.73 (d, *J* = 7.2 Hz, 1H), 7.12 (d, *J* = 2.0 Hz, 1H), 6.89 (dd, *J* = 7.4, 2.6 Hz, 1H), 3.90 (s, 3H), 3.85 – 3.78 (m, 2H), 1.64 – 1.52 (m, 2H), 0.88 (t, *J* = 7.4 Hz, 3H)

**General procedure for the synthesis of fluorosulfonylbenzoic acids (9a–b)**. To a solution of chlorosulfonylbenzoic acid (**8a-b**) (2.2 g, 10 mmol, 1.0 equiv) in dioxane (25 mL) was added a solution of HF:KF (15 mL, 2.0 M, 3.0 equiv). The mixture was stirred at room temperature. After 1 h, the reaction mixture was dilute with EtOAc (80 mL). The organic phase was washed with H<sub>2</sub>O (50 mL), dried over MgSO<sub>4</sub>, filtered and concentrated *in vacuo*.

**3-(fluorosulfonyl)benzoic acid (9a)**. White solid (1.9 g, 8.7 mmol, 87%). <sup>1</sup>H NMR (400MHz, DMSO-*d*<sub>6</sub>): δ 8.47-8.44 (m, 2H), 8.4 (d, *J* = 8.0 Hz, 1H), 7.94 (t, *J* = 7.6 Hz, 1H).

**4-(fluorosulfonyl)benzoic acid (9b)**. White solid (2.0 g, 9.0 mmol, 90%). <sup>1</sup>H NMR (400 MHz, DMSO-*d*<sub>6</sub>): δ 13.86 (s, 1H), 8.28 (s, 4H)

**General procedure for the synthesis of bromoalkyl (fluorosulfonyl)benzoates (11a-c and 12a-c)** A mixture of thionyl chloride (8 mL) and fluorosulfonylbenzoic acid (**9a-b**) (1 equiv) was refluxed at 75 °C for 3 h. The solvent was removed under vacuum. And the product was used in the next step without further analysis. Dry dioxane (6 mL) was added to the (fluorosulfonyl)benzoyl chloride (**10a-b**). To this solution the corresponding bromoalkylalcohol (0.85 equiv) was added and the mixture was refluxed overnight. After

completion was observed on TLC (CH<sub>2</sub>Cl<sub>2</sub>) the volatiles were removed *in vacuo* and the crude product was purified by column chromatography using CH<sub>2</sub>Cl<sub>2</sub> as an eluent to afford the products.

**2-bromoethyl-4-(fluorosulfonyl)benzoate (11a)** Colorless oil (0.088 g, 0.28 mmol, 23%) <sup>1</sup>H NMR (400 MHz, DMSO-*d*<sub>6</sub>): δ 8.31 (d, *J* = 8.2 Hz, 2H), 8.11 (d, *J* = 8.5 Hz, 2H), 4.69 (t, *J* = 5.9 Hz, 2H), 3.67 (t, *J* = 5.9 Hz, 2H).

**3-bromopropyl-4-(fluorosulfonyl)benzoate (11b)** White solid (2.0 g, 6.2 mmol, 50%) <sup>1</sup>H NMR (400 MHz, CDCl<sub>3</sub>): δ 8.27 (d, *J* = 8.4 Hz, 2H), 8.09 (d, *J* = 8.4 Hz, 2H), 4.54 (t, *J* = 6.0 Hz, 2H), 3.54 (d, *J* = 6.4 Hz, 2H), 2.35 (m, 2H).

**4-bromobutyl-4-(fluorosulfonyl)benzoate (11c)** White solid (0.30 g, 0.89 mmol, 45%) Compound was used without further purification.

**2-bromoethyl-3-(fluorosulfonyl)benzoate (12a).** Colorless Oil (0.51 g, 1.7 mmol, 55%) <sup>1</sup>H NMR (400 MHz, CDCl<sub>3</sub>): δ 8.69 (s, 1H), 8.47 (d, *J* = 7.6 Hz, 1H), 8.25 – 8.20 (m, 1H), 7.78 (t, *J* = 8.0 Hz, 1H), 4.71 (t, *J* = 6.0 Hz, 2H), 3.68 (t, *J* = 6.0 Hz, 2H).

**3-bromopropyl-3-(fluorosulfonyl)benzoate (12b).** Colorless oil (0.12 g, 0.38 mmol, 23%) <sup>1</sup>H NMR (400 MHz, CDCl<sub>3</sub>) δ 8.65 (t, *J* = 1.6 Hz, 1H), 8.44 (d, *J* = 7.8 Hz, 1H), 8.21 (d, *J* = 8.0 Hz, 1H), 7.76 (t, *J* = 7.9 Hz, 1H), 4.55 (t, *J* = 6.1 Hz, 1H), 3.55 (t, *J* = 6.4 Hz, 1H), 2.37 (p, *J* = 6.3 Hz, 1H).

**4-bromobutyl-3-(fluorosulfonyl)benzoate (12c).** Colorless Oil (0.84 g, 2.5 mmol, 83%) <sup>1</sup>H NMR (400 MHz, CDCl<sub>3</sub>): δ 8.65 (s, 1H), 8.45 (d, *J* = 8.0 Hz, 1H), 8.21 (d, *J* = 8.0 Hz, 1H), 7.78 (t, *J* = 7.6 Hz, 1H), 4.44 (t, *J* = 6.0 Hz, 2H), 3.50 (t, *J* = 6.4 Hz, 2H), 2.11 – 1.85 (m, 4H).

#### General procedure for the synthesis of 13a–c and 14a–c

The synthesis of these compounds were adapted from the conditions previously described by Priego et al [6]. The scaffold, 8-methoxy-3-propyl-1*H*,3*H*-pyrido[2,1-*f*]purine-2,4-dione **7** (1.0 equiv), and K<sub>2</sub>CO<sub>3</sub> (1.6 equiv) were suspended in anhydrous DMF. The mixture was added dropwise to a stirred solution of the corresponding bromoalkyl (fluorosulfonyl)benzoate (**11a–c** or **12a–c**) (1.0 equiv) in anhydrous DMF (4 mL). The reaction was stirred at 50 °C overnight. After conversion on TLC was observed, excess amount of CH<sub>2</sub>Cl<sub>2</sub> was added. Then the mixture was washed with 1M HCl (aq.), water and brine. The organic layer was dried over MgSO<sub>4</sub>, filtered and concentrated *in vacuo*. The crude product was purified by column chromatography, followed to a prep TLC was used to further purify the compound if necessary.

**2-(8-methoxy-2,4-dioxo-3-propyl-3,4-dihydropyrido[2,1-*f*]purine-1(2*H*)-yl)ethyl 4-(fluorosulfonyl)benzoate (13a)** Prepared from **11a** and purified by column chromatography

(1% CH<sub>3</sub>OH in CH<sub>2</sub>Cl<sub>2</sub>) to give the desired product as white solid (0.038 g, 0.07 mmol, 52%). <sup>1</sup>H NMR (400 MHz, CDCl<sub>3</sub>): δ 8.80 (d, *J* = 8.0 Hz, 1H), 8.17 (d, *J* = 8.0 Hz, 2H), 7.98 (d, *J* = 8.4 Hz, 2H), 6.76-6.73 (m, 2H), 4.78 (t, *J* = 4.8 Hz, 2H), 4.64 (t, *J* = 5.2 Hz, 2H), 4.00 (t, *J* = 7.6 Hz, 2H), 3.89 (s, 3H), 1.73-1.62 (m, 2H), 0.95 (t, *J* = 7.2 Hz, 3H). MS: [ESI+H]<sup>+</sup>: 505.1. HPLC: 9.99 min

**3-(8-methoxy-2,4-dioxo-3-propyl-3,4-dihydropyrido[2,1-*f*]purine-1(2*H*)-yl)propyl 4-(fluorosulfonyl)benzoate (13b)** Prepared from **11b** and purified by column chromatography (1% CH<sub>3</sub>OH in CH<sub>2</sub>Cl<sub>2</sub>) to give the desired product as white solid (0.096 g, 0.19 mmol, 76%). <sup>1</sup>H NMR (400 MHz, CDCl<sub>3</sub>): δ 8.76 (d, *J* = 7.2 Hz, 1H), 8.23 (d, *J* = 8.0 Hz, 2H), 8.06 (d, *J* = 8.4 Hz, 2H), 6.77 (d, *J* = 2.4 Hz, 1H), 6.73 (dd, *J* = 7.2, 2.4 Hz, 1H), 4.50 (t, *J* = 6.0 Hz, 2H), 4.41 (t, *J* = 6.8 Hz, 2H), 4.00 (t, *J* = 7.2 Hz, 2H), 3.90 (s, 3H), 2.38 (pentet, *J* = 6.0 Hz, 2H), 1.71 (sextet, *J* = 7.2 Hz, 2H), 0.99 (t, *J* = 7.6 Hz, 3H). MS: [ESI+H]<sup>+</sup>: 519.1. HPLC: 10.18 min

**4-(8-methoxy-2,4-dioxo-3-propyl-3,4-dihydropyrido[2,1-*f*]purine-1(2*H*)-yl)butyl 4-(fluorosulfonyl)benzoate(13c)** Prepared from **11c** and purified by column chromatography (2% CH<sub>3</sub>OH in CH<sub>2</sub>Cl<sub>2</sub>) to give the desired product as white solid (0.010 g, 0.019 mmol, 5.2%). <sup>1</sup>H NMR (400 MHz, CDCl<sub>3</sub>): δ 8.83 (dd, *J* = 7.6, 0.8 Hz, 1H), 8.27 (d, *J* = 8.0 Hz, 2H), 8.07 (d, *J* = 8.8 Hz, 2H), 6.93 (d, *J* = 2.4 Hz, 1H), 6.76 (dd, *J* = 7.6, 2.4 Hz, 1H), 4.46 (t, *J* = 6.4 Hz, 2H), 4.28 (t, *J* = 6.8 Hz, 2H), 4.02 (t, *J* = 7.2 Hz, 2H), 3.93 (s, 3H), 2.05 – 1.90 (m, 4H), 1.77 – 1.68 (m, 2H), 0.99 (t, *J* = 7.2 Hz, 3H). MS: [ESI+H]<sup>+</sup>: 533.1. HPLC: 9.40 min

**2-(8-methoxy-2,4-dioxo-3-propyl-3,4-dihydropyrido[2,1-*f*]purine-1(2*H*)-yl)ethyl 3-(fluorosulfonyl)benzoate (14a)** Prepared from **12a** and without purification to give the desired product as white solid (0.19 g, 0.36 mmol, 57%). <sup>1</sup>H NMR (400 MHz, CDCl<sub>3</sub>): δ 8.80 (d, *J* = 7.2 Hz, 1H), 8.51 (s, 1H), 8.36 (d, *J* = 7.6 Hz, 1H), 8.14 – 8.09 (m, 1H), 7.66 (t, *J* = 7.8 Hz, 1H), 6.84 (d, *J* = 2.4 Hz, 1H), 6.74 (dd, *J* = 7.6, 2.6 Hz, 1H), 4.78 (t, *J* = 4.8 Hz, 2H), 4.65 (t, *J* = 4.8 Hz, 2H), 4.04 – 3.97 (m, 2H), 3.90 (s, 3H), 1.68 (sextet, *J* = 7.6 Hz, 2H), 0.96 (t, *J* = 7.4 Hz, 3H). MS: [ESI+H]<sup>+</sup>: 505.1. HPLC: 8.47 min

**3-(8-methoxy-2,4-dioxo-3-propyl-3,4-dihydropyrido[2,1-*f*]purine-1(2*H*)-yl)propyl 3-(fluorosulfonyl)benzoate (14b)** Prepared from **12b** and purified by column chromatography (1% CH<sub>3</sub>OH in CH<sub>2</sub>Cl<sub>2</sub>) to give the desired product as white solid (0.035 g, 0.068 mmol, 34%). <sup>1</sup>H NMR (400 MHz, CDCl<sub>3</sub>): δ 8.74 (d, *J* = 7.6 Hz, 1H), 8.65 (s, 1H), 8.36 (d, *J* = 8.0 Hz, 1H), 8.18 (d, *J* = 8.0 Hz, 1H), 7.73 (t, *J* = 8.0 Hz, 1H), 6.86 (d, *J* = 2.0 Hz, 1H), 6.72 (dd, *J* = 7.2, 2.4 Hz, 1H), 4.51 (t, *J* = 6.0 Hz, 2H), 4.41 (t, *J* = 6.0 Hz, 2H), 3.99 (t, *J* = 7.6 Hz, 2H),

3.91 (s, 3H), 2.39 (pentet,  $J = 6.0$  Hz, 2H), 1.70 (sextet,  $J = 7.6$  Hz, 2H), 0.98 (t,  $J = 7.6$  Hz, 3H). MS: [ESI+H]<sup>+</sup>: 519.1. HPLC: 8.84 min

**4-(8-methoxy-2,4-dioxo-3-propyl-3,4-dihydropyrido[2,1-*f*]purine-1(2*H*)-yl)butyl 3-(fluorosulfonyl)benzoate(14c)** Prepared from **12c** and purified by column chromatography (first 30% DCM in EtOAc). Further purification by another column (4:1= MTBE: PET) gives the desired product as white solid (0.20g, 0.37 mmol, 38%). <sup>1</sup>H NMR (400 MHz, CDCl<sub>3</sub>):  $\delta$  8.85 (d,  $J = 7.2$  Hz, 1H), 8.67 (s, 1H), 8.45 (d,  $J = 8.0$  Hz, 1H), 8.21 (d,  $J = 8.0$  Hz, 1H), 7.75 (t,  $J = 8.0$  Hz, 1H), 6.97 (d,  $J = 2.4$  Hz, 1H), 6.77 (dd,  $J = 7.2, 2.4$  Hz, 1H), 4.49 (t,  $J = 6.4$  Hz, 2H), 4.30 (t,  $J = 7.2$  Hz, 2H), 4.08 – 4.01 (m, 2H), 3.95 (s, 3H), 2.10 – 2.00 (m, 2H), 2.00 – 1.89 (m, 2H), 1.81 – 1.69 (m, 2H), 1.01 (t,  $J = 7.2$  Hz, 3H). MS: [ESI+H]<sup>+</sup>: 533.1. HPLC: 9.14 min

**General procedure for the synthesis 1-(2-(1,3-dioxoisindolin-2-yl)alkyl)-8-methoxy-3-propyl-1*H*,3*H*-pyrido-[2,1-*f*]purine-2,4-dione (15a-c).** To a mixture of the core (**7**) (0.8 mmol, 1 equiv), *N*-(bromoalkyl)phthalimide (1.2 mmol, 1.5 equiv) and K<sub>2</sub>CO<sub>3</sub> (1.2 mmol, 1.5 equiv) was added anhydrous DMF (8 mL). The mixture was refluxed at 100 °C. After completion of the reaction, monitored by TLC (1% MeOH in CH<sub>2</sub>Cl<sub>2</sub>), the mixture was concentrated *in vacuo* and diluted with EtOAc (30 mL). The organic layer was washed with H<sub>2</sub>O (3 × 30 mL), brine (15 mL) and dried over MgSO<sub>4</sub>. The solvent was evaporated under reduced pressure, and the residue was purified by column chromatography using 1% MeOH as an eluent to give **15a-c** as solids.

**1-(2-(1,3-dioxoisindolin-2-yl)ethyl)-8-methoxy-3-propyl-1*H*,3*H*-pyrido-[2,1-*f*]purine-2,4-dione (15a)** Prepared from *N*-(2-bromoethyl)phthalimide and purified by column chromatography to give the desired product as white solid (0.20 g, 0.44 mmol, 5%). <sup>1</sup>H NMR (CDCl<sub>3</sub>):  $\delta$  8.77 (d,  $J = 6.8$  Hz, 1H), 7.73 (s, 2H), 7.64 (s, 2H), 6.69 (d,  $J = 14.0$  Hz, 2H), 4.53 (s, 2H), 4.17 (s, 2H), 3.89 (d,  $J = 6.2$  Hz, 2H), 3.85 (s, 3H), 1.58 – 1.45 (m, 3H), 0.86 (t,  $J = 7.2$  Hz, 3H).

**1-(2-(1,3-dioxoisindolin-2-yl)propyl)-8-methoxy-3-propyl-1*H*,3*H*-pyrido-[2,1-*f*]purine-2,4-dione (15b)** Prepared from *N*-(3-bromoethyl)phthalimide and purified by column chromatography to give the desired product as yellow solid (0.31 g, 0.66 mmol, 66%). <sup>1</sup>H NMR (400 MHz, CDCl<sub>3</sub>):  $\delta$  8.81 – 8.75 (m, 1H), 7.86 – 7.76 (m, 2H), 7.73 – 7.61 (m, 2H), 6.80 (s, 1H), 6.72 (dd,  $J = 7.2, 2.4$  Hz, 1H), 4.29 (t,  $J = 6.8$  Hz, 2H), 4.04 – 3.93 (m, 2H), 3.90 (s, 3H), 3.86 – 3.78 (m, 2H), 2.35 – 2.20 (m, 2H), 1.78 – 1.60 (m, 2H), 1.06 – 0.87 (m, 3H).

**1-(2-(1,3-dioxoisindolin-2-yl)butyl)-8-methoxy-3-propyl-1*H*,3*H*-pyrido-[2,1-*f*]purine-2,4-dione (15c)** Prepared from *N*-(4-bromoethyl)phthalimide and purified by column

chromatography to give the desired product as white solid (0.37 g, 0.76 mmol, 96%). <sup>1</sup>H NMR (400 MHz, CDCl<sub>3</sub>): δ 8.82 (d, *J* = 7.2 Hz, 1H), 7.82 (dd, *J* = 5.2, 2.8 Hz, 2H), 7.70 (dd, *J* = 5.2, 2.8 Hz, 2H), 6.93 (d, *J* = 2.4 Hz, 1H), 6.74 (dd, *J* = 7.2, 2.4 Hz, 1H), 4.22 (d, *J* = 7.2 Hz, 2H), 4.04 – 3.96 (m, 2H), 3.92 (s, 3H), 3.75 (d, *J* = 7.2 Hz, 2H), 1.95 – 1.85 (m, 2H), 1.85 – 1.77 (m, 2H), 1.74 – 1.65 (m, 3H), 0.97 (d, *J* = 7.6 Hz, 3H).

**General procedure for the synthesis 1-(2-aminoalkyl)-8-methoxy-3-propyl-1*H*,3*H*-pyrido-[2,1-*f*]purine-2,4-dione (16a-c).** To a stirred suspension of **15a-c** (0.66 mmol, 1 equiv) in MeOH (8 mL) was added excess hydrazine monohydrate (4.8 mL, 99 mmol). The mixture was stirred for 2–4 h at reflux. After conversion of the starting material, the mixture was cooled to room temperature. The solvents were removed under vacuum and the residue was dissolved in 2 M NaOH (aq.) (25 mL). This aqueous phase was extracted three times with CH<sub>2</sub>Cl<sub>2</sub> (25 mL). The organic layers were combined, dried over MgSO<sub>4</sub> and concentrated *in vacuo* to obtain **16a-c**.

**1-(2-aminoethyl)-8-methoxy-3-propyl-1*H*,3*H*-pyrido-[2,1-*f*]purine-2,4-dione (16a).**

Prepared from **15a** and purified by column chromatography to give the desired product as white solid (0.13 g, 0.39 mmol, 90%). <sup>1</sup>H NMR (400 MHz, CDCl<sub>3</sub>): δ 8.84 (d, *J* = 7.6 Hz, 1H), 6.95 (d, *J* = 2.4 Hz, 1H), 6.75 (dd, *J* = 7.2, 2.4 Hz, 1H), 4.27 (t, *J* = 6.4 Hz, 2H), 4.05 – 3.99 (m, 2H), 3.93 (s, 3H), 3.15 (t, *J* = 6.4 Hz, 2H), 1.78 – 1.67 (m, 2H), 0.99 (d, *J* = 7.6 Hz, 3H).

**1-(3-aminopropyl)-8-methoxy-3-propyl-1*H*,3*H*-pyrido-[2,1-*f*]purine-2,4-dione (16b).**

Prepared from **15b** and purified by column chromatography to give the desired product as white solid (0.25 g, 0.75 mmol, 97%). <sup>1</sup>H NMR (400 MHz, CDCl<sub>3</sub>): δ 8.82 (d, *J* = 7.2 Hz, 1H), 6.95 (d, *J* = 2.4 Hz, 1H), 6.75 (dd, *J* = 7.6, 2.4 Hz, 1H), 4.29 (t, *J* = 6.8 Hz, 2H), 4.07 – 3.98 (m, 2H), 3.93 (s, 3H), 2.75 (t, *J* = 6.6 Hz, 2H), 1.98 (p, *J* = 6.6 Hz, 2H), 1.78 – 1.65 (m, 2H), 0.99 (t, *J* = 7.4 Hz, 3H).

**1-(4-aminobutyl)-8-methoxy-3-propyl-1*H*,3*H*-pyrido-[2,1-*f*]purine-2,4-dione (16c).**

Prepared from **15c** and purified by column chromatography to give the desired product as white solid (0.23 g, 0.66 mmol, 86%). <sup>1</sup>H NMR (400 MHz, CDCl<sub>3</sub>): δ 8.84 (d, *J* = 7.6 Hz, 1H), 6.97 (d, *J* = 2.4 Hz, 1H), 6.75 (dd, *J* = 7.2, 2.4 Hz, 1H), 4.20 (t, *J* = 7.2 Hz, 2H), 4.06 – 3.98 (m, 2H), 3.92 (s, 3H), 2.77 (d, *J* = 6.8 Hz, 2H), 1.92 – 1.82 (m, 2H), 1.78 – 1.66 (m, 2H), 1.63 – 1.53 (m, 2H), 0.99 (t, *J* = 7.2 Hz, 3H).

**4-((2-(8-methoxy-2,4-dioxo-3-propyl-3,4-dihydropyrido[2,1-*f*]purin-1(2*H*)-yl)ethyl)carbamoyl)benzenesulfonyl fluoride (17a)** EDC (0.12 g, 0.60 mmol, 1.2 equiv) was dissolved in CHCl<sub>3</sub> (4 mL). To this stirring solution was added the acid (**9a**) (0.11g, 0.55 mmol, 1.1 equiv). The amine (**16a**) (0.16 g, 0.50 mmol, 1.0 equiv) was suspended in CHCl<sub>3</sub> (6



mL), then was added dropwise via an automatic syringe at a rate of 0.2 mL/min. The reaction was stirred for 1.5 h at room temperature and monitored by TLC (CH<sub>2</sub>Cl<sub>2</sub>: acetone = 3:2). After completion the solvent was removed under vacuum and the residue was redissolved in CHCl<sub>3</sub> (40 mL). The organic layer was washed with 1 M HCl (40 mL), H<sub>2</sub>O (2 × 40 mL), dried over MgSO<sub>4</sub> and concentrated *in vacuo* to obtain **17a** as white solid (0.20 g, 0.39 mmol, 78%). <sup>1</sup>H NMR (400 MHz, CDCl<sub>3</sub>): δ 8.83 (d, *J* = 7.2 Hz, 1H), 8.07 – 8.00 (m, 5H), 6.91 (d, *J* = 2.4 Hz, 1H), 6.80 (dd, *J* = 7.2, 2.0 Hz, 1H), 4.62 – 4.55 (m, 2H), 4.03 (t, *J* = 7.6 Hz, 2H), 3.95 (s, 3H), 3.94 – 3.89 (m, 2H), 1.68 (sextet, *J* = 7.6 Hz, 2H), 0.97 (t, *J* = 7.2 Hz, 3H). MS: [ESI+H]<sup>+</sup>: 504.1. HPLC: 7.93 min.

#### 4-((3(8-methoxy-2,4-dioxo-3-propyl-3,4-dihydropyrido[2,1-*f*]purin-

#### 1(2*H*)yl)propyl)carbamoyl)benzenesulfonyl fluoride (**17b**). To a suspension of EDC (0.22 g, 0.80 mmol, 1.5 equiv) and **9a** (0.16 g, 0.80 mmol 1.05 equiv) was dissolved in CH<sub>2</sub>Cl<sub>2</sub> (4 mL). To this stirring solution was added the amine (**16b**) (0.25 g, 0.76 mmol, 1.0 equiv) at room temperature. The reaction was stirred for 2 h and monitored by TLC (3% MeOH in CH<sub>2</sub>Cl<sub>2</sub>). After completion, the solvent was removed *in vacuo* and the residue was dissolved in CHCl<sub>3</sub> (40 mL). The organic layer was washed with 1 M HCl (40 mL), twice with H<sub>2</sub>O (2 × 40 mL), dried over MgSO<sub>4</sub> and concentrated *in vacuo*. The product was purified by column chromatography using 2% MeOH in CH<sub>2</sub>Cl<sub>2</sub> to afford the title compound as white solid (0.26 g, 0.50 mmol, 66%). <sup>1</sup>H NMR (400MHz, CDCl<sub>3</sub>) δ: 8.86 (d, *J* = 7.2 Hz, 1H), 8.38 (t, *J* = 5.6 Hz, 1H), 8.25 (d, *J* = 8.4 Hz, 2H), 8.16 (d, *J* = 8.4 Hz, 2H), 6.85 (d, *J* = 2.4 Hz, 1H), 6.81 (dd, *J* = 7.2, 2.4 Hz, 1H), 4.35 (t, *J* = 6.0 Hz, 2H), 4.05 (t, *J* = 7.6 Hz, 2H), 3.92 (s, 3H), 3.47 (q, *J* = 6.4 Hz, 2H), 2.19–2.13 (m, 2H), 1.73 (sextet, *J* = 7.6 Hz, 2H), 1.00 (t, *J* = 7.6 Hz, 3H). <sup>13</sup>C NMR (600 MHz, DMSO-*d*<sub>6</sub>, 348K) δ 164.0, 160.9, 153.4, 150.6, 150.5, 149.1, 141.3, 133.3 (d, *J* = 96 Hz), 128.5, 127.9, 127.3, 107.0, 99.8, 95.4, 55.7, 41.5, 40.6, 36.8, 27.1, 20.5, 10.6. MS: [ESI+H]<sup>+</sup>: 518.1. HRMS-ESI<sup>+</sup>: [M + H]<sup>+</sup> calcd: 518.1510 found: 518.1540, C<sub>23</sub>H<sub>25</sub>O<sub>6</sub>N<sub>5</sub>FS. HPLC: 8.27 min.

#### 4-((4(8-methoxy-2,4-dioxo-3-propyl-3,4-dihydropyrido[2,1-*f*]purin-1(2*H*)-

#### yl)butyl)carbamoyl)benzenesulfonyl fluoride (**17c**) The acid **9a** (0.11 g, 0.53 mmol, 1.5 equiv) was dissolved in an excess of thionyl chloride (20 mL) at 75 °C under nitrogen for 3 h. After removal of solvent and other volatiles in vacuum, **10a** was obtained as colorless oil. Subsequently the amine **16c** (0.12 g, 0.35 mmol, 1.0 equiv), K<sub>2</sub>CO<sub>3</sub> (0.073 g, 0.53 mmol, 1.5 equiv) and dry DMF were added and the reaction as stirred at 40 °C overnight. After completion of the reaction, 1M HCl (200 mL) was added and extracted with CH<sub>2</sub>Cl<sub>2</sub> (150 mL). The organic layer was washed with water (100 mL) and brine (100 mL). The organic layer

was dried, filtered and concentrated *in vacuo*. The residue was purified by column chromatography using CH<sub>2</sub>Cl<sub>2</sub> with 1% methanol as eluent to give **17c** as white solid (5.0 mg, 0.0094 mmol, 4%). <sup>1</sup>H NMR (400 MHz, CDCl<sub>3</sub>): δ 8.87 (d, *J* = 7.6 Hz, 1H), 8.17 (d, *J* = 8.4 Hz, 2H), 8.09 (d, *J* = 8.4 Hz, 2H), 7.54 (brs, 1H), 6.85 (s, 1H), 6.80 (dd, *J* = 7.2, 2.4 Hz, 1H), 4.29 (t, *J* = 7.6 Hz, 2H), 4.06 (t, *J* = 7.6 Hz, 2H), 3.92 (s, 3H), 3.68 (q, *J* = 6.0 Hz, 2H), 2.01 (pent, *J* = 6.8 Hz, 2H), 1.84-1.70 (m, 4H), 1.02 (t, *J* = 7.6 Hz, 3H). MS: [ESI+H]<sup>+</sup>: 532.3 . HPLC: 8.28 min.

**3-((2-(8-methoxy-2,4-dioxo-3-propyl-3,4-dihydropyrido[2,1-f]purin-1(2H)-yl)ethyl)carbamoyl)benzenesulfonyl fluoride (18a)** EDC (0.12 g, 0.60 mmol, 1.2 equiv) was dissolved in CHCl<sub>3</sub> (4 mL). To this stirring solution was added the acid **9b** (0.11 g, 0.55 mmol, 1.1 equiv). The amine **16a** (0.16 g, 0.50 mmol, 1.0 equiv) was suspended in CHCl<sub>3</sub> (6 mL), then was added dropwise via an automatic syringe at a rate of 0.2 mL/min. The reaction was stirred for 3 h at room temperature and monitored by TLC (CH<sub>2</sub>Cl<sub>2</sub>: Acetone = 3:2). After completion, the solvent was removed *in vacuo* and the residue was resolubilized in CHCl<sub>3</sub> (40 mL). The organic layer was washed with 1 M HCl (40 mL), twice with H<sub>2</sub>O (2 × 40 mL), dried over MgSO<sub>4</sub> and concentrated *in vacuo* to give **18a** as white solid (0.17g, 0.35 mmol, 70%). <sup>1</sup>H NMR (400 MHz, CDCl<sub>3</sub>): δ 8.81 (d, *J* = 7.6 Hz, 1H), 8.37 (s, 1H), 8.29 (d, *J* = 8.0 Hz, 1H), 8.11 (d, *J* = 7.6 Hz, 1H), 8.04 (br s, 1H), 7.71 (t, *J* = 8.0 Hz, 1H), 7.02 (d, *J* = 2.4 Hz, 1H), 6.77 (dd, *J* = 7.6, 2.4 Hz, 1H), 4.61 – 4.54 (m, 2H), 4.03 (t, *J* = 7.6 Hz, 2H), 3.96 (s, 3H), 3.94 – 3.89 (m, 2H), 1.76 – 1.63 (m, 2H), 0.97 (t, *J* = 7.6 Hz, 3H). MS: [ESI+H]<sup>+</sup>: 504.1. HPLC: 7.67 min.

**3-((3-(8-methoxy-2,4-dioxo-3-propyl-3,4-dihydropyrido[2,1-f]purin-1(2H)-yl)propyl)carbamoyl) benzenesulfonyl fluoride (18b)** The acid **9b** (0.42 g, 2.0 mmol, 3.0 equiv) was dissolved in thionylchloride (20 mL) and stirred for 3 h at 75 °C. The thionylchloride was evaporated and the residue was co-evapped twice with toluene. Then the amine **14b** (0.23 mg, 0.7 mmol, 1.00 equiv), K<sub>2</sub>CO<sub>3</sub> (0.073 g, 0.53 mmol, 1.5 equiv) and dry DMF were added and the reaction as stirred at 40 °C overnight. 1M HCl (200 mL) was added and extracted with CH<sub>2</sub>Cl<sub>2</sub> (150 mL). The organic layer was washed with water (100 mL) and brine (100 mL). The organic layer was dried, filtered and concentrated *in vacuo*. The residue was purified by column chromatography using CH<sub>2</sub>Cl<sub>2</sub> with 1% methanol as eluent to give **18b** as white solid (0.0050g, 0.01 mmol, 2.7%). <sup>1</sup>H NMR (400MHz, CDCl<sub>3</sub>) δ: 8.88 (d, *J* = 7.2 Hz, 1H), 8.68 (s, 1H), 8.55-8.50 (m, 2H), 8.20 (d, *J* = 8.0 Hz, 1H), 7.82 (t, *J* = 8 Hz, 2H), 7.00 (d, *J* = 2.4 Hz, 1H), 6.80 (dd, *J* = 7.2, 2.4 Hz, 1H), 4.33 (t, *J* = 6.0 Hz, 2H), 4.05 (t, *J* =

7.6 Hz, 2H), 3.94 (s, 3H), 3.47 (q,  $J = 6.0$  Hz, 2H), 2.17-2.12 (m, 2H), 1.74 (sextet,  $J = 7.6$  Hz, 2H), 1.00 (t,  $J = 7.6$  Hz, 3H). MS: ESI  $[M+H]^+$ : 518.1 HPLC: 8.28 min.

**3-((4-(8-methoxy-2,4-dioxo-3-propyl-3,4-dihydropyrido[2,1-*f*]purin-1(2*H*)-**

**yl)butyl)carbamoyl)benzenesulfonyl fluoride (18c)** EDC (0.13 g, 0.69 mmol, 1.2 equiv) was dissolved in CH<sub>2</sub>Cl<sub>2</sub> (3 mL). The acid **9b** (0.13 g, 0.63 mmol, 1.1 equiv) was added to this solution and the mixture was stirred. The amine **16c** (0.20 g, 0.57 mmol, 1 equiv) was dissolved in CHCl<sub>3</sub> (8 mL) and added dropwise via an automatic syringe at a rate of 0.2 mL/min to the stirring solution. After 3 h at room temperature the reaction was completed and the mixture was concentrated *in vacuo*. The residue was dissolved in CH<sub>2</sub>Cl<sub>2</sub> (40 mL) and washed with 1 M HCl (40 mL) and twice with H<sub>2</sub>O (2 × 40 mL). The organic layer was dried over MgSO<sub>4</sub> and concentrated *in vacuo*. Purification by column chromatography (CH<sub>2</sub>Cl<sub>2</sub>: acetone = 3:2) gave the **18c** as a white solid (0.14 g, 0.26 mmol, 47%). <sup>1</sup>H NMR (400 MHz, CDCl<sub>3</sub>): δ 8.84 (d,  $J = 7.2$  Hz, 1H), 8.54 (s, 1H), 8.36 (d,  $J = 7.6$  Hz, 1H), 8.12 (d,  $J = 7.6$  Hz, 1H), 7.72 (t,  $J = 7.6$  Hz, 1H), 7.62 (br s, 1H), 6.84 (s, 1H), 6.80 – 6.70 (m, 1H), 4.27 (t,  $J = 7.2$  Hz, 2H), 4.04 (t,  $J = 8.0$  Hz, 2H), 3.89 (s, 3H), 3.74 – 3.60 (m, 2H), 2.07 – 1.92 (m, 2H), 1.85 – 1.64 (m, 4H), 0.98 (t,  $J = 7.2$  Hz, 3H). MS:  $[ESI+H]^+$ : 532.3. HPLC: 8.21 min.

**N-(3-(8-methoxy-2,4-dioxo-3-propyl-3,4-dihydropyrido[2,1-*f*]purin-1(2*H*)-yl)propyl)-4-(methylsulfonyl)benzamide (19)**. To a solution of EDC (0.061 g, 0.32 mmol, 1.2 equiv) in CHCl<sub>3</sub> (5 mL) was added 4-(methylsulfonyl)benzoic acid (0.060 g, 0.30 mmol, 1.1 equiv). The amine **16b** (0.090 g, 0.27 mmol, 1 equiv) was taken up in CHCl<sub>3</sub> (5 mL) and was subsequently added dropwise via an automatic syringe at a rate of 0.15 mL/min. The reaction was stirred at room temperature and monitored by TLC (4% MeOH in CH<sub>2</sub>Cl<sub>2</sub>). After 3 h the reaction was completed and CHCl<sub>3</sub> (50 mL) was added. The organic layer was washed with 1 M HCl (60 mL), H<sub>2</sub>O (60 mL), brine (60 mL), dried over MgSO<sub>4</sub> and concentrated under vacuum. The product was purified by column chromatography using 2% MeOH in CH<sub>2</sub>Cl<sub>2</sub> to afford the title compound (0.075 g, 0.14 mmol, 54%). <sup>1</sup>H NMR (400 MHz, CDCl<sub>3</sub>): δ 8.86 (d,  $J = 7.2$  Hz, 1H), 8.36 (t,  $J = 5.6$  Hz, 1H), 8.19 (d,  $J = 8.4$  Hz, 2H), 8.09 (d,  $J = 8.4$  Hz, 2H), 6.90 – 6.71 (m, 2H), 4.45 – 4.28 (m, 2H), 4.13 – 3.99 (m, 2H), 3.91 (s, 3H), 3.55 – 3.41 (m, 2H), 3.11 (s, 3H), 2.27 – 2.09 (m, 2H), 1.83 – 1.61 (m, 2H), 1.00 (t,  $J = 7.4$  Hz, 3H). <sup>13</sup>C NMR (600 MHz, DMSO-*d*<sub>6</sub>, 318K): δ 164.7, 161.1, 153.5, 150.7, 150.6, 149.3, 142.8, 138.9, 127.9, 127.5, 126.7, 107.4, 99.9, 95.4, 56.0, 43.2, 41.6, 40.8, 36.8, 27.4, 20.7, 10.9. MS:  $[ESI+H]^+$ : 514.2. HRMS-ESI<sup>+</sup>:  $[M + H]^+$  calcd: 518.1760 found: 518.1791, C<sub>24</sub>H<sub>28</sub>O<sub>6</sub>N<sub>5</sub>S. HPLC: 6.89 min.

### 4.2. Computational studies

All calculations were performed using the Schrodinger Suite [31]. Since compound **17b** shares a high similarity with the ligands on which we previously published [7], the same homology model based on the high resolution antagonist-bound crystal structure of the adenosine A<sub>2A</sub> receptor (PDB: 4E1Y [27]) was used for the docking studies performed here. Based on those proposed docking poses, we used induced fit docking [32] with core constraints on the pyridopurinedione to dock the different ligands.

### 4.3. Biology

[<sup>3</sup>H]8-Ethyl-4-methyl-2-phenyl-(8R)-4,5,7,8-tetrahydro-1*H*-imidazo[2,1-*i*]-purin-5-one ([<sup>3</sup>H]PSB-11, specific activity 56 Ci·mmol<sup>-1</sup>) was a gift from Prof. C.E. Müller (University of Bonn, Germany). Unlabeled PSB-11, 1-deoxy-1-[6-(((3- and 2-chloro-N<sup>6</sup>-(3-iodobenzyl)-adenosine-5'-N-methyluronamide (2-Cl-IB-MECA) were purchased from Tocris Ltd. (Abingdon, UK). 5'-N-ethylcarboxamidoadenosine (NECA) was purchased from Sigma-Aldrich (Steinheim, Germany). Adenosine deaminase (ADA) was purchased from Boehringer Mannheim (Mannheim, Germany). Bicinchoninic acid (BCA) and BCA protein assay reagents were purchased from Pierce Chemical Company (Rockford, IL, USA). Chinese hamster ovary (CHO) cells stably expressing the human A<sub>3</sub> adenosine receptor (CHOhA<sub>3</sub>) were a gift from Dr. K-N Klotz (University of Würzburg, Germany). All other chemicals were obtained from standard commercial sources and were of analytical grade.

*Cell Culture and Membrane Preparation.* Chinese Hamster Ovary (CHO) cells, stably expressing the human A<sub>3</sub> adenosine receptor (CHOhA<sub>3</sub>), were cultured and membranes were prepared and stored as previously reported [7, 33]. Protein determination was performed based on the bicinchoninic acid (BCA) method [34].

*Y265F<sup>7.36</sup> Site-Directed Mutagenesis.* The single tyrosine mutation introduced in TM7 of the hA<sub>3</sub>AR was performed with the QuickChange II Site Directed Mutagenesis system (Stratagene, Huizen, The Netherlands). The wild type pcDNA3.1(+)-A<sub>3</sub>AR plasmid DNA with N-terminal 3 x HA-tag was used as a template for polymerase chain reaction (PCR) mutagenesis. Mutant primers for directional PCR product cloning were designed using the online Quickchange primer design program (Agilent Technologies, Santa Clara, CA), and obtained from Eurogentec (Maastricht, The Netherlands). Forward primer used for this procedure was 5'-cacagcttgctgttcatgggcatcctgct-3' and the reverse primer was 5'-agcaggatgcccatgaacagcacaagctgtg-3'. All DNA sequences were verified by Sanger sequencing at LGTC (Leiden, The Netherlands).

*Transient Expression of Wild Type (WT) and Mutant Receptors in CHO-K1 Cells.* CHO-K1 cells were seeded into 150-mm culture dishes to achieve 60% confluence in the presence of 20 ml culture medium consisting of DMEM/F12 (1:1) supplemented with 10% (v/v) newborn calf serum, streptomycin (50 µg/mL) and penicillin (50 IU/mL). Cells were transfected approximately 24 h later with plasmid DNA (20 µg of DNA/dish) by the PEI method [35] (PEI:DNA = 3:1) and left for 24 h. Subsequently medium was removed and fresh medium containing 5 mM sodium butyrate was added (to enhance the receptor expression level [36]), and cells were grown for an additional 24 h at 37 °C and 5% CO<sub>2</sub>. Membrane preparation followed the procedure described above for the CHO cell membranes stably expressing hA<sub>3</sub>AR. [7, 33]

*Radioligand Displacement Assay.* Radioligand displacement experiments were performed as in previously published methods [7]. Membrane aliquots containing 15 µg of protein were incubated in a total volume of 100 µL assay buffer (50 mM Tris-HCl, 5 mM MgCl<sub>2</sub>, supplemented with 0.01% CHAPS and 1 mM EDTA, pH 7.4) at 25 °C for 120 min. Displacement experiments were performed using six concentrations of competing antagonist in the presence of ~10 nM [<sup>3</sup>H]PSB-11. Nonspecific binding (NSB) was determined in the presence of 100 µM NECA and represented less than 10% of total binding. Incubation was terminated by rapid filtration performed on 96-well GF/B filter plates (Perkin Elmer, Groningen, the Netherlands) in a PerkinElmer Filtermate-harvester (Perkin Elmer, Groningen, the Netherlands). After the filter plate was dried at 55 °C for 30 min, the filter-bound radioactivity was determined by scintillation spectrometry using a 2450 MicroBeta<sup>2</sup> Plate Counter (Perkin Elmer, Boston, MA).

*Radioligand Competition Association Assay.* The competition association assay was performed by incubation of ~10 nM [<sup>3</sup>H]PSB-11 in the absence or presence of competing hA<sub>3</sub>AR antagonist at its IC<sub>50</sub> concentration with membrane aliquots. The amount of receptor-bound radioligand was determined at different time points up to 240 min. Incubations were terminated and samples were obtained as described under *Radioligand Displacement Assay*.

*[<sup>35</sup>S] GTPγS Binding Assay.* The assays were started by adding 15 µg of homogenized CHO<sub>hA3</sub> membranes in an ice-cold assay buffer to a total volume of 80 µL containing 50 mM Tris-HCl buffer, 5 mM MgCl<sub>2</sub>, 1 mM EDTA, 0.05% BSA and 1 mM DTT, 100 mM NaCl, pH 7.4, supplemented with 1 µM GDP and 5 µg saponin. The assays were performed in a 96-well plate format, where stock solutions of the compounds were added to a total volume

## Chapter 4

of 100  $\mu\text{L}$  using an HP D300 Digital Dispenser (Tecan, Männedorf, Switzerland). The final concentration of DMSO per assay point was  $\leq 0.1\%$ . The basal level of [ $^{35}\text{S}$ ] GTP $\gamma\text{S}$  binding was determined in the absence of ligand, whereas the maximal level of [ $^{35}\text{S}$ ] GTP $\gamma\text{S}$  binding was determined in the presence of 10  $\mu\text{M}$  2-Cl-IBMECA. For the insurmountability experiments, membrane preparations were pre-incubated with or without antagonists (1-, 3-, 10-fold  $K_i$  values) for 60 min at 25  $^\circ\text{C}$ , prior to the addition of 2-Cl-IBMECA (10  $\mu\text{M}$  to 0.1 nM) and 20  $\mu\text{l}$  [ $^{35}\text{S}$ ] GTP $\gamma\text{S}$  (final concentration  $\sim 0.3$  nM), after which incubation continued for another 30 min at 25  $^\circ\text{C}$ . For the surmountability (control) experiments, antagonists (1-, 3-, 10-fold  $K_i$  values) and 2-Cl-IBMECA (10  $\mu\text{M}$  to 0.1 nM) were co-incubated with [ $^{35}\text{S}$ ] GTP $\gamma\text{S}$  for 30 min at 25  $^\circ\text{C}$ . For all experiments, incubations were terminated and samples were obtained as described under *Radioligand Displacement Assay*, by using GF/B filters (Whatman International, Maidstone, UK).

*Data Analysis.* All experimental data were analyzed using the nonlinear regression curve fitting program GraphPad Prism 7.0 (GraphPad Software, Inc., San Diego, CA). Data from the radioligand displacement assays were fit into one-site binding mode, and the obtained  $\text{IC}_{50}$  values were converted into  $K_i$  values using the Cheng-Prusoff equation to determine the affinity of the ligands [37]. The observed association rate constants ( $k_{\text{obs}}$ ) derived from both assays were obtained by fitting association data using one phase exponential association. The dissociation rate constants were obtained by fitting dissociation data to a one phase exponential decay model. The  $k_{\text{obs}}$  values were converted into association rate constants ( $k_{\text{on}}$ ) using the equation  $k_{\text{on}} = (k_{\text{obs}} - k_{\text{off}})/[L]$ , where  $[L]$  is the amount of radioligand used for the association experiments. Association and dissociation rate constants for unlabeled compounds were calculated by fitting the data into the competition association model using “kinetics of competitive binding” [22].

$$\begin{aligned}
 K_A &= k_1[L] \cdot 10^{-9} + k_2 \\
 K_B &= k_3[I] \cdot 10^{-9} + k_4 \\
 S &= \sqrt{(K_A - K_B)^2 + 4 \cdot k_1 \cdot k_3 \cdot L \cdot I \cdot 10^{-18}} \\
 K_F &= 0.5(K_A + K_B + S) \\
 K_S &= 0.5(K_A + K_B - S) \\
 Q &= \frac{B_{\text{max}} \cdot k_1 \cdot L \cdot 10^{-9}}{K_F - K_S} \\
 Y &= Q \cdot \left( \frac{k_4 \cdot (K_F - K_S)}{K_F \cdot K_S} + \frac{k_4 - K_F}{K_F} e^{(-K_F \cdot X)} - \frac{k_4 - K_S}{K_S} e^{(-K_S \cdot X)} \right)
 \end{aligned}$$

Where X is the time (min), Y is the specific [<sup>3</sup>H]PSB-11 binding (DPM), k<sub>1</sub> and k<sub>2</sub> are the k<sub>on</sub> (nM<sup>-1</sup>min<sup>-1</sup>) and k<sub>off</sub> (min<sup>-1</sup>) of [<sup>3</sup>H]PSB-11, B<sub>max</sub> is the total binding (DPM), L is the radioligand concentration (nM), I is the concentration of the unlabeled competitor (nM). Association and dissociation rate constants for [<sup>3</sup>H]PSB-11 (k<sub>1</sub> = 0.281 ± 0.04 × 10<sup>8</sup> M<sup>-1</sup>·min<sup>-1</sup> and k<sub>2</sub> = 0.3992 ± 0.02 min<sup>-1</sup>) were obtained from Xia *et al* [7]. With that the k<sub>3</sub>, k<sub>4</sub> and B<sub>max</sub> were calculated, where k<sub>3</sub> represents the k<sub>on</sub> (nM<sup>-1</sup>min<sup>-1</sup>) of the unlabeled ligand, k<sub>4</sub> stands for the k<sub>off</sub> (min<sup>-1</sup>) of the unlabeled ligand and B<sub>max</sub> equals the total binding (DPM). All competition association data were globally fitted. The residence time (RT, in min) was calculated using the equation RT = 1/ k<sub>off</sub>, as k<sub>off</sub> values are expressed in min<sup>-1</sup>. [<sup>35</sup>S] GTPγS binding curves were analyzed by nonlinear regression using “log (agonist) vs response-variable slope” to obtain potency, inhibitory potency or efficacy values of agonists and antagonists (EC<sub>50</sub> and E<sub>max</sub>, respectively). In the (in)surmountability assays, Schild EC<sub>50</sub> shift equations were used to obtain Schild-slopes and pA<sub>2</sub> values. All experimental values obtained are means of three independent experiments performed in duplicate.

### Supporting Information

4

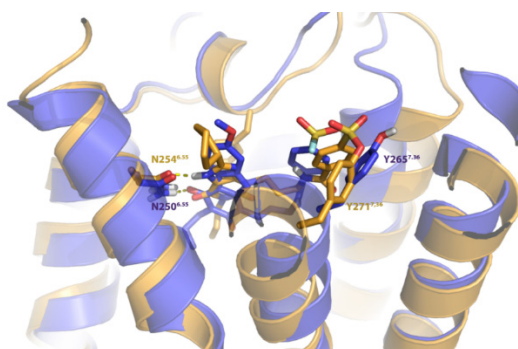


Figure S1. Overlay of a view from crystal structure of compound **2** (mustard carbon sticks) bound to human adenosine A<sub>1</sub> receptor (mustard; PDB: 5UEN)[11] and the hA<sub>3</sub>AR (violet) homology model docking with **17b** (violet carbon sticks). Atoms color code: red = oxygen, blue = nitrogen, white = hydrogen, yellow = sulfur, cyan = fluorine. Hydrogen bonds between ligands and relevant amino acid residues are indicated by dashed lines.

### Abbreviations used

ADA, adenosine deaminase. BCA, bicinchoninic acid. CHAPS, 3-[(3-Cholamidopropyl) dimethylammonio]-1-propanesulfonate. CHO, Chinese hamster ovary. CHO-K1, a subclone from the parental CHO cell line. 2-Cl-IB-MECA, 1-[2-chloro-6-[[[(3-iodophenyl) methyl] amino]-9H-purin-9-yl]-1-deoxy-N-methyl-β-D-ribofuranuronamide. DBU, 1,8-diazabicyclo [5.4.0] undec-7-ene. EDC, 1-ethyl-3-(3-dimethylaminopropyl) carbodiimide. E<sub>max</sub>, maximum response elicited by an unlabeled ligand in a functional assay (relatively to 2-Cl-IB-MECA) at

## Chapter 4

---

membranes of CHO cells stably expressing the A<sub>3</sub> adenosine receptor. EtOAc, ethylacetate. FBS, fetal bovine serum. G418, geneticin. GTP $\gamma$ S, guanosine 5'-O-[ $\gamma$ -thio] triphosphate. hA<sub>1</sub>AR, human A<sub>1</sub> Adenosine Receptor. hA<sub>3</sub>AR, human A<sub>3</sub> Adenosine Receptor. MeCN, acetonitrile. NECA, 5'-(N-ethylcarboxamide) adenosine. PSB-11, 8-Ethyl-4-methyl-2-phenyl-(8R)-4,5,7,8-tetrahydro-1H-imidazo[2,1-*i*]-purin-5-one. PET, petroleum ether

### References

1. Fredholm B.B., IJzerman A.P., Jacobson K.A., Klotz K.N., and Linden J. *Pharmacol Rev.* **2001**. 53(4): 527-552.
2. Ali H., Cunhamelo J.R., Saul W.F., and Beaven M.A. *J Biol Chem.* **1990**. 265(2): 745-753.
3. Borea P.A., Varani K., Vincenzi F., Baraldi P.G., Tabrizi M.A., Merighi S., and Gessi S. *Pharmacol Rev.* **2015**. 67(1): 74-102.
4. Yang H., Avila M.Y., Peterson-Yantorno K., Coca-Prados M., Stone R.A., Jacobson K.A., and Civan M.M. *Cur Eye Res.* **2005**. 30(9): 747-754.
5. Brown R.A., Spina D., and Page C.P. *Br J Pharmacol.* **2008**. 153 Suppl 1: S446-456.
6. Priego E.M., Perez-Perez M.J., von Frijtag Drabbe Kuenzel J.K., de Vries H., IJzerman A.P., Camarasa M.J., and Martin-Santamaria S. *ChemMedChem.* **2008**. 3(1): 111-119.
7. Xia L., Burger W.A.C., van Veldhoven J.P.D., Kuiper B.J., van Duijl T.T., Lenselink E.B., Paasman E., Heitman L.H., and AP I. *J Med Chem.* **2017**. 60(17): 7555-7568.
8. Priego E.M., Kuenzel J.V., IJzerman A.P., Camarasa M.J., and Perez-Perez M.J. *J Med Chem.* **2002**. 45(16): 3337-3344.
9. Weichert D., and Gmeiner P. *ACS Chem Bio.* **2015**. 10(6): 1376-1386.
10. Murrison E.M., Goodson S.J., Edbrooke M.R., and Harris C.A. *Febs Letters.* **1996**. 384(3): 243-246.
11. Glukhova A., Thal D.M., Nguyen A.T., Vecchio E.A., Jorg M., Scammells P.J., May L.T., Sexton P.M., and Christopoulos A. *Cell.* **2017**. 168(5): 867-877.
12. Li A.H., Chang L., Ji X.D., Melman N., and Jacobson K.A. *Bioconjugate Chem.* **1999**. 10(4): 667-677.
13. Baraldi P.G., Cacciari B., Moro S., Romagnoli R., Ji X.D., Jacobson K.A., Gessi S., Borea P.A., and Spalluto G. *J Med Chem.* **2001**. 44(17): 2735-2742.
14. Biochemical and Biophysical Research Communications Ji X.D., Gallorodriguez C., and Jacobson K.A. *Biochem. and Biophys Res Commun.* **1994**. 203(1): 570-576.
15. Yang X., Michiels T.J.M., de Jong C., Soethoudt M., Dekker N., Gordon E., van der Stelt M., Heitman L.H., van der Es D., and IJzerman A.P. *J Med Chem.* **2018**. 61(17): 7892-7901.
16. Picone R.P., Fournier D.J., and Makriyannis A. *J Pept Res.* **2002**. 60(6): 348-356.
17. Narayanan A., and Jones L.H. *Chem Sci.* **2015**. 6(5): 2650-2659.
18. Grimster N.P., Connelly S., Baranczak A., Dong J.J., Krasnova L.B., Sharpless K.B., Powers E.T., Wilson I.A., and Kelly J.W. *J Am Chem Soc.* **2013**. 135(15): 5656-5668.
19. Muller C.E., Diekmann M., Thorand M., and Ozola V. *Bioorg Med Chem Lett.* **2002**. 12(3): 501-503.
20. Weichert D., Kruse A.C., Manglik A., Hiller C., Zhang C., Hubner H., Kobilka B.K., and Gmeiner P. *Proc. Natl. Acad. Sc U.S.A.* **2014**. 111(29): 10744-10748.
21. Yang X., Dong G., Michiels T.J.M., Lenselink E.B., Heitman L., Louvel J., and IJzerman A.P. *Purinergic Signalling.* **2017**. 13(2): 191-201.
22. Motulsky H.J., and Mahan L.C. *Mol Pharmacol.* **1984**. 25(1): 1-9.



23. Doornbos M.L.J., Wang X., Vermond S.C., Peeters L., Perez-Benito L., Trabanco A.A., Lavreysen H., Cid J.M., Heitman L.H., Tresadern G., and IJzerman A.P., *J Med Chem.* **2018**. In Press: 10.1021/acs.jmedchem.8b00051.
24. Jorg M., Glukhova A., Abdul-Ridha A., Vecchio E.A., Nguyen A.T.N., Sexton P.M., White P.J., May L.T., Christopoulos A., and Scammells P.J. *J Med Chem.* **2016**. 59(24): 11182-11194.
25. van Muijlwijk-Koezen J.E., Timmerman H., van der Sluis R.P., van de Stolpe A.C., Menge W.M.P.B., Beukers M.W., van der Graaf P.H., de Groot M., and IJzerman A.P. *Bioorg. Med. Chem. Lett.* **2001**. 11(6): 815-818.
26. Strange P.G. *Br J Pharmacol.* **2010**. 161(6): 1238-1249.
27. Liu W., Chun E., Thompson A.A., Chubukov P., Xu F., Katritch V., Han G.W., Roth C.B., Heitman L.H., IJzerman A.P., Cherezov V., and Stevens R.C. *Science.* **2012**. 337(6091): 232-236.
28. Picone R.P., Khanolkar A.D., Xu W., Ayotte L.A., Thakur G.A., Hurst D.P., Abood M.E., Reggio P.H., Fournier D.J., and Makriyannis A. *Mol Pharmacol.* **2005**. 68(6): 1623-1635.
29. Singh J., Petter R.C., Baillie T.A., and Whitty A. *Nat Rev Drug Discov.* **2011**. 10(4): 307-317.
30. Soethoudt M., Stolze S.C., Westphal M.V., van Stralen L., Martella A., van Rooden E.J., Guba W., Varga Z.V., Deng H., van Kasteren S.I., Grether U., IJzerman A.P., Pacher P., Carreira E.M., Overkleeft H.S., Ioan-Facsinay A., Heitman L.H., and van der Stelt M. *J Am Chem Soc.* **2018**. 140(19): 6067-6075.
31. Goebel U., Siepe M., Schwer C., Schlensak C., and Loop T. *Eur J Anaesthesiol.* **2010**. 27(1): 72-72.
32. Sherman W., Day T., Jacobson M.P., Friesner R.A., and Farid R. *J Med Chem.* **2006**. 49(2): 534-553.
33. Heitman L.H., Göblyös A., Zweemer A.M., Bakker R., Mulder-Krieger T., van Veldhoven J.P.D., de Vries H., Brussee J., and IJzerman A.P. *J Med Chem.* **2009**. 52(4): 926-931.
34. Smith P.K., Krohn R.I., Hermanson G.T., Mallia A.K., Gartner F.H., Provenzano M.D., Fujimoto E.K., Goeke N.M., Olson B.J., and Klenk D.C. *Anal Biochem.* **1985**. 150(1): 76-85.
35. Boussif O., Lezoualch F., Zanta M.A., Mergny M.D., Scherman D., Demeneix B., and Behr J.P. *Proc. Natl. Acad. Sci. U.S.A.* **1995**. 92(16): 7297-7301.
36. Gorman C.M., Howard B.H., and Reeves R. *Nucleic Acids Res.* **1983**. 11(21): 7631-7648.
37. Cheng Y.-C., and Prusoff W.H. *Biochem Pharmacol.* **1973**. 22(23): 3099-3108



# Chapter 5

## Design, Synthesis and Pharmacological Profiles of LUF7746, a Novel Covalent Partial Agonist for the Adenosine A<sub>1</sub> Receptor

*Xue Yang*

*Majlen A. Dilweg*

*Dion Osemwengie*

*Lindsey Burggraaff*

*Daan van der Es*

*Laura H. Heitman*

*Adriaan P. IJzerman\**

To be submitted



### Abstract

Partial agonists for G protein-coupled receptors (GPCRs) provide opportunities for novel pharmacotherapies with enhanced on-target safety compared to full agonists. For the human adenosine A<sub>1</sub> receptor (hA<sub>1</sub>AR) this has led to the discovery of capadenoson, which has been in phase IIa clinical trials for heart failure. Accordingly, the design and profiling of novel hA<sub>1</sub>AR partial agonists has become an important research focus. In this study, we report on LUF7746, a capadenoson derivative bearing an electrophilic fluorosulfonyl moiety, as an irreversibly binding hA<sub>1</sub>AR modulator. Meanwhile, a nonreactive ligand bearing a methylsulfonyl moiety, LUF7747, was designed as a control probe in our study.

In a radioligand binding assay LUF7746's apparent affinity increased to nanomolar range with longer pre-incubation time, suggesting an increasing level of covalent binding over time. Moreover, compared to the reference full agonist CPA, LUF7746 was a partial agonist in a hA<sub>1</sub>AR-mediated G protein activation assay, and resistant to blockade with an antagonist/inverse agonist. An *in silico* structure-based docking study combined with site-directed mutagenesis of the hA<sub>1</sub>AR demonstrated that amino acid Y271<sup>7,36</sup> was the primary anchor point for the covalent interaction. Additionally, a label-free whole-cell assay was set up to identify LUF7746's irreversible activation of an A<sub>1</sub> receptor-mediated cell morphological response.

These results led us to conclude that LUF7746 is a novel covalent hA<sub>1</sub>AR partial agonist and a valuable chemical probe for further mapping the receptor activation process. It may also serve as a prototype for a therapeutic approach in which a covalent partial agonist may cause less on-target side effects, conferring enhanced safety compared to a full agonist.

### Keywords

G protein-coupled receptors, adenosine A<sub>1</sub> receptor, covalent ligand, partial agonist, radioligand binding, label-free assay

### 1. Introduction

G protein-coupled receptors (GPCRs) are one of the largest families of drug targets [1]. Being transmembrane proteins they, however, pose problems in studying their structure and function, due to their low expression and profound instability. To solve these problems, covalent ligands have been shown to be useful tools for the structure elucidation of active/inactive receptor structures and mapping of the ligand-binding domains [2]. Beyond that, covalent ligands are beginning to be applied in GPCR chemical biology and proteomics applications [3].

Historically, the few covalent agonists for the human adenosine A<sub>1</sub> receptor (hA<sub>1</sub>AR) available have all been derivatives of the endogenous ligand adenosine, containing an intact ribose moiety. Chemical modification of the adenosine structure at the N<sup>6</sup> position has yielded several selective chemo-reactive agonists [4, 5]. One such example is N<sup>6</sup>-[4-[[[4-[[[[2-[[[(m-isothiocyanatophenyl)amino]-thiocarbonyl]amino]ethyl]amino] carbonyl]methyl]aniline]-carbonyl] methyl]phenyl]adenosine (m-DITC-ADAC), an adenosine analogue incorporating a chemoreactive isothiocyanate group to form a covalent bond with the receptor [5]. These covalent agonists were validated as full agonists for adenosine A<sub>1</sub> receptor [5, 6]. However, full activation of the hA<sub>1</sub>AR influences a broad physiologic spectrum of cardiac functions associated with unwanted effects, such as atrioventricular block [7]. Thus, partial agonists, triggering submaximal effects compared to a full agonist, have emerged as a new therapeutic option in treating cardiovascular indications [8]. Research from Bayer and our group has unveiled the existence of 2-aminopyridine-3,5-dicarbonitrile derivatives such as capadenoson and LUF5853 as non-ribose agonists for the hA<sub>1</sub>AR [9-11]. Here, we used the 2-aminopyridine-3,5-dicarbonitrile scaffold as a starting point in our design and synthesis efforts towards a covalent partial agonist probe for the hA<sub>1</sub>AR, the fluorosulfonyl-equipped derivative LUF7746. Meanwhile, a chemically similar, but non-reactive methylsulfonyl-equipped ligand, LUF7747, was designed to be used as a reversible control ligand. We then validated LUF7746 to bind covalently and partially activate the receptor in a series of *in vitro* experiments. We finally provided evidence for its point of attachment to the receptor. The results presented here constitute the initial report and pharmacological profiling of a novel, non-ribose covalent partial agonist and also shed light on the rational design of partial agonists as therapeutics. Furthermore, this reported covalent ligand could serve as a valuable pharmacological tool to investigate the contribution of partial activation of hA<sub>1</sub>AR physiological functions.

## 2. Materials and Methods

### 2.1. Chemistry

All solvents and reagents were purchased from commercial sources and were of analytical grade. Demineralised water is referred to as H<sub>2</sub>O, as was used in all cases unless stated otherwise (i.e., brine). All reactions were routinely monitored with thin layer chromatography (TLC), using aluminium silica gel coated 60 F<sub>254</sub> plates from Merck. Purification by column chromatography was carried out with the use of VWR silica gel irregular ZEOprep<sup>®</sup> particles (60-200 μm). Solutions were concentrated using a Heidolph Hei-VAP Value rotary evaporator. Nuclear magnetic resonance (NMR) spectra were recorded on a Bruker AV-400 liquid spectrometer (<sup>1</sup>H NMR, 400 MHz) at ambient temperature and subsequently analysed with MestReNova v.12 software. Chemical shifts are reported in parts per million (ppm), designated by δ and corrected to the internal standard tetramethylsilane (δ = 0). Coupling constants are reported in Hz and are designated as *J*. Mass analyses were performed with liquid chromatography mass spectrometry (LC-MS) using an LCQ<sup>™</sup> Advantage MAX system from Thermo Finnigan together with a Phenomenex Gemini<sup>®</sup> C18 110Å column (50 mm × 4.6 mm × 3 μm). Samples were eluted using an isocratic system of H<sub>2</sub>O/CH<sub>3</sub>CN/1% TFA in H<sub>2</sub>O, through decreasing the polarity of the solvent mixture from 80:10:10 to 0:90:10 in an elution time of 15 minutes. Analytical purity of the obtained final compounds was determined with high performance liquid chromatography (HPLC) using a Shimadzu HPLC system with a Phenomenex Gemini<sup>®</sup> C18 110Å column (50 mm × 4.6 mm × 3 μm) coupled to a 254 nm UV detector. Samples were eluted using the same method as mentioned for LC-MS. For both LC-MS and HPLC, 0.3-0.8 mg of compound was dissolved in 1 mL of a 1:1:1 mixture of CH<sub>3</sub>CN/H<sub>2</sub>O/tBuOH as sample preparation. All reactions were performed under nitrogen atmosphere unless stated otherwise. Ligands were synthesized in two step protocol from compound **1** (Fig.1) as described below.

#### **4-((3-((6-amino-4-(benzo[*d*][1,3]dioxol-5-yl)-3,5-dicyanopyridin-2-yl)thio)propyl)carbomoyl)benzenesulfonylfluoride (**4**, LUF7746).**

A mixture of 4-(fluorosulfonyl)benzoic acid (1.5 mmol, 0.30 g, 1.0 equiv), 3-bromopropylamine hydrobromide (1.9 mmol, 0.42 g, 1.3 equiv) and EDC·HCl (1.8 mmol, 0.33 g, 1.2 equiv) in anhydrous DMF was cooled down to 0 °C. Subsequently, DIPEA (3.0 mmol, 0.52 mL, 2.0 equiv) was added dropwise and the solution was stirred for 4 h at 0 °C, followed by overnight stirring at room temperature. After completion was observed on TLC, the mixture was concentrated *in vacuo*. Water was added to the residue and the mixture was

## Chapter 5

---

extracted three times with ethyl acetate. The combined organic layers were washed three times with 1M HCl three times, dried over MgSO<sub>4</sub>, filtered and concentrated *in vacuo*. The crude product was purified by column chromatography (PE: EtOAc = 2:1) to give the N-(3-bromopropyl)-4-(fluorosulfonyl)benzamide (**2**) as a white solid (1.1 mmol, 0.35 g, 74%). Compound **2** was used without further purification. 2-amino-4-(benzo[d][1,3]dioxol-5-yl)-6-mercaptopyridine-3,5-dicarbonitrile **1** (0.48 mmol, 0.14 g, 1.0 equiv) was dissolved in anhydrous DMF in the presence of **2** (0.48 mmol, 0.15 g, 1.0 equiv) and NaHCO<sub>3</sub> (0.73 mmol, 0.061 g, 1.5 equiv) and stirred at room temperature until completion of the reaction. Water was added to the mixture which was extracted with EtOAc four times. Subsequently, the combined organic layers were washed with brine 4 times, dried over MgSO<sub>4</sub>, filtered and concentrated *in vacuo*. The crude product was purified via column chromatography (EtOAc:PE = 1:1) to yield the desired compound as white solid (0.039 mmol, 0.021 g, 8%). <sup>1</sup>H NMR (400 MHz, CDCl<sub>3</sub>) δ 8.10 (d, *J* = 8.4 Hz, 2H), 8.02 (d, *J* = 8.3 Hz, 2H), 7.00 (dd, *J* = 8.0, 1.6 Hz, 1H), 6.97-6.92 (m, 2H), 6.55 (t, *J* = 5.6 Hz, 1H), 6.07 (s, 2H), 5.92 (br s, 2H), 3.65 (q, *J* = 6.7 Hz, 2H), 3.27 (t, *J* = 7.1 Hz, 2H), 2.16 (quin, *J* = 7.1 Hz, 2H) ppm. MS: [ESI+H]<sup>+</sup>: 540.0. HPLC *t*<sub>R</sub> = 8.36 min, purity 97%.

**N-(3-((6-amino-4-(benzo[d][1,3]dioxol-5-yl)-3,5-dicyanopyridin-2-yl)thio)propyl)-4-(methylsulfonyl)benzamide (5, LUF7747)**. A mixture of (4-methyl sulfonyl)-benzoic acid (0.82 mmol, 0.16 g, 1.0 equiv), 3-bromopropylamine hydrobromide (1.1 mmol, 0.23 g, 1.3 equiv) and EDC·HCl (0.98 mmol, 0.19 g, 1.2 equiv) in anhydrous DMF was stirred for 1 h at rt. Subsequently, DIPEA (1.7 mmol, 0.29 mL, 2.0 equiv) was added dropwise to the suspension and the reaction was stirred overnight at room temperature. After completion was observed on TLC, the mixture was concentrated *in vacuo*. Water was added to the residue and the mixture was extracted three times with ethyl acetate. The combined organic layers were washed three times with 1M HCl, dried over MgSO<sub>4</sub>, filtered and concentrated *in vacuo*. The crude product was purified by column chromatography (EtOAc : PE = 2:1) to give N-(3-bromopropyl)-4-(methylsulfonyl)benzamide (**3**) as a white solid (0.21 mmol, 0.068 g, 26%). Compound **3** was used without further purification. 2-amino-4-(benzo[d][1,3]dioxol-5-yl)-6-mercaptopyridine-3,5-dicarbonitrile **1** (0.21 mmol, 0.062 g, 1.0 equiv) was dissolved in anhydrous DMF in the presence of **3** (0.21 mmol, 0.067 g, 1.0 equiv) and NaHCO<sub>3</sub> (0.31 mmol, 0.026 g, 1.5 equiv) and stirred at room temperature until completion of the reaction. Water was added to the mixture which was extracted with EtOAc four times. Subsequently, the combined organic layers were washed with brine 4 times, dried over MgSO<sub>4</sub>, filtered and concentrated *in vacuo*. The crude product was purified via column chromatography



(EtOAc:PE = 2:1) to yield the desired compound as off-white solid (0.093 mmol, 0.050 g, 45%). <sup>1</sup>H NMR (400 MHz, DMSO-*d*<sub>6</sub>) δ 8.80 (t, *J* = 5.6 Hz, 1H), 8.07 (d, *J* = 8.4 Hz, 2H), 8.02 (d, *J* = 8.4 Hz, 2H) 7.15 (d, *J* = 1.8 Hz, 1H), 7.10 (d, *J* = 8.1 Hz, 1H), 7.02 (dd, *J* = 8.1, 1.8 Hz, 1H), 6.15 (s, 2H), 3.43 (q, *J* = 6.6 Hz, 2H), 3.31-3.24 (m, 5H), 1.96 (quin, *J* = 7.0 Hz, 2H) ppm. MS: [ESI+H]<sup>+</sup>: 535.9 HPLC t<sub>R</sub> = 7.41 min, purity 99%.

## 2.2. Biology

Both radioligands 1,3-[<sup>3</sup>H]-dipropyl-8-cyclopentylxanthine ([<sup>3</sup>H]DPCPX, specific activity of 120 Ci × mmol<sup>-1</sup>) and [2-<sup>3</sup>H]-4-(2-[7-amino-2-(2-furyl)-[1,2,4]-triazolo-[2,3-*a*]-[1,3,5]-triazin-5-yl amino]ethyl ([<sup>3</sup>H] ZM241385, specific activity of 50 Ci × mmol<sup>-1</sup>) were purchased from ARC Inc. (St.Louis, MO). [<sup>3</sup>H]PSB603 ([<sup>3</sup>H]8-(4-(4-(4-Chlorophenyl)piperazine-1-sulfonyl)phenyl)-1-propylxanthine, specific activity 79 Ci × mmol<sup>-1</sup>) and [<sup>3</sup>H]8-Ethyl-4-methyl-2-phenyl-(8R)-4,5,7,8-tetrahydro-1H-imidazo[2,1-*i*]-purin-5-one ([<sup>3</sup>H]PSB-11, specific activity 56 Ci × mmol<sup>-1</sup>) were obtained with kind help of Prof. C.E. Müller (University of Bonn, Germany). [<sup>35</sup>S]-Guanosine 5'-(γ-thio)triphosphate ([<sup>35</sup>S]GTPγS, specific activity 1250 Ci × mmol<sup>-1</sup>) was purchased from PerkinElmer, Inc. (Waltham, MA, USA). 5'-N-ethylcarboxamidoadenosine (NECA) was purchased from Sigma-Aldrich (Steinheim, Germany). N<sup>6</sup>-cyclopentyladenosine (CPA) was purchased from Abcam (Cambridge, UK). Unlabeled ZM241385 was a gift from Dr. S.M.Poucher (Astra Zeneca, Macclesfield, UK). Adenosine deaminase (ADA) was purchased from Boehringer Mannheim (Mannheim, Germany). Bicinchoninic acid (BCA) and BCA protein assay reagent were obtained from Pierce Chemical Company (Rockford, IL, USA). Chinese hamster ovary cells stably expressing the hA<sub>1</sub>AR (CHOhA<sub>1</sub>AR) were provided by Prof. S. J. Hill (University of Nottingham, UK). Chinese hamster ovary cells stably expressing low levels of hA<sub>1</sub>AR (CHO-hA<sub>1</sub>AR-low) were obtained from Prof. Andrea Townsend (University College London, UK). HEK293 cells stably expressing the hA<sub>2A</sub> adenosine receptor (HEK293 hA<sub>2A</sub>AR) were kindly provided by Dr J Wang (Biogen/IDEC, Cambridge, MA, USA). Chinese hamster ovary cells stably expressing the human adenosine A<sub>2B</sub> (CHOhA<sub>2B</sub>AR) and A<sub>3</sub> receptor (CHOhA<sub>3</sub>AR) were obtained from Dr. S. Rees (AstraZeneca, Macclesfield, UK) and Dr. K-N. Klotz (University of Würzburg, Germany), respectively. All other chemicals were of analytical grade and obtained from standard commercial sources.

### Site-directed mutagenesis

Site-directed mutant hA<sub>1</sub>AR-Y271<sup>7.36</sup>F was constructed by polymerase chain reaction mutagenesis using pcDNA3.1(+)-hA<sub>1</sub>AR with N-terminal HA and C-terminal His tag as the template plasmid. Mutant primers for directional polymerase chain reaction product cloning

## Chapter 5

---

were designed using the online QuikChange® Primer Design Program (Agilent Technologies, Santa Clara, CA, USA) and obtained from Eurogentec Nederland b.v. (Maastricht, The Netherlands). All DNA sequences were verified by Sanger sequencing at the Leiden Genome Technology Center (Leiden, The Netherlands).

### **Cell culture, transfection and membrane preparation**

Cell culture and membranes preparation were performed as previously described [12, 13].

### **Transient expression of wild type (WT) and mutant receptors in CHO cells.**

CHO cells were seeded into 150-mm culture dishes to achieve 50-60 % confluence containing 20 ml of medium consisting of DMEM/F12 (1:1) supplemented with 10% (v/v) newborn calf serum, streptomycin (50 µg/mL), and penicillin (50 IU/mL). Cells were transfected approximately 24 h later with plasmid DNA (20 µg of DNA/dish) by the PEI method (PEI:DNA = 3:1) and left for 48 h [14]. Subsequently, medium was removed and fresh medium was added, and cells were grown for an additional 24 h at 37 °C and 5% CO<sub>2</sub>. Membranes were prepared in the same way as previously described [12] and stored in 250 µL aliquots at -80 °C until further use.

### **Radioligand displacement assays**

*hA<sub>1</sub>AR* [15]. Membrane aliquots containing 5 µg were incubated in a total volume of 100 µL assay buffer (50 mM Tris HCl, pH 7.4) at 25 °C for 60 min. Displacement experiments were performed using six concentrations of competing antagonist in the presence of ~1.6 nM [<sup>3</sup>H]DPCPX. Nonspecific binding was determined in the presence of 100 µM CPA and represented less than 10% of total binding. Incubation was terminated by rapid filtration performed on 96-well GF/B filter plates (Perkin Elmer, Groningen, the Netherlands) in a PerkinElmer Filtermate-harvester (Perkin Elmer, Groningen, the Netherlands) and washed with buffer (50 mM Tris, pH 7.4) After the filter plate was dried at 55 °C for 30 min, the filter-bound radioactivity was determined by scintillation spectrometry using a 2450 MicroBeta<sup>2</sup> Plate Counter (Perkin Elmer, Boston, MA).

*Adenosine A<sub>2A</sub> Receptor* [13]. Membrane aliquots containing 20 µg of protein were incubated in a total volume of 100 µL of assay buffer (50 mM Tris-HCl, pH 7.4) at 25 °C for 120 min. Displacement experiments were performed using 1 µM of competing compound in the presence of ~2.5 nM [<sup>3</sup>H]ZM241385. Nonspecific binding was determined in the presence of 100 µM NECA. Incubations were terminated, washed and samples were obtained and analysed as described under hA<sub>1</sub>AR.

*Adenosine A<sub>2B</sub> Receptor* [16]. Membrane aliquots containing 25 µg of protein were incubated in a total volume of 100 µL of assay buffer (50 mM Tris-HCl, pH 7.4, supplemented with

0.1% (w/v) CHAPS) at 25 °C for 120 min. Displacement experiments were performed using 1 μM of competing compound in the presence of ~1.5 nM [<sup>3</sup>H]PSB603. Nonspecific binding was determined in the presence of 10 μM ZM241385. Incubations were terminated, filters were washed with buffer (50 mM Tris-HCl, pH 7.4, supplemented with 0.1% BSA and 0.1% (w/v) CHAPS) and samples were obtained and analyzed as described under hA<sub>1</sub>AR.

*Adenosine A<sub>3</sub> Receptor* [17]. Membrane aliquots containing 15 μg of protein were incubated in a total volume of 100 μL of assay buffer (50mM Tris, 10mM MgCl<sub>2</sub>, 1mM EDTA, 0.01% CHAPS, pH 8.0) at 25 °C for 120 min. Displacement experiments were performed using 1 μM of competing compound in the presence of ~10 nM [<sup>3</sup>H]PSB11. Nonspecific binding was determined in the presence of 100 μM NECA. Incubations were terminated, washed with buffer (50mM Tris, 10mM MgCl<sub>2</sub>, 1mM EDTA, pH 8.0) and samples were obtained and analyzed as described under hA<sub>1</sub>AR.

### Competition association assays

The binding kinetics of unlabeled ligands were assessed as described previously [15]. Briefly, the association of the radioligand was followed over time in the absence or presence of a concentration corresponding to 10 × K<sub>i</sub> value of unlabeled LUF7746 and LUF7747. In practice, to the mixture of equal volumes of 2.5 nM [<sup>3</sup>H]DPCPX, unlabeled compound and assay buffer (50 mM Tris-HCl supplemented with 5 mM MgCl<sub>2</sub> and 0.1% CHAPS) was added a 25 μL membrane aliquot containing 5 μg of protein at each time point from 0.5 min to 240 min at 25°C. Incubation was terminated as described above (radioligand displacement assay).

### Wash-out assay on both wild type hA<sub>1</sub>AR and hA<sub>1</sub>AR-Y<sup>7.36</sup>F cell membranes

100 μL of assay buffer containing either 1% DMSO (blank control) or 1 μM of ligands (LUF7746 or LUF7747) and 200 μL additional assay buffer were added to a 2 mL Eppendorf tube containing 100 μL cell membrane suspension (20 μg and 40 μg of protein for wild type and Y7.36F, respectively, to obtain an assay window of 3000 dpm in both cases) to achieve a total volume of 400 μL. The tubes were incubated for 2 h in an Eppendorf® Thermomixer® at 900 rpm and 25 °C. After incubation the tubes were centrifuged for 5 min at 16 000 × g and 4 °C and subsequently the buffer containing unbound ligands was removed. The membrane pellet was resuspended in 1 mL of assay buffer, incubated for 10 min at 25 °C and 900 rpm after which the tubes were centrifuged for 5 min at 16 000 × g and 4 °C and the cycle was repeated three more times. After the final washing step, the membrane pellet was resuspended in 300 μL assay buffer to determine the radioligand binding activity. All samples were transferred to the test tubes and incubated with 100 μL of 1.6 nM [<sup>3</sup>H]DPCPX for 2 h at 25 °C. The

## Chapter 5

---

incubation was terminated by vacuum filtration through a GF/B filter using a Brandel M24 Scintillation Harvester to separate bound and free radioligand. The filters were washed three times with ice-cold wash buffer (50 mM Tris-HCl, pH 7.4). After drying the filters, 3.5 mL of scintillation liquid was added and the filter-bound radioactivity was determined in a Tri-Carb 2900TR Liquid Scintillation Analyzer (PerkinElmer, Inc., Waltham, MA, USA). Results are expressed as percentage normalized to the maximum specific binding in the control group (100%).

### **Computational modelling**

All calculations were performed using the Schrödinger Suite [18]. The X-ray structure of the hA<sub>1</sub>AR was extracted from the PDB (PDB: 5UEN) [19, 20]. The co-crystallized ligand DU172 was removed and protein chain A was prepared for docking with the Protein Preparation tool. Additionally, missing side chains were added using Prime [21].

### **Functional [<sup>35</sup>S]GTPγS binding assay**

Binding of [<sup>35</sup>S]GTPγS to membranes was adapted from a previously reported method [16]. The assays were performed in a 96-well plate format, where stock solutions of the compounds were added using an HP D300 Digital Dispenser (Tecan, Männedorf, Switzerland). The final concentration of DMSO per assay point was ≤0.1%. For concentration-response assays transiently transfected membranes (hA<sub>1</sub>AR-WT, 5 μg and hA<sub>1</sub>AR-Y271<sup>7.36</sup>F, 20 μg to obtain an assay window of 3000 dpm in both cases) in 80 μL total volume of assay buffer containing 50 mM Tris-HCl buffer, 5 mM MgCl<sub>2</sub>, 1 mM EDTA, 100 mM NaCl, 0.05% BSA and 1 mM DTT pH 7.4 supplemented with 3 μM GDP and saponin (hA<sub>1</sub>AR-WT, 5 μg and hA<sub>1</sub>AR-Y271<sup>7.36</sup>F, 20 μg) were added to a range of concentrations of ligand (10<sup>-10</sup> to 10<sup>-5</sup>) for 30 min at 25 °C. After this, 20 μL of [<sup>35</sup>S]GTPγS (final concentration of 0.3 nM) was added and incubation continued for another 90 min at 25 °C. The basal level of [<sup>35</sup>S] GTPγS binding was determined in the absence of ligand, whereas the maximal level of [<sup>35</sup>S]GTPγS binding was determined in the presence of 1 μM CPA. For receptor activation/inhibition studies, hA<sub>1</sub>AR-WT or hA<sub>1</sub>AR-Y271<sup>7.36</sup>F cell membranes were pre-incubated with LUF7746 or LUF7747 (EC<sub>80</sub> concentration) for 60 min. After this, [<sup>35</sup>S]GTPγS (final concentration of 0.3 nM) was added in the absence or presence of DPCPX (1 μM) for another 90 min. For all experiments, incubations were terminated by rapid vacuum filtration to separate the bound and free radioligand through Whatman™ UniFilter™ 96-well GF/B microplates using a PerkinElmer's FilterMate™ Universal Harvester (PerkinElmer, Groningen, Netherlands). Filters were subsequently washed three times with 2 mL of ice-cold buffer (50 mM Tris-HCl, pH 7.4 supplemented with 5 mM MgCl<sub>2</sub>). The filter-bound radioactivity was determined by

scintillation spectrometry using a PerkinElmer MicroBeta2 2450 Microplate Counter (PerkinElmer, Groningen, Netherlands).

### Label-free whole-cell assays

Label-free whole-cell assays were adapted from a previously reported method [22, 23] using the real-time cell analyser (RTCA) xCELLigence SP system (ACEA Biosciences, San Diego, CA, USA) [24]. The system measures electrical impedance generated by adherence of cells to gold-coated electrodes at the bottom of 96 wells PET E-plates (obtained from Bioké, Leiden, the Netherlands). Changes in impedance ( $Z$ ) were measured continuously and are displayed as Cell Index (CI), which is defined as  $(Z_i - Z_0) \Omega / 15\Omega$ .  $Z_i$  is the impedance at a given time and  $Z_0$  is the baseline impedance measured at the start of the experiment in the absence of cells. CHO cells stably expressing a relatively low level hA<sub>1</sub>AR (CHO-hA<sub>1</sub>AR-low) were cultured in medium of DMEM/F12 (1:1) supplemented with 10% (v/v) newborn calf serum, streptomycin (50  $\mu\text{g}/\text{mL}$ ), penicillin (50 IU/mL), and G418 (0.2 mg/mL) at 37 °C in 5% CO<sub>2</sub> as a monolayer on 10-cm  $\varnothing$  culture plates to 70-80% confluency and subsequently harvested and centrifuged twice at 200 $\times$ g for 5 min [25]. Initially, 60  $\mu\text{L}$  of culture medium was added to wells in E-plates 96 to obtain background readings ( $Z_0$ ) followed by the addition of 40  $\mu\text{L}$  of cell suspension containing 40,000 cells per well. After resting at room temperature for 30 min, the plate was mounted in the RTCA recording station within a humidified 37°C, 5% CO<sub>2</sub> incubator. Impedance was measured every 15 min overnight. For agonist assays, after 17 hours, medium was replaced with 95  $\mu\text{L}$  serum free medium plus 1.2 IU ADA and kept in the 37°C, 5% CO<sub>2</sub> incubator for 3 h of starvation. After that, cells were stimulated with increasing concentrations of agonists or vehicle (final concentration of 0.25 % DMSO) in a final well volume of 100  $\mu\text{L}$ . For the inverse agonist reversal assay, cells were placed in 90  $\mu\text{L}$  serum free medium containing 1.2 IU/ml ADA for 3 h starvation. Then cells were stimulated with 5  $\mu\text{L}$  indicated compound (final concentration 1  $\mu\text{M}$ ) for 30 min, followed by the addition of 100 nM DPCPX in a final well volume of 100  $\mu\text{L}$ . For both assays, to record the signal changes, CI was recorded for at least 30 min with a recording schedule of 15 s intervals for 20 min, followed by intervals of 1 min, 5 min and finally 15 min. For data analysis, the individual CI traces were normalized, by subtracting the baseline (vehicle control), to correct for any agonist-independent signals.

### Data analysis

All the experimental data were analyzed with GraphPad Prism 7.0 software (GraphPad Software Inc., San Diego, CA).  $p\text{IC}_{50}$  values in radioligand displacement assays were obtained by non-linear regression curve fitting into a sigmoidal concentration-response curve

## Chapter 5

using the equation:  $Y = \text{Bottom} + (\text{Top} - \text{Bottom}) / (1 + 10^{-(X - \text{LogIC}_{50})})$ .  $pK_i$  values were obtained from  $pIC_{50}$  values using the Cheng-Prusoff equation [26]. Association data for the radioligand were fitted using one-phase exponential association. Values for  $k_{on}$  were obtained by converting  $k_{obs}$  values using the following equation:  $k_{on} = (k_{obs} - k_{off}) / [\text{radioligand}]$ , where  $k_{off}$  values ( $0.21 \pm 0.01 \text{ min}^{-1}$ ) were cited from Guo *et al* [15]. Association and dissociation rates for unlabeled ligands were calculated by fitting the data in the competition association model using ‘kinetics of competitive binding’ [15, 27].

$$\begin{aligned}
 K_A &= k_1[L] \cdot 10^{-9} + k_2 \\
 K_B &= k_3[I] \cdot 10^{-9} + k_4 \\
 S &= \sqrt{(K_A - K_B)^2 + 4 \cdot k_1 \cdot k_3 \cdot L \cdot I \cdot 10^{-18}} \\
 K_F &= 0.5(K_A + K_B + S) \\
 K_S &= 0.5(K_A + K_B - S) \\
 Q &= \frac{B_{\max} \cdot k_1 \cdot L \cdot 10^{-9}}{K_F - K_S} \\
 Y &= Q \cdot \left( \frac{k_4 \cdot (K_F - K_S)}{K_F \cdot K_S} + \frac{k_4 - K_F}{K_F} e^{-(K_F \cdot X)} - \frac{k_4 - K_S}{K_S} e^{-(K_S \cdot X)} \right)
 \end{aligned}$$

Where X is the time (min), Y is the specific [ $^3\text{H}$ ]DPCPX binding (dpm),  $k_1$  and  $k_2$  are the  $k_{on}$  and  $k_{off}$  of [ $^3\text{H}$ ]DPCPX and were obtained from Guo *et al.* [15], L is the concentration of [ $^3\text{H}$ ]DPCPX used (nM),  $B_{\max}$  the total binding (dpm) and I the concentration of unlabeled ligand (nM). Fixing these parameters allows the following parameters to be calculated:  $k_3$ , which is the  $k_{on}$  value ( $\text{M}^{-1}\text{min}^{-1}$ ) of the unlabeled ligand and  $k_4$ , which is the  $k_{off}$  value ( $\text{min}^{-1}$ ) of the unlabeled ligand. The residence time (RT) was calculated using  $\text{RT} = 1/k_{off}$ .  $pEC_{50}$  and  $EC_{80}$  values in the [ $^{35}\text{S}$ ]GTP $\gamma$ S binding assays were determined using non-linear regression curve fitting into a sigmoidal dose-response curve with variable slope. For the label-free whole-cell assays, ligand responses were normalized to obtain normalized cell index (NCI) and then subtracted baseline (vehicle control), which correct for ligand-independent effects. Area-under-curve (AUC) values from the NCI were determined for a 100 min period after compound addition, which were used for concentration-response curves.  $pEC_{50}$  values from the label-free whole-cell assays were determined using the same non-linear regression as for the [ $^{35}\text{S}$ ]GTP $\gamma$ S binding assays. Data shown represent the mean  $\pm$  SEM of three individual experiments each performed in duplicate or a representative graph is shown. Statistical analysis was performed as indicated. If p-values were below 0.05, observed differences were considered statistically significant.

### 3. Results

#### 3.1. Design and synthesis of LUF7746 and LUF7747

Over the years our research group has explored a series of hA<sub>1</sub>AR agonists based on the 6-amino-4-aryl-3,5-dicyano-2-thiopyridine template, to investigate their structure-activity and structure-kinetics relationships (SAR and SKR) [9, 28]. We learned that the benzo[1,3]dioxol-5-yl moiety generally provided selective and potent agonists for hA<sub>1</sub>AR. Based on that finding, we used 2-amino-4-(benzo[*d*][1,3]dioxol-5-yl)-6-mercaptopyridine-3,5-dicarbonitrile as a scaffold (Fig.1), and developed a potentially covalent ligand by incorporating the fluorosulfonyl moiety as a warhead through an amide linker at the position of the sulfur atom. Hence, LUF7746, 4-((3-(((6-amino-4-(benzo[*d*][1,3]dioxol-5-yl)-3,5-dicyanopyridin-2-yl)thio)propyl)carbonyl)benzenesulfonyl)fluoride (Fig.1), was synthesized in one step by alkylating the template with the corresponding alkyl bromide. Additionally, to remove the reactivity of the warhead a methylsulfonyl substitution was used to replace the fluorosulfonyl moiety, which yielded a nonreactive control compound, *N*-(3-(((6-amino-4-(benzo[*d*][1,3]dioxol-5-yl)-3,5-dicyanopyridin-2-yl)thio)propyl)-4-(methylsulfonyl)benzamide (LUF7747, Fig.1). The reaction conditions and other reagents used in the synthesis of both compounds are described in Materials and Methods.

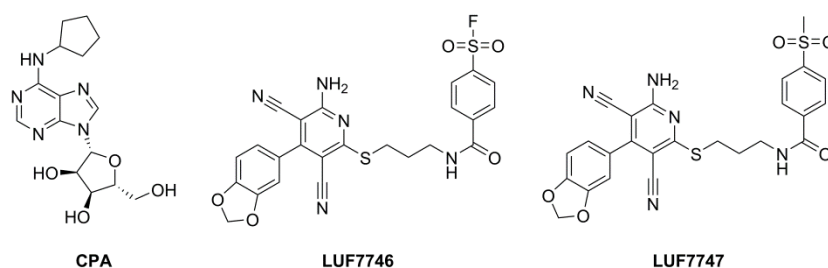
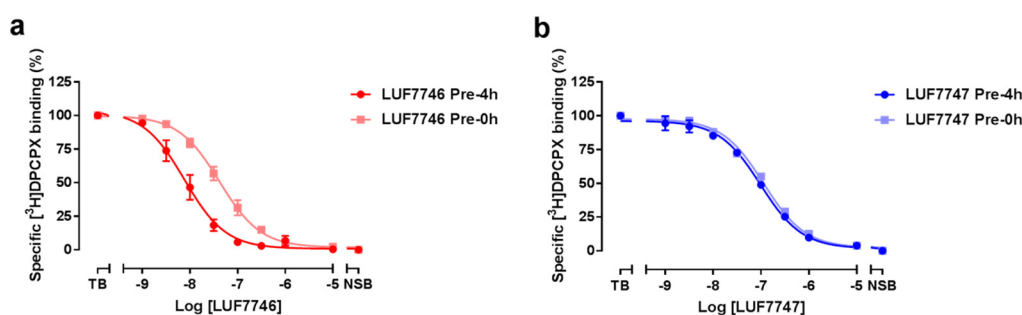


Fig. 1 Chemical structures of the hA<sub>1</sub>AR agonists examined in this study.

#### 3.2. Affinity characterization at different incubation times for LUF7746 and LUF7747

To determine the affinity of the synthesized ligands we tested both ligands in a [<sup>3</sup>H]DPCPX displacement assay at 25 °C. After 0.5 h co-incubation time, both compounds were able to concentration-dependently inhibit specific [<sup>3</sup>H]DPCPX binding to the hA<sub>1</sub>AR (Fig.2). As presented in Table 1, both compounds showed similar binding affinities in the submicromolar range ( $pK_i = 7.7 \pm 0.2$  and  $7.3 \pm 0.04$  for LUF7746 and LUF7747, respectively). We then tested the time dependency of the affinity for both compounds. In detail, the CHO cell membranes overexpressing hA<sub>1</sub>AR were pre-incubated with the indicated compound for 4 h,



**Fig.2 Time-dependent affinity assessment of LUF7746 and LUF7747.** Displacement of specific [ $^3\text{H}$ ]DPCPX binding from the adenosine CHO $\text{hA}_1\text{AR}$  receptor at 25°C by LUF7746 (a), and LUF7747 (b) with or without a pre-incubation of 4h. Data are normalized to 100% of the total binding and represent the mean  $\pm$  SEM of three individual experiments performed in duplicate.

followed by a 0.5 h co-incubation with the radioligand [ $^3\text{H}$ ]DPCPX. LUF7746 showed a significantly increased affinity with 4 h preincubation time ( $pK_i = 8.4 \pm 0.1$ ; Table 1), while LUF7747's affinity did not change ( $pK_i = 7.3 \pm 0.02$ ; Table 1). Representative graphs for this effect are shown in Fig.2, in which the curve representing a concentration-dependent inhibition of specific [ $^3\text{H}$ ]DPCPX binding was shifted to the left with 4 h pre-incubation of LUF7746 (Fig.2a), with no difference for LUF7747 (Fig.2b). It is worth to mention that for a covalent ligand no dynamic equilibrium can be reached. We thus expressed LUF7746's affinity for  $\text{hA}_1\text{AR}$  as "apparent  $K_i$ ". Compared to the reversible ligand LUF7747 covalent LUF7746 showed an increase in apparent  $pK_i$  with 0.7 log unit. The increased receptor affinity by LUF7746 with prolonged incubation time, indicated an increased level of covalent, non-displaceable binding over time.

Additionally, we tested these compounds in a single-point radioligand binding assay for other adenosine receptor subtypes (Table 1). Both compounds displaced less than 50% of the total radioligand binding at 1  $\mu\text{M}$  for other subtypes of human adenosine receptors (i.e. yielding estimated  $\text{IC}_{50}$  values higher than 1  $\mu\text{M}$ ), even when the incubation time was doubled. Thus, both ligands are selective towards the  $\text{hA}_1\text{AR}$ .

### 3.3. Kinetic characterization of LUF7746 and LUF7747 in a competition association binding assay

The apparent affinity shift of LUF7746 inspired us to examine the kinetic characteristics of the ligand-receptor interaction and to investigate the ligand's dissociation rate. In our previous research, the kinetic binding parameters  $k_{on}$  ( $k_1 = 1.2 \pm 0.1 \times 10^8 \text{ M}^{-1} \cdot \text{min}^{-1}$ ) and  $k_{off}$  ( $k_2 = 0.23 \pm 0.01 \text{ min}^{-1}$ ) of [ $^3\text{H}$ ]DPCPX at 25 °C had been determined in traditional association and



**Table 1.** Binding affinities of LUF7746 and LUF7747 for all adenosine receptor subtypes and mutant hA<sub>1</sub>AR-Y271F<sup>7,36</sup>.

cpd	<i>pK<sub>i</sub></i> <sup>a</sup> (pre-0h)	<i>pK<sub>i</sub></i> <sup>b</sup> (pre-4h)	Displacement at 1 μM (%)			<i>pIC<sub>50</sub></i>
	hA <sub>1</sub> AR		hA <sub>2A</sub> AR <sup>c</sup>	hA <sub>2B</sub> AR <sup>d</sup>	hA <sub>3</sub> AR <sup>e</sup>	hA <sub>1</sub> AR-Y271F <sup>7,36</sup> <sup>f</sup>
LUF7746 <sup>g</sup>	7.7 ± 0.2	8.4 ± 0.1**	26% (18,34)	26% (28,24)	25% (17,33)	7.2 ± 0.05
LUF7747	7.3 ± 0.04	7.3 ± 0.02	11% (10, 11)	16% (14,19)	7% (9, 5)	7.0 ± 0.06

Values represent *pK<sub>i</sub>* ± SEM (n=3) or mean percentage displacement at 1 μM (n=2) of separate experiments each performed in duplicate. \*\*P < 0.01 compared with the *pK<sub>i</sub>* values in displacement experiments without pre-incubation; Student's t-test.

<sup>a</sup>Affinity determined from displacement of specific [<sup>3</sup>H]DPCPX binding on CHO cell membranes stably expressing hA<sub>1</sub>AR at 25 °C after 0.5 h co-incubation;

<sup>b</sup>Affinity determined from displacement of specific [<sup>3</sup>H]DPCPX binding on CHO cell membranes stably expressing hA<sub>1</sub>AR at 25 °C with compounds pre-incubated for 4 h, followed up by a 0.5 h co-incubation with [<sup>3</sup>H]DPCPX ;

<sup>c</sup>% displacement at 1 μM concentration of specific [<sup>3</sup>H]ZM241385 binding on HEK293 cell membranes stably expressing human adenosine A<sub>2A</sub> receptors at 25 °C after 2 h co-incubation;

<sup>d</sup>% displacement at 1 μM concentration of specific [<sup>3</sup>H]PSB-603 binding on CHO cell membranes stably expressing human adenosine A<sub>2B</sub> receptors at 25 °C after 2 h co-incubation;

<sup>e</sup>% displacement at 1 μM concentration of specific [<sup>3</sup>H]PSB11 binding on CHO cell membranes stably expressing human adenosine A<sub>3</sub> receptors at 25 °C after 2 h co-incubation;

<sup>f</sup>Affinity determined from displacement of specific [<sup>3</sup>H]DPCPX binding on CHO cell membranes transiently expressing hA<sub>1</sub>AR-Y271F<sup>7,36</sup> at 25 °C after 2 h co-incubation ;

<sup>g</sup>For LUF7746, affinity values can only be apparent, as true equilibrium cannot be reached.

dissociation assays [15, 27, 29]. In this study we derived the kinetic binding parameters for the two unlabeled ligands by performing a competition association assay at a concentration of IC<sub>50</sub> value. The association in the presence of LUF7747 (Fig.3) reached a plateau within 30 mins, indicating a dynamic equilibrium was reached between [<sup>3</sup>H]DPCPX, ligand and hA<sub>1</sub>AR. Interestingly, LUF7746's behavior caused an initial 'overshoot' of [<sup>3</sup>H]DPCPX binding in the competition association curve which decreased over time (Fig.3). Analysing these curves with the (equilibrium) Motulsky and Mahan model [27] led to the summarized data in Table 2. Reversible ligand LUF7747 showed an association rate constant of 6.3 ± 0.9 × 10<sup>6</sup> M<sup>-1</sup>min<sup>-1</sup>, and a fast dissociation rate constant (0.42 ± 0.03 M<sup>-1</sup>min<sup>-1</sup>) which equalled to a receptor residence time (RT) of 2.3 ± 0.2 min. For LUF7746, this competition association assay generated a negligible dissociation rate constant (*k<sub>off</sub>* = 0.0046 ± 0.0020 min<sup>-1</sup>) and thus an infinite RT for LUF7746 (>1000 min, Table 2). These data provided further evidence for a putative irreversible binding mode between LUF7746 and the hA<sub>1</sub>AR.

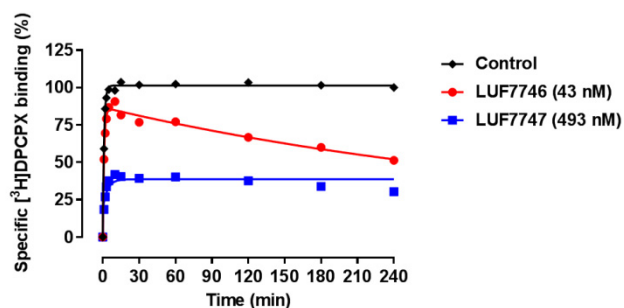


**Fig.3 Characterization of target binding kinetics of LUF7746 and LUF7747.** Competition association radioligand binding assay with [<sup>3</sup>H]DPCPX in the absence or presence of indicated compounds (at 10 x K<sub>i</sub> value) at 25°C. Data were fitted to the equations described in the methods to calculate the  $k_{on}$  ( $k_3$ ) and  $k_{off}$  ( $k_4$ ) values of unlabeled ligands by using the  $k_1$  and  $k_2$  values of [<sup>3</sup>H]DPCPX. Representative graphs from one experiment performed in duplicate. Parameters obtained from these graphs are listed in Table 2.

**Table 2.** Kinetic binding parameters ( $k_{on}$ ,  $k_{off}$ , RT) for LUF7746 and LUF7747

Compound	$k_{on}$ (M <sup>-1</sup> min <sup>-1</sup> ) <sup>a</sup>	$k_{off}$ (min <sup>-1</sup> ) <sup>a</sup>	RT (min)
LUF7746 <sup>b</sup>	((4.1±0.9) x 10 <sup>5</sup> )	(0.0046±0.0020)	(1118±963)
LUF7747	(6.3±0.9) x 10 <sup>6</sup>	0.42±0.03	2.3±0.2

<sup>a</sup>Association ( $k_{on}$ ) and dissociation ( $k_{off}$ ) rate constants were determined by competition association assay at 25 °C; all values were determined using the mathematical model described by Motulsky and Mahan [27]

<sup>b</sup>No equilibrium between receptors and ligand was reached for LUF7746; the values obtained are therefore shown in parentheses and are considered to provide qualitative insight only.

### 3.4. Washout assay between LUF7746 and hA<sub>1</sub>AR

We then performed a “washout” experiment to investigate the irreversibility of the ligand-receptor interaction. We first exposed hA<sub>1</sub>AR cell membranes to LUF7746 or LUF7747 at 1 μM concentration with [<sup>3</sup>H]DPCPX for 2 h, without any washing step, to assess the binding capacity of the receptor (“Unwashed” group; Fig.4a). Both ligands achieved a high receptor occupancy, resulting in a lower radioligand-occupied receptor population of 23 ± 2% for LUF7746 and 38 ± 4% for LUF7747, respectively. For the “washed” groups, the pre-incubated hA<sub>1</sub>AR membranes were washed four times to remove the non-covalently bound ligands (“washed” group; Fig.4a), after which they were exposed to [<sup>3</sup>H]DPCPX. Membranes pretreated with LUF7746 showed no increase in specific [<sup>3</sup>H]DPCPX binding with only 9 ± 4% recovery despite the intensive washing treatment. In contrast, membranes pretreated with LUF7747 showed a full recovery of radioligand binding (104 ± 6%), ensuring the efficiency of the washing procedure to remove the reversible ligand.

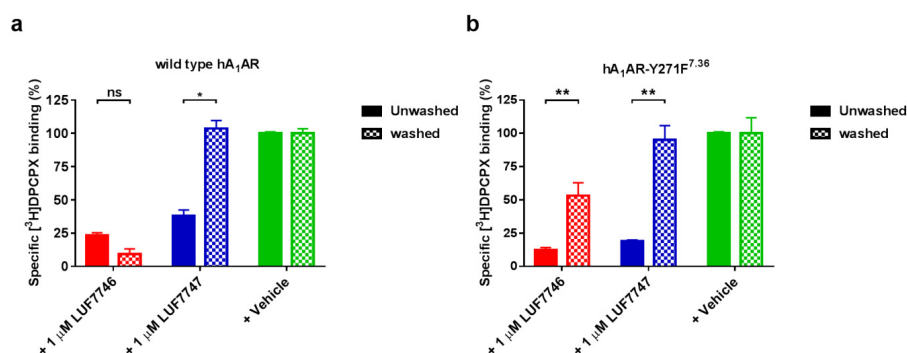


**Fig.4 Involvement of Y271<sup>7.35</sup> in the covalent binding of LUF7746.** CHO<sub>hA<sub>1</sub>AR</sub> wild-type cell membranes (a) or mutant hA<sub>1</sub>AR-Y271F<sup>7.36</sup> cell membranes (b) were pre-treated with 1 μM LUF7746, LUF7747 or buffer (vehicle) followed by no washing (filled column) or four washing cycles (hatched column). The membranes were then subjected to a standard [<sup>3</sup>H]DPCPX radioligand binding assay. Data are expressed as the percentage of vehicle group (100%) and represent mean ± SEM of three individual experiments performed in triplicate. Statistical analyses were performed using unpaired Student's *t*-test between groups. ns: no significant difference; Significant difference: (\*) *p* < 0.05; (\*\*) *p* < 0.01.

### 3.5. Functional characterization of LUF7746 and LUF7747 in a [<sup>35</sup>S]GTPγS assay

To extend the functional profiling of what emerged from the data presented above from the radioligand binding assays, we evaluated the compounds' functional activities in a GTPγS-binding assay on CHO cell membranes transiently transfected with wild type hA<sub>1</sub>AR (hA<sub>1</sub>AR-WT). This assay reflects the functional response of ligands at the level of GDP/GTP exchange by the ternary G protein complex, or G protein activation [30].

The results showed that LUF7746 is a partial agonist ( $E_{max} = 56 \pm 5\%$ ) in comparison to CPA, a reference full agonist with a  $pEC_{50}$  value of  $8.1 \pm 0.1$  ( $E_{max}$  set to 100%, at a concentration of 1 μM). The potency of LUF7746 ( $pEC_{50} = 7.3 \pm 0.1$ ; Fig.5a, Table 3) was comparable to its affinity ( $pK_i = 7.7 \pm 0.2$ ; Fig.2a, Table 1). In addition, LUF7747 was also identified as a partial hA<sub>1</sub>AR receptor agonist ( $E_{max} = 53 \pm 2\%$ ) with a potency ( $pEC_{50} = 7.2 \pm 0.02$ ; Fig.5a, Table 3) that corresponded to its affinity ( $pK_i = 7.3 \pm 0.04$  and  $pK_i = 7.3 \pm 0.02$ ; Fig.2b, Table 1).

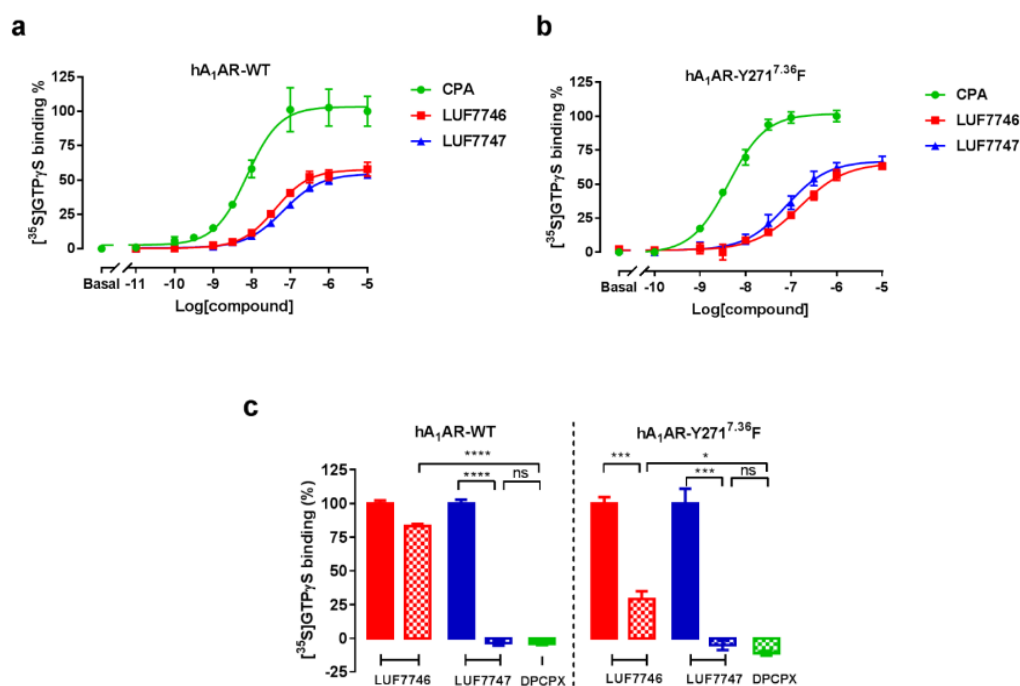


**Fig.5 Functional profile of LUF7746 and LUF7747 in [<sup>35</sup>S]GTP $\gamma$ S binding assays on both hA<sub>1</sub>AR-WT and hA<sub>1</sub>AR-Y271<sup>7.36</sup>F** (a) Functional ([<sup>35</sup>S]GTP $\gamma$ S binding) concentration-effect curves for CPA, LUF7746 and LUF7747 on transiently transfected hA<sub>1</sub>AR-WT cell membranes. Data are expressed as the percentage of maximal response induced by 10 $\mu$ M CPA (100%) and represent the mean  $\pm$  SEM of three individual experiments performed in duplicate. (b) Functional ([<sup>35</sup>S]GTP $\gamma$ S binding) concentration-effect curves for CPA, LUF7746 and LUF7747 on transiently transfected hA<sub>1</sub>AR-Y271<sup>7.36</sup>F cell membranes. Data are expressed as the percentage of maximal response induced by 1  $\mu$ M CPA (100%) and represent the mean  $\pm$  SEM of three individual experiments performed in duplicate. Parameters obtained from these graphs are described in Table 3. (c) hA<sub>1</sub>AR-WT or hA<sub>1</sub>AR-Y271<sup>7.36</sup>F cell membranes were pre-incubated with LUF7746 or LUF7747 (EC<sub>80</sub>, obtained from figure 6a or 6b) for 1 h, followed by incubation with [<sup>35</sup>S] GTP $\gamma$ S in the absence (filled columns) or presence (hatched columns) of DPCPX (1  $\mu$ M) to determine residual [<sup>35</sup>S]GTP $\gamma$ S binding. Data are expressed as the percentage of response induced by LUF7746 at EC<sub>80</sub> (100%) and represent the mean  $\pm$  SEM of three individual experiments performed in duplicate. Statistical analyses were performed using unpaired Student's t-test between groups. ns: no significant difference; Significant difference: (\*)  $p < 0.05$ ; (\*\*\*)  $p < 0.005$ ; (\*\*\*\*)  $p < 0.001$ .

To investigate the irreversible agonistic effect of LUF7746, we added an inverse agonist, DPCPX to hA<sub>1</sub>AR-WT pre-incubated with the designed agonist at EC<sub>80</sub> concentration. In the absence of agonist pre-incubation, DPCPX showed a (small, but significant) reduction in the basal level of G protein activity ( $-4 \pm 1\%$ ; Fig.5c), consistent with an inverse agonistic behavior. Moreover, the G protein activation induced by LUF7746 and LUF7747 at EC<sub>80</sub> concentration was inhibited by subsequent addition of DPCPX to varying degrees. Specifically, LUF7747 stimulation of G protein activity was completely reversed ( $-4 \pm 2\%$ ; Fig.5c), to an extent that was also obtained by treatment with DPCPX alone ( $-4 \pm 1\%$ ; Fig.5c). [<sup>35</sup>S]GTP $\gamma$ S binding upon LUF7746 stimulation was only slightly reversed by DPCPX ( $83 \pm$

2%; Fig.5c), possibly due to the fact that not all receptors are irreversibly labeled by LUF7746 at an EC<sub>80</sub> concentration.

**Table 3.** Functional characterization of LUF7746 and LUF7747 in [<sup>35</sup>S]GTPγS binding assays

Compound	CHOhA <sub>1</sub> AR-WT		CHOhA <sub>1</sub> AR-Y271F <sup>7,36</sup>	
	pEC <sub>50</sub>	E <sub>max</sub> (%) <sup>a</sup>	pEC <sub>50</sub>	E <sub>max</sub> (%) <sup>b</sup>
CPA	8.1 ± 0.1	100 ± 13	8.4 ± 0.03	100 ± 4
LUF7746	7.3 ± 0.1	56 ± 5*	6.8 ± 0.1	66 ± 1***
LUF7747	7.2 ± 0.02	53 ± 2*	7.1 ± 0.1	66 ± 4***

Values represent the mean ± SEM of three individual experiments performed in duplicate.

<sup>a</sup>Expressed as percentage of [<sup>35</sup>S]GTPγS binding induced by 10 μM CPA (set at 100%).

\*P < 0.05, compared to CPA efficacy (E<sub>max</sub>) using one way ANOVA with Dunnett's post-test.

<sup>b</sup>Expressed as percentage of [<sup>35</sup>S]GTPγS binding induced by 1 μM CPA (set at 100%).

\*\*\*P < 0.001, compared to CPA efficacy (E<sub>max</sub>) using one way ANOVA with Dunnett's post-test.

### 3.6. Binding mode of LUF7746 in the hA<sub>1</sub>AR binding pocket

The characterization of the irreversible binding nature between LUF7746 and hA<sub>1</sub>AR prompted us to further investigate the target residue of the reactive warhead. Thus, we first retrieved the receptor atomic coordinates from a reported hA<sub>1</sub>AR X-ray crystal structure (PDB: 5UEN) [19] and constructed a receptor model in which hA<sub>1</sub>AR and LUF7746 interact. The binding pose of LUF7746 (Fig.6), is comparable to that of DU172, the ligand present in the crystal structure. Specifically, one cyano group at the C<sup>5</sup> position participated in H-bond formation with Nδ2 of N254<sup>6,55</sup>. The dioxomethylene substituent functioned as H-bond acceptor with T91<sup>3,36</sup>, while carbonyl-oxygen in the amide position of the linker hydrogen-bonded with N70<sup>2,65</sup>. Of note, the flexibility of the three-carbon linker allowed the warhead, the fluorosulfonyl group of LUF7746, to form a covalent sulfonyl amide bond with the phenolic hydroxyl group of Y271<sup>7,36</sup>.

### 3.7. Tyrosine Y271<sup>7,36</sup> residue is the possible anchor point for covalent bond formation

To verify this structural feature of the ligand-receptor interaction, we mutated the potential target tyrosine to phenylalanine (hA<sub>1</sub>AR-Y271<sup>7,36</sup> F) and determined the affinities of both ligands for the mutant construct. As presented in Table 1, both compounds showed similar binding affinities in the submicromolar range (pIC<sub>50</sub> = 7.2 ± 0.05 and 7.0 ± 0.06 for LUF7746 and LUF7747, respectively; Table 1). Then we repeated the “washout” assay. As shown in Fig.4b, LUF7746 caused a significant recovery (53 ± 10 % remaining) compared to the unwashed group (12 ± 2%). This significant recovery was in striking contrast to the washout

## Chapter 5

---

assay on hA<sub>1</sub>AR-WT, which showed no recovery at all (Fig.4a). As a control, LUF7747 was rapidly washed off the membranes overexpressing hA<sub>1</sub>AR-Y271<sup>7.36</sup>F, as a full recovery of radioligand binding was observed (95 ± 11 %).

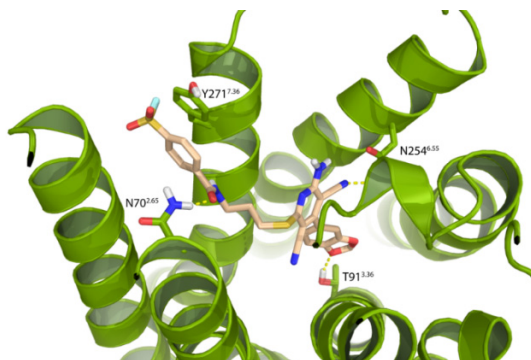


**Fig.6 Binding model of LUF7746 in the hA<sub>1</sub>AR-binding pocket.** The ligand binding pocket present in the hA<sub>1</sub>AR crystal structure (PDB: 5UEN) was used for the modeling of LUF7746 into it. Receptor helices are in green with some amino acids marked. LUF7746 is represented by light brown carbon sticks, together with oxygen, nitrogen, sulfur and hydrogen atoms (colored red, blue, yellow and white, respectively). The hydrogen bonds between ligand and receptor are indicated by yellow dashed lines. The ligand's fluorosulfonyl group and Y271<sup>7.36</sup> are in close proximity to facilitate covalent bond formation.

In addition to the radioligand binding assay, potency and efficacy of both ligands were also evaluated in a GTP $\gamma$ S-binding assay on cell membranes transiently transfected with hA<sub>1</sub>AR-Y271<sup>7.36</sup>F. Both LUF7746 and LUF7747 showed a comparable  $E_{max}$  value (66 ± 1% and 66 ± 4%; Fig.5b; Table 3) compared to reference full agonist CPA that had a  $pEC_{50}$  value of 8.4 ± 0.03 (maximum response  $E_{max}$  set to 100%, at a concentration of 1  $\mu$ M). This indicates that the two compounds are still partial agonists on mutant hA<sub>1</sub>AR-Y271<sup>7.36</sup>F receptors. The potency of LUF7746 was slightly decreased on hA<sub>1</sub>AR-Y271<sup>7.36</sup>F ( $pEC_{50}$  = 6.8 ± 0.1; Fig.5b, Table 3) compared to hA<sub>1</sub>AR-WT ( $pEC_{50}$  = 7.3 ± 0.1; Fig.5a, Table 3), while the potency value of LUF7747 was identical between hA<sub>1</sub>AR-Y271<sup>7.36</sup>F ( $pEC_{50}$  = 7.1 ± 0.1; Fig.5b, Table 3) and hA<sub>1</sub>AR-WT ( $pEC_{50}$  = 7.2 ± 0.02; Fig.5a, Table 3). Then on hA<sub>1</sub>AR-Y271<sup>7.36</sup>F, we repeated the DPCPX inhibition experiments on cell membranes pretreated with both LUF7746 and LUF7747 at EC<sub>80</sub> concentration. As shown in Fig.5c, DPCPX caused a more pronounced effect to reverse the stimulation of [<sup>35</sup>S]GTP $\gamma$ S binding induced by LUF7746 (29 ± 6%) on the mutant membranes, compared to the inhibition on hA<sub>1</sub>AR-WT (83 ± 2 %). As a control, LUF7747's stimulation on hA<sub>1</sub>AR-Y271<sup>7.36</sup>F was completely reversed (-5 ± 4%), comparable to the group only treated with DPCPX (-11 ± 2%).



### 3.8. Characterization of the covalent interaction in a label-free whole cell assay

To further evaluate receptor activation by these ligands, we used a label-free, impedance-based technology (xCELLigence) capable of real-time monitoring of hA<sub>1</sub>AR-mediated cell

**Table 4.** Pharmacological characterization of LUF7746 and LUF7747 in a label-free whole-cell assay

Compound	CHO-hA <sub>1</sub> AR-low cells	
	<i>p</i> EC <sub>50</sub>	<i>E</i> <sub>max</sub> (%) <sup>a</sup>
CPA	8.9 ± 0.06	100 ± 6
LUF7746	7.7 ± 0.1	61 ± 1**
LUF7747	7.6 ± 0.03	69 ± 4**

Values represent the mean ± SEM of three individual experiments performed in duplicate.

<sup>a</sup>Data were normalized to the CPA response at 1 μM (100%). \*\*P < 0.01, compared to CPA efficacy (*E*<sub>max</sub>) response using one way ANOVA with Dunnett's post-test.

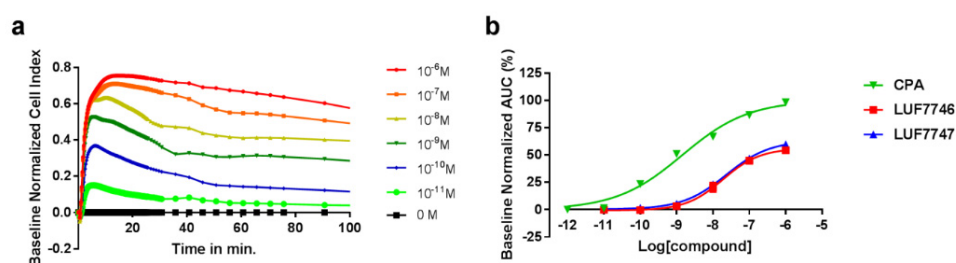


**Fig. 7 Functional characterization of CPA, LUF7746 and LUF7747 in a label-free whole cell assay.** CHO-hA<sub>1</sub>AR-low cells were seeded into E-plate 96 wells (40,000 cells/well) for 17 h, followed by 3 h serum free medium plus ADA (1.2 IU/ml) starvation, prior to the indicated agonist effects. (a) Representative example of a baseline-corrected CPA response [1 μM–10 pM]. (b) Concentration-response curves of the three agonists, derived from similar curves as in (a). Data are expressed as the percentage of maximal response induced by 1 μM CPA (analysis of area-under-curve (AUC) at 100 min, 100%) and represent mean ± SEM of three individual experiments performed in duplicate.

morphological changes over time [24]. Typically, CHO cells stably expressing a relative low level of hA<sub>1</sub>AR (CHO-hA<sub>1</sub>AR-low) were plated on an E-plate 17 h before the experiment [31]. Upon agonist addition to these cells, the impedance (shown as cell index, CI) was dose-dependently increased, followed by a gradual decrease until reaching a plateau in most cases after 100 min. A representative experiment of CPA-induced impedance changes is shown in Fig.7a. Dose-response curves for CPA and the two LUF compounds were derived from the area under curve (AUC) of corresponding agonist-induced changes within 100 min (Fig.7b).

## Chapter 5

Specifically, compared to CPA, LUF7746 and LUF7747 again behaved as partial agonists with similar  $E_{\max}$  values and potencies (see Fig.7b and Table 4).

To probe the putative irreversibility of the designed agonist, we used this label-free assay to determine whether the activation of the receptor is reversed by subsequent addition of the A<sub>1</sub>AR antagonist/inverse agonist DPCPX (i.e. similar to the GTPγS experiments of membranes). After the CHO-hA<sub>1</sub>AR-low cells were incubated with compounds for 30 min

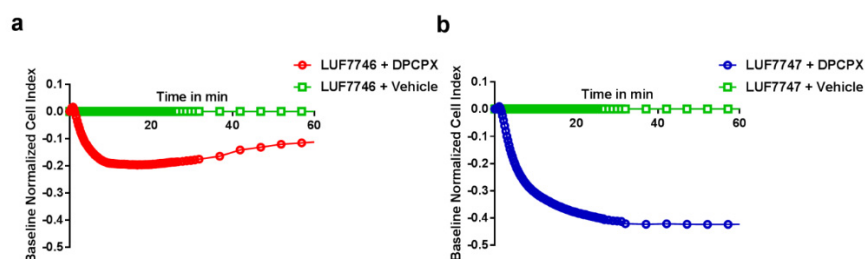


**Fig. 8 Characterization of the irreversible receptor activation induced by LUF7746 in a label-free whole assay.** CHO-hA<sub>1</sub>AR-low cells were pre-incubated with 1  $\mu$ M LUF7746 (a) or LUF7747 (b) for 30 min, followed by the addition of vehicle (0.25% DMSO) or 100 nM DPCPX (in 0.25% DMSO) to track the cell index changes for another 60 min. Representative graphs from one experiment performed in duplicate.

DPCPX (100 nM) or 0.25% DMSO (vehicle) was added and the impedance change was measured until 100 min. As shown in Fig.8a, cells exposed to LUF7746 showed a slight drop of CI values with a recovery trend back to control (0.25% DMSO). A more outspoken decrease of CI was detected upon antagonist exposure of cells pretreated with LUF7747 (Fig.8b). This behavior showed that LUF7746-pretreated cells were quite resistant to DPCPX compared to LUF7747, consistent with an irreversible mode of receptor activation.

### 4. Discussion

Covalent ligands have been invaluable in the study of ligand-receptor interactions and in GPCR structural biology. Recently, several GPCR structures, such as cannabinoid receptor CB<sub>1</sub> [32] and adenosine A<sub>1</sub> receptor [19], have been determined in the presence of chemoreactive ligands contributing to the formation of stable and functional ligand-receptor complexes. More generally, the use of covalent affinity probes for the exploration of the ligand binding pocket is widespread in GPCR research [2].

The non-ribose agonists' design dates back to the discovery of a former drug candidate, capadenoson, withdrawn from phase IIa clinical studies when it failed to show heart rate reduction for patients with atrial fibrillation [10, 11]. The structure modifications in capadenoson derivatives revealed that the dicyanopyridine scaffold with a benzo[1,3]dioxol-



5-yl moiety at the C<sup>4</sup> position showed good selectivity and efficacy at the hA<sub>1</sub>AR [9, 28]. Building on that, we introduced a reactive warhead (i.e. sulfonyl fluoride), connected to the scaffold's sulfur atom with an amide bond linked spacer, yielding the covalent dicyanopyridine ligand LUF7746. Meanwhile, a nonreactive methylsulfonyl derivative LUF7747, was designed and synthesized as a reversible control compound.

The first hint of covalent interaction of LUF7746 was found in time-dependent radioligand displacement assays, while the control ligand LUF7747 reached equilibrium independent of pre-incubation time. Similar experiments were performed on other subtypes of GPCRs, such as the M<sub>4</sub> muscarinic receptor and cannabinoid CB<sub>1</sub> receptor. All of the functionalized covalent ligands generated a time-dependent affinity increase [33, 34]. Subsequently, a continuing decrease of specific radioligand binding was observed for LUF7746 when the kinetic experiments were performed over a 4 h incubation at 25°C (Fig.3). The inadequacy of the Motulsky-Mahan model to fit this data is further evidence for the non-equilibrium features of the binding of LUF7746 to the receptor. In addition, extensive washing failed to restore [<sup>3</sup>H]DPCPX binding (Fig.4a) to membranes pretreated with LUF7746, validating the irreversible nature of LUF7746 to hA<sub>1</sub>AR. Likewise, on other GPCR subtypes, there are reported cases showing a covalent interaction was wash-resistant [13, 35, 36]. Furthermore, receptor activation induced by LUF7746 was not or hardly inhibited by the inverse agonist DPCPX (Fig.5c). This confirmed the covalent nature of LUF7746 binding to the receptor from a functional perspective, similar to other subtypes of GPCRs, where an excess of inverse agonist was unable to reverse covalent ligand-induced G protein activation [37]. Taking all data together we concluded LUF7746 showed a covalent interaction with hA<sub>1</sub>AR under many different experimental conditions.

The next step was to identify the anchor point of the covalent probe. The reported active structure of the hA<sub>1</sub>AR is in the presence of the ribose-based full agonist adenosine, which is structurally and functionally distinct from our non-ribose partial agonist LUF7746 [38]. In addition, our previous study on the dicyanopyridine scaffold showed that upon the addition of GTP this compound class only caused a minor shift to a lower affinity on hA<sub>1</sub>AR [39]. It is thus possible that this non-ribose partial agonist-bound receptor adopts a conformation distinct from the fully active state. Therefore, we adopted the inactive state of the hA<sub>1</sub>AR receptor (PDB:5UEN) for our docking studies [19]. Based on the LUF7746 binding pose in our model of the hA<sub>1</sub>AR, we hypothesized that LUF7746 covalently interacts with a tyrosine residue, Y271<sup>7,36</sup>, resulting in a sulfonamide bond formation (Fig.6).

## Chapter 5

---

To investigate our hypothesis, this tyrosine was mutated to phenylalanine (hA<sub>1</sub>AR-Y271<sup>7.36</sup>F) to remove the nucleophilic reactivity of the phenolic hydroxyl group and potentially prevent the covalent bond from being formed. Since control compound LUF7747 showed a similar affinity for both the Y271<sup>7.36</sup>F ( $pIC_{50} = 7.0 \pm 0.06$ ) and WT receptors ( $pIC_{50} = 7.0 \pm 0.02$ ), we assumed that the difference in radioligand binding recovery was not due to a point mutation within the receptor binding site, which has the potential to affect ligand binding properties. Moreover, there were no marked affinity differences on hA<sub>1</sub>AR-Y271<sup>7.36</sup>F between LUF7746 ( $pIC_{50} = 7.2 \pm 0.05$ ) and LUF7747 ( $pIC_{50} = 7.0 \pm 0.06$ ). This suggests that the chemically dissimilar ligands LUF7746 (reactive) and LUF7747 (nonreactive) exhibit a similar binding interaction with hA<sub>1</sub>AR-Y271<sup>7.36</sup>F. Lastly, the extensive washing treatment caused a four-fold increase of [<sup>3</sup>H]DPCPX binding recovery on hA<sub>1</sub>AR-Y271<sup>7.36</sup>F pre-incubated with LUF7746 (Fig. 4b), which is in sharp contrast to the findings in the wild type washout assay. Hence, we concluded Y271<sup>7.36</sup> is involved in the covalent attachment of LUF7746's fluorosulfonyl group within the hA<sub>1</sub>AR binding pocket.

A similar result was observed in the functional [<sup>35</sup>S]GTP $\gamma$ S assay. Since LUF7747 showed a comparable potency for hA<sub>1</sub>AR-Y271<sup>7.36</sup>F and hA<sub>1</sub>AR-WT, the receptor functionality was not altered by the point mutation. Furthermore, receptor stimulation by LUF7746 was largely reversed by DPCPX due to the amino acid Y271<sup>7.36</sup> mutation, unlike in the WT receptor (Fig. 5c). This marked contrast confirms the hypothesized covalent interaction between ligand and receptor and validates the primary role of the tyrosine residue in the formation of the covalent activation. It may be though that a second site of covalent interaction exists, as the reversal of the functional effect was not complete under the experimental conditions examined. Similar results from functionalized covalent probes were also obtained on other GPCR subtypes. On M<sub>1</sub> and M<sub>2</sub> muscarinic receptors, nitrogen mustard analogs alkylate more than one residue besides a well-known reactive center Asp3.32 [40]. Likewise, on the human cannabinoid 2 receptor, two possible cysteines were validated to mediate the covalent binding of affinity probe AM1336 [41]. Mutagenesis of nucleophilic residues near the orthosteric binding pocket is useful to study the mode and site of interaction, but may also drive the covalent ligand to react with secondary nucleophilic amino acid residues.

Building on our understanding of the chemical properties of LUF7746, we further performed an *in vitro* A<sub>1</sub> receptor-mediated whole-cell assay. To reveal the partial agonistic behavior, the cell line used for this label-free assay has a relatively low hA<sub>1</sub>AR expression level ( $B_{max} = 0.968 \pm 0.014$  pmol/mg protein for [<sup>3</sup>H] DPCPX derived from saturation experiments) [25]. In

particular, the inhibition of reversible activation (LUF7747, Fig.8b) demonstrated a continued decrease in cell impedance, whereas covalent activation by LUF7746 (Fig.8a) was first inhibited by DPCPX, although less than for LUF7747, and appeared to return towards the activation state. Hence, we substantiated that the intrinsic cellular effect induced by LUF7746 is vastly different from cellular responses generated by LUF7747. This phenomenon was found in other studies as well. For instance, in the case of the cannabinoid CB<sub>1</sub> receptor, covalent agonist AM841 generates an inhibition on synaptic transmission, which cannot be reversed by antagonist [42]. In another study, Jorg *et al* found that hA<sub>1</sub>AR modulation by covalent agonists appeared to be insensitive to post-reversal by antagonist [4].

In conclusion, we report the rational design of non-ribose hA<sub>1</sub>AR ligand LUF7746, with a chemically reactive electrophilic (SO<sub>2</sub>F) warhead at a judiciously selected position. A series of assays, comprising time-dependent affinity determination, kinetic assay, washout experiments and [<sup>35</sup>S]GTPγS binding assays, then validated LUF7746 as the first covalent partial agonist for the hA<sub>1</sub>AR. A combined *in silico* hA<sub>1</sub>AR-structure based docking and site-directed mutagenesis-study was performed to demonstrate amino acid residue Y271<sup>7,36</sup> was responsible for the covalent interaction. Furthermore, we demonstrated that LUF7746 behaved as covalent partial agonist under near-physiological conditions at the cellular level. Thus, our covalent ligand LUF7746 behaves as a covalent partial agonist on membranes and intact cells and may serve as a tool compound for further studies on receptor desensitization or internalization and target validation in *in vivo* studies. This useful approach for investigating ligand-receptor interactions can be enhanced through the design of other higher affinity electrophiles, and it can be applied to study molecular mechanisms involved in partial agonism. Future work in this regard could involve proteomics studies with LUF7746 e.g., peptide-level LC/MS/MS, to experimentally identify other potential amino acid residues critical to hA<sub>1</sub>AR orthosteric ligand binding and function and would serve to map structural features and the topology of the hA<sub>1</sub>AR non-ribose partial agonist binding pocket.

### References

1. A.S. Hauser, M.M. Attwood, M. Rask-Andersen, H.B. Schiøth, D.E. Gloriam, *Nat. Rev. Drug Discov.* **2017**.16(12): 829-842.
2. D. Weichert, P. Gmeiner, *ACS Chem. Bio.* **2015**. 10(6): 1376-1386.
3. D.W. Szymanski, M. Papanastasiou, K. Melchior, N. Zvonok, R.W. Mercier, D.R. Janero, et al., *J. Proteome Res.* **2011**. 10(10): 4789-4798.
4. M. Jorg, A. Glukhova, A. Abdul-Ridha, E.A. Vecchio, A.T. Nguyen, P.M. Sexton, et al. *J. Med. Chem.* **2016**. 59(24):11182-11194.

## Chapter 5

---

5. K.A. Jacobson, S. Barone, U. Kammula, G.L. Stiles. *J Med Chem.* **1989.** 32(5): 1043-1051.
6. J. Zhang, L. Belardinelli, K.A. Jacobson, D.H. Otero, S.P. Baker. *Mol. Pharmacol.* **1997.** 52(3): 491-498.
7. W.F. Kiesman, E. Elzein, J. Zablock, *Adenosine Receptors in Health and Disease, Springer Berlin Heidelberg, Berlin, Heidelberg, 2009.* 25-58.
8. S.J. Greene, H.N. Sabbah, J. Butler, A.A. Voors, B.E. Albrecht-Kupper, H.D. Dungen. *Heart Fail. Rev.* **2016.** 21(1): 95-102.
9. L.C.W. Chang, J.K.V.F. Kunzel, T. Mulder-Krieger, R.F. Spanjersberg, S.F. Roerink, G. van den Hout, et al. *J Med Chem.* **2005.** 48(6): 2045-2053.
10. W. Sherman, T. Day, M.P. Jacobson, R.A. Friesner, R. Farid, s, J. Med. Chem. **2006.** 49(2), 534-553.
11. U.H. Rosentreter, R., Bauser, M.; Krämer, T., Vaupel, A., W.D. Hübsch, K., Salcher-Schraufstätter, O., Stasch, J.-P.T.P. Krahn, E.WO2001/025210, April 12, 2001.
12. L.H. Heitman, A. Goblyos, A.M. Zweemer, R. Bakker, T. Mulder-Krieger, J.P.D. van Veldhoven, et al. *J. Med. Chem.* **2009.** 52(4): 926-931.
13. X. Yang, G. Dong, T.J.M. Michiels, E.B. Lenselink, L. Heitman, J. Louvel, et al. *Purinergic Signal,* **2017.** 13(2): 191-201.
14. O. Boussif, F. Lezoualch, M.A. Zanta, M.D. Mergny, D. Scherman, B. Demeneix, et al., , *Proc. Natl. Acad. Sci. USA.* **1995** 92(16): 7297-7301.
15. D. Guo, E.J. van Dorp, T. Mulder-Krieger, J.P. van Veldhoven, J. Brussee, A.P. IJzerman, et al. *J Biomol Screen.* **2013.** 18(3): 309-320.
16. J. Louvel, D. Guo, M. Agliardi, T.A. Mocking, R. Kars, T.P. Pham, et al. *J. Med. Chem.* **2014.** 57(8): 3213-3222.
17. L. Xia, A. Kyrizaki, D.K. Tosh, T.T. van Duijl, J.C. Roorda, K.A. Jacobson, et al. *Biochem. Pharmacol.* **2018.** 153: 248-259.
18. S. Schrödinger Release 2018-3: LigPrep, LLC, New York, NY, 2018.
19. A. Glukhova, D.M. Thal, A.T. Nguyen, E.A. Vecchio, M. Jorg, P.J. Scammells, et al. *Cell* **2017.** 168(5): 867-877.
20. W.J. Berman HM, Feng Z, et al The Protein Data Bank, *Nucleic Acids Research*, 28: 235-242. [www.rcsb.org](http://www.rcsb.org)
21. S. Schrödinger Release 2017-4: Prime, LLC, New York, NY, 2017.
22. D. Guo, T. Mulder-Krieger, A.P. IJzerman, L.H. Heitman. *Br J Pharmacol.* **2012.** 166(6):: 1846-1859.
23. J.M. Hillger, J. Schoop, D.I. Boomsma, P.E. Slagboom, A.P. IJzerman, L.H. Heitman, *Biosens. Bioelectron.* **2015.** 74: 233-242.
24. N. Yu, J.M. Atienza, J. Bernard, S. Blanc, J. Zhu, X. Wang. *Anal. Chem.* **2006.** 78(1): 35-43.
25. A. Dalpiaz, A. Townsend-Nicholson, M.W. Beukers, P.R. Schofield, IJzerman A. P. *Biochem. Pharmacol.* **1998.** 56(11): 1437-45.
26. Y. Cheng, W.H. Prusoff. *Biochem. Pharmacol.* **1973.** 22(23): 3099-3108.
27. H.J. Motulsky, L.C. Mahan. *Mol. Pharmacol.* **1984.** 25(1): 1-9.
28. J. Louvel, D. Guo, M. Soethoudt, T.A.M. Mocking, E.B. Lenselink, T. Mulder-Krieger, et al., *Eur J Med Chem.* **2015.** 101: 681-691.
29. D. Guo, S.N. Venhorst, A. Massink, J.P.D. van Veldhoven, G. Vauquelin, A.P. IJzerman, et al., , *Br J Pharmacol.* **2014.** 171(23): 5295-5312.
30. P.G. Strange, *Br J Pharmacol.* **2010.** 161(6): 1238-1249.

31. A. Townsend-Nicholson, P.R. Schofield. *J Biol Chem.* **1994.** 269(4):2373-2376.
32. T. Hua, K. Vemuri, S.P. Nikas, R.B. Laprairie, Y. Wu, L. Qu, et al. *Nature.* **2017.** 547(7664): 468-471.
33. H. Suga, F.J. Ehlert. *Biochemistry.* **2013.** 52(29): 4914-4928.
34. C. Li, W. Xu, S.K. Vadivel, P. Fan, A. *J Med Chem.* **2005.** 48(20) (2005): 6423-6429.
35. M.L.J. Doornbos, X. Wang, S.C. Vermond, L. Peeters, L. Perez-Benito, A.A. Trabanco, et al., *J Med Chem.* **2019** Jan 10; 62(1): 223–233.
36. K.W. Figueroa, H. Suga, F.J. Ehlert, *Br. J. Pharmacol.* 160(6) (2010), pp. 1534-1549
37. D. Weichert, A.C. Kruse, A. Manglik, C. Hiller, C. Zhang, H. Hubner, et al. *Proc. Natl. Acad. Sci. USA.* **2014.** 111(29): 10744-10748.
38. C.J. Draper-Joyce, M. Khoshouei, D.M. Thal, Y.L. Liang, A.T.N. Nguyen, S.G.B. Furness, et al. *Nature,* **2018.** 558(7711): 559-563.
39. L.H. Heitman, T. Mulder-Krieger, R.F. Spanjersberg, J.K. von Frijtag Drabbe Kunzel, A. Dalpiaz, A.P. IJzerman, *Br J Pharmacol.* **2006.** 147(5): 533-541.
40. H. Suga, G.W. Sawyer, F.J. Ehlert. *Mol Pharmacol.* **2010.** 78(4) (2010):745-755.
41. R.W. Mercier, Y. Pei, L. Pandarinathan, D.R. Janero, J. Zhang, A. *Chem Biol.* **2010.** 17(10): 1132-1142.
42. C.M. Keenan, M.A. Storr, G.A. Thakur, J.T. Wood, J. Wager-Miller, A. Straiker, et al. *Br Pharmacol.* **2015.** 172(9) (2015): 2406-2418.



# Chapter 6

## An Affinity-based Probe for the human Adenosine A<sub>2A</sub> Receptor

*Xue Yang,*

*Thomas J.M. Michiels,*

*Coen de Jong,*

*Marjolein Soethoud<sup>§</sup>,*

*Niek Dekker,*

*Euan Gordon<sup>‡</sup>,*

*Mario van der Stelt,*

*Laura H. Heitman,*

*Daan van der Es*

*Adriaan P. IJzerman\**

J Med Chem. 2018 Sep 13;61(17):7892-7901.

doi: 10.1021/acs.jmedchem.8b00860.





### Abstract

Using activity-based protein profiling (ABPP) functional proteins can be interrogated in their native environment. Despite their pharmaceutical relevance G protein-coupled receptors (GPCRs), have been difficult to address through ABPP. In the current study we took the prototypical human adenosine A<sub>2A</sub> receptor (hA<sub>2A</sub>R) as the starting point for the construction of a chemical toolbox allowing two-step affinity-based labeling of GPCRs.

Firstly, we equipped an irreversibly binding hA<sub>2A</sub>R ligand with a terminal alkyne to serve as probe. We showed that our probe irreversibly and concentration-dependently labeled purified hA<sub>2A</sub>R. Click-ligation with a sulfonated cyanine-3 fluorophore allowed us to visualize the receptor on SDS-PAGE. We further demonstrated that labeling of the purified hA<sub>2A</sub>R by our probe could be inhibited by selective antagonists. Lastly, we showed successful labeling of the receptor in cell membranes overexpressing hA<sub>2A</sub>R making our probe a promising affinity-based probe that sets the stage for the further development of probes for GPCRs.

### 1. Introduction

The adenosine receptors, belonging to the family of G protein-coupled receptors (GPCRs), have been coined adenosine A<sub>1</sub>, A<sub>2A</sub>, A<sub>2B</sub>, and A<sub>3</sub>. These receptors are widely distributed through the human body and are considered promising targets for a wide range of diseases [1]. Regadenoson, a selective human adenosine A<sub>2A</sub> receptor (hA<sub>2A</sub>R) agonist used to increase vasodilation during cardiac imaging, has been approved by the FDA, exemplifying the potential therapeutic applications for the hA<sub>2A</sub>R. Likewise, hA<sub>2A</sub>R antagonists are currently being pursued as potential treatment of Parkinson's disease and as adjuvants in cancer immunotherapy [2, 3].

The hA<sub>2A</sub>R was one of the first GPCRs for which a crystal structure was elucidated [4]. However, the challenges in structural biology of GPCRs, including the low expression level in native tissue and inherent poor protein stability, still exist [5]. To overcome these obstacles, covalent probes have been developed as useful pharmacological tools. Such probes, also named affinity labels, represent compounds that feature a reactive cross-linking moiety, which can irreversibly and specifically bind to a receptor. For example, an irreversible antagonist was used to stabilize the adenosine A<sub>1</sub> receptor for co-crystallization, resulting in the visualization of key amino acids important for ligand-receptor binding [6].

The design of covalent probes for GPCRs generally follows a similar strategy, which is to incorporate a warhead in a high-affinity, reversibly binding ligand. Based on the type of warhead used, two categories of irreversible ligands can be discerned: photoaffinity- and chemoreactive ligands [7, 8]. Whereas in the former type a photoreactive warhead is employed, the latter is equipped with an electrophilic chemical moiety capable of binding nucleophilic residues in the target protein. A commonly used warhead is aryl sulfonyl fluoride, which is capable of covalently binding to many nucleophilic amino acid residues, such as serine, threonine, lysine, and cysteine [9]. This warhead has been incorporated in several reported covalent ligands for the adenosine receptors, including FSCPX [10], FSPTP [11], fluorosulfonyl functionalized pyrimidine derivatives [12] and LUF7445 [13]. Likewise, fluorescent tags have been incorporated into adenosine receptor ligands to visualize the receptor, which yielded e.g., FITC-ADAC [14], MRS5422 [15] and NBD-NECA [16]. However, fluorescent moieties are of significant size and *a priori* derivatization of a ligand with such a group may negatively affect receptor affinity. Here, two-step affinity-based probes (AfBPs) might be a better alternative, as a reporter tag is added after the reactive ligand has bound its target [17].

Interestingly, from the field of activity-based protein profiling (ABPP), combined with click chemistry, many techniques have emerged that could potentially be applied to GPCRs using our covalent ligand. Normally in ABPP, an irreversible ligand is equipped with a ligation handle and after binding to the protein of interest is paired with a clickable fluorophore. In this way, via a Huisgen 1,3-dipolar cycloaddition, a stable triazole-linked product is formed, effectively attaching a fluorescent label to the protein [18-20]. Currently, this technique serves as a tool to profile the activities of drug targets (currently mainly enzymes) in native biological systems. One-step labeling, where the reporter group is pre-attached to the probe, has been applied on GPCRs before [21-23]. Moreover, similar two-step labeling strategies have been applied for other targets [24, 25]. However, due to their low abundance GPCRs are difficult to address with this otherwise promising technique. Within the entire GPCR family with over 800 members, until recently, only the mGlu<sub>5</sub> receptor had been the subject of this approach, albeit with limited success [26]. Very recently, the type 2 cannabinoid receptor (CB<sub>2</sub>R) has been probed with a two-step photoaffinity probe, leading to great insights into receptor localization and target engagement [27].

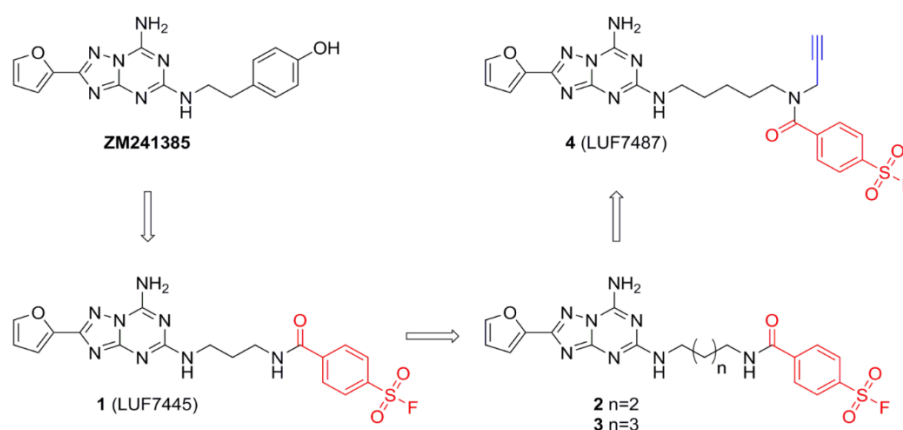


**Figure 1.** Chemical structures of the hA<sub>2A</sub>R antagonists examined in this study. The lead compound ZM241385, a selective hA<sub>2A</sub>R antagonist, inspired the design of covalent antagonist **1**.<sup>13</sup> In the current study the effect of the linker length between scaffold and warhead on affinity was further examined, yielding compound **2** and, preferably, compound **3**. The affinity-based probe **4** was then synthesized from compound **3**, bearing an alkyne ligation-handle and a fluorosulfonyl electrophilic warhead. The electrophilic warhead is in red and the click-ligation handle is in blue.

In this study, we describe our efforts to obtain a clickable affinity-based probe, with an electrophilic warhead, as a logical extension of our previous research on the successful design of a covalent antagonist of hA<sub>2A</sub>R, compound **1** (LUF7445) [13]. We used the antagonist ZM241385 as the starting point in our design efforts, and synthesized a series of fluorosulfonyl derivatives with diverse linker lengths (compounds **1-3**, Figure 1). The most

potent ligand, with low nanomolar affinity, was retained for further structural modification and was equipped with an alkyne-click handle, resulting in probe **4**, as shown in Figure 1. We then validated that the ligand's binding to the receptor was wash-resistant. Additionally, we demonstrated the ligand's covalent labeling capacity of purified receptors via a bioorthogonal copper catalyzed azide-alkyne ligation reaction with a fluorescent moiety, sulfonated cyanine 3 ((E)-2-((E)-3-(1-(6-((3-azidopropyl)amino)-6-oxohexyl)-3,3-dimethyl-5-sulfo-3*H*-indol-1-ium-2-yl)allylidene)-3,3-dimethyl-1-(3-sulfopropyl)indoline-5-sulfonate). Finally, this probe was able to profile the presence of hA<sub>2A</sub>R in a relatively complex biological sample. Hence, this is one of the first AfBPs for a GPCR, and may set the stage for similar probes to facilitate target discovery and bioanalysis of GPCRs associated with human disease.

## 2. Results and discussions

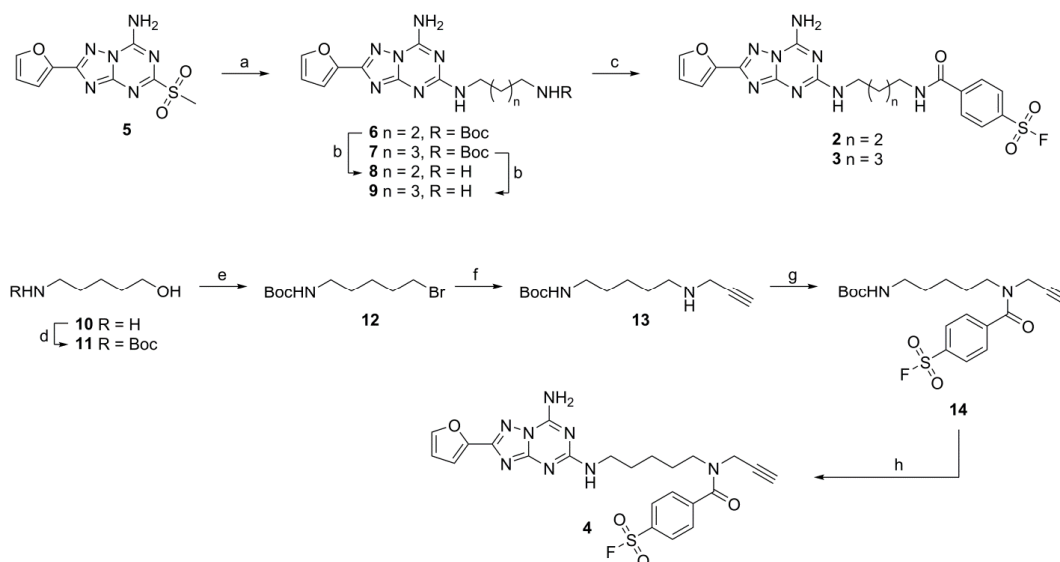
### 2.1. Chemistry.

In the past, our research group has been evaluating structural modifications of triazolotriazine derivatives based on the selective adenosine A<sub>2A</sub> antagonist 4-(2-(7-amino-2-(furan-2-yl)-[1,2,4]triazolo[1,5-*a*][1,3,5]triazin-5-ylamino)ethyl)phenol (ZM241385), to obtain a covalent ligand for the hA<sub>2A</sub>R. The rational design of this covalent ligand originated from a reported hA<sub>2A</sub>R crystal structure (PDB: 4EIY) in complex with ZM241385 [4]. In it, the ligand binding pocket demonstrated a deep, planar and narrow cavity embracing the aromatic core and furan ring of ZM241385. Therefore, an extension of the hydroxyphenethylamine moiety into the extracellular domain of the receptor offered us the playground for integration of the electrophilic reactive groups. Our earlier covalent antagonist, compound **1** (Figure 1), in which the 4-hydroxyphenylethylamine-side chain in ZM241385 was replaced with a similar side chain harboring an electrophilic fluorosulfonyl moiety, was recognized by hA<sub>2A</sub>R with an apparent  $pK_i$  of 8.99 [13]. In order to optimize the irreversible binding potential of our compound, with our current aim of developing an AfBP in mind, an exploration of linker length was performed, varying the linker between the fluorosulfonyl warhead moiety and the aromatic recognition element from three to five carbon atoms. To this end, compounds **2** and **3** were synthesized as detailed in Scheme 1. The synthesis starts from 2-(furan-2-yl)-5-(methylsulfonyl)-[1,2,4]triazolo[1,5-*a*][1,3,5]triazin-7-amine **5**, synthesized as previously reported [13], and involves a linear sequence comprising aromatic substitution with either commercially available mono-Boc-protected butyldiamine or pentyldiamine and subsequent Boc-deprotection towards intermediates **8** and **9**. Introduction of the fluorosulfonylbenzoyl

warhead proceeded with low yields due to difficult purification, providing ligands **2** and **3** in 4% and 2% yield respectively.

The synthetic route towards probe **4** (LUF7487, Figure 1) is depicted in Scheme 1. First, the amino group of 5-aminopentanol was protected with a Boc group and the hydroxyl was converted to a bromide using an Appel reaction, providing intermediate **12**. Nucleophilic substitution of the bromide with propargylamine afforded amine **13**, which was acylated with 4-fluorosulfonylbenzoylchloride to give Boc-protected bi-functional spacer **14** uneventfully. Finally, in a two-step process, the spacer was deprotected and coupled to scaffold **5**, to provide probe **4** in 45% yield.

**Scheme 1.** Synthesis of compounds **2**, **3** and **4**.



Reagents and conditions: a) *tert*-butyl (4-aminobutyl)carbamate or *tert*-butyl (5-aminopentyl)carbamate, DiPEA, MeCN, 70-85°C, 46-74%; b) TFA, quant; c) 4-fluorosulfonylbenzoylchloride, DiPEA, MeCN, 70°C, 2-4%; d) Boc<sub>2</sub>O, DCM, quant; e) PPh<sub>3</sub>, CBr<sub>4</sub>, 90%; f) propargylamine, DiPEA, 46%; g) 4-fluorosulfonylbenzoylchloride, DiPEA, MeCN, quant; h) i. **5**, TFA, DCM, ii. DiPEA, MeCN, 70°C, 45%

## 2.2. Biology

To assess the affinity for the hA<sub>2A</sub>R, compounds **2** and **3** were tested in [<sup>3</sup>H]ZM241385 displacement experiments (n = 3), which demonstrated a concentration-dependent inhibition of radioligand binding to hA<sub>2A</sub>R overexpressed in HEK293 cells. To better understand the time-dependent binding characteristics of these compounds, we then carried out displacement assays performed with two different incubation times. Representative graphs for these

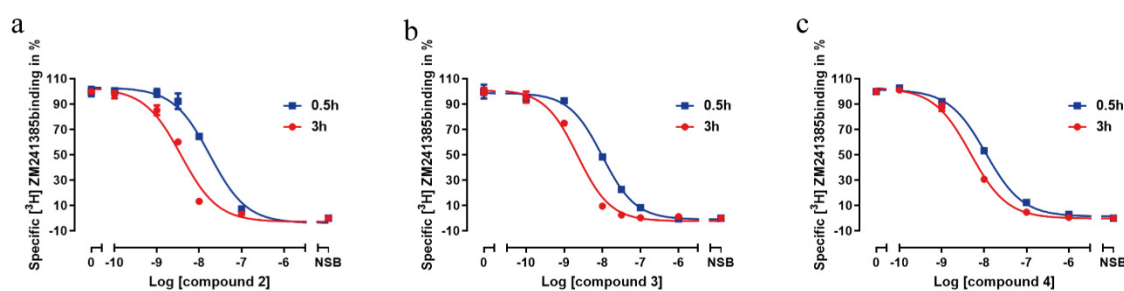


**Figure 2.** Displacement of specific [ $^3\text{H}$ ]ZM241385 binding from HEK293 cell membranes stably expressing the  $\text{hA}_{2\text{A}}\text{R}$  receptor at  $25^\circ\text{C}$  by compound **2** (a), **3** (b) and **4** (c) with an incubation time of 0.5h (blue curve) and 3h (red curve), respectively. Representative graphs are from one experiment performed in duplicate. Independent experiments performed in duplicate with error bars representing SEM values

experiments are given in Figure 2a and 2b, in which the concentration-dependent inhibition of specific [ $^3\text{H}$ ]ZM241385 binding shifted to the left with an incubation time extension from 0.5 h (standard) to 3 h. As detailed in Table 1, the affinities of both compound **2** and **3** significantly increased by approximately 5-fold to sub-nanomolar values with longer incubation times. In other words, both designed covalent ligands became more potent in displacing the radioligand [ $^3\text{H}$ ]ZM241385 from the receptor over time. Similarly, to **1** [13], this pronounced affinity increase may be attributed to an irreversible binding nature of the compounds, leading to a higher receptor occupancy with a longer incubation time. It should be kept in mind that due to the covalent nature of the interaction; affinity values can only be apparent as no dynamic equilibrium can be reached. Compound **3** inhibited the specific [ $^3\text{H}$ ]ZM241385 binding to the  $\text{hA}_{2\text{A}}\text{R}$  with a  $\text{pK}_i$  of 9.21, compared to the affinity of compound **2** ( $\text{pK}_i = 9.05 \pm 0.07$ ) and **1** ( $\text{pK}_i = 8.99 \pm 0.01$ ). Thus, the extension of the linker to five carbon atoms slightly increased the apparent affinity. This could be caused by more steric freedom allowing the fluorosulfonyl group to orient towards the adjacent nucleophilic residue in the receptor binding site compared to ligands with a shorter linker. A similar example is an electrophilic probe for the cannabinoid  $\text{CB}_1$  receptor, 7'-NCS-1',1'-DMH- $\Delta^8$ -THC, in which lengthening the C-3 alkyl side chain to seven carbons, resulted in a significantly improved affinity [28]. Above all, high affinity is a key requirement for the development of irreversible ligands, as it increases the presence of the chemoreactive moiety in proximity to a nucleophilic residue in the binding site, thereby improving receptor occupancy and causing a

**Table 1.** (Apparent) affinities of synthesized ligands for the human A<sub>2A</sub> adenosine receptor<sup>a</sup>

Compound <sup>b</sup>	pK <sub>i</sub> <sup>c</sup> (0.5h)	pK <sub>i</sub> <sup>d</sup> (3h)	pK <sub>i</sub> shift <sup>e</sup>
<b>1</b> <sup>f</sup>	8.27 ± 0.04	8.99 ± 0.01 <sup>***</sup>	0.72
<b>2</b>	8.20 ± 0.13	9.05 ± 0.07 <sup>***</sup>	0.85
<b>3</b>	8.56 ± 0.03	9.21 ± 0.01 <sup>***</sup>	0.65
<b>4</b>	8.41 ± 0.02	8.82 ± 0.02 <sup>***</sup>	0.41

<sup>a</sup>Data are expressed as means ± SEM of three separate experiments each performed in duplicate. \*\*\*P < 0.001 compared with the pK<sub>i</sub> values in displacement experiments with a 0.5h incubation time; Student's t-test.

<sup>b</sup>For all the designed covalent antagonists, pK<sub>i</sub> values can only be apparent, as true equilibrium cannot be reached;

<sup>c</sup>Affinity, expressed as pK<sub>i</sub> value, determined from displacement of specific [<sup>3</sup>H]ZM241385 binding from the hA<sub>2A</sub>R at 25°C during a 0.5h incubation;

<sup>d</sup>Affinity, expressed as pK<sub>i</sub> value, determined from displacement of specific [<sup>3</sup>H]ZM241385 binding from the hA<sub>2A</sub>R at 25°C during a 3h incubation;

<sup>e</sup>Affinity shift was calculated as [pK<sub>i</sub>(3h)-pK<sub>i</sub>(0.5h)];

<sup>f</sup>Data previously reported provided for comparison [13].

decrease in non-specific binding to other unrelated targets. As we anticipated a greater demand for steric freedom for the incorporation of the alkyne group and the subsequent ligation between the alkyne moiety and a bulky fluorescent dye, we retained the preferable five carbon atom linker length for the design of our probe.

Inspired by the most promising compound **3**, we incorporated the alkyne click-handle to afford a novel covalent probe, compound **4** (LUF7487, Figure 1). As detailed in Table 1, affinity-based probe **4** demonstrated a high affinity, displacing [<sup>3</sup>H]ZM241385 with an apparent pK<sub>i</sub> value of 8.82. Under these conditions **4** was at least 10-fold selective over human A<sub>1</sub> and A<sub>3</sub> receptors (SI Table S1). In a time-dependent study, probe **4** generated a significant increase in specific [<sup>3</sup>H]ZM241385 displacement over time (Table 1). In analogy to the covalent ligand **3**, the designed probe was markedly influenced by prolonged incubation times (Figure 2c), suggesting an increasing level of covalent binding over time. However, compared to **3**, the slight decrease in affinity may be attributed to the incorporation of the click handle, possibly leading to a steric hindrance in the ligand-receptor complex, and/or the formation of a covalent bond between the warhead and other nucleophilic residues.

To better understand the receptor-ligand binding nature, the novel affinity-based probe was then evaluated for its covalent nature by determining its capacity to irreversibly block [<sup>3</sup>H]ZM241385 to hA<sub>2A</sub>R binding sites. Membranes overexpressing hA<sub>2A</sub>R were pretreated with probe **4** or ZM241385 at the indicated concentration (IC<sub>50</sub> or 0.3-fold IC<sub>50</sub>) for 3 hours,

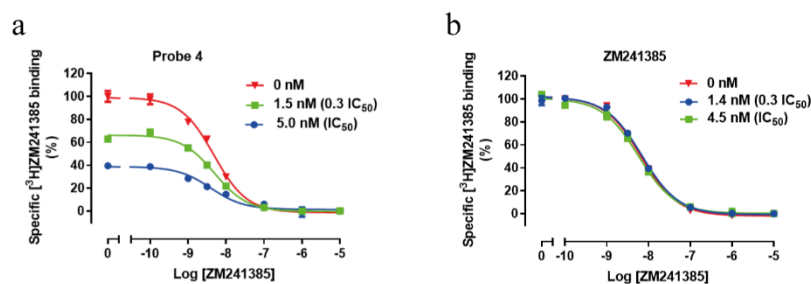


**Figure 3.** Probe 4 irreversibly binds to hA<sub>2A</sub>R HEK293 cell membranes stably expressing hA<sub>2A</sub>R were pre-incubated with probe 4 (a) or ZM241385 (b) at the indicated comparable concentrations. Pretreated membranes were washed three times extensively before further displacement studies of specific [<sup>3</sup>H]ZM241385 binding from the hA<sub>2A</sub>R at 25°C by non-labelled ZM241385 were performed. Representative graphs are from three independent experiments performed in duplicate with error bars representing SEM values

followed by a three-cycle washing step to remove the non-covalently bound material. The membranes pretreated with probe 4 (Figure 3a) at increasing concentrations revealed a concomitant decline in specific [<sup>3</sup>H]ZM241385 binding, which was reduced from  $65 \pm 2\%$  to  $43 \pm 2\%$ . However, membranes pretreated with the reversible antagonist ZM241385 (Figure 3b) at increasing concentrations showed no decrease in specific [<sup>3</sup>H]ZM241385 binding, proving that the washing procedure was extensive enough to remove all non-covalently binding compound. Meanwhile, the affinity of unlabeled ZM241385 was not influenced significantly by the preincubation and washing procedure, indicating that the extensive washing did not damage the membrane integrity or alter the membrane binding sites (SI Table S2). Therefore, it could be concluded that the concentration-dependent decrease in specific [<sup>3</sup>H]ZM241385 binding observed with probe 4 resulted from an irreversible occupancy of the hA<sub>2A</sub> receptor binding pocket. Similar results have been obtained on other GPCRs, e.g., for the adenosine A<sub>1</sub> receptor irreversible antagonist FSCPX [29, 30] and the covalent histamine H<sub>4</sub> receptor partial agonist VUF14480 [31], although these compounds lack the alkyne moiety to perform a click chemistry approach.

### 2.3. Fluorescent labeling of the hA<sub>2A</sub>R.

Having shown that the designed probe 4 meets the requirement of covalent binding, we then set out to evaluate its ability to function as an affinity-based probe. Purified hA<sub>2A</sub>R was first incubated with the alkyne-containing probe 4 to ensure formation of a covalent probe-hA<sub>2A</sub>R adduct. Then all samples were subjected to a copper (I)-catalyzed sulfonated cyanine 3-azide



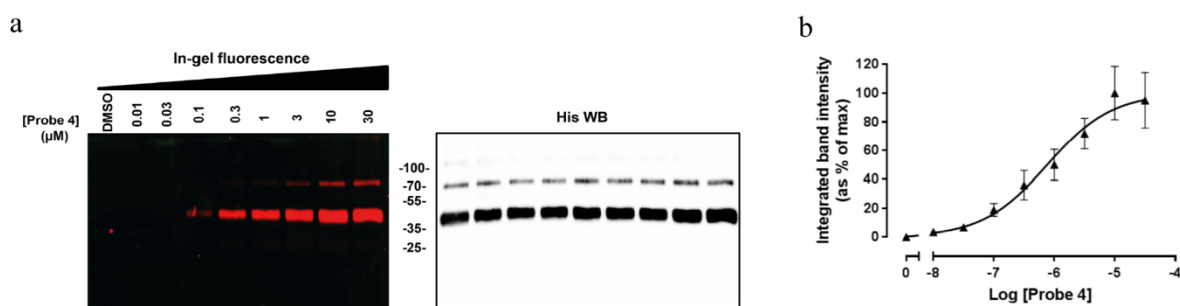


**Figure 4.** Concentration-dependent affinity labeling of purified, His-tagged hA<sub>2A</sub>R by probe 4. (a) Purified hA<sub>2A</sub>R material was incubated with the indicated concentrations of probe 4 or vehicle (1% DMSO), and subjected to click chemistry ligation with Cy3-azide, followed by SDS-PAGE separation and in-gel fluorescence scanning (left). The blotted membranes were probed with anti-histidine antibody, wherein bands corresponding to purified hA<sub>2A</sub>R molecular weight (~47 kDa) were evident in all samples (right). (b) Quantification of fluorescence intensity from purified hA<sub>2A</sub>R labeled by probe 4 clicked to Cy3-azide. Representative graphs are from three independent experiments, with errors bars representing SEM values. In-gel fluorescence of the hA<sub>2A</sub>R band at ~47 kDa was normalized to the corresponding hA<sub>2A</sub>R immunoreactivity in each sample.

(Cy3-azide) attachment to the terminal alkyne [32, 33]. The subsequent fluorescence scanning of a SDS-PAGE showed that in the presence of fluorescent dye Cy3-azide (Figure 4a), probe 4 was concentration-dependently incorporated into a fixed amount of purified hA<sub>2A</sub>R, while in the absence of probe, little fluorescence intensity was detected. Importantly, western blot analysis using the purified hA<sub>2A</sub>R receptor and specific anti-histidine antibodies unambiguously validated the labeling band was hA<sub>2A</sub>R (Figure 4a). Interestingly, a second band was observed in both affinity labeling results and western blots, most likely resulting from posttranslationally modified receptors,<sup>34</sup> as has been shown before on CB<sub>2</sub>R [27]. Quantification of the fluorescence intensity of the main labeling bands in the hA<sub>2A</sub>R is reflected in the concentration-effect curve in Figure 4b. This revealed that clickable probe 4 labeled hA<sub>2A</sub>R with a pEC<sub>50</sub> value of  $6.10 \pm 0.04$ , resulting in a maximal labeling achieved with 10 μM probe 4 when incubated with 0.1 mg mL<sup>-1</sup> of purified hA<sub>2A</sub>R. Collectively, these data demonstrate that probe 4 can be used as an affinity-based probe for purified hA<sub>2A</sub>R.

To further characterize our affinity-based probe, we then investigated whether competitive antagonists could inhibit the labelling of purified receptors by probe 4. We chose to evaluate

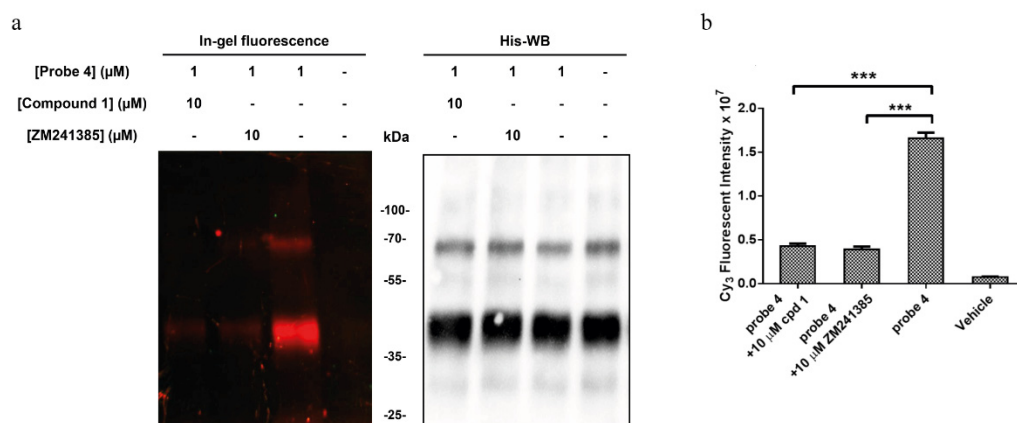


**Figure 5.** Competitive affinity labeling of the purified hA<sub>2A</sub>R by probe 4 (a) Affinity labeling of purified hA<sub>2A</sub>R by probe 4 (1  $\mu\text{M}$ ) is inhibited by preincubation with either compound 1 (10  $\mu\text{M}$ ) or ZM241385 (10  $\mu\text{M}$ ) (left). The blotted membranes were probed with anti-histidine antibody, wherein bands corresponding to purified hA<sub>2A</sub>R molecular weight ( $\sim 47$  kDa) were evident in all samples (right). (b) Quantification of fluorescence intensity from pretreated purified hA<sub>2A</sub>R labeled by probe 4 clicked to Cy3-azide. Representative graphs are from three independent experiments, with errors bars representing SEM values. \*\*\* $P < 0.001$  compared with the fluorescent intensity of purified hA<sub>2A</sub>R labeled by probe 4 (1  $\mu\text{M}$ ); Student's t-test. In-gel fluorescence of the hA<sub>2A</sub>R band at  $\sim 47$  kDa was normalized to the corresponding hA<sub>2A</sub>R immunoreactivity in each sample

reversible antagonist ZM241385 and irreversible compound 1, at saturating concentrations (10  $\mu\text{M}$ , i.e. 10 times higher than the concentration of the clickable probe 4). Purified hA<sub>2A</sub>R, preincubated with the competitors and subsequently treated as mentioned before to incorporate the sulfonated cyanine 3 fluorophore, showed little if any fluorescence intensity of labelling bands under these conditions. This revealed that both a reversible and an irreversible antagonist competed with probe 4 (Figure 5a, left panel) for the same binding site at the hA<sub>2A</sub>R, which was available at identical amounts in all conditions (as evidenced by His-tagging: Figure 5a, right panel). Theoretically, both reversible and irreversible ligands inhibit affinity labelling, provided that they target the same receptor binding site and are present in a sufficient concentration. Of note, in practice, this is not always easily observed, as in the competition between reversible ligand and covalently binding probe there is an inherent bias towards the irreversible pathway, hindering the interaction between the receptor and a reversible ligand. For instance, in the few other studies where an AfBP has been used on GPCRs it was found that a reversible mGlu<sub>5</sub> negative allosteric modulator, MPEP, could not inhibit the tandem photoaffinity labeling of purified mGlu<sub>5</sub>, whereas on CB<sub>2</sub>R, inhibition of labeling by various competitors was observed [26, 27]. Apparently, this was less of a problem on the hA<sub>2A</sub>R. Our results demonstrate that the developed AfBP system can serve as an effective chemical tool for profiling the purified hA<sub>2A</sub>R in vitro, prompting us to further

evaluate the potency and selectivity of probe **4** in profiling the activity of the adenosine A<sub>2A</sub> receptor in more complex biological samples.

We further explored the ability of probe **4** to label hA<sub>2A</sub>R in cell membranes prepared from HEK293 cells, which were transiently transfected with N-terminally FLAG-tagged and C-terminally His-tagged human adenosine A<sub>2A</sub> receptors (FLAG-hA<sub>2A</sub>R-His). Therefore, FLAG-hA<sub>2A</sub>R-His cell membranes were incubated with probe **4** at room temperature for 1 h, followed by click ligation to Cy3-azide treatment. As detailed in Figure 6, a band corresponding to the molecular weight of the FLAG-hA<sub>2A</sub>R-His was observed on fluorescent SDS-PAGE scanning, which was then validated by Western blot using specific anti-FLAG antibodies. In these initial proof-of-concept experiments we highlighted the versatility of probe **4**, which can be efficiently used to label the adenosine A<sub>2A</sub> receptor in cell membrane samples. Background signals caused by nonspecific labeling of abundant proteins in complex proteomes may sometimes confound the analysis of on-target labeling of low expression proteins such as GPCRs.

Thus, we utilized cell membranes transiently transfected with FLAG-hA<sub>2A</sub>R-His, which have a relatively high level of receptor expression. Additionally, instead of premixing the copper sulfate and sodium ascorbate reagents, we slightly altered the click procedure by adding the copper sulfate last to achieve efficient and selective labeling of the A<sub>2A</sub> receptors [35, 36].

Although we were able to decrease the strong background signals, a significant non-specific fluorescent dyes and labeled receptors, non-specific protein binding of the probe due to the inherently reactive warhead and the sensitivity of the used detection method. Hence, further technological refinement should help us in achieving better labeling of endogenously expressed GPCRs, e.g. in human tissues as has been shown recently on CB<sub>2</sub>R [27]. The monitoring of endogenous GPCR expression and target engagement in human cells holds promise for future GPCRs studies.

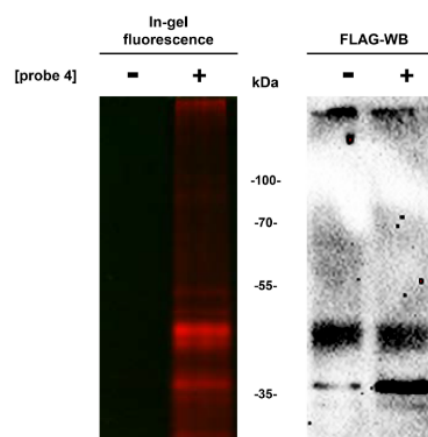


**Figure 6.** Affinity labeling of hA<sub>2A</sub>R in HEK293 cell membranes transiently expressing FLAG-tagged hA<sub>2A</sub>R using probe **4**. (a) cell membranes overexpressing FLAG-tagged hA<sub>2A</sub>R were incubated with either 1 μM probe **4** or vehicle (1% DMSO), then subjected to click chemistry ligation with Cy3-azide, followed by SDS-PAGE separation and in-gel fluorescence scanning (left). The blotted membranes were probed with anti-FLAG antibody, wherein bands corresponding to the hA<sub>2A</sub>R molecular weight (~50 kDa) are evident in all samples.

### 3. Conclusion

Starting from a selective antagonist, ZM241385, we designed and synthesized a series of covalent ligands using the electrophilic nature of sulfonyl fluorides, eventually yielding probe **4**, the first affinity-based probe for the hA<sub>2A</sub>R. We successfully demonstrated a concentration-dependent labelling of purified receptor by probe **4** via an experimental two-step labeling strategy, which could be inhibited by both reversible and irreversible competing ligands. Additionally, probe **4** displayed target selectivity in cell membranes overexpressing the hA<sub>2A</sub>R, indicating that it may become a useful pharmacological tool to identify the hA<sub>2A</sub>R in living organisms for target validation or to assess receptor subtype distribution. In this strategy a probe depicts the native binding with less perturbation, which bridges the chemical biology study with molecular pharmacology to better investigate receptor-ligand interactions.

In future research, different tags may be introduced; for instance, a biotin-tag would allow for streptavidin-mediated receptor enrichment followed by LC/MS analysis. Similarly, the approach developed in this study may be applied to other GPCRs, such as the other adenosine receptor subtypes.

### 4. Experimental sections

#### 4.1. Chemistry

All solvents and reagents were purchased from commercial sources and were of analytical grade. <sup>1</sup>H NMR spectra were recorded on a Bruker AV 400 liquid spectrometer (<sup>1</sup>H NMR, 400 MHz) at ambient temperature. Chemical shifts are reported in parts per million (ppm) and are designated by  $\delta$ . Coupling-constants are reported in Hz and are designated as  $J$ . Analytical purity of the final compounds was determined by high pressure liquid chromatography (HPLC) with a Phenomenex Gemini 3 $\mu$  C18 110A column (50  $\times$  4.6 mm, 3  $\mu$ m), measuring UV absorbance at 254 nm. Sample preparation and HPLC method was as follows: 0.5 mg of compound was dissolved in 1 mL of a 1:1:1 mixture of CH<sub>3</sub>CN/H<sub>2</sub>O/tBuOH and eluted from the column within 15 min, with a three component system of H<sub>2</sub>O/CH<sub>3</sub>CN/1% TFA in H<sub>2</sub>O, decreasing polarity of the solvent mixture in time from 80/10/10 to 0/90/10. All compounds showed a single peak at the designated retention time and are at least 95% pure. Liquid chromatography–mass spectrometry (LC–MS) analyses were performed using Thermo Finnigan Surveyor – LCQ Advantage Max LC-MS system and a Gemini C18 Phenomenex column (50  $\times$  4.6 mm, 3  $\mu$ m). The sample preparation was the same as for HPLC analysis. The elution method was set up as follows: 1–4 min isocratic system of H<sub>2</sub>O/CH<sub>3</sub>CN/1% TFA in H<sub>2</sub>O, 80:10:10; from the 4th min, a gradient was applied from 80:10:10 to 0:90:10 within 9

min, followed by 1 min of equilibration at 0:90:10 and 1 min at 80:10:10. Thin-layer chromatography (TLC) was routinely performed to monitor the progress of reactions, using aluminum coated Merck silica gel F254 plates. Purification by column chromatography was achieved by use of Grace Davison DAVISIL silica column material (LC60A 30–200 micron). Solutions were concentrated using a Heidolph laborota W8 2000 efficient rotary evaporation apparatus and by a high vacuum on a Binder APT line Vacuum Drying Oven.

**4-((4-((7-amino-2-(furan-2-yl)-[1,2,4]triazolo[1,5-*a*][1,3,5]triazin-5-yl)amino)butyl)carbonyl)benzene sulfonyl fluoride (2)** Previously synthesized N<sup>5</sup>-(4-aminobutyl)-2-(furan-2-yl)-[1,2,4]triazolo[1,5-*a*][1,3,5]triazine-5,7-diamine **8** (TFA salt, 250 mg, 0.40 mmol, 1.0 eq) was suspended in acetonitrile (10 mL) and purged with N<sub>2</sub>. Then DiPEA (0.42 mL, 2.4 mmol, 6.0 eq) was added after which 4-fluorosulfonylbenzoylchloride (134 mg, 0.60 mmol, 1.5 eq) was added last and the mixture was heated to 70 °C for 7 h, and then stirred at room temperature for another 17 h. A flash column (MTBE + 1% AcOH → 90% MTBE + 10% EtOAc + 1% AcOH), a subsequent preparative TLC (1:1 MTBE:EtOAc + 1% MeOH) and an extraction using acetonitrile (10 mL) and petroleum ether (4 x 10 mL) afforded the product as a white solid (8 mg, 0.017 mmol, 4% yield). <sup>1</sup>H NMR (DMSO-*d*<sub>6</sub>, 400 MHz): δ 8.29–8.18 (m, 5H), 7.75 (s, 1H), 7.40 (br s, 2H), 7.05 (d, *J* = 3.2 Hz, 1H), 6.73 (m, 1H), 6.62 (s, 1H), 3.55–3.46 (m, 4H), 1.75–1.74 (m, 4H). HPLC: 96.5 %, RT 7.478 min. LC-MS: [ESI+H]<sup>+</sup>: 475.20

**4-((5-((7-amino-2-(furan-2-yl)-[1,2,4]triazolo[1,5-*a*][1,3,5]triazin-5-yl)amino)pentyl)carbonyl) benzenesulfonyl fluoride (3)** N<sup>5</sup>-(5-aminopentyl)-2-(furan-2-yl)-[1,2,4]triazolo[1,5-*a*][1,3,5]triazine-5,7-diamine **9** (TFA salt, 674 mg, 0.85 mmol, 1 eq) was suspended in acetonitrile (5 mL). 4-Fluorosulfonylbenzoylchloride (208 mg, 0.94 mmol, 1.1 eq) was added, along with DiPEA (0.8 mL, 5 mmol, 5.8 eq). The mixture was heated at 70 °C under N<sub>2</sub> atmosphere for 2.5 h. A flash column (DCM → 60% DCM, 40% EtOAc) with subsequent preparative TLC (100% EtOAc) was used to obtain the title compound as a colorless solid (9 mg, 0.018 mmol, 2% yield). <sup>1</sup>H NMR (C<sub>3</sub>D<sub>6</sub>O, 400 MHz): δ 8.27–8.16 (m, 4H), 7.73 (dd, *J* = 1.7, 0.8 Hz, 1H), 7.39 (s, 2H), 7.05 (d, *J* = 3.2 Hz, 1H), 6.80–6.63 (m, 1H), 6.62 (dd, *J* = 3.4, 1.8 Hz, 1H), 3.52–3.38 (m, 4H), 1.78–1.62 (m, 4H), 1.56–1.44 (m, 2H). HPLC: 100%, RT 7.637 min, LC-MS:[ESI+H]<sup>+</sup>: 489.00

**4-((5-((7-amino-2-(furan-2-yl)-[1,2,4]triazolo[1,5-*a*][1,3,5]triazin-5-yl)amino)pentyl)(prop-2-yn-1-yl)carbonyl)benzenesulfonyl fluoride (4)** *tert*-butyl (5-(4-(fluorosulfonyl)-*N*-(prop-2-yn-1-yl)benzamido)pentyl)carbamate **14** (586 mg, 1.38 mmol, 1 eq) was dissolved in DCM (10 mL). To this solution TFA (10 mL) was added. After 2 min the

solvents were removed *in vacuo*. This crude intermediate was suspended in acetonitrile (10 mL), 2-(furan-2-yl)-5-(methylsulfonyl)-[1,2,4]triazolo[1,5-*a*][1,3,5]triazin-7-amine **5** (386 mg, 1.38 mmol, 1 eq) was added, along with DiPEA (2 mL, 11.0 mmol, 8 eq). The reaction mixture was heated at 70 °C for 2 h. Then the reaction mixture was concentrated and purified by a flash column (EtOAc) to yield a yellow solid (330 mg, 0.62 mmol, 45%). <sup>1</sup>H NMR (DMSO-*d*<sub>6</sub>, 353K, 400 MHz,) δ 8.17 (d, *J* = 8.3 Hz, 2H), 7.93–7.73 (m, 5H), 7.12 (t, *J* = 5.3 Hz, 1H), 7.03 (d, *J* = 3.3 Hz, 1H), 6.64 (dd, *J* = 3.0, 1.5 Hz, 1H), 4.17 (s, 2H), 3.41 (s, 2H), 3.29 (d, *J* = 6.2 Hz, 2H), 3.14 (s, 1H), 1.73–1.61 (m, 2H), 1.61–1.44 (m, 2H), 1.40–1.23 (m, 2H) ppm. HPLC: 95.772%, RT: 8.117 min, MS: [ESI+H]<sup>+</sup>: 527.20

**tert-butyl(4-((7-amino-2-(furan-2-yl)-[1,2,4]triazolo[1,5-*a*][1,3,5]triazin-5-yl)amino)butyl)carbamate (6)** 2-(Furan-2-yl)-5-(methylsulfonyl)-[1,2,4]triazolo[1,5-*a*][1,3,5]triazin-7-amine **5** (435 mg, 1.55 mmol, 1.0 eq), synthesized as previously reported,<sup>13</sup> was suspended in acetonitrile to yield a 0.1 M solution. *tert*-butyl (4-aminopropyl) carbamate (0.33 mL, 1.71 mmol, 1.1 eq) was added, followed by the addition of *N,N*-diisopropylethylamine (1.08 mL, 6.21 mmol, 4 eq). The mixture was heated at 85 °C for 29 hours and stirred at r.t. for another 18 hours. A flash column (DCM:EtOAc, 0% → 90% EtOAc) was used to purify the crude mixture. This gave a yellowish solid (444 mg, 1.14 mmol, 74% yield). <sup>1</sup>H NMR (DMSO-*d*<sub>6</sub>, 400 MHz): δ 8.49–7.92 (m, 2H), 7.86 (s, 1H), 7.51 (t, *J* = 5.9 Hz, rotamer 1, 0.3H), 7.44 (t, *J* = 5.7 Hz, rotamer 2, 0.7H), 7.07–7.00 (m, 1H), 6.87–6.76 (m, 1H), 6.67 (dd, *J* = 3.2, 1.7 Hz, 1H), 3.29–3.19 (m, 2H), 2.92 (d, *J* = 6.5 Hz, 2H), 1.48 (d, *J* = 7.2 Hz, 2H), 1.44–1.29 (m, 11H).

**tert-butyl (5-((7-amino-2-(furan-2-yl)-[1,2,4]triazolo[1,5-*a*][1,3,5]triazin-5-yl)amino)pentyl)carbamate (7)** 2-(Furan-2-yl)-5-(methylsulfonyl)-[1,2,4]triazolo[1,5-*a*][1,3,5]triazin-7-amine **5** (280 mg, 1.0 mmol, 1.0 eq) and commercially available *tert*-butyl (5-aminopentyl)carbamate (0.2 mL, 1.0 mmol, 1.1 eq) were put in a microwave tube and dissolved in acetonitrile (1.5 mL). DIPEA (0.3 mL, 1.7 mmol) was added, the tube was charged with a stirring bar, sealed and heated at 70 °C for 1.5 h. After 1.5 h HPLC analysis indicated full conversion. The mixture was concentrated, EtOAc (50 mL) and HCl (1M in H<sub>2</sub>O, 50 mL) were added for extraction. The organic layer was washed with H<sub>2</sub>O (50 mL) and brine (50 mL). After drying over MgSO<sub>4</sub> the solvent was removed *in vacuo* to give the title compound as a yellow foam (186 mg, 0.46 mmol, 46% yield). <sup>1</sup>H NMR (DMSO-*d*<sub>6</sub>, 400 MHz,) δ 8.48–7.96 (m, 2H), 7.86 (s, 1H), 7.48 (t, *J* = 5.1 Hz, rotamer, 0.38H), 7.41 (t, *J* = 5.7 Hz, rotamer, 0.62H), 7.10–7.01 (m, 1H), 6.77 (t, *J* = 5.0 Hz, 1H), 6.67 (dd, *J* = 3.0, 1.7 Hz, 1H), 3.28–3.17 (m, 2H), 2.90 (d, *J* = 6.6 Hz, 2H), 1.57–1.44 (m, 2H), 1.44–1.21 (m, 13H).

**N<sup>5</sup>-(4-aminobutyl)-2-(furan-2-yl)-[1,2,4]triazolo[1,5-*a*][1,3,5]triazine-5,7-diamine (8)**

TFA (4.3 mL, 57 mmol, 50 eq) was added to the suspension of Boc-protected amine **6** (444 mg, 1.14 mmol, 1 eq) in DCM (equal volume as TFA). Solvents were removed under reduced pressure after completion of the reaction (5 min). This gave the product as brown oil (899 mg, 1.13 mmol, quantitative yield). Products were confirmed by <sup>1</sup>H NMR first and then stored under N<sub>2</sub> until used. <sup>1</sup>H NMR (DMSO-*d*<sub>6</sub>, 400 MHz): δ 8.49–8.05 (m, 3H (R-NH<sub>3</sub><sup>+</sup>)), 7.88 (dd, *J* = 1.7, 0.7 Hz, 1H), 7.62 (br s, 3H (R-NH<sub>3</sub><sup>+</sup>)), 7.52 (t, *J* = 6.0 Hz, 1H), 7.09–7.02 (m, 1H), 6.68 (dd, *J* = 3.4, 1.7 Hz, 1H), 3.35–3.23 (m, 2H), 2.87–2.76 (m, 2H), 1.63–1.50 (m, 4H).

**N<sup>5</sup>-(5-aminopentyl)-2-(furan-2-yl)-[1,2,4]triazolo[1,5-*a*][1,3,5]triazine-5,7-diamine (9)**

TFA (3 mL, 40 mmol, 50 eq) was added to the suspension of Boc protected amine **7** (324 mg, 0.8 mmol, 1 eq) in DCM. Once the reaction was completed, the solvent was removed and the mixture was co-evaporated twice with water and dried using high vacuum. This gave a brown oil (556 mg, 0.8 mmol, quantitative yield) as a TFA salt. The crude product was used without further purification.

**tert-butyl (5-hydroxypentyl) carbamate (11)** 5-amino-1-pentanol **10** (4.2 mL, 38.8 mmol) was dissolved in DCM (20 mL). Di-*tert*-butyl dicarbonate (8.4 g, 38.8 mmol) was slowly added as a solid. The reaction was left stirring at r.t. for 18 h, then the solvent was removed to give a yellow oil (8.83 g, quantitative yield, some *t*-BuOH left). <sup>1</sup>H NMR (CDCl<sub>3</sub>, 400 MHz) δ 4.57 (s, 1H), 3.65 (t, *J* = 6.5 Hz, 2H), 3.13 (t, *J* = 6.5 Hz, 2H), 1.67 – 1.35 (m, 15H (under water peak)).

**tert-butyl (5-bromopentyl) carbamate (12)** *tert*-butyl (5-hydroxypentyl) carbamate **11** (8.83 g, 38.8 mmol, 1 eq) and PPh<sub>3</sub> (15.3 g, 58.2 mmol, 1.5 eq) were dissolved in THF (120 mL). A solution of CBr<sub>4</sub> (19.3 g, 58.2 mmol, 1.5 eq) in THF (40 mL), was added over 2 h using a syringe pump. After 3 h at room temperature the reaction mixture was filtered and the filtrate was concentrated. This crude product was dissolved in DCM (~5 mL) and purified by flash column chromatography (100% PE → 90% PE + 10% EtOAc). This gave the product as a colorless oil (9.31 g, 35.0 mmol, 90% yield). <sup>1</sup>H NMR (400 MHz, CDCl<sub>3</sub>) δ 4.54 (s, 1H), 3.41 (t, *J* = 6.7 Hz, 2H), 3.13 (m, 2H), 1.97–1.80 (m, 2H), 1.58–1.36 (m, 13H) ppm. <sup>13</sup>C NMR (101 MHz, CDCl<sub>3</sub>) δ 40.5, 33.8, 32.5, 29.4, 28.6, 25.5.

**tert-butyl (5-(prop-2-yn-1-ylamino) pentyl) carbamate (13)** Propargylamine (1 mL, 15 mmol, 3 eq) was dissolved in acetonitrile (10 mL). To this stirred solution a solution of *tert*-butyl (5-bromopentyl) carbamate **12** (798 mg, 3 mmol, 1 eq) and DiPEA (1 mL, 6 mmol, 2 eq) in acetonitrile (18 mL) was added using a syringe pump. Afterwards the solvent was removed and the product purified by flash column chromatography (EtOAc). This gave a yellowish oil



(331 mg, 1.38 mmol, 46% yield) with EtOAc as an impurity.  $^1\text{H}$  NMR ( $\text{CDCl}_3$ , 400 MHz)  $\delta$  4.54 (s, 1H), 3.44 (d,  $J = 2.0$  Hz, 2H), 3.12 (q,  $J = 6.4$  Hz, 2H), 2.70 (t,  $J = 7.1$  Hz, 2H), 2.22 (t,  $J = 2.2$  Hz, 1H), 1.55–1.34 (m, 15H) ppm.

***tert*-butyl (5-(4-(fluorosulfonyl)-*N*-(prop-2-yn-1-yl)benzamido)pentyl)carbamate (14)**

*tert*-butyl (5-(prop-2-yn-1-ylamino)pentyl)carbamate **13** (664 mg, 1.38 mmol, 1 eq) was dissolved in acetonitrile (10 mL), 4-fluorosulfonyl benzoylchloride (338 mg, 1.52 mmol, 1.1 eq) was added and followed by the addition of DiPEA (0.75 mL, 4.14 mmol, 3 eq). Once the reaction was completed, the solvent was removed and the crude mixture purified by flash column chromatography (DCM + 5% MTBE  $\rightarrow$  DCM + 7.5% MTBE). This yielded a yellow oil (586 mg, 1.52 mmol, quantitative yield).  $^1\text{H}$  NMR ( $\text{DMSO-}d_6$ , 332K, 400 MHz)  $\delta$  8.19 (d,  $J = 8.0$  Hz, 2H), 7.77 (d,  $J = 7.9$  Hz, 2H), 6.37 (brs, 1H), 4.16 (brs, 2H), 3.37 (brs, 2H), 2.90 (m, 2H), 1.61 (m, 2H), 1.44–1.29 (m, 9H), 1.29–1.14 (m, 4H).

### 4.2. Biology

The radioligand [ $^3\text{H}$ ]ZM241385 with a specific activity of  $50 \text{ Ci} \times \text{mmol}^{-1}$  was purchased from ARC Inc. (St. Louis, MO). Unlabeled ZM241385 was a kind gift from Dr. S.M. Poucher (Astra Zeneca, Macclesfield, UK). 5'-*N*-ethylcarboxamidoadenosine (NECA) was purchased from Sigma-Aldrich (Steinheim, Germany). Adenosine deaminase (ADA) was purchased from Sigma-Aldrich Chemie N.V. Bicinchoninic acid (BCA) and BCA protein assay reagent were obtained from Pierce Chemical Company (Rockford, IL, USA). Human embryonic kidney (HEK) 293 cells stably expressing the hA<sub>2A</sub> receptor (hA<sub>2A</sub>R-WT) were kindly provided by Dr J Wang (Biogen/IDEC, Cambridge, MA, USA). The purified hA<sub>2A</sub> receptor material was kindly provided by Dr. Niek Dekker and Dr. Euan Gordon (AstraZeneca). All other chemicals were of analytical grade and obtained from standard commercial sources.

*Cell culture, transfection and membrane preparation.* We followed the procedures reported previously.<sup>13, 37</sup> Briefly, HEK293 cells were grown as monolayers in Dulbecco's modified Eagle's medium supplemented with 2 mM glutamine, 10% newborn calf serum, 50  $\mu\text{g mL}^{-1}$  streptomycin, and 50 IU  $\text{mL}^{-1}$  penicillin at 37°C and 7% CO<sub>2</sub> atmosphere. Cells were subcultured twice a week at a ratio of 1:20 on 10 cm  $\varnothing$  culture plates. The cells were transfected with pcDNA3.1(-) plasmid containing the hA<sub>2A</sub>R with N terminal FLAG and C-terminal His tags (FLAG-hA<sub>2A</sub>R-His<sup>4</sup>) using the calcium phosphate precipitation method (1  $\mu\text{g}$  plasmid DNA), followed by a 48-hour incubation, as previously described.<sup>38</sup> Stably transfected hA<sub>2A</sub>R-WT cells were grown in the same medium but with the addition of G-418 (500 mg  $\text{mL}^{-1}$ ). For both transiently transfected cells and stably hA<sub>2A</sub>R-WT cells were



detached from the plates by scraping them into PBS and centrifuged to remove PBS buffer. The pellets were resuspended in ice-cold Tris-HCl buffer (50 mM, pH 7.4) and then homogenized. The cell membrane suspensions were centrifuged at  $100,000 \times g$  at 4°C for 20 minutes, after which the procedure was repeated one more time. After this, the same Tris-HCl buffer was used to resuspend the pellet, and adenosine deaminase was added to break down endogenous adenosine. HEK293 cells stably expressing hA<sub>2A</sub>R were grown as monolayers in same culture medium and detached from plates by same treatment for membrane preparation. For both membranes were stored in 250  $\mu$ L aliquots at -80°C until further use. Membrane protein concentrations were measured using the BCA method.<sup>39</sup>

*[<sup>3</sup>H]ZM241383 radioligand displacement assay.* Radioligand displacement experiments were performed as previously described.<sup>13</sup> hA<sub>2A</sub>R-WT cell membrane aliquots stably expressing hA<sub>2A</sub>R containing 10  $\mu$ g of protein were incubated in a total volume of 100  $\mu$ L of assay buffer to obtain an assay window of approximately 3000 DPM of receptor-specific radioligand binding. Nonspecific binding was determined in the presence of 100  $\mu$ M NECA and represented less than 10% of the total binding. Briefly, to each tube were added 25  $\mu$ L cell membranes (10  $\mu$ g of protein), 25  $\mu$ L of radioligand [<sup>3</sup>H]ZM241383, 25  $\mu$ L of assay buffer [25 mM Tris-HCl, pH 7.4 at 25°C, supplemented with 5 mM MgCl<sub>2</sub> and 0.1% (w/v) CHAPS and 25  $\mu$ L of the indicated compounds in increasing concentrations in the same assay buffer. The mixture was incubated at 25°C for 60 min to reach equilibrium. Incubations were terminated by rapid vacuum filtration to separate the bound and free radioligand through 96-well GF/B filter plates using a Perkin Elmer Filtermate-harvester (PerkinElmer, Groningen, Netherlands). Filters were subsequently washed three times with 2 mL of ice-cold buffer (25 mM Tris-HCl, pH 7.4, supplemented with 5 mM MgCl<sub>2</sub>). The filter-bound radioactivity was determined by scintillation spectrometry using a P-E 1450 Microbeta Wallac Trilux scintillation counter (PerkinElmer).

*Heterologous displacement binding of probe 4 and ZM241385 to hA<sub>2A</sub>R-WT cell membranes.* To assess the irreversible binding level, cell membranes stably expressing hA<sub>2A</sub>R were incubated with either 50 mM Tris-HCl (pH = 7.4) or two concentrations (0.3 IC<sub>50</sub> and IC<sub>50</sub>) of probe 4 or ZM241385 for 3h at 25°C on a Eppendorf Thermomixer. Subsequently, the mixture was centrifuged at  $16,100 \times g$  at 4°C for 5 minutes and the supernatant was removed, followed by a resuspension of the pellet in 1 mL assay buffer and spun again for 5 min at  $16,100 \times g$  at 4°C. This washing procedure was repeated three times. 50  $\mu$ L aliquots of these pretreated membranes were incubated with 25  $\mu$ L of radioligand [<sup>3</sup>H]ZM241383 and 25  $\mu$ L of

## Chapter 6

---

a concentration range (100 pM-1  $\mu$ M) of unlabeled ZM241385 for 1h at 25 °C. Incubation was terminated as described under [<sup>3</sup>H]ZM241385 radioligand displacement assay.

*Expression and purification of wild type hA<sub>2A</sub>R.* The gene coding for hA<sub>2A</sub>R (residues 1-316) was synthesised by Genscript and cloned into pPICZb with an N-terminal  $\alpha$ -factor signal sequence from *Saccharomyces cerevisiae* (MRFPSIFTAVLFAASSALAAPVNTTTEDETAQIPAEAVIGYSDLEGDFDVAVLPSNS TNNGLLFINTTIASIAAKEEGVSLEKRLVPRGS), followed by hA<sub>2A</sub>R and a C-terminus biotinylation domain from *Propionibacterium shermanii* (TSEFENLYFQGQFGGGTGG APAPAAGGAGAGKAGEGEIPAPLAGTVSKILVKEGDTVKAGQTVLVLEAMKMETEINA PTDGKVEKVLVKERDAVQGGQGLIKI) for enhanced expression<sup>40</sup> and a decaHis tag (GHHHHHHHHHGS).

The receptor was expressed in *Pichia pastoris* SMD1168 at 3 L scale in a fermentor essentially as described,<sup>41</sup> except that dissolved oxygen was maintained at 25%, and 2.5% DMSO and 10 mM theophylline were included in the fermentation media. Approximately 200 grams of wet cells were harvested per liter. 200 g cells were resuspended using a Turax in 600 mL ice-cold lysis buffer (50 mM HEPES pH 7.4, 200 mM NaCl, Complete EDTA free protease inhibitor tablets (Roche) at 1/50 mL). Cells were lysed by a single passage through a Constant Cell system at 30 kpsi with extensive cooling. Cell debris was removed by centrifugation at 1000  $\times$  g for 10 min at 4°C. Membranes were collected by ultracentrifugation at 100,000  $\times$  g for 45 minutes at 4°C. Membrane pellet was resuspended in buffer to a total protein concentration of 20 mg mL<sup>-1</sup> (final volume of 180 mL) and stored at -80°C.

Membranes (20 mL) were resuspended in 200 mL solubilization buffer (25 mM HEPES, pH7.4, 300 mM NaCl, 20% glycerol, 1% DDM/0.1% CHS, Complete tablets (1/50 mL), 200  $\mu$ M theophylline). The suspension was incubated for 2 hours at 4°C on a rolling table, prior to centrifugation for 30 min at 100,000  $\times$  g to remove unsolubilized material. Imidazole was added to a final concentration of 15 mM and the clarified solution was loaded on a 5 mL HisTrap crude column at 2.5 mL min<sup>-1</sup>. The column was washed with 100 mL buffer A (25 mM HEPES, 25 mM imidazole pH 7.4, 300 mM NaCl, 10% glycerol, 0.05% DDM/0.0005% CHS, 100  $\mu$ M theophylline) to which imidazole was added to final concentration of 25 mM to reduce nonspecific binding, followed by step wise washes with increasing concentrations of imidazole in this buffer (50 mM and 75 mM) and hA<sub>2A</sub>R was eluted in 25 mM HEPES pH

7.4, 300 mM NaCl, 10% glycerol, 0.05% DDM/0.0005%CHS, 300 mM imidazole, 100 μM theophylline. Fractions were analyzed on SDS-PAGE and those containing hA<sub>2A</sub>R were pooled and concentrated to 2.5 mL using a 50 kDa filter. High imidazol is harmful to hA<sub>2A</sub>R and the buffer was changed to buffer A on a PD10 G25 column. Eluted fraction was further concentrated to 0.5 mL and loaded on a Superdex-200 10/30 column running in in 25mM NaPi pH7.2, 100 mM NaCl, 10 μM LMNG, 500 μM Caffeine. Fractions were analyzed on SDS-PAGE. hA<sub>2A</sub>R eluted as single peak at expected position for the detergent-protein complex (around 80kDa). Fractions were pooled and concentrated on a 50 kDa filter to final volume of 0.4 mL and stored at -80°C. Protein concentration was determined using absorbance measurement against buffer A (Abs<sub>280</sub>(0.1%) =1.05). Final concentration was 7 mg mL<sup>-1</sup> with a total of ~2mg hA<sub>2A</sub>R.

*Affinity-based protein labeling assay on purified hA<sub>2A</sub>R with probe 4.* For purified hA<sub>2A</sub>R, both affinity labeling and click reactions were performed on ice, unless indicated otherwise. Purified hA<sub>2A</sub>R was diluted to a concentration of 0.1 mg mL<sup>-1</sup> in assay buffer (25 mM HEPES pH 7.5, 100 mM NaCl and 10 μM LMNG). 38 μL samples were incubated with 2 μL probe 4 at indicated concentrations or vehicle control (1% DMSO) for 1 h. To initiate the click reaction, 5.6 mM CuSO<sub>4</sub> (2.5 μL / reaction, from a 100 mM stock solution in water) was mixed vigorously with 33 mM sodium ascorbate (1.5 μL / reaction, freshly made as a 1 M stock solution in water) to obtain a yellow mixture, followed by the immediate addition of 1.1 mM THPTA (0.5 μL / reaction, from a 100 mM stock solution in water) and 4.4 μM fluorescent tag Cy3-azide (0.5 μL / reaction, from a 400 μM stock solution in DMSO). The reaction mixtures were incubated for 1h and quenched with 15 μL 4xSDS loading buffer. Proteins in the mixture were separated by SDS-PAGE on 10% polyacrylamide gels. In-gel fluorescence was detected with a ChemiDoc MP system (605/50 filter). Proteins were transferred from gel to a PVDF membrane by Trans-Blot®Turbo (BioRad). Then the membrane was washed in 20 mL TBS for 10 min on a roller bench, followed by a three times wash with TBST (PBS with 0.1% Tween-20). Afterwards, the membrane was blocked in 5% (w/v) non-fat milk for 1h at room temperature and probed with rabbit-anti-His antibody (Rockland)(1:1000 [v/v] dilution in blocking buffer) overnight at 4 °C, washed three times again with TBST and incubated with goat-anti-rabbit IgG-HRP (1:5000 in 5% milk in TBST; Santa Cruz) for 1 h at room temperature. After two wash cycles in TBST and one in TBS, the blot was developed in the dark using a 10 mL luminal solution, with 100 μL ECL enhancer and 3 μL H<sub>2</sub>O<sub>2</sub>. Chemiluminescence was visualized with ChemiDoc XRS (BioRad).

## Chapter 6

---

*Competitive labeling assays in purified hA<sub>2A</sub> AR by probe 4.* Prior to the two-step labeling experiment purified hA<sub>2A</sub>AR was diluted to a concentration of 0.1 mg mL<sup>-1</sup> in assay buffer and incubated with 10 μM compound **1**, ZM241385 or vehicle control (1% DMSO) for 1h on ice, followed by labeling with 1 μM probe **4** for 0.5 h on ice. Samples were then subjected to the click chemistry procedure using the protocol described above.

*Affinity-based protein labeling of membranes transiently overexpressing FLAG-HA-hA<sub>2A</sub>AR-His.* hA<sub>2A</sub>AR-FLAG-His membranes were diluted to a concentration of 1 mg mL<sup>-1</sup> in 50 mM Tris-HCl (pH = 7.4 at 25 °C). Either 2 μL probe **4** at indicated concentrations (0.1 μM, 0.3 μM, 1 μM and 3 μM) or vehicle control (1% DMSO) was added to 38 μL samples for 1 h incubation at room temperature. Then all samples were subjected to the click chemistry conjugation reaction. The click reagents were added in the following sequence: 4.4 μM fluorescent Cy3-azide (0.5 μL / reaction, 400 μM stock in DMSO) was added to the mixture followed by 33 mM sodium ascorbate (1.5 μL / reaction, freshly made in 1M stock in water) and 1.1 mM THPTA (0.5 μL / reaction, 100 mM stock in water). Finally, 5.6 mM CuSO<sub>4</sub> (2.5 μL / reaction, 100 mM stock in water) was added to start and run the cycloaddition reaction for 1 h at room temperature. Then, the reaction was quenched with 15 μL 4xSDS loading buffer and protein material denatured for 30 min at 37 °C. Proteins (60 μL sample) were separated by SDS-PAGE on 10% polyacrylamide gels. In-gel fluorescence was detected with the ChemiDoc MP system (605/50 filter). Proteins were transferred from gel to a PVDF membrane by Trans-Blot®Turbo (BioRad). Then the membrane was washed in 20 mL TBS for 10 min on a roller bench, followed by a three times wash with TBST (PBS with 0.1% Tween-20). Then the membrane was blocked in 5% (w/v) non-fat milk and incubated with mouse-anti-FLAG (Sigma) (1:5000 [v/v] dilution in blocking buffer) as primary antibody. Thereafter, the membrane was washed in TBST three times and incubated with goat-anti-mouse HRP (Sigma) (1:5000 [v/v] dilution in blocking buffer) as secondary antibody. After two wash cycles in TBST and one in TBS, the blot was developed in the dark using a 10 mL luminal solution, with 100 μL ECL enhancer and 3 μL H<sub>2</sub>O<sub>2</sub>. Chemiluminescence was imaged using a ChemiDoc XRS (BioRad).

### Abbreviations used

ADA, Adenosine deaminase; BCA, Bicinchoninic acid; CHAPS,3-[(3-cholamidopropyl) dimethylammonio]-1-propane sulfonate; Cy3-azide, sulfonated Cyanine 3 dye azide; DiPEA, Di-isopropylethylamine; ECL, enhanced chemiluminescence; HEPES, 4-(2-hydroxyethyl)-1-piperazineethanesulfonic acid; LMNG, Lauryl Maltose Neopentyl Glycol; MTBE, Methyl

*tert*-butyl ether; NaPi, Sodium Phosphate Buffer; NECA, 5'-N-ethylcarboxamidoadenosine; TBS, Tris-buffered saline; TBST, Tris Buffered Saline with 0.05% Tween; THPTA, Tris(3-hydroxypropyl triazolylmethyl)amine; TFA, Trifluoroacetic acid; PVDF, Polyvinylidene difluoride; ZM241385, 4-(2-[7-Amino-2-(2-furyl)[1,2,4]triazolo[2,3-a][1,3,5]triazin-5-ylamino]ethyl)phenol.

### Supporting Information

**Table S1. Apparent affinities of 4 at the human A<sub>1</sub> and A<sub>3</sub> adenosine receptor subtypes.** Data are expressed as pK<sub>i</sub> values (means ± SEM) of three separate experiments each performed in duplicate.

Compound	pK <sub>i</sub>		
	hA <sub>1</sub> <sup>a</sup>	hA <sub>2A</sub> <sup>b</sup>	hA <sub>3</sub> <sup>c</sup>
4	7.72 ± 0.05	8.82 ± 0.02	7.22 ± 0.01

<sup>a</sup>Affinity determined from displacement of specific [<sup>3</sup>H]DPCPX binding on CHO cell membranes stably expressing human adenosine A<sub>1</sub> receptors at 25°C during 3h incubation; <sup>b</sup>Affinity determined from displacement of specific [<sup>3</sup>H]ZM241385 binding from the hA<sub>2A</sub>R at 25°C during 3h incubation; <sup>c</sup>Affinity determined from displacement of specific [<sup>3</sup>H]PSB-11 binding on CHO cell membranes stably expressing human adenosine A<sub>3</sub> receptors at 25°C during 3h incubation.

**Table S2. Affinities of ZM241385 on hA<sub>2A</sub>R preincubated with different concentrations of the indicated compounds<sup>a</sup>**

Preincubated Compound	pK <sub>i</sub> IC <sub>50</sub>	pK <sub>i</sub> 0.3IC <sub>50</sub>	pK <sub>i</sub> control
4 <sup>b</sup>	9.01 ± 0.05 <sup>ns</sup>	8.84 ± 0.04 <sup>ns</sup>	9.03 ± 0.10
ZM241385 <sup>c</sup>	8.94 ± 0.07 <sup>ns</sup>	8.84 ± 0.03 <sup>ns</sup>	8.77 ± 0.04

<sup>a</sup>Data are expressed as means ± SEM of three separate experiments each performed in duplicate. ns indicates a non-significant difference with p>0.05 when compared with the pK<sub>i</sub> values in control groups; One-way ANOVA test. <sup>b</sup>Affinity of ZM241385, expressed as pK<sub>i</sub> value, determined from displacement of specific [<sup>3</sup>H]ZM241385 binding from the hA<sub>2A</sub>R cell membranes preincubated with compound 4 at indicated concentrations for 3h at 25°C and then treated with a three-cycle washing step. <sup>c</sup>Affinity of ZM241385, expressed as pK<sub>i</sub> value, determined from displacement of specific [<sup>3</sup>H]ZM241385 binding from the hA<sub>2A</sub>R cell membranes preincubated with ZM241385 at indicated concentrations for 3h at 25°C and then treated with a three-cycle washing step.

### References

1. Fredholm, B. B.; IJzerman, A. P.; Jacobson, K. A.; Linden, J.; Muller, C. E.. *Pharmacol. Res.* **2011**, 63, 1-34.
2. Schwarzschild, M. A.; Agnati, L.; Fuxe, K.; Chen, J. F.; Morelli, M. *Trends Neurosci.* **2006**, 29, 647-654.
3. Adams, J. L.; Smothers, J.; Srinivasan, R.; Hoos, A. *Nat. Rev. Drug Discov.* **2015**, 14, 603-622.
4. Jaakola, V. P.; Griffith, M. T.; Hanson, M. A.; Cherezov, V.; Chien, E. Y.; Lane, J. R.; IJzerman, A. P.; Stevens, R. C. *Science* **2008**, 322, 1211-1217.

## Chapter 6

---

5. Rosenbaum, D. M.; Rasmussen, S. G. F.; Kobilka, B. K. *Nature* **2009**, 459, 356-363.
6. Glukhova, A.; Thal, D. M.; Nguyen, A. T.; Vecchio, E. A.; Jorg, M.; Scammells, P. J.; May, L. T.; Sexton, P. M. *Cell* **2017**, 168, 867-877.
7. Weichert, D.; Gmeiner, P. *ACS Chem. Biol.* **2015**, 10, 1376-1386.
8. Jorg, M.; Scammells, P. J. *ChemMedchem* **2016**, 11, 1488-1498.
9. Narayanan, A.; Jones, L. H. *Chem. Sci.* **2015**, 6, 2650-2659.
10. Srinivas, M.; Shryock, J. C.; Scammells, P. J.; Ruble, J.; Baker, S. P.; Belardinelli, L. *Mol. Pharmacol.* **1996**, 50, 196-205.
11. Shryock, J. C.; Snowdy, S.; Baraldi, P. G.; Cacciari, B.; Spalluto, G.; Monopoli, A.; Ongini, E.; Baker, S. P.; Belardinelli, L. *Circulation* **1998**, 98, 711-718.
12. Baraldi, P. G.; Cacciari, B.; Moro, S.; Romagnoli, R.; Ji, X.; Jacobson, K. A.; Gessi, S.; Borea, P. A.; Spalluto, G. *J. Med. Chem.* **2001**, 44, 2735-2742.
13. Yang, X.; Dong, G.; Michiels, T. J. M.; Lenselink, E. B.; Heitman, L.; Louvel, J.; IJzerman, A. P. *Purinergic Signal.* **2017**, 13, 191-201.
14. Jacobson, K. A.; Ukena, D.; Padgett, W.; Kirk, K. L.; Daly, J. W. *Biochem. Pharmacol.* **1987**, 36, 1697-1707.
15. Kecskes, A.; Tosh, D. K.; Wei, Q.; Gao, Z. G.; Jacobson, K. A. *Bioconjugate Chem.* **2011**, 22, 1115-1127.
16. Macchia, M.; Salvetti, F.; Bertini, S.; Di Bussolo, V.; Gattuso, L.; Gesi, M.; Hamdan, M.; Klotz, K. N.; Laragione, T.; Lucacchini, A.; Minutolo, F.; Nencetti, S.; Papi, C.; Tuscano, D.; Martini, C. *Bioorg. Med. Chem. Lett.* **2001**, 11, 3023-3026.
17. Blair, J. A.; Rauh, D.; Kung, C.; Yun, C. H.; Fan, Q. W.; Rode, H.; Zhang, C.; Eck, M. J.; Weiss, W. A.; Shokat, K. M. *Nat. Chem. Biol.* **2007**, 3, 229-238.
18. Speers, A. E.; Adam, G. C.; Cravatt, B. F. *J. Am. Chem. Soc.* **2003**, 125, 4686-4687.
19. Kolb, H. C.; Sharpless, K. B. *Drug Discov. Today* **2003**, 8, 1128-1137.
20. Speers, A. E.; Cravatt, B. F. *Chem. Biol.* **2004**, 11, 535-546.
21. Blex, C.; Michaelis, S.; Schrey, A. K.; Furkert, J.; Eichhorst, J.; Bartho, K.; Gyapon Quast, F.; Marais, A.; Hakelberg, M.; Gruber, U.; Niquet, S.; Popp, O.; Kroll, F.; Sefkow, M.; Schulein, R.; Dreger, M.; Koster, H. *Chembiochem* **2017**, 18, 1639-1649.
22. Grunbeck, A.; Sakmar, T. P. *Biochemistry* **2013**, 52, 8625-8632.
23. Burgermeister, W.; Nassal, M.; Wieland, T.; Helmreich, E. J. *Biochim. Biophys. Acta* **1983**, 729, 219-228.
24. Tam, E. K.; Li, Z.; Goh, Y. L.; Cheng, X.; Wong, S. Y.; Santhanakrishnan, S.; Chai, C. L.; Yao, S. Q. *Chem. Asian J.* **2013**, 8, 1818-1828.
25. Cheng, X. M.; Li, L.; Uttamchandani, M.; Yao, S. Q. *Chem. Commun.* **2014**, 50, 2851-2853.
26. Gregory, K. J.; Velagaleti, R.; Thal, D. M.; Brady, R. M.; Christopoulos, A.; Conn, P. J.; Lapinsky, D. J. *ACS Chem. Biol.* **2016**, 11, 1870-1879.
27. Soethoudt, M.; Stolze, S. C.; Westphal, M. V.; van Stralen, L.; Martella, A.; van Rooden, E. J.; Guba, W.; Varga, Z. V.; Deng, H.; van Kasteren, S. I.; Grether, U.; AP, I. J.; Pacher, P.; Carreira, E. M.; Overkleeft, H. S.; Ioan-Facsinay, A.; Heitman, L. H.; van der Stelt, M. *J. Am. Chem. Soc.* **2018**, 140, 6067-6075.
28. Picone, R. P.; Fournier, D. J.; Makriyannis, A. *J. Pept. Res.* **2002**, 60, 348-356.
29. Jorg, M.; Glukhova, A.; Abdul-Ridha, A.; Vecchio, E. A.; Nguyen, A. T.; Sexton, P. M.; White, P. J.; May, L. T.; Christopoulos, A.; Scammells, P. J. *J. Med. Chem.* **2016**, 59, 11182-11194.

30. van Muijlwijk-Koezen, J. E.; Timmerman, H.; van der Sluis, R. P.; van de Stolpe, A. C.; Menge, W. M. P. B.; Beukers, M. W.; van der Graaf, P. H.; de Groote, M.; IJzerman, A. P. *Bioorg. Med. Chem. Lett.* **2001**, 11, 815-818.
31. Nijmeijer, S.; Engelhardt, H.; Schultes, S.; van de Stolpe, A. C.; Lusink, V.; de Graaf, C.; Wijtmans, M.; Haaksma, E. E. J.; de Esch, I. J. P.; Stachurski, K.; Vischer, H. F.; Leurs, R. *Br. J. Pharmacol.* **2013**, 170, 89-100.
32. Worrell, B. T.; Malik, J. A.; Fokin, V. V. *Science* **2013**, 340, 457-460.
33. Himo, F.; Lovell, T.; Hilgraf, R.; Rostovtsev, V. V.; Noodleman, L.; Sharpless, K. B.; Fokin, V. *V. J. Am. Chem. Soc.* **2005**, 127, 210-216.
34. Barrington, W. W.; Jacobson, K. A.; Stiles, G. L. *Mol. Pharmacol.* **1990**, 38, 177-183.
35. Krysiak, J. M.; Kreuzer, J.; Macheroux, P.; Hermetter, A.; Sieber, S. A.; Breinbauer, R. *Angew. Chem. Int. Ed.* **2012**, 51, 7035-7040.
36. Hong, V.; Presolski, S. I.; Ma, C.; Finn, M. G. *Angew. Chem. Int. Ed.* **2009**, 48, 9879-9883.
37. Guo, D.; Mulder-Krieger, T.; IJzerman, A. P.; Heitman, L. H. *Br. J. Pharmacol.* **2012**, 166, 1846-1859.
38. Sambrook J; Fritsch EF; Maniatis T. In *Molecular Cloning : A Laboratory Manual*, 2nd ed.; Cold Spring Harbor Laboratory Press: New York, 1990; Vol. 343, pp 604-605.
39. Smith, P. K.; Krohn, R. I.; Hermanson, G. T.; Mallia, A. K.; Gartner, F. H.; Provenzano, M. D.; Fujimoto, E. K.; Goeke, N. M.; Olson, B. J.; Klenk, D. C. *Anal. Biochem.* **1985**, 150, 76-85.
40. Andre, N.; Cherouati, N.; Prual, C.; Steffan, T.; Zeder-Lutz, G.; Magnin, T.; Pattus, F.; Michel, H.; Wagner, R.; Reinhart, C. *Protein Sci.* **2006**, 15, 1115-1126.
41. Wohri, A. B.; Hillertz, P.; Eriksson, P. O.; Mueller, J.; Dekker, N.; Snijder, A. *Mol. Membr. Biol.* **2013**, 30, 169-183





|

# **Chapter 7**

## **Conclusions and Future Perspectives**



This thesis delves into the design and pharmacological profiling of covalent ligands for adenosine receptors (ARs). In this chapter, insights gained from case studies at three adenosine receptor subtypes are elaborated on, and remarks for further research on covalent probes for GPCRs are presented.

### 1. Conclusions

#### 1.1. Guidelines for the design of covalent probes targeting ARs

Covalent probes, or affinity labels, are pharmacological tools that can be used to study the structural and functional properties of GPCRs [1]. As illustrated in **Chapter 2**, these ligands comprise three elements: a pharmacophore, a linker and a reactive group. The pharmacophore generates affinity and selectivity towards a specific adenosine receptor subtype, whereas a linker moiety connects the pharmacophore to the reactive moiety that forms a covalent bond with an amino acid residue near the binding pocket. An ideal reactive moiety, also referred to as warhead, shows a low nonspecific reactivity in solution or outside the binding pocket. Once accommodated in the binding pocket, it has the capacity to react with a neighboring nucleophilic amino acid residue to form a covalent interaction. In this regard, sulfonyl fluorides were chosen as warhead for all the covalent ligand design in this thesis (**Chapters 3-6**). This privileged functionality holds a good combination of physiochemical properties (i.e., aqueous or thermodynamic stability) and electrophilic reactivity [2]. The targeted nucleophilic amino acid residues include serine, threonine, tyrosine, lysine, cysteine and histidine. Building on that, throughout this thesis I present examples that demonstrate the rational ligand design based on a well-defined structure-activity relationship (SAR) profile of the pharmacophore and extensive structural information of the binding site of the adenosine receptor.

First, a high-affinity pharmacophore is deemed to be an important starting point towards a successful design, as it increases the ligand concentration in the binding site, eventually triggering covalent interaction. Logically, it is essential that the introduction of a warhead to the original pharmacophore should not jeopardize the key properties of the ligand such as affinity and selectivity. As shown in Figure 1, the design of the covalent antagonist LUF7445 (**Chapter 3**) was based on a high-affinity non-xanthine antagonist, ZM241385, a molecular template co-crystallized with hA<sub>2A</sub>R (PDB: 4EIY) [3]. Analysis of the binding site in the crystal structure shows that the phenylethylamine chain in ZM241385 is directed toward the more solvent exposed extracellular region (EL2 and EL3), where this hydrophobic/hydrophilic interface offers us tremendous substituent flexibility. Based on

## Chapter 7

extensive SAR studies performed by our group [4, 5], we introduced the electrophilic fluorosulfonyl group at the phenylethylamine side chain to achieve a covalent interaction with amino acid K153<sup>ECL2</sup>.

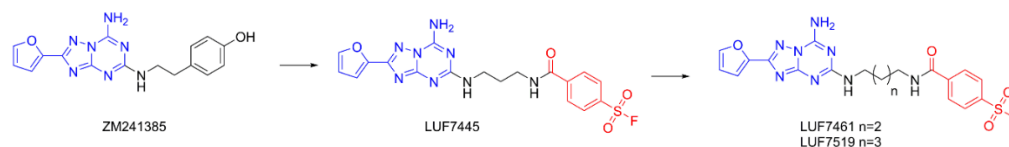


**Figure 1. Chemical structures of covalent ligands for hA<sub>2A</sub>R examined in Chapters 3 and 6.** Here, the effect of the linker length between scaffold and warhead on affinity was further examined, yielding compound LUF7461 and, preferably, compound LUF7519 with an improved affinity.

A case based on an agonist scaffold is described in **Chapter 5**. The non-ribose agonists' scaffold was inspired by a former drug candidate, capadenoson [6, 7]. This dicyanopyridine scaffold with a benzo[1,3]dioxol-5-yl moiety at the C<sup>4</sup> position (LUF7174, Figure 2) showed good selectivity and efficacy at the hA<sub>1</sub>R [8, 9]. This pharmacophore led to the discovery of a covalent partial agonist, LUF7746 (Figure 2), which maintained its high affinity and selectivity toward hA<sub>1</sub>R.

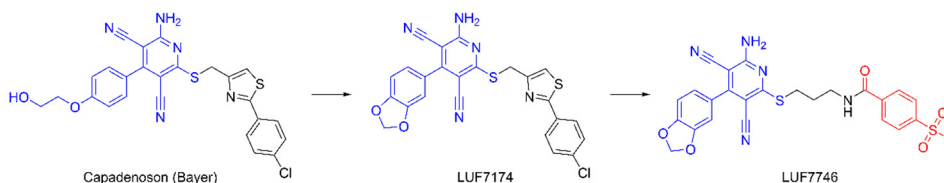


**Figure 2. Chemical structures of covalent partial agonists examined in Chapter 5.** The lead compound, capadenoson, a selective hA<sub>1</sub>R partial agonist inspired the design of covalent partial agonist, LUF7746.

Of note, in the case with limited structural insights of the receptor binding pocket, altering the linker length is not the only way in which key properties of ligands (affinities) can be affected. **Chapter 4** presents the case of covalent antagonist design for the hA<sub>3</sub>R, in which both the linker type and orientation of the warhead appeared relevant. The position of the warhead and linker type and length were given equal weight to the design strategy. It was found that the 4-position of the sulfonyl fluoride on the warhead's phenyl group was favored for high affinity. More importantly, the replacement of the ester group with the more metabolically stable amide linker resulted in irreversible probes with a slightly increased affinity. This led to the discovery of LUF7602 (Figure 3) as a best-in-class ligand among the series.

Lastly, in some cases the incorporation of a linker unit can be likewise important to maintain the properties of the pharmacophore and orient the ligand into a suitable direction for covalent interaction. As illustrated in **Chapter 6**, an extension of linker length based on LUF7445 (Figure 1) slightly increased the apparent affinity. This concurs with available literature reporting an electrophilic probe for the cannabinoid CB<sub>1</sub> receptor, also demonstrating that a significantly improved affinity resulted from a longer linker [10]. This might be the result of more steric freedom allowing the warhead to reach the adjacent nucleophilic amino acid residue in the receptor binding site more efficiently.

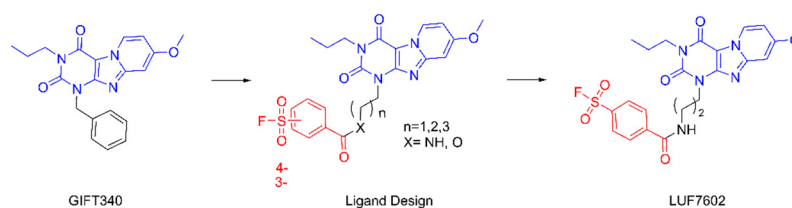


**Figure 3. Chemical structures examined in Chapter 4.** The antagonist scaffold, 1H,3H-pyrido[2,1-f]purine-2,4-dione (blue color), was employed to study the effect of the linker length, type and position of warheads on affinity. It led to the discovery of LUF7602 as a best-in-class covalent antagonist in this study.

In summary, cases presented in this thesis provide insight and clues towards a universal strategy for the design of covalent ligands. The efficiency of the ligation reaction is ultimately dependent on an optimal combination of 1) the affinity of the pharmacophore for the target receptor, 2) the warhead's proximity to an appropriate nucleophilic amino acid residue and 3) the warhead's reactivity.

### 1.2. Research workflow to characterize the covalent ligands

The examples summarized in thesis (**Chapter 3-6**) demonstrate a research workflow (Figure 4) to profile the pharmacological activities of the covalent ligand-receptor interaction. As summarized in section 7.1.1, the design of covalent ligands needs to be balanced between high-affinity pharmacophore, linker unit and reactive functionality. Moreover, a control ligand is required to maintain a similar binding mode but in a nonreactive reversible manner, where it is crucial to maintain a structural similarity with the corresponding covalent ligand. In **Chapter 3** for instance, both a long residence time compound LUF6632 and a short-residence time prototypical ligand ZM241385 are employed as control ligands to perform the pharmacological evaluations. Although, these control compounds were structurally very similar to the covalent ligand, even closer analogues were possible. Hence, in the cases presented in **Chapters 4** and **5** non-reactive electron-withdrawing methylsulfonyl derivatives

were designed as control ligands, resulting in significant, if not the best possible, structural similarities with covalent ligand. Subsequently, both covalent ligand and control ligand are subjected to streamlined biological evaluation, including time-dependent affinity determination, binding kinetics investigation, wash-out assays, mutagenesis study and functional characterization (Figure 4).



**Figure 4. Research workflow to design, select and validate covalent ligands for GPCRs**

In detail, the first hint of a covalent interaction by the probe is represented by a leftward shift of the concentration-dependent radioligand displacement curve at different incubation times. A longer incubation time renders the covalent ligand to be more potent in displacing the radioligand from the receptor, resulting in an increased apparent affinity. However, it is far from conclusive to verify a covalent interaction from an affinity shift alone, as pseudo-irreversible interactions can also occur caused by slow dissociation rates. This is actually shown in **Chapter 3**, where a long residence time compound, LUF6632, also achieves a better affinity with a longer incubation time. To this end, the binding kinetic profiles are explored as a second hint for covalence, with specific focus on a ligand's dissociation rate constant ( $k_{off}$ ) and residence time ( $RT = 1/k_{off}$ ; Figure 4). The covalent ligands presented in **Chapters 3-5** cause an initial 'overshoot' of the competition association curve, followed by a linear decline over time indicating that no equilibrium was reached. The data analysis of these cases yield a negligible dissociation rate, and a concomitant, almost infinite residence time. In addition, the inadequacy of the Motulsky-Mahan equations to fit this data is further evidence for the non-equilibrium features of the irreversible interaction with the receptor [11]. Thirdly, a "washout" experiment to ascertain the irreversible ligand-receptor interaction are often performed (Figure 4). Here, the washing treatment failed to regenerate the binding capacity of the radioligand used, which demonstrated wash-resistance of the covalent ligand at the receptor.

A final (fourth) confirmation, is obtained by locating the target amino acid of the warhead responsible for the covalent interaction of the ligand in the receptor binding pocket (Figure 4). Structural knowledge of the receptor binding pocket greatly aids in docking the covalent compound, and thus pinpointing towards a potential anchor point. Finding the anchor point for covalent probes of GPCR families is always challenging. Mutagenesis of nucleophilic residues near the ligand's binding pocket appears to be one of the most useful tools to identify where the ligands bind covalently. Under the circumstance that receptor mutation does not alter the receptor binding site and functionality, a regained recovery of radioligand binding capacity in “wash-out” assays demonstrates the involvement of covalent bonding with the selected amino acid residue. In the studies of LUF7445 (**Chapter 3**) and LUF7746 (**Chapter 5**), the mutation led to the identification of the primary anchor point engaged in the covalent interaction. Still, this recovery failed to regenerate a 100% radioligand binding capacity, suggesting that other unidentified residues may play a similar role. In this context, an incomplete receptor activation recovery was observed in the functional [<sup>35</sup>S] GTP $\gamma$ S assay for covalent partial agonist (LUF7746, **Chapter 5**). Of note, site-directed mutagenesis studies for hA<sub>3</sub>R (**Chapter 4**) showed that removal of the nucleophilic group of the targeted amino acid residue resulted in the complete loss of covalent binding, validating that Y265<sup>7,36</sup> is the only anchor point of reactive covalent ligand LUF7602. The results presented in this thesis therefore agree with previous investigations to some degree, i.e. a high-affinity pharmacophore is a crucial starting point for a successful design of covalent ligands. Nevertheless, in future research, more extensive knowledge of receptor structure may improve the feasibility to locate the covalent interaction anchoring point. Overall, mutagenesis of nucleophilic residues near the ligand binding pocket is useful to study the mode and site of interaction, but may also drive the covalent ligand to react with secondary nucleophilic amino acid residues.

Although covalence can be confirmed by the experiments listed above, the irreversible activation/inhibition can be further evaluated on receptor function (Figure 4). For example, the covalent antagonistic nature of LUF7445 (**Chapter 3**) was confirmed in a cAMP functional assay, as it irreversibly blocked hA<sub>2A</sub>R-mediated cAMP accumulation by agonist NECA. For G<sub>i</sub>-coupled receptors, a membrane functional assay using [<sup>35</sup>S]GTP $\gamma$ S was employed. An insurmountable antagonism caused by the covalent interaction was demonstrated for LUF7602 (**Chapter 4**), while a persistent activation by LUF7746 (**Chapter 5**) was validated by its resistance to be blocked by an inverse agonist. Importantly, ligands of

interest in **Chapter 5** were further evaluated for their covalent partial agonistic behavior in the label-free xCELLigence assay detecting changes in cell morphology. Compared to conventional *in vitro* functional assays, these assays provide new opportunities, as they determine integrated receptor-mediated responses under near-physiological conditions at the cellular level that are recorded in real time without the need for any labels. Consistent with an irreversible mode of receptor activation in a membrane-based [<sup>35</sup>S]GTP $\gamma$ S assay, the obtained results validated the irreversible activation induced by LUF7746, also by its resistance to inhibition by antagonist DPCPX.

### 1.3. Applications of covalent ligands

The application of covalent ligands summarized in this thesis mainly focuses on the investigation of the topography of the GPCR-ligand binding pockets, as well as on receptor-signaling. However, in **Chapter 6**, we developed a covalent antagonist LUF7445 into an affinity-based probe LUF7487, which was used for two-step labeling of adenosine receptors. The previously synthesized covalently binding ligand LUF7445 (described in **Chapter 3**) was diversified to yield a few novel derivatives with different linker lengths. The most potent ligand was further equipped with a terminal alkyne allowing conjugation to azide-tailed fluorescent dyes, yielding probe LUF7487. Once bound, probe LUF7487 was concentration-dependently reacted with a fluorescent Cy3 moiety onto purified hA<sub>2A</sub>Rs via a bio-orthogonal copper catalyzed azide-alkyne click-ligation reaction. We further demonstrated that this affinity-based covalent labeling of the purified hA<sub>2A</sub>R by probe LUF7487 was inhibited by hA<sub>2A</sub>R selective antagonists. Lastly, we showed successful labeling of the receptor in cell membranes overexpressing hA<sub>2A</sub>R making probe LUF7487 a promising affinity-based probe (AfBP) that will be useful in identifying and profiling the presence of the hA<sub>2A</sub>R in complex biological samples.

In summary, by applying this research workflow (Figure 4), including rational design of covalent ligands and non-reactive control compounds, covalent interaction characterization and anchoring position capture, we shed light on the molecular mechanism of covalent modulation of the adenosine receptors. The obtained insights are valuable for the design of covalent antagonists (**Chapter 3 and 4**) and agonists (**Chapter 5**) for the orthosteric ligand binding site, for which novel assays were set up to study receptor pharmacology (**Chapters 3, 4 and 5**). The results obtained with novel tool compounds (**Chapters 6**) depict native receptor binding, and bridge the fields of chemical biology and molecular pharmacology to better investigate receptor-ligand interactions. Together, these insights are valuable in future



discovery projects for drugs targeting the adenosine receptor, and this research methodology may serve as an example to study the structural details on ligand recognition for other GPCR subtypes.

## 2. Future perspectives

### 2.1. The “druggability” of adenosine receptors

Adenosine receptors have been recognized as therapeutic targets for various diseases, such as cerebral and cardiac ischemic diseases [12], sleep disorders [12], immune and inflammatory disorders [13] and cancer [14]. Therefore, numerous attempts to develop potent and selective ligands have been made in recent decades [12, 15]. In the end, the first approved AR ligand is a selective A<sub>2A</sub>R agonist, regadenoson (Lexiscan®), for medical use related to myocardial perfusion imaging [16]. Another example is a xanthine-derived A<sub>2A</sub>R antagonist, istradefylline, (NOURIAST®), for the treatment of Parkinson’s disease in Japan [17]. Many other clinical trials targeting ARs are currently in progress with a focus on indications including Parkinson’s disease, chronic heart failure and inflammatory and autoimmune disorders [15, 18]. More recently, with the discovery of the adenosine-mediated immunosuppressive mechanism in cancer therapy [14], several A<sub>2A</sub> antagonists, initially developed for the CNS system, have entered clinical trials as immune-oncology agents alone and in combination with anti-PD1 or anti-PDL1 therapies [19]. Since oxygen deprivation in the tumor microenvironment causes an augmented extracellular adenosine level [14], it is essential that high-affinity adenosine antagonists are able to maintain their potencies in competition with the local adenosine levels, especially for small molecule antagonists with a fairly short *in vivo* half-life. In this regard, a covalently binding antagonist such as LUF7445 (described in **Chapter 3**), potentially prolonging the duration of action, may be a better proposition under these conditions. Moreover, as discussed in **Chapter 1**, the complexity of adenosine-mediated signaling and potential side effects compromises the development of pharmacological agents for specific applications. In such cases, the current fundamental research efforts on receptor structure and function still provide novel insights to facilitate the development of clinical candidates for adenosine receptors. More importantly, novel covalent AR ligands, including those discussed in this thesis, should be developed to investigate the topography of the GPCR-ligand binding pocket, as well as receptor-signaling and further pharmacological research. It is anticipated that such future molecules will possess enhanced properties and may therefore emerge as future drugs targeting ARs.

### 2.2. Covalent inhibitors for drug targets - what are the future opportunities?

In this thesis I have presented a design strategy for covalent probes that entails the identification of a reversibly binding lead compound, which is further optimized and used as a scaffold to incorporate a warhead for the targeted receptor. Notwithstanding the successful cases studied in this thesis, there are concerns that the addition of warheads and/or linkers might alter the key properties of the synthesized ligands. Meanwhile, the full dependency on the topology information of the binding pocket sometimes limits the successful application of this strategy to new targets. As in the hA<sub>3</sub>R study in **Chapter 4**, one solution is to build a homology model based on other target, in this case hA<sub>2A</sub>R subtype, with similar binding pockets. Knowledge of targets with similar binding pockets and anchoring locations is a valuable resource for designing selective compounds, as overlaying structures can often highlight where modifications can be made to gain selectivity. Still, this strategy can only be applicable if a suitable reversible lead exists.

Alternatively, covalent fragment screening appears to be a potential solution to cases where no available reversible ligands/inhibitors for the targets are known [20, 21]. It starts with a low molecular weight or drug-like fragment with an electrophilic reactive center, which is then developed into a fragment library. Specifically, when the electrophilic fragments bind proximal to the nucleophilic residue on the target protein, they will be covalently trapped on the target protein surface and detected using X-ray crystallography, mass spectrometry and digestion studies to identify the residue targeted [22]. The robust discovery of covalent ligands relies on the size of fragment libraries covering a broad range of reactivity. Nevertheless, potential issues that arise from this approach reveal that such simple hits will be dominated by strong reactivity of the fragments instead of specific recognition (as is the case for a pharmacophore), consequently increasing the risk of non-specific labeling, off-target toxicity, and promiscuous activity [21].

In addition, the availability of proper bioassays to measure covalent binding is essential. The examples illustrated in this thesis focus on the time-dependent radioligand binding assay and site-directed mutagenesis studies aided by computational docking studies. Another technique, mass spectrometry (MS)-based proteomics, emerged as a powerful structural biological tool to characterize protein conformation providing further structural insight [23, 24]. Depending on the availability of high-resolution structures, MS-based structural strategies can provide valuable, previously inaccessible information on protein conformational changes and dynamics, protein flexibility, and ligand-protein binding [25, 26].

The power of combining mass spectrometry-based proteomics and site-directed covalent labeling in the elucidation of GPCR ligand binding sites has shown great impact on the understanding of the structural features involved in ligand binding [27-29]. As summarized in **Chapter 2**, so far there is only one case that uses a photoaffinity probe to investigate the precise nucleophilic anchor point in the hA<sub>2A</sub>R binding pocket by mass spectrometry [30]. In this regard, the development of diverse experimental paradigms opens promising avenues for covalent ligands to obtain focused insights in structure-enabled GPCR ligand design. Ultimately, this may help in increasing the number and the quality of drug candidates targeting adenosine receptors as well as other GPCRs in the near future.

### 2.3. Covalent probes for GPCRs - where should we go?

Covalent ligands for GPCRs have shown to be valuable tool compounds to facilitate GPCR structure and function determination [31]. In the field of the adenosine A<sub>3</sub> receptor, an experimental crystal or cryo-EM structure would be a valuable addition to the currently available structures in the adenosine receptor family. The covalent ligands described in **Chapter 4** could be valuable tools for the elucidation of the inactive state of the human adenosine A<sub>3</sub> receptor structure.

The advent of covalent probes for chemical biology has been assisted by the development of click chemistry methods [32-34]. As demonstrated in **Chapter 6**, these covalent probes equipped with a ligation handle are paired with tags (e.g., biotin and/or a fluorophore) after they covalently bound to the receptors. This strategy underlays chemical biology or proteomics studies, to gain deeper insights into receptor localization and target engagement. The uncoupling of the ligand binding from the reporter tag labeling steps by click chemistry allows for tracking tissue and organ distribution of covalent probes *in vivo* [35]. In future research on adenosine receptors, different tags may be introduced; for instance, a biotin-tag would allow for streptavidin-mediated receptor enrichment for in-depth profiling using the Multi-dimensional Protein Identification Technology (MudPIT) analysis [36]. Similarly, the approach developed in this study may be applied to other GPCRs in similar physiological and pathological conditions.

### 2.4. Covalent drugs for GPCRs - worth a try?

In the history of drug discovery, covalent drugs have returned to the stage of the drug market in recent years, despite the past reluctance to pursue a covalent mechanism of interaction due to potential off-target toxicities. In approximately one-third of all enzyme targets for which there is an FDA-approved inhibitor, there is an example of an approved covalent drug [37].

## Chapter 7

---

The number of literature citations concerning covalent drugs appears to be rapidly increasing [37-41]. The continued and renewed interest in covalent drugs came from several recognized benefits, such as increased target potency, prolonged duration of action and the decreased therapy-induced drug resistance in clinical studies of cancer or infection. There is currently only one covalent drug targeting GPCR families, chopidogrel [42, 43]. It blocks the P2Y<sub>12</sub> receptor to inhibit platelet aggregation, occurring in e.g., thrombosis. However, clopidogrel can come with unwanted (on target) side-effects, such as extensive bleeding and thrombotic thrombocytopenic purpura.

In general, the bar to introduce a covalent drug for GPCRs is higher than is the case for kinases, a target class which has so far been well recognized and represented by several recently approved covalent drugs (ibrutinib, afatinib, and osimertinib) [44, 45]. Part of the reason is owing to the absence of an active reaction center in receptors and thus in the deficiency of mechanism-based inhibitors. Several considerations for rational design summarized in the conclusion paragraph may increase the rate of success. In addition, designing a compound targeting a poorly conserved residue may improve the selectivity of a compound. For instance, cysteine residues are in low abundance in proteins and possess a high nucleophilicity, appealing to be targeted with a low-reactivity warhead, Michael acceptors being key examples [46, 47]. This warhead reactivity is certainly an important consideration, demonstrating a balance between target engagement and idiosyncratic adverse drug reactions. To this end, warheads with low reactivity are generally preferred as a “safer” choice for a future drug candidate. Overall, the successful development of covalent kinase inhibitors as safe and efficacious cancer therapies will support the efforts towards other targets, such as GPCRs. If the selectivity and thus the safety of covalent molecules can be guaranteed these molecules provide valuable opportunities for future drug therapy.

### Final notes

This thesis is focused on rational design and pharmacological profiling paradigms of covalent probes for adenosine receptors. The results obtained in this thesis contribute to an improved understanding of the molecular aspects of receptor structure and function. We provide evidence that covalent modulation of GPCRs adds indispensable information on structural insights. Besides, we set up a work flow of *in vitro* pharmacological assays as a robust tool for measuring and quantifying covalent modulation. Finally, we developed affinity-based probes, which allow monitoring of GPCR expression in cell fragments.

Hopefully, all findings from this thesis add to a further molecular understanding of covalent ligand-receptor interactions, and contribute to the design of better covalent ligands with an appropriate profile, multiple tool compounds for future target validation, and ultimately suitable evaluation schemes for a better translation towards effective and safe drugs.

### References

1. Jorg M., and Scammells P.J. *ChemMedChem*. **2016**. 11(14): 1488-1498.
2. Narayanan A., and Jones L.H. *Chem Sci*. **2015**. 6(5): 2650-2659.
3. Jaakola V.P., Griffith M.T., Hanson M.A., Cherezov V., Chien E.Y., Lane J.R., IJzerman A.P., and Stevens R.C. *Science*. **2008**. 322(5905): 1211-1217.
4. Guo D., Xia L.Z., van Veldhoven J.P.D., Hazeu M., Mocking T., Brussee J., IJzerman A.P., and Heitman L.H. *Chemmedchem*. **2014**. 9(4): 752-761.
5. de Zwart M., Vollinga R.C., Beukers M.W., Slegers D.F., von Frijtag Drabbe Künzel J.K., de Groote M., and IJzerman A.P. *Drug Dev Res*. **1999**. 48(3): 95-103.
6. Sherman W., Day T., Jacobson M.P., Friesner R.A., and Farid R. *J Med Chem*. **2006**. 49(2): 534-553.
7. Rosentreter U., Henning R., Bauser M., Krämer T., Vaupel A., Hübsch W., Dembowski K., Salcher-Schraufstätter O., Stasch J.-P., Krahn T., and Perzborn E. *WO2001/025210*, . **2001**: April 12.
8. Chang L.C.W., Kunzel J.K.V.F., Mulder-Krieger T., Spanjersberg R.F., Roerink S.F., van den Hout G., Beukers M.W., Brussee J., and IJzerman A.P. *J Med Chem*. **2005**. 48(6): 2045-2053.
9. Louvel J., Guo D., Soethoudt M., Mocking T.A.M., Lenselink E.B., Mulder-Krieger T., Heitman L.H., and IJzerman A.P. *Eur J Med Chem*. **2015**. 101: 681-691.
10. Picone R.P., Fournier D.J., and Makriyannis A. *J Pept Res*. **2002**. 60(6): 348-356.
11. Motulsky H.J., and Mahan L.C. *Mol Pharmacol*. **1984**. 25(1): 1-9.
12. Jacobson K.A., and Gao Z.G. *Nat Rev Drug Discov*. **2006**. 5(3): 247-264.
13. Hasko G., Linden J., Cronstein B., and Pacher P. *Nat Rev Drug Discov*. **2008**. 7(9): 759-770.
14. Vijayan D., Young A., Teng M.W.L., and Smyth M.J. *Nat Rev Drug Discov*. **2017**. 17(12): 765-765.
15. Muller C.E., and Jacobson K.A. *Biochim Biophys Acta*. **2011**. 1808(5): 1290-1308.
16. Ghimire G., Hage F.G., Heo J., and Iskandrian A.E. *J Nucl Cardiol*. **2013**. 20(2): 284-288.
17. Dungo R., and Deeks E.D. *Drugs*. **2013**. 73(8): 875-882.
18. Chen J.F., Eltzschig H.K., and Fredholm B.B. *Nat Rev Drug Discov*. **2013**. 12(4): 265-286.
19. Congreve M., Brown G.A., Borodovsky A., and Lamb M.L. *Expert Opin Drug Discov*. **2018**. 13(11): 997-1003.
20. Lonsdale R., and Ward R.A. *Chem Soc Rev*. **2018**. 47(11): 3816-3830.
21. Kathman S.G., and Statsyuk A.V. *Medchemcomm*. **2016**. 7(4): 576-585.
22. Tailor A., Waddington J.C., Meng X.L., and Park B.K. *Chem Res Toxicol*. **2016**. 29(12): 1912-1935.
23. Xiao K., Chung J., and Wall A. *J Recept Signal Transduct Res*. **2015**. 35(3): 213-229.
24. Shukla A.K., Westfield G.H., Xiao K., Reis R.I., Huang L.Y., Tripathi-Shukla P., Qian J., Li S., Blanc A., Oleskie A.N., Dosey A.M., Su M., Liang C.R., Gu L.L., Shan J.M., Chen X., Hanna R., Choi M., Yao X.J., Klink B.U., Kahsai A.W., Sidhu S.S., Koide S., Penczek P.A., Kossiakkoff

## Chapter 7

---

- A.A., Woods V.L., Jr., Kobilka B.K., Skiniotis G., and Lefkowitz R.J. *Nature*. **2014**. 512(7513): 218-222.
25. Qin S.S., Meng M.M., Yang D.H., Bai W.W., Lu Y., Peng Y., Song G.J., Wu Y.R., Zhou Q.T., Zhao S.W., Huang X.P., McCorvy J.D., Cai X.Q., Dai A.T., Roth B.L., Hanson M.A., Liu Z.J., Wang M.W., Stevens R.C., and Shui W.Q. *Chem Sci*. **2018**. 9(12): 3192-3199.
26. Massink A., Holzheimer M., Holscher A., Louvel J., Guo D., Spijksma G., Hankemeier T., and IJzerman A.P. *Purinergic Signal*. **2015**. 11(4): 581-594.
27. Mallipeddi S., Kreimer S., Zvonok N., Vemuri K., Karger B.L., Ivanov A.R., and Makriyannis A. *J Proteome Res*. **2017**. 16(7): 2419-2428.
28. Zvonok N., Xi W., Williams J., Janero D.R., Krishnan S.C., and Makriyannis A. *J Proteome Res*. **2010**. 9(4): 1746-1753.
29. Szymanski D.W., Papanastasiou M., Melchior K., Zvonok N., Mercier R.W., Janero D.R., Thakur G.A., Cha S.W., Wu B., Karger B., and Makriyannis A. *J Proteome Res*. **2011**. 10(10): 4789-4798.
30. Muranaka H., Momose T., Handa C., and Ozawa T. *ACS Med Chem Lett*. **2017**. 8(6): 660-665.
31. Weichert D., and Gmeiner P. *Acs Chem Biol*. **2015**. 10(6): 1376-1386.
32. Gregory K.J., Velagaleti R., Thal D.M., Brady R.M., Christopoulos A., Conn P.J., and Lapinsky D.J. *ACS Chem Biol*. **2016**. 11(7): 1870-1879.
33. Soethoudt M., Stolze S.C., Westphal M.V., van Stralen L., Martella A., van Rooden E.J., Guba W., Varga Z.V., Deng H., van Kasteren S.I., Grether U., IJzerman A.P., Pacher P., Carreira E.M., Overkleeft H.S., Ioan-Facsinay A., Heitman L.H., and van der Stelt M. *J Am Chem Soc*. **2018**. 140(19): 6067-6075.
34. Yang X., Michiels T.J.M., de Jong C., Soethoudt M., Dekker N., Gordon E., van der Stelt M., Heitman L.H., van der Es D., and IJzerman A.P. *J Med Chem*. **2018**. 61(17): 7892-7901.
35. Speers A.E., and Cravatt B.F. *Chem Biol*. **2004**. 11(4): 535-546.
36. Speers A.E., and Cravatt B.F. *Curr Protoc Chem Biol*. **2009**. 1: 29-41.
37. Singh J., Petter R.C., Baillie T.A., and Whitty A. *Nat Rev Drug Discov*. **2011**. 10(4): 307-317.
38. Kalgutkar A.S., and Dalvie D.K. *Expert Opin Drug Discov*. **2012**. 7(7): 561-581.
39. Bauer R.A. *Drug Discov Today*. **2015**. 20(9): 1061-1073.
40. Adeniyi A.A., Muthusamy R., and Soliman M.E.S. *Expert Opin Drug Discov*. **2016**. 11(1): 79-90.
41. De Cesco S., Kurian J., Dufresne C., Mittermaier A.K., and Moitessier N. *Eur J Med Chem*. **2017**. 138: 96-114.
42. Savi P., Pereillo J.M., Uzabiaga M.F., Combalbert J., Picard C., Maffrand J.P., Pascal M., and Herbert J.M. *Thromb Haemost*. **2000**. 84(5): 891-896.
43. Ding Z., Kim S., Dorsam R.T., Jin J., and Kunapuli S.P. *Blood*. **2003**. 101(10): 3908-3914.
44. Baillie T.A. *Angew Chem Int Ed*. **2016**. 55(43): 13408-13421.
45. Liu Q., Sabnis Y., Zhao Z., Zhang T., Buhrlage S.J., Jones L.H., and Gray N.S. *Chem Biol*. **2013**. 20(2): 146-159.
46. Abranyi-Balogh P., Petri L., Imre T., Szijj P., Scarpino A., Hrast M., Mitrovic A., Fonovic U.P., Nemeth K., Barreateau H., Roper D.I., Horvati K., Ferenczy G.G., Kos J., Ilas J., Gobec S., and Keseru G.M. *Eur J Med Chem*. **2018**. 160: 94-107.
47. Shannon D.A., and Weerapana E. *Curr Opin Chem Biol*. **2015**. 24: 18-26

---

# Summary

Most of the small-molecular drugs are tailored to reversibly interact with their biological targets. There are concerns that the formation of a covalent bond with their target may yield off-target reactivity and this has led to these covalent drugs being disfavored as a drug class. Nevertheless, a common focus in modern drug discovery programs to maximize the strength of the desired drug-protein interactions has brought the concept of ‘covalent interactions’ back into the drug discovery track. These interactions may cause prolonged duration of action and improved potency and selectivity, providing advantages as both chemical probes and drug candidates. It has been recognized that the deficiencies of covalent modes of action may be tuned by designing compounds that carefully combine reactivity with specific complementarity to the target. Hence, in this thesis a covalent strategy is applied and shown to be compatible with a target-directed, structure-guided discovery paradigm, with a focus on G protein-coupled receptors as drug targets.

**Chapter 1** covers the main concepts studied throughout the thesis. The chapter starts with an introduction to G protein-coupled receptors (GPCRs), with a focus on the adenosine receptors. Subsequently, the concepts of covalent ligands for GPCRs and current state-of-the-art and challenges are described. **Chapter 2** continues with discussing the emerging molecular probes to profile adenosine receptors’ biological effects and summarizes the utilization of the probes to characterize and interrogate adenosine receptor subtypes both *in vitro* and *in vivo*, and to study their behaviors in physiological and disease conditions. The following **Chapters 3-6** demonstrate the design of covalently binding ligands targeting adenosine receptors and highlight their utility to profile pharmacological effects.

In **Chapter 3**, LUF7445 was introduced and characterized extensively. This covalent antagonist was designed based on a high affinity non-xanthine antagonist, ZM241385. This ligand has been co-crystalized with hA<sub>2A</sub>R, providing a clear blueprint of ligand-binding interactions. Analysis of the shape of the binding site shows that the phenylethylamine chain in ZM241385 is directed toward the more solvent-exposed extracellular region (EL2 and EL3), such that the ligand-receptor interactions offer us tremendous substituent flexibility to introduce the electrophilic fluorosulfonyl group responsible for the covalent interaction. Using time-dependent affinity shift and kinetic competition association assays, LUF7445 was likely identified as a covalent antagonist, which was further confirmed in wash-out assay. An *in*

---

*in silico* A<sub>2A</sub>-structure-based docking model combined with site-directed mutagenesis studies suggested the binding mode of LUF7445 with an anchor point at lysine amino acid K153<sup>ECL2</sup>. Meanwhile, a functional assay combined with wash-out experiments was set up to investigate the efficacy of covalent binding of LUF7445. These findings advance the studies of covalent ligands to serve as a prototype for a therapeutic approach in which a covalent antagonist may be needed to counteract prolonged and persistent presence of the endogenous ligand adenosine.

Inspired by the successful design of LUF7445, **Chapter 4** starts with a structure-based design of covalent antagonists for human adenosine A<sub>3</sub> receptors, a case with few structural insights of the receptor binding pocket. Starting from the 1H,3H-pyrido[2,1-*f*]purine-2,4-dione antagonist scaffold, a series of ligands bearing a fluorosulfonyl warhead with a varying linker length was obtained. The follow-up streamlined workflow to characterize these ligands was adapted from **Chapter 3**, suggesting LUF7602 behaves as a covalent antagonist for the human adenosine A<sub>3</sub> receptor. Of note, in this research, a non-reactive methylsulfonyl derivative LUF7714 was developed as a reversible control compound. When combined with *in silico* hA<sub>3</sub>R-homology modeling and site-directed mutagenesis, LUF7602 was used to characterize the spatial orientation and topography of the receptor ligand binding site, demonstrating that amino acid residue Y265<sup>7,36</sup> was the unique anchor point of the covalent interaction. In the end, using this structured approach a well-defined covalent ligand was quickly obtained and profiled.

Of note, this research workflow, including rational design of covalent ligands and non-reactive sulfonyl-bearing control compound, covalent interaction identification combined with *in silico* modeling and site-directed mutagenesis, may serve as a streamline to study the structural details of ligand recognition for other GPCR subtypes.

Subsequently, **Chapter 5** reports on the design, synthesis and application of a Capadenoson-based covalent partial agonist probe, LUF7746, bearing an electrophilic fluorosulfonyl moiety. Similarly, a nonreactive ligand bearing a methylsulfonyl moiety, LUF7747, was designed as a control ligand. In addition to the streamlined workflow to profile covalent ligands, a hA<sub>1</sub>R-mediated G protein activation assay was used to identify LUF7746 as a partial agonist and it is resistant to blockade with an antagonist/inverse agonist. An *in-silico* structure-based docking study combined with site-directed mutagenesis of the hA<sub>1</sub>R demonstrated that amino acid Y271<sup>7,36</sup> was the primary anchor point for the covalent



---

interaction, as it was for the adenosine A<sub>3</sub> receptor. In the end, a label-free whole-cell assay was set up to identify LUF7746's irreversible activation of an A<sub>1</sub> receptor-mediated cell morphological response.

After these demonstrations of covalent ligands to investigate adenosine receptor's pharmacological effects, **Chapter 6** reports on the development of A<sub>2A</sub>R covalent ligands into an affinity-based probe. In detail, an irreversible ligand LUF7445 was equipped with a terminal alkyne to serve as an affinity-based probe, LUF7487. After binding to the purified hA<sub>2A</sub>R, this probe was paired with a clickable fluorophore Cy3-azide, and irreversibly and concentration-dependently labelled purified hA<sub>2A</sub>R, which was visualized by SDS-PAGE. This labelling of the purified hA<sub>2A</sub>R by LUF7487 could be inhibited by both reversible and irreversible antagonists, provided that they target the same receptor binding site. In the end, a successful labeling of the receptor in cell membranes overexpressing hA<sub>2A</sub>R was demonstrated, making LUF7487 a promising affinity-based probe that sets the stage for the further development of probes for GPCRs.

In summary, the approach to design and pharmacologically profile covalent ligands for adenosine receptors has been explored and detailed throughout this thesis. A universal strategy of covalent ligands' design has been investigated, and the findings highlight several elements that can profoundly influence the covalent ligand-receptor interaction. These factors manifest an optimal combination dependent on the affinity of the pharmacophore, the warhead's proximity to an appropriate nucleophilic amino acid residue and the warhead's reactivity. The overall conclusion from the results described in this thesis and emerging opportunities for drug discovery are discussed in detail in **Chapter 7**. In concert, the novel insights that have been obtained in this thesis may provide valuable information for drug discovery targeting the adenosine receptor as well as other GPCRs.



---

# Samenvatting

De meeste geneesmiddelen zijn op maat gemaakt om een reversibele interactie aan te gaan met hun biologische aangrijpingspunten, genaamd target eiwitten. Het vormen van eecovalente en irreversibele binding met een target eiwit kan mogelijk leiden tot nadelige gevolgen wat tot bedenkingen heeft geleid om covalente geneesmiddelen als een medicijnklasse te zien. Echter, gezamenlijke inspanningen en successen in het veld van medicijnontwikkeling om de sterkte van geneesmiddel-eiwitinteracties te maximaliseren, hebben het concept van "covalente interacties" nieuw leven ingeblazen. Covalente interacties kunnen de werkingsduur verlengen en de activiteit en selectiviteit verbeteren, wat voordelen biedt voor zowel chemische probes als kandidaat-geneesmiddelen. Mogelijke tekortkomingen van covalente werkingsmechanismen kunnen worden aangepast door verbindingen te ontwerpen die gecontroleerde activiteit vertonen en die uit te rusten met selectiviteit voor het target eiwit. Daarom wordt in dit proefschrift een covalente strategie toegepast die compatibel is met een target-gerichte, structuur-gestuurde ontdekkingsparadigma, met een focus op G-eiwit-gekoppelde receptoren (GPCR's) als aangrijpingspunten voor geneesmiddelen.

**Hoofdstuk 1** behandelt de belangrijkste concepten die in het proefschrift zijn bestudeerd. Het hoofdstuk begint met een inleiding over GPCR's, waarbij de focus ligt op de adenosine receptoren. Vervolgens worden de concepten van covalente liganden voor GPCR's en de huidige situatie en uitdagingen beschreven. **Hoofdstuk 2** gaat verder met het bespreken van de opkomst van moleculaire probes om de biologische effecten van adenosine receptoren in kaart te brengen en vat samen hoe probes worden gebruikt om adenosine receptorsubtypen zowel *in vitro* als *in vivo* te karakteriseren. Verder wordt de rol van deze receptoren in fysiologische en ziektecondities bestudeerd. De **hoofdstukken 3-6** beschrijven het ontwerpproces van covalente liganden voor adenosine receptoren en demonstreren het gebruik van deze liganden om farmacologische effecten te bewerkstelligen.

In **hoofdstuk 3** wordt LUF7445 geïntroduceerd en uitgebreid gekarakteriseerd. Deze covalente antagonist is ontworpen op basis van een niet-xanthine antagonist met hoge affiniteit, ZM241385. Deze moleculaire "mal" werd gecokristalliseerd met hA<sub>2A</sub>R, wat een heldere blauwdruk van de ligand-binding interacties opleverde. Analyse van de vorm van de bindingsplaats toont aan dat de fenylethylamine-keten in ZM241385 is gericht op het meer aan oplosmiddel blootgestelde extracellulaire gebied (EL2 en EL3), waar ook veel ruimte is om de elektrofiele fluorosulfonyl groep te introduceren die verantwoordelijk is voor de

---

covalente interactie. Met behulp van tijdsafhankelijke affiniteitsverschuiving en kinetische competitie associatie experimenten, werd LUF7445 geïdentificeerd als een waarschijnlijk covalente antagonist, wat verder werd bevestigd met wash-out experimenten. Een docking model gebaseerd op de structuur van de adenosine A<sub>2A</sub> receptor gecombineerd met plaatsgerichte mutagenesestudies suggereert een bindingsmodus van LUF7445 met als ankerpunt lysine-aminozuur K153<sup>ECL2</sup>. Ondertussen werd een functioneel experiment, gecombineerd met wash-out experimenten, opgezet om de sterkte van de covalente binding van LUF7445 te onderzoeken. Deze bevindingen bevorderen studies van covalente liganden en dienen als een prototype voor een therapeutische benadering waarbij een covalente antagonist nodig kan zijn om langdurige en persistente aanwezigheid van het endogene ligand adenosine tegen te gaan.

Geïnspireerd door het succesvolle ontwerp van LUF7445, begint **hoofdstuk 4** met het op structuur gebaseerd ontwerpen van covalente antagonisten voor menselijke adenosine A<sub>3</sub>-receptoren, waarvoor maar weinig structurele inzichten in de receptor-bindingsplaats zijn. Uitgaande van de 1H,3H-pyrido[2,1-*f*]purine-2,4-dion-antagonist basisstructuur werd een reeks liganden gesynthetiseerd die een fluorosulfonyl “warhead” met een variërende linker dragen. De gestroomlijnde follow-up workflow om deze liganden te karakteriseren werd overgenomen van **hoofdstuk 3**, en de bevindingen suggereren dat LUF7602 zich gedraagt als een covalente antagonist voor de menselijke adenosine A<sub>3</sub>-receptor. Daarnaast werd in dit onderzoek een niet-reactief methylsulfonyl-derivaat LUF7714 ontwikkeld als een reversibel bindende controleverbinding. In combinatie met *in silico* hA<sub>3</sub>R-homologiemodellering en plaatsgerichte mutagenese werd LUF7602 gebruikt om de ruimtelijke oriëntatie en topografie van de receptor-ligandbindingsplaats te karakteriseren, waarbij werd aangetoond dat aminozuurresidu Y265<sup>7,36</sup> het unieke ankerpunt van de covalente interactie is. Uiteindelijk werd uit deze gestructureerde benadering snel een goed gedefinieerd covalent ligand verkregen en geprofileerd.

Notabene, deze onderzoekswerkstroom, inclusief rationeel ontwerp van covalente liganden en een niet-reactieve sulfonyl-dragende controleverbinding, alsmede de identificatie van covalente interactie gecombineerd met *in silico*-modellering en plaatsgerichte mutagenese, kan dienen als een gestroomlijnde aanpak om de structurele details over ligandherkenning voor andere GPCR's te bestuderen.

---

Vervolgens beschrijft **hoofdstuk 5** het ontwerp, de synthese en de toepassing van een op capadenoson gebaseerde covalente partiële agonist voor de adenosine A<sub>1</sub> receptor, LUF7746, die een elektrofiele fluorosulfonylgroep bevat. Tevens werd een niet-reactief ligand met een methylsulfonylgroep, LUF7747, ontworpen als controle ligand. Naast de eerder genoemde gestroomlijnde aanpak om covalente liganden te karakteriseren, werd een analyse van hA<sub>1</sub>R-gemedieerde G-eiwit-activering gebruikt om LUF7746 als een partiële agonist te identificeren alsook de ongevoeligheid voor blokkering door een antagonist/inverse agonist. Een *in silico* structuur-gebaseerde docking-studie gecombineerd met plaatsgerichte mutagenese van de hA<sub>1</sub>R toonde aan dat ook hier aminozuur Y271<sup>7,36</sup> het primaire aangrijpingspunt was voor de covalente interactie. Uiteindelijk werd een label-vrij intacte-cel experiment opgezet om de morfologische celrespons te identificeren als gevolg van de onomkeerbare LUF7746-activering van de A<sub>1</sub>-receptor.

Volgend op deze demonstraties van covalente liganden om de farmacologische effecten van adenosine receptoren te onderzoeken, beschrijft **hoofdstuk 6** de ontwikkeling van A<sub>2A</sub>R covalente liganden tot een op affiniteit gebaseerde probe. Hier werd een covalent ligand, LUF7445, uitgerust met een terminale alkyngroep om te dienen als een op affiniteit gebaseerde probe, LUF7487. Na binding aan de gezuiverde hA<sub>2A</sub>R werd deze probe gekoppeld aan de klikbare fluorofoor Cy3-azide en werd onomkeerbare en concentratieafhankelijke labelling aan gezuiverd hA<sub>2A</sub>R gevisualiseerd met behulp van SDS-PAGE. Het labellen van het gezuiverde hA<sub>2A</sub>R door LUF7487 kon worden geremd door zowel reversibele als irreversibele antagonisten, op voorwaarde dat ze zich richten op dezelfde receptor-bindingsplaats. Uiteindelijk werd een succesvolle labeling van de receptor in celmembranen die hA<sub>2A</sub>R tot overexpressie brachten aangetoond, wat LUF7487 tot een veelbelovende op affiniteit gebaseerde probe maakt die hopelijk de basis vormt voor de verdere ontwikkeling van probes voor GPCR's.

Samenvattend is de benadering van ontwerp en farmacologisch karakteriseren van covalente liganden voor adenosine receptoren onderzocht en gedetailleerd in dit proefschrift. Een universele strategie voor het ontwerp van covalente liganden is onderzocht en de bevindingen benadrukken verschillende elementen die de covalente ligand-receptor interactie sterk kunnen beïnvloeden. Deze factoren vertonen een optimale combinatie afhankelijk van de affiniteit van de farmacofoor, de nabijheid van de chemisch reactieve groep ('warhead') tot een geschikt nucleofiel aminozuurresidu en de reactiviteit van de 'warhead'. De algemene conclusie van de resultaten beschreven in dit proefschrift en de komende mogelijkheden voor

---

de ontdekking van geneesmiddelen worden in **hoofdstuk 7** gedetailleerd besproken. Met andere woorden, de nieuwe inzichten, verkregen door dit proefschrift, geven mogelijk waardevolle informatie voor geneesmiddelenonderzoek gericht op de adenosine receptoren alsook op andere GPCR's.

---

# List of publications

## *Part of this thesis:*

Yang X, Heitman LH, van der Es D, IJzerman AP. *Molecular probes for the human adenosine receptors*, In preparation.

Yang X, Dilweg M.A., Osemwengie, D., Burggraaff L, van der Es D, Heitman LH, IJzerman AP. *Design, Synthesis and Pharmacological Profiles of LUF7746, a Novel Covalent Partial Agonist for the Adenosine A<sub>1</sub> Receptor*, In preparation.

Yang X, van Veldhoven JPD, Offringa J, Kuiper BJ, Lenselink EB, Heitman LH, van der Es D, IJzerman AP, *Development of Covalent Ligands for G Protein-Coupled Receptors: A Case for the Human Adenosine A<sub>3</sub> Receptor*. J Med Chem. **2019** Apr 11;62(7):3539-3552. doi: 10.1021/acs.jmedchem.8b 02026.

Rouquette M, Lepetre-Mouelhi S, Dufrancais O, Yang X, Mouglin J, Pieters G, Garcia-Argote S, IJzerman AP, Couvreur P. *Squalene-Adenosine Nanoparticles: Ligands of Adenosine Receptors or Adenosine Prodrug?* J Pharmacol Exp Ther. **2019** Apr;369(1):144-151. doi: 10.1124/jpet.118.254961.

Yang X, Michiels TJM, de Jong C, Soethoudt M, Dekker N, Gordon E, van der Stelt M, Heitman LH, van der Es D, IJzerman AP. *An Affinity-Based Probe for the Human Adenosine A<sub>2A</sub> Receptor*. J Med Chem. **2018** Sep 13;61(17):7892-7901. doi: 10.1021/acs.jmedchem.8b00860.

Xia L, de Vries H, Yang X, Lenselink EB, Kyrizaki A, Barth F, Louvel J, Dreyer MK, van der Es D, IJzerman AP, Heitman LH. *Kinetics of human cannabinoid 1 (CB1) receptor antagonists: Structure-kinetics relationships (SKR) and implications for insurmountable antagonism*. Biochem Pharmacol. **2018** May; 151:166-179. doi: 10.1016/j.bcp.2017.10.014.

Yang X, Dong G, Michiels TJM, Lenselink EB, Heitman L, Louvel J, IJzerman AP. *A covalent antagonist for the human adenosine A<sub>2A</sub> receptor*. Purinergic Signal. **2017** Jun;13(2):191-201. doi: 10.1007/s113 02-016-9549-9.

---

**Not part of this thesis:**

Zhang H, Zhu P, Liu J, Yang X, Xu S, Yao H, Jiang J, Ye W, Wu X, Xu J. *Synthesis and antitumor activity of novel 3-oxo-23-hydroxybetulinic acid derivatives*. Eur J Med Chem. **2014** Nov 24; 87:159-67. doi: 10.1016/j.ejmech.2014.09.058.

Liu J, Liu Q, Yang X, Xu S, Zhang H, Bai R, Yao H, Jiang J, Shen M, Wu X, Xu J. *Design, synthesis, and biological evaluation of 1,2,4-triazole bearing 5-substituted biphenyl-2-sulfonamide derivatives as potential antihypertensive candidates*. Bioorg Med Chem. **2013** Dec 15;21(24):7742-51. doi: 10.1016/j.bmc.2013.10.017.

Bai R, Huang X, Yang X, Hong W, Tang Y, Yao H, Jiang J, Liu J, Shen M, Wu X, Xu J. *Novel hybrids of natural isochroman-4-one bearing N-substituted isopropanolamine as potential antihypertensive candidates*. Bioorg Med Chem. **2013** May 1;21(9):2495-502. doi: 10.1016/j.bmc.2013.02.044.

Bai R, Yang X, Zhu Y, Zhou Z, Xie W, Yao H, Jiang J, Liu J, Shen M, Wu X, Xu J. *Novel nitric oxide-releasing isochroman-4-one derivatives: Synthesis and evaluation of antihypertensive activity*. Bioorg Med Chem. **2012** Dec 1;20(23):6848-55. doi: 10.1016/j.bmc.2012.09.043.

Bai R, Liu J, Zhu Y, Yang X, Yang C, Kong L, Wang X, Zhang H, Yao H, Shen M, Wu X, Xu J. *Chiral separation, configurational identification and antihypertensive evaluation of (±)-7,8-dihydroxy-3-methyl-isochromanone-4*. Bioorg Med Chem Lett. **2012** Oct 15;22(20):6490-3. doi: 10.1016/j.bmcl.2012.08.040.

### **Oral and poster communications**

2018-Dec CHAINS Veldhoven, the Netherlands, oral communication

2018-Oct FIGON DMD Ede, the Netherlands, oral communication

**(selected poster abstract)**

2018-Sep EFMC-ISMIC 2018 XXV EFMC International Symposium on Medicinal

Chemistry, poster presentation **(funded by FIGON traveling grant)**

2018-Oct LACDR Spring Symposium, poster presentation **(best poster prize)**

2017-Oct FIGON DMD Ede, the Netherlands, oral communication

**(selected poster abstract)**

2017-Oct K4DD Meeting - Binding kinetics: Time is of the essence,

Berlin, Germany, poster presentation



---

# Curriculum Vitae

Xue Yang was born on March 6<sup>th</sup>, 1988 in Zhengzhou, Henan, China. After graduating from No.1 High School of Zhengzhou in 2007, she studied pharmaceutical science at China Pharmaceutical University. She was awarded first-grade scholarships and a CTTO Pharma Scholarship in 2007-2011.

At her last year undergraduate study, she was admitted as a recommended postgraduate specializing in medicinal chemistry. Since then, she started her scientific journey as a medicinal chemist working on the structure modifications of a natural product, XJP, at the division of Medicinal Chemistry under the supervision of Dr. Renren Bai. and Prof. dr. Jinyi Xu. This natural product was isolated from banana peel with potent antihypertensive activity in renal hypertensive rats. In the same year, she graduated with an honor degree and continued her research in the same group. In June 2014, she obtained her MSc degree. For her overall study results she was awarded the China National Scholarship, an annual award by the Chinese central government for outstanding students from each university.

In the same year, she was sponsored by the China Scholarship Council (CSC) to perform her PhD research at the Division of Drug Discovery and Safety under the supervision of Dr. Julien Louvel and Prof. dr. Ad IJzerman. Her research started from the design and synthesize novel covalent ligands targeting at adenosine receptors. Afterwards, she expanded her interest into the pharmacological profiling of these bioactive molecules *in vitro* under the supervision of Dr. Laura Heitman, Dr. Daan van der Es and Prof. dr. Ad IJzerman. Among other techniques, a range of *in vitro* assays were set up to investigate the covalent ligand-receptor interaction and fluorescently labeling of the adenosine receptors, for which she collaborated with Prof. Mario van der Stelt from the Leiden Institute of Chemistry. Throughout her PhD studies she presented work described in this thesis at various (inter)national conferences, including FIGON Dutch Medicines Days (2015-2018) and the Dutch Chemistry Conference CHAINS 2018. In 2018, she was awarded the 1<sup>st</sup> poster prize at the LACDR Spring Symposium and a FIGON Travel Grant to one of the EFMC-ISMC conferences.



---

# Acknowledgements

The work presented in this thesis took the past few years to complete, throughout which I gained input and support from so many people, many of whom became more than just workmates. I appreciate the input and contributions that enabled my PhD work to arrive at the current state.

It has been a wonderful opportunity to join our research group. Ad, thanks for your inspiration, encouragement and trust not just in the lab work, but also for the moments when I was facing challenges. I'm grateful to Laura and Daan for your practical input and insightful advice. In particular, I was so lucky to be supervised by a talented chemist, Julien (you will be missed). Thank you all for the thumbs up and constructive criticism. It has been a pleasure to work in this research group for these years.

I would like to thank all my colleagues and students for all the fun times and laughter in the lab. To the students, especially my master students Thomas, Coen, Dion, Jelle and Majlen, who have greatly contributed to parts of this thesis and gave me great inspiration to work on these projects. To my collaborators, Bart, Lindsey, Hui, Marjolein and Mario, who have broadened my vision and greatly facilitated my research projects. To my officemates, Jaco, Sebastian, and Tasia for their persistent invitations for coffee breaks and interesting pop-science discussions. To Thea and Henk, for the steady support with the many years of hands-on experience in the lab.

Special thanks to Anna, Natalia, Maarten, Rongfang, Xuesong and Lindsey for all the funny moments and distress activities we have been through. To the many other great people I have ever met, Bert, Huub, Olivier, Brandon, Lisa, Jara, Cas, Hein and Gerard for shared conversations, sport activities and drinks.

I would also like to thank my friends, Inge, Mike, Lance, Haoyu, Weichun, Xinyang, Jing, Liang, Mingqian, Ming, Qiang, Xuhan, Xiaobing, Yazhi, Huayu and Gangqi, for their endless efforts to burnish my journey in the Netherlands.

Finally, to my beloved family, who have become my backbones throughout so many years. I am immoderately grateful to my parents and brother for their long-term support and understanding. I much appreciate to go through this "covalent" phase with all of you.

